PFC/RR-95-3 DOE/DE-FG02-91ER40648

Interaction of Intense Lasers with Plasmas

Gennady Shvets

February, 1995

This work was supported by the U.S. Department of Energy Contract No. DOE/DE-FG02-91ER40648. Reproduction, translation, publication, use and disposal, in whole or in part by or for the United States government is permitted.

Interaction of Intense Lasers with Plasmas

by

Gennady Shvets

Submitted to the Department of Physics
in partial fulfillment of the requirements for the degree of

Doctor of Philosophy in Physics

at the

MASSACHUSETTS INSTITUTE OF TECHNOLOGY

February 1995

Author .....
Department of Physics
January 23, 1995

Certified by .....
Jonathan S. Wurtele
Associate Professor
Thesis Supervisor

Accepted by .....
George F. Koster
Chairman, Departmental Committee on Graduate Students

Interaction of Intense Lasers with Plasmas

by

Gennady Shvets

Submitted to the Department of Physics
on January 23, 1995, in partial fulfillment of the
requirements for the degree of
Doctor of Philosophy in Physics

Abstract

This thesis addresses two important topics in nonlinear laser plasma physics: the interaction of intense lasers with a non thermal homogeneous plasma, the excitation of laser wakefields in hollow plasma channels, and the stability of channel guided propagation of laser pulses.

In the first half of this thesis a new theoretical approach to the nonlinear interaction of intense laser pulses with underdense plasmas is developed. Unlike previous treatments, this theory is three-dimensional, relativistically covariant, and does not assume that $a \ll 1$, where $a = eA/mc^2$ is a dimensionless vector potential. This formalism borrows the diagrammatic techniques from quantum field theory, yet remains *classical*. This classical field theory, which treats cold plasma as a relativistic field interacting with the electromagnetic fields, introduces an artificial length scale which is smaller than any physically relevant spatial scale. By adopting a special (Arnowitt-Fickler) gauge, electromagnetic waves in a cold relativistic plasma are separated into "photons and "plasmons which are the relativistic extensions of electrostatic and electromagnetic waves in a cold stationary plasma.

The field-theoretical formalism is applied to a variety of nonlinear problems including harmonic generation, parametric instabilities, and nonlinear corrections to the index of refraction. For the first time the rate of the second harmonic emission from a homogeneous plasma is calculated and its dependence on the polarization of the incident radiation is studied. An experimental check of this calculation is suggested, based on the predicted non-linear polarization rotation (the second harmonic is emitted polarized perpendicularly to polarization of the incident signal). The concept of renormalization is applied to the plasma and electromagnetic radiation (photons and plasmons). To the lowest order, this corresponds to relativistically correcting the electron mass for its oscillation in an intense EM field and to replacing the vacuum dispersion relation by the usual relativistic plasma dispersion relation. This renormalization procedure is then carried to higher order in $\epsilon = \omega_p^2 a^2/[(1 + a^2/2)^{3/2}\omega^2]$. This yields the nonlinear modification of the index of refraction of a strong electromagnetic wave and the dispersion of a weak probe in the presence of the wave.

In the second part of this thesis the stability of short laser pulses propagating

through parabolic channels and the wake excitation of hollow plasma channels are studied. The stability of a channel guided short laser pulse propagation is analyzed for the first time. Perturbations to the laser pulse are shown to modify the ponderomotive pressure, which distorts the dielectric properties of the plasma channel. The channel perturbation then further distorts the laser pulse. A set of coupled mode equations is derived, and a matrix dispersion relation is obtained analytically. As an example, the spacio-temporal growth of a pure dipole perturbation is evaluated in various parameter regimes. A mechanism for suppressing the instability, analogous to BNS damping in linear accelerators, is proposed and evaluated analytically and numerically.

The ponderomotive excitation of wakefields in a hollow plasma channel by an intense laser pulse is studied analytically. We demonstrate that the laser excites an accelerating mode in the channel. This mode has a higher degree of transverse uniformity than could be realized by the same laser pulse in a homogeneous plasma, making it more desirable for the acceleration of a high quality beam. A convolution equation for the excitation of this mode is found. For the first time the modifications to the mode due to finite thickness of the channel walls are derived and the interaction of the mode with inhomogeneous plasma inside the channel wall is analyzed. An important finding is that the resonant absorption in the channel wall dissipates the accelerating wake, thereby introducing a finite quality factor of the hollow plasma channel and reducing the number of electron bunches that can be accelerated in the wake of a single laser pulse.

Thesis Supervisor: Jonathan S. Wurtele
Title: Associate Professor

Acknowledgments

The time I spent at MIT was both intellectually challenging and immensely rewarding. For that my greatest thanks go to my research advisor Professor Jonathan Wurtele. From him I learned how a theorist can create something beautiful as well as useful. Being critical of my own ideas (as well as of those of other people) is one of the qualities I have acquired working with Jonathan. His never failing willingness to "talk physics", diversity of the research interests, and the scientific freedom I enjoyed have been inspirational to me over these years.

In the beginning of my graduate career I was involved in microwave FEL research at RLE. For this invaluable introduction to the world of experiments (and experimentalists) I am greatly indebted to Professor George Bekefi and Manoel Conde.

My summer research at Lawrence Berkeley Lab opened the rich world of laser-plasma physics to me. My great thanks go to Dr. Andrew Sessler for being both critical and encouraging supervisor and for tolerating my attempts to solve all the problems at the same time. I am also grateful to the team of our collaborators on the West coast: to Rick Savage for inspiring discussions of the experiment, to Warren Mori, Tom Katsouleas, and Chris Decker for introducing me to the world of plasma simulations, and to Professor Chan Joshi for taking my ideas seriously.

When working on my thesis I have received many valuable suggestions from Professors Barton Zwiebach and Arthur Kerman, for which I am very grateful.

My life in graduate school would have been much poorer without the company of my fellow students. I want to thank Paul Volfbeyn for being a wonderful friend and officemate, with whom I spent endless hours discussing physics, physicists, and life. I would also like to thank my co-author and friend Ge Zhang for her encouragement and kindness.

I want to thank Alma Ourazalinova for her companionship and patience during my final year in graduate school.

And finally I wish to thank my Mom and Dad for giving me the strength and support over these years and for everything they have done for me before.

Contents

List of Figures

Chapter 1

Introduction

Over the past decade a revolution has occurred in our ability to produce high-power and high-intensity laser pulses [1]. Chirped-pulse amplification (CPA) [2, 3] has led to tabletop laser systems producing multi-Terawatt powers and focused irradiances in excess of $10^{18}\mathrm{W/cm^2}$. The CPA technique makes possible efficient energy extraction from high energy-storage materials by short (sub-picosecond) pulses without incurring nonlinear effects associated with high intensity. This is accomplished by first stretching a femtosecond pulse by a factor of up to 10^4, then amplifying the resulting long pulse by $10-11$ orders of magnitude, and finally, compressing the pulse to its near original value. The future CPA based laser systems will produce even higher power outputs since the theoretical power limit is yet to be reached. For example, the construction of a PW (petawatt) laser is under way at Lawrence Livermore National Laboratory (LLNL). The development of these intense short pulse lasers has opened up a new parameter regime in the interaction of intense lasers with plasmas, creating a surge of experimental [1]-[11] and theoretical [12]-[41] investigations.

These multi-Terawatt lasers operate with pulses sufficiently short (< 100 fs) so that hydrodynamic motions during the pulse [4, 10] are eliminated. The enormous electric and magnetic fields at a laser focus make electron motion mildly relativistic at the 1TW power level and highly relativistic at 1 PW powers. For example, plasma electrons subjected to linear polarized laser fields of a 1 TW laser with $I\lambda^2 = 10^{18}\mathrm{W}\mu^2/\mathrm{cm}^2$ acquire a time-averaged kinetic energy of about 100keV, while

a 1 PW laser would generate $\sim$ 10 MeV energy in the oscillatory motion. This new relativistic regime allows for the study of such fundamental laser-plasma phenomena as relativistic self-focusing [15], harmonic generation [14, 15, 16, 17], emission of terahertz radiation [5], strongly coupled scattering [6], and development of applications such as Compton side-scatter x-ray sources [18], laser-based accelerating schemes, and laser drivers for photon (gamma-gamma) colliders.

High intensity short laser pulses offer a new mechanism for producing hot electrons: plasma electrons are ponderomotively accelerated to relativistic velocities, then collisionally thermalize to quasi-Maxwellian distributions, with the total (thermal) energy in good agreement with ponderomotive energy. This mechanism for the production of hot electrons and hard X- rays has been predicted [38] and experimentally observed [8]. While hard X-rays have been observed in a number of earlier experiments with long pulse lasers ($>$ 100 ps) [9], in the majority of those experiments the hot electrons were produced by stimulated Raman scattering.

Another interesting phenomenon in intense laser-plasma interactions is the enormous light pressure, which for laser pulses of intensity $10^{18}\mathrm{W/cm^2}$ is of order 300Mbarr. This pressure significantly changes laser absorption in the plasma. For low intensity, long laser pulses most of the absorption occurs at the critical surface, where the local plasma frequency matches the laser frequency. High-intensity short pulses can strongly modify the plasma density profile, penetrating past the critical surface [38]. This effect was observed by Liu and Umstadter [7] for laser intensities exceeding $5 \times 10^{16}\mathrm{W/cm^2}$.

A potentially important application of laser-plasma interactions is inertial confinement fusion (ICF). The traditional approach of ICF is to compress the deuterium-tritium (D-T) fuel to a high density and temperature, sufficient to ensure the thermonuclear synthesis. The compression is achieved by irradiating the target with electromagnetic radiation, either directly from several lasers (direct drive), or with X-rays emitted by a holhraum (a hollow cylinder made of high-Z material),the inside of which is irradiated through small entrance holes by the lasers. Heating is accomplished when the incident X-rays generate a shock compression wave which propagates towards the

center of the target. This approach requires a very high symmetry of the incident radiation and a high degree of compression.

A recently developed [39] alternative approach envisions a two-stage heating process. The fuel is first compressed at relatively low temperature (a few hundred eV) and then rapidly heated to ignition temperatures (5-10 keV). The heating is accomplished by energetic electrons which are produced when a short high-power laser pulse bores a hole into the target. This method decouples the compression and heating stages, thus relieving the requirements on the symmetry and degree of compression.

High-intensity, ultra-short laser-plasma interactions can be used in a number of applications requiring unusually high fields that would cause a breakdown of any other medium. For instance, as was first realized by Tajima and Dawson [28], the ability of plasma to support strong longitudinal waves makes it a possible (although not in the immediate future) candidate for high energy particle acceleration. Various schemes of plasma based accelerators have been proposed such as the Laser Wakefield Accelerator [23, 25], Plasma Beat-Wave Accelerator [11] and others [21]. All of these employ high-intensity lasers to excite a strong plasma wave with a phase velocity near the speed of light.

Plasma is also an attractive nonlinear medium for harmonic generation. The idea behind harmonic generation is very straightforward— plasma density is perturbed by the high-frequency ponderomotive force of the pump wave, thus producing a high-frequency moving grating that the pump can scatter off, thereby producing harmonics. But it was only recently realized [14, 15] that the relativistic nature of the electron motion has to included to obtain a correct prediction of the harmonic generation rate. More precisely, the ponderomotive force (which is responsible for the excitation of the density ripple) scales quadratically with the laser amplitude, as do the relativistic corrections to the electron dynamics. Hence, the necessity to treat both nonlinearity and relativistic corrections simultaneously.

The availability of the multi-Terawatt laser sources and the numerous applications provide a strong motivation for constructing a systematic approach to laser-plasma interactions which does not treat the normalized amplitude of the laser $a = e \mid \vec{A} \mid$

$/mc^2$ (where $\vec{A}$ is a vector potential of the laser field, $-e$ is the electron charge, and m is the electron mass) as a small parameter. That a can be much greater than unity is evident from typical numbers for the Pettawatt project at Livermore [1]: a $1.0kJ$ of 1.053μ light, with pulse duration between 0.5 and 20 ps, focused to twice the diffraction limit, can provide normalized laser amplitudes as high as 30.

One of the first attempts at circumventing the now obsolete assumption that $a < 1$, was in a paper by Rax and Fisch, who pointed out that

$$\epsilon = \omega_p^2 a^2/[(1 + a^2/2)^{3/2}\omega^2] \tag{1.1}$$

(where $\omega_p^2 = 4\pi e^2 n_0/m$, n_0 is the plasma density, and ω is the laser frequency) is a useful small parameter. The rate of the third harmonic generation was computed in [14, 15, 16, 17] to the lowest order in ϵ. Nevertheless, since diffraction limits the interaction length of the incident laser pulse with the plasma, the use of plasma as a practical medium for harmonic generation will require that the rate is maximized. This implies operating at slightly under-critical densities, which clearly violates the condition $\omega_p^2 \ll \omega^2$ and makes the retention of only the first order in ϵ insufficient.

The importance of developing a systematic higher-order perturbation theory is illustrated by an example in which a first order calculation yields a vanishing emission rate. It was thought for some time [16] that there is no second harmonic emission from a homogeneous plasma even when a finite transverse size of the laser is taken into account (or, alternatively, several plane electromagnetic waves propagating at finite angles to each other are present). This was based on a calculation which assumed that a is small and was carried out to the order a^2 in laser amplitude. We will show that a higher-order calculation yields a non-zero rate of second harmonic generation (see Eq.(4.50)). This result was only obtained because the perturbation formalism allowed for both higher order nonlinearities and three-dimensional effects (the finite transverse size of the incident radiation). Thus a suitable theory must be three-dimensional, relativistically covariant, and calculable to any order in ϵ. The diagrammatic formalism presented in the first half of this thesis is such a theory.

Diagrammatic perturbation expansions have been used in laser and plasma physics before. Nonlinear optical susceptibilities were calculated using diagrammatic perturbation theory in quantum optics [42]. Pioneering use of diagrams was made in nonlinear plasma physics [43] to study turbulence [44], Landau damping [45] and other processes in thermal plasmas. However, the diagrams in these calculations were not derived from first principles but, rather, were used as convenient visualizations for various nonlinear processes whose rates were obtained using certain assumptions about stochastic processes in plasma, etc. On the other hand, the diagrammatic theory presented in this thesis is derived from first principles, is relativistically covariant, and predicts new phenomena (such as the second harmonic generation) which are technically hard to obtain using conventional techniques. Unlike the previous treatments that employed diagrams, this thesis uses the diagrammatic perturbation theory to address the physical problems that involve *collective* processes in *non-thermal* plasma.

Diagrams have also been used to analyze the radiation of a single electron in the field of intense electromagnetic wave [46]-[49]. Yet no serious attempt was made to self-consistently study the effect of the plasma on the EM wave.

Much excitement over the past decade was brought about by the idea of using laser-plasma for high-energy particle acceleration. For instance, one of the schemes of laser-plasma accelerator is the so-called Laser Wakefield Accelerator (LWA). In LWA an intense short laser pulse is injected into the plasma where it excites a strong plasma wave—wake. The name originates from the similarity of the excited plasma wave with the wake left behind a motor boat on the lake. Since the electric field of the plasma wave is longitudinal (in the direction of the laser propagation) and its phase velocity is equal to the group velocity of the laser pulse in the plasma (which is close to the speed of light for very underdense plasmas, see Sec. 5.1), this plasma wake can be used for particle acceleration. Acceleration to high energies requires long propagation distances. Diffraction imposes the most stringent constraint on the interaction length over which acceleration can take place. Transverse variation of the plasma density offers a mechanism for guiding the light over many diffraction lengths.

Since the index of refraction of the electromagnetic wave in the plasma *decreases*

with plasma density, a plasma channel which has a lower plasma density *on axis* than *off axis* can guide the laser pulse similarly to an optical fiber. The crucial distinction between a plasma channel and an optical fiber is that the laser does not leave wakes in the fiber while it certainly excites plasma wakes in the channel. The desired wake provides the accelerating longitudinal field, but other wakes can also be excited. Initial research into channel propagation [15] of short pulse lasers was axisymmetric and did not include the action of plasma wakes on the laser itself. In a three-dimensional calculation we have found and analyzed, for a parabolic channel, a new instability by which the initial distortions in the transverse laser profile are amplified as the laser propagates along the channel. The physics of the amplification is straightforward— distortions in the laser profile generate density perturbations which act back on the laser. By analogy with techniques developed and used in linear accelerators we propose and study a method of damping the instability.

One of the promising schemes for laser-plasma acceleration [40], as will be discussed in the second half of this thesis, is the hollow channel laser wakefield accelerator. In this scheme an evacuated channel in the plasma serves as an optical fiber which guides the laser pulse over many Rayleigh lengths. At the same time, the ponderomotive force of the laser excites wakefields at the surface of the channel, which extend to the center where they can be used for particle acceleration. The attraction of the hollow channel laser wakefield accelerator comes both from the ability of the channel to guide the laser pulse and the transverse uniformity of the accelerating mode. We find the accelerating mode of the hollow channel with a step-function plasma density profile, derive its frequency and an equation for its excitation by the ponderomotive force of the laser pulse acting on the channel walls. We further examine the more general case of a finite thickness wall. We then perturbatively study the influence of the finite-thickness channel wall on the structure and the frequency of the accelerating mode and examine the interaction of this mode with electrons inside the channel wall. We find that there exists a region of resonant absorption inside the wall, where the local plasma frequency matches the frequency of the wake. This resonant absorption dissipates the wake, thereby introducing an effective quality factor Q of the hollow

channel.

This thesis consists of two major parts—(i) the diagrammatic approach to laser-plasma interactions (Chapters 2-5) and (ii) laser propagation in plasma channels (Chapters 5-7). Chapter 2 introduces the diagrammatic methods as applied to nonlinear problems. It develops an original formalism for treating laser-plasma interactions as a field theory. Chapter 3 introduces a relativistically covariant classification for electromagnetic waves in cold plasma (by utilizing a non-traditional Arnowitt-Fickler gauge) and renormalization (which is applied, to the lowest order in ϵ, to radiation and electrons). Chapter 4 presents most of the calculations using the diagrammatic formalism. These include the non-linear dispersion of EM waves, a dispersion relation for small-angle Raman scattering (without the assumption that $a < 1$) and the rate for the second harmonic emission from homogeneous plasmas.

Chapter 5 reviews the acceleration schemes based on the ponderomotive excitation of plasma wakes by high intensity short laser pulses. It motivates the study of channel guided laser propagation, which is the main subject of the second part of this thesis. Chapter 6 studies the instabilities of the propagation of laser pulses in parabolic channels. It is largely based on the work by G. Shvets and J. S. Wurtele [41]. Chapter 7 contains an original treatment of wake excitation in inhomogeneous plasma channels. Chapter 8 concludes this thesis by summarizing the obtained results and outlining some extensions and further applications of this work.

Appendix A describes laser plasma interactions through Klein-Gordon equation and compares the results with the diagrammatic calculation. Linear large angle Raman scattering instability is also considered and the growth rate for Raman backscattering, previously derived in [12], is recovered as a particular case. This appendix suggests an idea of perturbatively solving the classical Hamilton-Jacobi equation for the relativistic action, expressing it as a series of canonical transformations. Appendix B serves as a tutorial on the usage of diagrams by analyzing in great detail three typical problems from laser-plasma interactions. Appendix C presents the list of commonly used notation to facilitate the reading of the thesis.

Chapter 2

Basic Concepts of the Diagrammatic Approach to Laser Plasma Interactions

2.1 Introduction

Laser-plasma interactions has been a mature sub-field of plasma physics for over a two decades [50]. A great number of theoretical approaches have been developed. Yet all these approaches are distinguished by different ways of treating the *plasma*. This is by far the hardest part in any laser-plasma problem. The electrodynamics, aside from minor subtleties associated with propagation in inhomogeneous medium [51], the applicability of electrostatic [40] or quasistatic [52, 15] assumptions, etc., is relatively straightforward. At the same time, the dynamics of the plasma, in different physical circumstances, has to be analyzed using very different theoretical models.

The most straightforward description of the plasma is the Klimontovich model [53, 54], which treats plasma as a collection of interacting point-like particles. This model is used if the main focus of the problem is defined by the single particle motion: incoherent emission, electron-electron and electron- ion collisions, etc. When the discrete nature of plasma particles is less important, various truncations of the Klimontovich

equation are used. For example, collisional plasmas are described by kinetic equations in phase-space, with a Boltzman-like collisional operator (see, for example, Ref. [56] and references therein). Collisionless plasmas are described by a phase space density that evolves according to the Vlasov equation [57] and self-consistent Maxwell's equations for the fields. As kinetic effects become less important, plasmas can be described by truncations of the Vlasov equation that characterize the plasma by its global properties, such as fluid velocity, density, temperature and pressure. For a thermal plasma interacting with a long-pulse, low power laser, this would be a model of choice [50]. In general, both ion and electron dynamics have to be included.

For shorter laser pulses, the ion motion becomes less important, and the significant interactions occur between the radiation and the electrons in the plasma. Depending on how the thermal energy compares with the jitter energy in the laser field, and on the significance of kinetic effects, such as particle trapping and wave-breaking, either a fluid or kinetic description of the electron plasma is appropriate [58].

We notice that in all these descriptions of plasma (Klimontovich, Boltzmann, Vlasov, fluid), there is an important formal difference in the treatment of electrodynamic quantities and plasma. Electrodynamic quantities are described as fields whereas plasma is described in some other way. In this thesis we develop a diagrammatic perturbation theory that treats electrons and electromagnetic fields on the same footing, namely as *fields*. Ions are assumed to be a stationary neutralizing background due to the short duration of the intense laser pulses. The theory is fully relativistic, covariant and three dimensional. The normalized laser vector potential a is not assumed small.

Since plasma is described as a field, this implies that electrons are treated as waves with a very short wavelength. Yet the theory developed here is essentially classical. This may seem a bit puzzling at first but a few simple arguments convince one that there is no inconsistency in developing a *classical* theory that treats particles as waves.

The first and the most obvious objection against this approach is the uncertainty principle. It states that the position and the momentum of a particle can not be both determined exactly. Yet the degree of uncertainty is proportional to the constant that

has the same dimension as $\hbar$, the Plank constant, and can be chosen to be arbitrarily small.

Another phenomenon present in quantum physics (and derived from the wave description of particles) and seemingly absent from the classical physics, is the spreading of a wave packet. Any particle initially localized in space will eventually spread out due to the uncertainty in its momentum. Yet this spreading due to uncertainty in momentum is not at all quantum mechanical and is indeed reproduced in a classical calculation. One can represent a density clump by a distribution function of finite extent in momentum space, and choose the momentum spread in agreement with uncertainty principle. Then, as was demonstrated by R. Littlejohn [59], the results of a classical calculation are in perfect agreement with the exact solution of the Schroedinger equation.

The most important advantage of describing particles as fields comes from the realization that all the powerful apparatus of QED, including the diagrammatic expansion, mass renormalization, "dressed particles" and so on, can be utilized in the calculations. The calculation remains classical so long as (1) The perturbation theory is applied as described in Section 2.2, that is, characterizing the plasma by canonical coordinates and using classical Poisson brackets (instead of characterizing the plasma by operators and using quantum mechanical commutators). This eliminates the loops which are incompatible with classical physics. (2) By choosing the effective "Plank's constant", (e.g. the scale length where the wave-particle effects are important) sufficiently small. Precisely how small is explained in Section 2.3.1.

The diagrammatic expansion in Poisson brackets introduced here can be obtained from a quantum mechanical expansion of a Feynman path integral if the action in the integrand is computed to lowest order in Plank's constant. This expansion is known in field theory as a tree expansion since it can then be shown [64] that the lowest order in Plank's constant contributions to the action are given by Feynman diagrams that contain no loops. Since this thesis is not concerned with quantum mechanical effects, the expansion in Poisson brackets (which does not contain any loops) and description of the EM and electron fields by complex numbers (as opposed to operators) is more

appropriate.

The field-theoretical description of the plasma is, in principle, as complete as the Klimontovich approach in a sense that all the components of energy-momentum tensor of the collection of electrons can be specified at any point in space, averaged over length larger than the scale defined by $\hbar$. But this scale can be made as small as desired. Yet the perturbation theory developed in this thesis will not converge if the kinetic effects such as particle trapping or wave-braking take place. The reason for this non-convergence is not the incompleteness of the field description (as it is the case with fluid description) but, rather, the method by which the perturbation calculation is performed. Constructing a perturbation theory that would properly describe the trapped particles is extremely hard and outside of the scope of this thesis. For the problems that we address, such as harmonic generation, non-linear modification of the index of refraction and rescaling of the electron mass and parametric instabilities, the particle-trapping will be assumed to be negligible. Even though this assumption limits our ability to predict the ultimate fate of some processes (for instance, saturation of parametric instabilities), the initial evolution is computed correctly, without resorting to weakly relativistic assumption.

The diagrammatic method is clearly not the only approach to calculating the harmonic generation, parametric instabilities, etc. For instance, the rate of the third harmonic generation was computed using the fluid model of the plasma [15] as well as the relativistically covariant Lagrangian for a single charged particle [14]. Both these calculations were one dimensional. The rate of the second harmonic generation from the uniform plasma was computed [16] in three dimensional geometry using the fluid description of plasma. It was found that the rate vanishes to first order in a^2. No attempts of extending the calculation to higher orders in a^2 in three dimensional geometry were discussed in the literature, to our knowledge. Despite the fact that the perturbation field theory developed here assumes (for convergence) that kinetic effects are not important and thus the plasma can be described as a fluid, we find that the diagrammatic approach is computationally easier, relies on the established techniques of QED, naturally extends to three dimensions, and allows to treat different processes

such as harmonic generation, nonlinear corrections to the index of refraction, and parametric instabilities, on a unified basis.

This Chapter is organized as follows: In Section 2.2 we develop a diagrammatic perturbation theory for a single particle (which is equivalent to zero dimension field theory). Section 2.3 extends the diagrammatic ideas of Section 2.2 to laser-plasma interactions. Section 2.4 illustrates the diagrammatic ideas using the simplest one-dimensional, lowest order calculation of the rate of third harmonic emission and compares the results for relativistic and nonrelativistic plasmas.

2.2 Diagrams in Nonlinear Single Particle Dynamics

2.2.1 Motivation

In this section we use the anharmonic oscillator to illustrate the use of diagrams in analyzing nonlinear problems. The choice of this simple example to introduce the powerful diagrammatic expansion, mainly reserved for quantum electrodynamics (QED), is surprising at first. Yet the two problems (anharmonic oscillator and QED) have a lot in common.

Standard technique for perturbative study of the nonlinear oscillator (nonlinearity is assumed small) is to re-calculate the fundamental frequency of the oscillator to each order in nonlinearity and use this frequency to compute the amplitudes of the harmonics, etc. [60]. A simple observation will clarify a conceptual similarity of this approach to nonlinear problems with the renormalization approach in high energy physics. The standard tool of high-energy physics which allows one to analyze various interactions systematically is Feynman diagrams. For example, in QED one has to account for the interactions between charged fields and photons. This is accomplished by breaking the full Lagrangian of the system into a zeroth order and an interaction parts. The zeroth order Lagrangian determines the unperturbed solutions that serve as a basis for a perturbative expansion of the interaction Lagrangian. If different

particles (i.e. electrons and photons) are considered as noninteracting at $t = -\infty$ and the interaction between them is adiabaticlly turned on at a later time, it is necessary to introduce extra terms into the zeroth order "free" Lagrangian and, of course, subtract these terms from the interaction Lagrangian. This avoids a mismatch in the vacuum energies of individual particles with and without interaction. A smallness parameter for such a theory is the interaction between different particles.

A similar problem occurs when one solves the equation of motion for a nonlinear oscillator. The smallness parameter here is the nonlinearity of the force acting on the oscillator. An expansion of the true solution as a series of terms with slowly varying coefficients that are harmonics of the unperturbed eigenfrequency leads to secularly growing terms in the second order of perturbation. The origin of the secular growth is that the eigenfrequency of the nonlinear oscillator is modified by the anharmonic force. Expressing the solution as a series in powers of nonlinearity, times the terms that are harmonics of the unperturbed frequency, is equivalent to

$$\sin\left((\omega_0 + \delta\omega)t\right) = \sin\left(\omega_0 t\right) + \delta\omega t \cos\left(\omega_0 t\right) + \ldots \tag{2.1}$$

No matter how small the nonlinearity $\delta\omega$ is, this expansion clearly fails for long enough times. This prompts us to attempt using the standard diagrammatic techniques from high-energy physics for treating nonlinear problems. Expressing physical quantities in terms of the observed (true) electron mass in QED and adding the appropriate counter-terms into the interaction Lagrangian, is, in a sense, equivalent to expressing the solution of a nonlinear oscillator in terms of solutions of a harmonic oscillator equation with a modified frequency. To be sure, there are fundamental differences between the two problems. Standard QED involves infinities that cancel each other out. In fact, the unmodified Lagrangian of QED would involve infinite mass for the electron. The diagrams that generate the infinities in QED contain loops, and are physically related to interaction with quantum fluctuations of the vacuum. On the contrary, quantum fluctuations are *absent* in the classical case, and, as we show in this section, so are the loops. At the same time we will prove a mathematical theorem

that reveals a formal similarity between the quantum field theory problems and the classical perturbation theory we develop in the rest of this section.

In the rest of this Chapter we develop a classical Hamiltonian perturbation theory similar to the Lie transforms widely applied to nonlinear problems in classical mechanics [61, 62, 63]. The dynamics of a single particle can be viewed as a field theory in zero dimensions, and we use the diagrammatic techniques of QED to develop a classical perturbation theory, with nonlinearity as a small parameter. Extending the theory to higher dimension will then be a matter of a straightforward generalization.

John Cary [63] developed Eq.(2.16) which relates the evolution of an arbitrary function of the coordinates f to the time-ordered exponential of the Poisson brackets, but then used Lie- transform techniques to solve it. In the next section we introduce the Green function of a harmonic oscillator (propagator) and develop a diagrammatic technique for solving Eq.(2.16).

2.2.2 Canonical Formalism

Consider a Hamiltonian system characterized by the canonical variables (q, p) that evolves in time according to Hamilton's equations of motion:

$$\begin{aligned} \dot{q} &= \frac{\partial H}{\partial p} \\ \dot{p} &= -\frac{\partial H}{\partial q}, \end{aligned} \tag{2.2}$$

where $H(p, q)$ is a Hamiltonian of the system. It is understood that the RHS of Eq.(2.2) is a function of time through the implicit dependence of q and p on time even when the Hamiltonian is not explicitly time-dependent.

The Poisson bracket is defined by a linear operation on two functions $f(p, q, t)$ and $g(p, q, t)$:

$$\{f, g\} = \frac{\partial f}{\partial q}\frac{\partial g}{\partial p} - \frac{\partial f}{\partial p}\frac{\partial g}{\partial q}. \tag{2.3}$$

It is then straightforward to show, from Eq. (2.2), that the time evolution of any

function $f(p,q,t)$ is given by

$$\frac{df}{dt} = -\{H, f\} + \frac{\partial f}{\partial t}. \tag{2.4}$$

We also introduce an operator $\hat{F}$ associated with an arbitrary function $F(q,p)$ by the identity:

$$\hat{F}\psi = \{F, \psi\}. \tag{2.5}$$

The evolution equation (2.4) can be rewritten as

$$\frac{df}{dt} = -\hat{H}f + \frac{\partial f}{\partial t}. \tag{2.6}$$

Now assume that the Hamiltonian describes an oscillator with a small nonlinearity:

$$H = H_0 + H_i,$$

where

$$H_0 = p^2/2 + \omega_0^2 q^2/2$$

and H_i stands for the nonlinear part of the Hamiltonian. We change to interaction coordinates, i.e. those that stay constant in the absence of H_i:

$$\begin{aligned} q_i &= e^{\hat{H}_0 t} q \\ p_i &= e^{\hat{H}_0 t} p. \end{aligned} \tag{2.7}$$

Here q_i and p_i are assumed to coincide with q and p at some arbitrary point in time, taken as $t = 0$. Therefore, the Poisson bracket algebra for q_i and p_i is the same as for the equal-time q and p:

$$\{q_i, p_i\} = 1, \qquad \{p_i, p_i\} = \{q_i, q_i\} = 0. \tag{2.8}$$

Another way of saying this is that the transformation given by Eq.(2.7) is a canonical transformation which guarantees the preservation of the Poisson bracket relationship.

From Eq. (2.7) it is straightforward to show that

$$q = q_i \cos(\omega_0 t) + \frac{p_i}{\omega_0} \sin(\omega_0 t)$$
$$p = p_i \cos(\omega_0 t) - \omega_0 q_i \sin(\omega_0 t). \tag{2.9}$$

Eq. (2.9) allows us to compute the Poisson brackets of the coordinates taken at nonequal times. For example, a relationship that we will extensively use in the future is

$$\{q(t_2), q(t_1)\} = \frac{\sin \omega_0 (t_1 - t_2)}{\omega_0}. \tag{2.10}$$

By substituting Eq.(2.7) into Eq.(2.6) we obtain the evolution equation for the interaction coordinate q_i (with the identical one holding for p_i):

$$\dot{q}_i = -\hat{\tilde{H}}_i q_i, \tag{2.11}$$

where

$$\hat{\tilde{H}}_i(q_i, p_i, t) \equiv \hat{H}_i(q, p) \tag{2.12}$$

and (q, p) to be inserted into Eq.(2.12) are given by (2.9). In words, the prescription to obtain the time-dependent interaction part of the Hamiltonian in the interaction picture is reduced to inserting time-dependent expressions for q and p from the Eq.(2.9) into the original interaction Hamiltonian. Similarly to Eq.(2.4) we find that the evolution of any function $f(q_i, p_i)$ which does not depend explicitly on time takes the form

$$\frac{df}{dt} = -\{\tilde{H}_i, f\} = -\hat{\tilde{H}}_i f. \tag{2.13}$$

Our usual choice will be $f = q_i$. The result of Eq.(2.13) can be stated simply: to find a derivative of a function of the coordinates q_i and p_i at time t take a Poisson bracket of this function with the Hamiltonian and *then* plug in the changed values of q_i and p_i at time t. The solution of Eq.(2.13) can be written as an infinite sum of integrals:

$$f(t) = f_0 - \int_{t_0}^{t} dt_1 \{\tilde{H}_i(t_1), f_0\} + \int_{t_0}^{t} dt_1 \int_{t_0}^{t_1} dt_2 \{\tilde{H}_i(t_2), \{\tilde{H}_i(t_1), f_0\}\} +$$

$$\ldots + (-1)^n \int_{t_0}^{t} dt_1 \ldots \int_{t_0}^{t_{n-1}} dt_n \{\tilde{H}_i(t_n), \{\ldots \tilde{H}_i(t_1), f_0\} \ldots\} + \ldots \qquad (2.14)$$

Here f_0 is the value of the function at the lower limit of the integration. Note that the Poisson brackets $\{\tilde{H}_i(t_k), \ldots\}$ in Eq.(2.14) are time ordered—if $t_k > t_j$ then $\tilde{H}_i(t_k)$ is positioned to the right of $\tilde{H}_i(t_j)$.

We formally introduce a time-ordering operator by the definition:

$$\begin{aligned} T(\hat{A}(t_2)\hat{B}(t_1)) &= \hat{A}(t_2)\hat{B}(t_1) \quad \text{if} \quad t_1 > t_2 \\ &= \hat{B}(t_1)\hat{A}(t_2) \quad \text{if} \quad t_1 < t_2. \end{aligned} \qquad (2.15)$$

Using Eq.(2.15), Eq.(2.14) can be rewritten in a more compact (and, as we will see later, more easily manipulated in computations) form:

$$f(t) = T e^{-\int^t dt' \tilde{H}_i(t')} f_0. \qquad (2.16)$$

This expression for $f(t)$ is still not amenable to practical calculations because of the time-ordering that appears in the integrand. Below we introduce a new definition, which we call a "contraction" because of its similarity with the contraction in quantum field theory. We also state and illustrate a mathematical theorem that relates the integral of a time-ordered product to the integral of the sum of all the possible contractions.

A contraction of $A(t_1)$ with $B(t_2)$ is defined by

$$\begin{aligned} \widehat{A(t_2)B}(t_1) &= \{A(t_2), B(t_1)\} \quad \text{for} \quad t_1 > t_2 \\ &= 0 \qquad \text{for} \quad t_1 < t_2. \end{aligned} \qquad (2.17)$$

For the unperturbed harmonic oscillator governed by the Hamiltonian H_0, Eq.(2.17) can be rewritten for $A(t_1) = q(t_1)$ and $B(t_2) = q(t_2)$, using Eq.(2.10), as

$$\widehat{q(t_2)q}(t_1) = -\int_{-\infty}^{+\infty} \frac{d\omega}{2\pi} \frac{e^{-i\omega(t_1 - t_2)}}{(\omega + i\epsilon)^2 - \omega_0^2}, \qquad (2.18)$$

where ϵ is an infinitely small positive number. We note that this definition is very similar to the contraction in quantum field theory [64], in fact, Eq.(2.18) is almost precisely the definition of the quantum propagator, except that the contour of integration is chosen differently.

Fundamental to our analysis, and to diagrammatic perturbation theory in QED are theorems relating time-ordering to contractions. For QED, the theorem is formulated for the time ordered product of *noncomuting operators* [64], and is known as Wick's theorem. For the first time, we formulate the Wick's theorem for the time-ordered string of *Poisson brackets of functions.*

Theorem: *An integral of a time-ordered string of Poisson brackets is equal to an integral of the sum of products of all contracted terms in the string of time-disordered operators, with no loops allowed.*

The "loop" is defined by an intuitively obvious rule: if an operator $A(t_1)$ contracts an operator $B(t_2)$, operator $B(t_2)$ contracts an operator $C(t_3)$, and $C(t_3)$ contracts $A(t_1)$, they are said to have formed a loop. Obviously, loops can be larger in size than in this example. Since in a string of Poisson brackets an operator can only contract another operator that is somewhere to the right from it, but not to the left, a "directiveness" is created that does not allow for the loops. Mathematically, the theorem is stated as

$$T\int_{t_0}^{t} dt_1 \ldots \int_{t_0}^{t_{n-1}} dt_n \{\tilde{H}_i(t_n), \{\ldots \tilde{H}_i(t_1), f_0\}\ldots\} = \int_{t_0}^{t} dt_1 \ldots \int_{t_0}^{t} dt_n \widehat{H_{in}H_{ik}}\widehat{H_{ik}H_{ij}}\ldots \widehat{H_{i1}f_0}, \tag{2.19}$$

where $H_{ik} \equiv H_i(t_k)$ and the sum stands for all possible contractions of every q in H_i with another q from H_i at another time, with no loops allowed.

To illustrate what is meant by a contraction of two operators, we calculate the contraction of two operators, $A(t_1)$ and $B(t_2)$, each of which is a power of the coordinate q, evaluated at the corresponding point in time: $A = q^l(t_1)$ and $B = q^k(t_2)$. Then, using the definitions of the Poisson bracket (2.3) and the contraction (2.17),

$$\widehat{A(t_1)B}(t_2) = k!l!q^{l-1}(t_1)q^{k-1}(t_2)\widehat{q(t_1)q}(t_2). \tag{2.20}$$

Expression (2.16) can now be rewritten in a form that does not contain time-ordering:

$$f(t) = \sum \frac{1}{n!}(-1)^n \int^t dt_1 \ldots \int^t dt_n \widehat{H_{in}} \widehat{H_{ik}} \widehat{H_{ik}} \widehat{H_{ij}} \ldots \widehat{H_{i1}} f_0, \qquad (2.21)$$

For notational simplicity we dropped the lower limit of integration in Eq.(2.21).

2.2.3 Example: Oscillator with a Quadric Nonlinearity

The third order expansion of the anharmonic oscillator with quadric nonlinearity $H_i = \beta q^4/4$ provides a clear illustration of how Eq.(2.21) is used. It is rather straightforward to generalize this idea to an arbitrary Hamiltonian.

From Eq.(2.14) we obtain the third-order term in nonlinearity parameter β,

$$f^{(3)}(t) = -\frac{\beta^3}{4^3} \int^t dt_1 \int^{t_1} dt_2 \int^{t_2} dt_3 \{q^4(t_3), \{q^4(t_2), \{q^4(t_1), f_0\}\}\}. \qquad (2.22)$$

For notational simplicity we will write

$$q_k \equiv q(t_k).$$

Assuming that f_0 is chosen as a linear function of q_i and p_i, so that the Poisson bracket of f with q is a complex number (not a function!), the simplification of the of the Poisson brackets in Eq.(2.22) results in the sum of two topologically different terms:

$$\begin{aligned} f(t) &= 9\beta^3 \int^t dt_1 \int^{t_1} dt_2 \int^{t_2} dt_3 q_3^3 q_2^2 q_1^2 \{q_3, q_2\}\{q_2, q_1\}\{q_1, f_0\} \\ &+ 6\beta^3 \int^t dt_1 \int^{t_1} dt_2 \int^{t_2} dt_3 q_3^3 q_2^3 q_1 \{q_3, q_1\}\{q_2, q_1\}\{q_1, f_0\}. \end{aligned} \qquad (2.23)$$

The first term in Eq.(2.23) represents the three interaction Hamiltonians connected in series whereas the second term represents two interaction Hamiltonians connected to the third one which contracts the function f_0 under investigation. By using the definition of the contraction, Eq.(2.17), we notice immediately that if we substitute

contractions in place of the Poisson brackets in the first term of Eq.(2.23), we can lift the requirement $t_1 > t_2 > t_3$, extending the region of integrations to $G = \{t_1, t_2, t_3 < t\}$. By inspecting the second term we notice that the value of the integrand does not change under the interchange of t_3 and t_2. Thus the second term in Eq.(2.23) can be rewritten as a one-half of the same integral over the extended region $G_3 = \{t_3, t_2 < t_1 < t\}$. By substituting the appropriate contractions in place of the Poisson brackets the region of integration G_3 extends to G. Overall, we obtain:

$$\begin{aligned} f(t) &= 9\beta^3 \int^t dt_1 \int^t dt_2 \int^t dt_3 q_3^3 q_2^2 q_1^2 \widehat{q_3 q_2} \widehat{q_2 q_1} \{q_1, f_0\} \\ &+ 3\beta^3 \int^t dt_1 \int^t dt_2 \int^t dt_3 q_3^3 q_2^3 q_1 \widehat{q_3 q_1} \widehat{q_2 q_1} \{q_1, f_0\}. \end{aligned} \tag{2.24}$$

It is a matter of simple counting to convince oneself that the expression obtained by expanding the exponential in Eq.(2.16) to third order and using Eq.(2.20), with $k = l = 4$, is exactly Eq.(2.24).

2.2.4 Diagrammatic Perturbation Theory and Renormalization

Since imaginary exponents are easier to deal with than trigonometric functions, it is computationally convenient to use a different set of interaction coordinates. In place of q_i and p_i we use their complex linear combinations, reminiscent of the creation and annihilation operators in quantum mechanics:

$$\begin{aligned} a^\dagger &= (\omega_0/2)^{1/2}(q_i - ip_i/\omega_0) \\ a &= (\omega_0/2)^{1/2}(q_i + ip_i/\omega_0) \end{aligned} \tag{2.25}$$

We emphasize that, unlike quantum mechanics, a and $a^\dagger$ *are not* operators, but just complex numbers that are more convenient in calculations than the interaction coordinates (q_i, p_i). It is straightforward to show that

$$\{a, a^\dagger\} = -i. \tag{2.26}$$

From Eqs.(2.9) and (2.25) q and p can be expressed in terms of the creation and annihilation operators yielding:

$$\begin{aligned} q &= \frac{1}{(2\omega_0)^{1/2}}\left(a^\dagger e^{i\omega_0 t} + a e^{-i\omega_0 t}\right) \\ p &= \frac{i\omega_0}{(2\omega_0)^{1/2}}\left(a^\dagger e^{i\omega_0 t} - a e^{-i\omega_0 t}\right). \end{aligned} \tag{2.27}$$

Using again the example of a weakly nonlinear harmonic oscillator, we will illustrate in detail the procedure involved in calculating the nonlinear corrections to the oscillation frequency. The problem that arises if we attempt to blindly sum up the infinite series from Eq.(2.16) is that, already to the second order, we encounter zero denominators. As was pointed out earlier in Eq.(2.1), this indicates that the expansion uses the "wrong" frequency. One of the modern approaches that avoids this problem is the Lie group technique, in which one seeks the canonical transformation that leads to the "true" action-angle variables. The Lie group-theoretical approach is not widely used for problems dealing with continuum variables. Having in mind the extension from single-particle dynamics to laser-plasma problems, a more appropriate technique for overcoming these zero denominators utilizes the methods of field theory.

For the sake of illustration we develop below a field theory in 0 dimensions which describes an anharmonic oscillator.

The Hamiltonian is

$$H = \frac{p^2}{2} + \omega_0^2\frac{q^2}{2} + \beta\frac{q^4}{4}, \tag{2.28}$$

where the mass was chosen to be unity for notational convenience. To utilize the interaction method developed above, we split the Hamiltonian into the unperturbed and interaction parts:

$$H = H_0 + H_i, \tag{2.29}$$

where

$$H_0 = \frac{p^2}{2} + \omega^2\frac{q^2}{2}$$

$$H_i = \sum_{n=1} C_2^{(n)} \frac{q^2}{2} + \beta \frac{q^4}{4}. \tag{2.30}$$

Since we cannot add and subtract terms from the Hamiltonian arbitrarily, the following relation should hold:

$$\omega_0^2 = \omega^2 + \sum_{n=1} C_2^{(n)}. \tag{2.31}$$

Here $C_2^{(n)}$ stands for the n-th order (in nonlinearity β) correction to the frequency. This approach allows us to express all the relevant physical properties in terms of ω, the true oscillation frequency of the nonlinear system. We will require that there are no secular terms in the equation of motion for the oscillator, which yields an expression for C_2^n's in terms of ω, the amplitude of the oscillation (with the correct frequency ω) and the nonlinearity coefficient β. Together with Eq.(2.31), this allows one to express ω_0 in terms of ω and thereby the dependence of ω on the nonlinearity coefficient and the energy in the system to all orders in β.

To determine $C_2^{(n)}$ we require that the interaction part of the Lagrangian does not produce secularly growing terms. It is sufficient to ensure that a and $a\dagger$ operators do not grow secularly with time, since they are given by the linear combinations of q_i and p_i. In this example we will calculate $C_2^{(1)}$ and $C_2^{(2)}$—the lowest order corrections to the eigenfrequency. Choosing $f_0 = a\dagger$ in Eq.(2.16) and using (2.30) we calculate $C_2^{(n)}$ order by order.

At this point we introduce the nonlinear diagrams which present a convenient way to visualize the perturbative results and keep track of all the contributions from the nonlinear part of the Hamiltonian. As it is clear from Eq.(2.21), a typical expansion term in the perturbation series is given by a string of interaction Hamiltonians connected by contractions. To reproduce these terms diagrammatically, we introduce three types of objects— an interaction vertex, a set of counter-terms and a propagator, shown in Fig. 2-1.

The annihilation and creation operators defined in (2.25) introduce a concept of "absorbing" or "emitting" an "oscillation". We assume the following conventions: to draw the line from the top whenever an "oscillation" is absorbed and draw the line

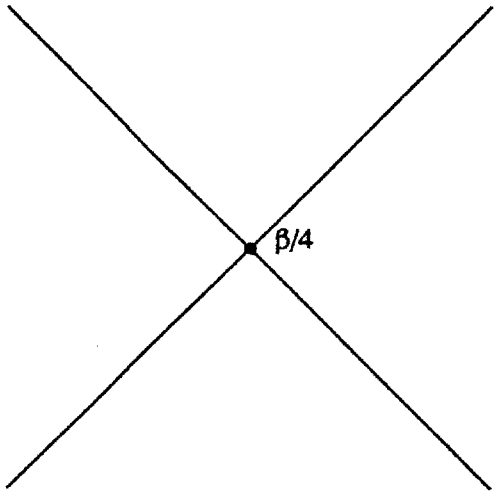

interaction vertex

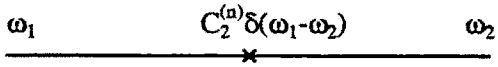

counter-term

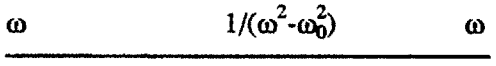

propagator

Figure 2-1: Diagrammatic elements for nonlinear oscillator.

from the bottom whenever an "oscillation" is emitted. When a quantity (usually a coordinate) has to be evaluated in the unperturbed state, it is marked by a cross. This is consistent with a standard notation of field theory where all the external fields are marked by crosses. The part of the Hamiltonian that is contracted with f_0, the evolution of which is being studied, is represented by a "loose" line—the line which is neither contracted nor marked with a cross. Examples below will illustrate these conventions.

First order:

$$a\dagger = \frac{i}{(2\omega)^{1/2}} \int^t dt' \left(C_2^{(1)} q(t') + \beta q^3(t') \right) e^{-i\omega t'}. \tag{2.32}$$

The coefficient $C_2^{(1)}$ is determined by the requirement that it cancels out the secularly growing terms arising from the nonlinear term βq^3. Using Eq. 2.27 we obtain

$$C_2^{(1)} = -3\beta a a\dagger /(2\omega). \tag{2.33}$$

Using the fact that

$$a a\dagger /(2\omega) = a_0^2/4,$$

where a_0 is the amplitude of oscillation with a new frequency ω, we obtain:

$$C_2^{(1)} = -\frac{3\beta a_0^2}{4}. \tag{2.34}$$

The diagram describing the nonlinear shift of the eigenfrequency (2.34) simply consists of one interaction vertex and is shown in Fig. 2-2. The "loose" line contract the $a^\dagger$ operator which we are evaluating. The process can be viewed as a scattering of one of the external lines into the "loose" line, in the presence of two other external lines, each of which is proportional to a_0.

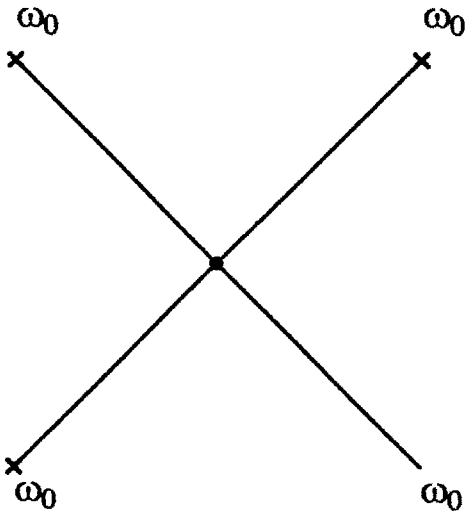

Figure 2-2: Lowest order in β frequency correction for a nonlinear oscillator.

Second order:

$$a\dagger = \frac{i}{(2\omega)^{1/2)}} \int^t dt_1 C_2^{(2)} q(t_1) e^{-i\omega t_1} - \frac{i}{(2\omega)^{1/2}} \int^t \int^t dt_1 dt_2 3\beta^2 q^3(t_2) q^2(t_1) q(t_2)\widehat{q}(t_1) e^{-i\omega t_1}, \tag{2.35}$$

where the contraction is given by Eq.(2.18). Here we will substitute the expression for $q(t)$ from Eq.(2.27) and follow the strategy similar to the first-order calculation (that is cancelling out the secular terms) but a few technical comments are in order. First, it is assumed that the integration time t is much longer compared to any frequency in the problem so that

$$\int^t dt' e^{i(\omega_1 - \omega_2)t'} = 2\pi\delta(\omega_1 - \omega_2). \tag{2.36}$$

Secondly, we drop all the terms in the integrand that contain vanishing denominators. Vanishing denominator in the $n-$th order of the expansion comes from the secularly growing term in the lower order which should have been taken care of at the previous steps. For instance, the only term in the Eq.(2.35) that has to be retained can be thought of as "absorbing" and then "reemitting" three "oscillations", that is having a value of $(3\omega)^2 - \omega^2$ in the denominator of the propagator. This also explains why we don't need to include the $C_2^{(1)}$ term to this order—it would inevitably include a

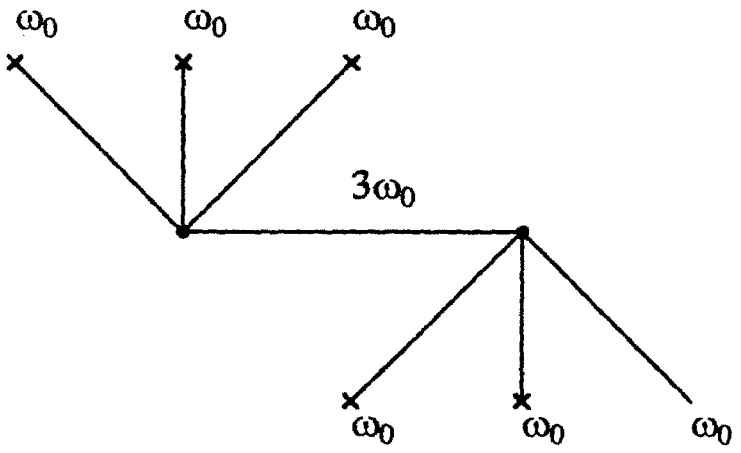

Figure 2-3: Second order in β frequency correction for nonlinear oscillator.

vanishing denominator. This is no longer true to the next order in nonlinearity.

Diagrammatically, the content of Eq.(2.35) is expressed in Fig. 2-3 by the only diagram contributing to the nonlinear frequency shift to the second order in β.

It is easy to see that $C_2^{(2)}$ is proportional to a_0^4. Indeed, each of the external lines is proportional to a_0. The diagram in Fig. 2-3 has *five* external lines, and has to be balanced by the counter term $C_2^{(2)}$, which itself has *one* external line. Thus $C_2^{(2)}$ is proportional to the *fourth* power of a_0.

Carrying out the outlined program results in

$$C_2^{(2)} = -\frac{3\beta^2 a_0^4}{128\omega^2}. \tag{2.37}$$

Combining Eqs.(2.34), (2.37) and (2.31) gives the nonlinear frequency correction (to the second order):

$$\omega^2 = \omega_0^2 + \frac{3\beta a_0^2}{4} + \frac{3\beta^2 a_0^4}{128\omega_0^2}. \tag{2.38}$$

in agreement with the conventional calculations [65].

Diagrams present a convenient way of visualizing the perturbatively computed results. The diagrammatic interpretation of the perturbative Hamiltonian calculation forms a basis for our field theory of the laser plasma interactions, which we construct in the next Section. In spite of the similarity of both the formulas and definitions in multi- dimensional classical field theory and single-particle diagram-

matic perturbation theory, there is also an important conceptual difference. For a single particle there can be no pumping of energy into other modes (since only one mode, with frequency ω, exists). The harmonics of this frequency do not represent a new type of mode, but rather are the result of the oscillatory motion at the true frequency ω. The origin of the harmonics here can be understood in the following way—the motion of the oscillator, governed by the full Hamiltonian, remains periodic with the period $T = 2\pi/\omega$ but no longer harmonic. Since any periodic motion can be expanded into Fourier series with frequencies being the multiples of ω, this gives rise to the higher harmonics of the oscillation. On the other hand, if we had a system of two nonlinearly coupled oscillators with commensurate eigenfrequences, one of them initially excited and the other one at rest, we could calculate the rate at which the energy of the excited oscillator flows into the resting one (neglecting the self-consistent energy depletion of the former). This observation sets the ground for the realistic three-dimensional calculation which will involve the scattering of energy of an initially strong laser pump into (initially absent) higher harmonics of the pump. These higher harmonics represent distinct modes of oscillation and should not be confused with the harmonics that were encountered in the above example of a single anharmonic oscillator.

2.3 Basic Concepts from Field Theory

2.3.1 Plasma Physics as a Field Theory

In this Section we introduce a semiclassical model of the interaction between charged particles and electromagnetic fields. An important conceptual difference of this model from more conventional approaches lies in the way the charged particles are treated. Instead of modeling the plasma as a collection of discrete particles (Klimontovich formalism), a fluid or a statistical distribution in phase space (kinetic formalism), we treat electrons as a field, very much like in quantum electrodynamics.

Any field theory starts with defining a Lagrangian of the system. The full Lagrangian of our system of interacting charged particles and electromagnetic fields is the sum of the Lagrangians of a free particle field, free electromagnetic field, and the interaction Lagrangian. For notational convenience, and to treat spatial and temporal coordinates on an equal footing, c, the speed of light, is chosen to be unity throughout this work.

The Lagrangian density of the free electromagnetic field is given by (see, for example, Ref. [66])

$$\mathcal{L}_{em} = -\frac{1}{4\pi}\frac{F_{\mu\nu}F^{\mu\nu}}{4}, \tag{2.39}$$

where $F_{\mu\nu} = \partial_\mu A_\nu - \partial_\nu A_\mu$ and A_μ is a four-vector potential describing electromagnetic field. The Lagrangian itself is an integral of $\mathcal{L}_{em}$ over the three-dimensional space:

$$L_{em} = \int d^3x \mathcal{L}_{em}. \tag{2.40}$$

For the rest of the work we will refer to Lagrangian densities as the Lagrangian, keeping in mind that the true Lagrangian is obtained by integration over the three-dimensional space.

To describe the electrons we have to introduce an artificial spatial (or temporal, since special relativity makes no distinction between the two) scale associated with the wavelength of the electron. The final results will be obtained in the limit that

this scale is infinitesimal. The Lagrangian density of the particle field is chosen to be

$$\mathcal{L}_m = \partial_\mu \psi \partial^\mu \psi^* - \frac{m^2}{\hbar^2} \psi \psi^*, \tag{2.41}$$

where ψ is the complex field describing the electrons and $\hbar$ is a constant with the same dimension as the Plank's constant. This constant can be chosen arbitrarily, as we explain below.

Conforming to the notation of quantum physics, we call the artificial length scale mentioned earlier "Compton length", λ_c, where

$$\lambda_c = \frac{\hbar}{mc}. \tag{2.42}$$

Note that this Compton length has nothing to do with the Compton length of a "real" quantum mechanical electron since $\hbar$ here *is not* the real Plank's constant but a quantity *chosen by us.* Thus it is easy to establish an upper limit on the value of $\hbar$ that still does not introduce any artificial "quantum mechanical" effects: the only restriction on the numerical value of $\hbar$ is that the "Compton" wavelength, as defined by (2.42), be much smaller than any spatial scale in the problem. For instance, if λ_{min} is the shortest wavelength in the problem, then the condition of smallness on $\hbar$ is

$$\frac{\hbar}{mc} \ll \lambda_{min}. \tag{2.43}$$

The reason $\hbar$ is introduced is to have consistent dimensions of all terms in the Lagrangian: the first term in the RHS of Eq.(2.41) has dimension of $[\text{Length}]^{-2}$ while the second term has dimension of $[\text{Energy}]^2/[\hbar^2]$. One, therefore, needs to introduce a conversion coefficient between the energy and the distance.

The use of field description of the electrons is by no means necessary. One can develop a perturbation theory based on a traditional fluid [16] or Lagrangian formalism [14]. Yet, we find that our approach used in this thesis greatly facilitates the calculations, is inherently covariant, and makes full use of the advanced techniques developed for QED. The use of the diagrammatic approach leads to new physical results.

For example, the rate of second harmonic generation from homogeneous plasma was computed for the first time because the calculation needs to be *both* three-dimensional *and* higher order in a. None of the previous approaches had this feature.

The Lagrangian density (2.41) of the electrons corresponds to a bosonic system. In fact, the problems addressed in this thesis are classical, no inclusion of quantum mechanical effects, such as spin, is made. Therefore, the choice of a boson-like field to describe the classical electron plasma is not problematic and does not lead to any unphysical results.

We also note that the charged matter has to be described by a complex field because the Lagrangian (2.41) possesses an additional symmetry— it is invariant with respect of changing the phase angle of the complex function ψ ("charge conjugation"). From Noethers theorem it follows that any invariant has a conservation law associated with it. The invariance with respect to charge conjugation results in charge conservation.

Before proceeding further we review those basic points and definitions of field theory that are essential to our analysis.

2.3.2 General Formalism

For a physical system characterized by a set of fields ϕ^a with Lagrangian density $\mathcal{L} = \mathcal{L}(\phi^a, \partial_\mu \phi^a)$ given as a function of the fields ϕ^a and their derivatives, one can define a set of canonical momenta:

$$\Pi^{a\mu} = \frac{\partial \mathcal{L}}{\partial(\partial_\mu \phi^a)} \tag{2.44}$$

associated with the fields ϕ^a. Similarly to Eq.(2.8) we require that

$$\{\phi^a(t, \vec{x}_1), \Pi^{0a}(t, \vec{x}_2)\} = \delta^3(\vec{x}_1 - \vec{x}_2), \tag{2.45}$$

which is also reminiscent of the equal-time commutation relations for the quantum mechanical position-momentum operators.

In general, the requirement of extremizing the action leads to Euler-Lagrange equation:

$$\partial_\mu \frac{\partial \mathcal{L}}{\partial(\partial_\mu \phi^a)} = \frac{\partial \mathcal{L}}{\partial \phi^a}, \tag{2.46}$$

which for the case of a free electron fluid takes the form of

$$\partial_\mu \partial^\mu \psi + \frac{m^2}{\hbar^2}\psi = 0 \tag{2.47}$$

and the same equation for ψ^*. The solution of Eq.(2.47) can be expanded as a sum of free-propagating plane waves:

$$\begin{aligned} \psi &= \hbar^{1/2} \int \frac{d^3\vec{p}}{(2\pi)^{3/2}(2p_0)^{1/2}} (b_{\vec{p}}\dagger\, e^{(-i\vec{p}\cdot\vec{x}+ip_0 t)} + c_{\vec{p}} e^{(i\vec{p}\cdot\vec{x}-ip_0 t)}) \\ \psi^* &= \hbar^{1/2} \int \frac{d^3\vec{p}}{(2\pi)^{3/2}(2p_0)^{1/2}} (b_{\vec{p}} e^{(i\vec{p}\cdot\vec{x}-ip_0 t)} + c_{\vec{p}}\dagger\, e^{(-i\vec{p}\cdot\vec{x}+ip_0 t)}), \end{aligned} \tag{2.48}$$

where $b_{\vec{p}}$,$b_{\vec{p}\dagger}$,$c_{\vec{p}}$ and $c_{\vec{p}}\dagger$ are introduced analogously to Eq.(2.27). Similarly to the single- particle theory of Section 2.2.2, where (q,p) formed a pair of canonical coordinate and momentum, complex fields ψ and ψ^*, with their corresponding momenta defined by Eq.(2.44), form pairs of canonical coordinates and momenta for the field theory. The two obvious differences of the field theory presented here from the Hamiltonian theory of a single oscillator is that (i) it is described by a complex field (to ensure charge conservation) and (ii) it has infinitely many canonical coordinates (at each point $\vec{x}$ in a three-dimensional space). Time evolution of the canonical coordinates will be expressed as a string of Poisson brackets, exactly as in Section 2.2.2. We emphasize here that, unlike quantum field theory, the fields ψ and ψ^* are just complex functions, *not operators*. The same holds for the Fourier coefficients $b_{\vec{p}}$, $b^\dagger_{\vec{p}}$, $c_{\vec{p}}$,$c^\dagger_{\vec{p}}$; daggers here are equivalent to complex conjugation. In Eq.(2.48) $p_0 = (\vec{p}^2 + m^2/\hbar^2)^{1/2}$ is the relativistic particle energy.

Substituting (2.48) into (2.45) yields the Poisson bracket algebraic rule: the only nonzero Poisson brackets are

$$\{b_{\vec{p}_1}, b^\dagger_{\vec{p}_2}\} = \{c_{\vec{p}_1}, c^\dagger_{\vec{p}_2}\} = -(i/\hbar)\delta^3(\vec{p}_1 - \vec{p}_2). \tag{2.49}$$

We introduce a contraction of ψ and ψ^* evaluated at different space-time points by the following expression:

$$\begin{aligned} \psi^*(\vec{x}_2, t_2)\widehat{\psi}(\vec{x}_1, t_1) &= \{\psi^*(\vec{x}_2, t_2)\psi(\vec{x}_1, t_1)\} \quad \text{for} \quad t_1 > t_2 \\ &= 0 \qquad \text{for} \quad t_1 < t_2. \end{aligned} \tag{2.50}$$

Substituting Eq.(2.48) into Eq.(2.50) and using Eq.(2.49) yields a convenient expression for the contraction:

$$\psi^*(\vec{x}_2, t_2)\widehat{\psi}(\vec{x}_1, t_1) = -\int \frac{d^4p}{(2\pi)^4} \frac{e^{ip\cdot(x_1 - x_2)}}{(p_0 + i\epsilon)^2 - \varepsilon_{\vec{p}}^2}, \tag{2.51}$$

where

$$\varepsilon_{\vec{p}}^2 = \vec{p}^2 + m^2/\hbar^2 \tag{2.52}$$

and $x = (t, \vec{x})$.

We note that even though the charged bosonic field ψ can in principle describe particles as well as antiparticles, we restrict our treatment to the case when $c_{\vec{p}} = c_{\vec{p}}^\dagger = 0$ initially, which is equivalent to considering only electrons without the positrons. Since we are restricting our calculations to the case $\lambda_c \ll \lambda_r$, where λ_r is a typical wavelength of electromagnetic radiation, $c_{\vec{p}}$ and $c_{\vec{p}}^\dagger$ will stay infinitesimally small at later times (to order λ_c/λ_r). At the same time, the formalism developed in this thesis is capable of describing the interaction of electromagnetic fields with electron-positron plasmas, provided that pair-creation/annihilation phenomena are not important. This kind of rarefied two-component plasmas might occur in astrophysical situations.

Another thing to note is that by introducing the dimensional constant $\hbar$ we have made the dimension of "momentum" $\vec{p}$ to be an inverse length. For the rest of this thesis we will use the following convention: momenta denoted with lower case p have dimensions of inverse length, whereas all momenta denoted by capital P have dimensions of energy (recall that $c = 1$). P and p are related to each other through $p = P/\hbar$.

As was mentioned earlier, a complex field $\psi(\vec{x},t)$ completely characterizes the state of a charged single-species plasma. To realize this, it is sufficient to recall that the motion of a collection of particles is completely characterized by the energy-momentum tensor at every point in space, which can be expressed in terms of ψ. Let us examine what function ψ describes a non-thermal plasma with density n_0, moving with a four-momentum p_0^μ.

It is easy to convince oneself that the desired function is

$$\psi = \hbar^{1/2} \frac{e^{ip_0^\mu \cdot x_\mu}}{(2p_0^0)^{1/2}} \sqrt{n_0}, \tag{2.53}$$

where

$$(p_0^0)^2 = \vec{p}_0 \cdot \vec{p}_0 + m^2/\hbar^2. \tag{2.54}$$

Indeed, density of the energy-momentum tensor $T^{\mu\nu}$ of a system with Lagrangian density $\mathcal{L}(\phi^a, \partial_\mu \phi^a)$ can be calculated (see, for example, Ref. [69]) as

$$T^{\mu\nu} = \sum_a \Pi^{\mu a} \partial^\nu \phi^a - g^{\mu\nu} \mathcal{L}. \tag{2.55}$$

For the unperturbed particle Lagrangian (2.41), the energy-momentum tensor is given by

$$T^{\mu\nu} = \partial^\mu \psi^* \partial^\nu \psi + \partial^\mu \psi \partial^\nu \psi^* - g^{\mu\nu}(\partial^\alpha \psi^* \partial_\alpha \psi - m^2/\hbar^2 \psi\psi^*). \tag{2.56}$$

Inserting the expression for ψ in (2.53) into (2.56) yields

$$T^{\mu\nu} = \frac{n_0}{\gamma} P_0^\mu P_0^\nu. \tag{2.57}$$

The energy-momentum density tensor of a collection of particles, with density n_0, all moving with four-momentum P_0, is indeed equal to (2.57) (see also Ref. [69]).

2.3.3 Radiation-particle Interaction

The electromagnetic and particle fields are coupled to each other. Both classical and quantum mechanics give a simple prescription for this coupling: substitute the

canonical momentum for the kinematic momentum in the particle Hamiltonian. For a single particle this implies

$$P_\mu \rightarrow P_\mu + eA_\mu. \tag{2.58}$$

In field-theoretical language this becomes a modification of the particle field Lagrangian:

$$\partial_\mu \rightarrow \partial_\mu + ieA_\mu/\hbar. \tag{2.59}$$

Equation (2.59) can be used with Eq.(2.41) to find the interaction Lagrangian between the plasma and the electromagnetic fields:

$$\mathcal{L}_i = \frac{e^2}{\hbar^2} A_\mu A^\mu \psi\psi^* - i\frac{e}{\hbar} A^\mu(\psi^*\partial_\mu\psi - \psi\partial_\mu\psi^*). \tag{2.60}$$

Equation (2.16) prescribes the evolution in time of an arbitrary function of the fields f in terms of the interaction Hamiltonian. The function we have obtained in Eq.(2.60) is the interaction Lagrangian, not the Hamiltonian. If Eq.(2.60) did not contain any derivative interactions, the prescription for transforming from the Lagrangian to the Hamiltonian would be very straightforward—the interaction Hamiltonian is equal to the interaction Lagrangian, with the opposite sign. If derivative interactions are present, as in Eq.(2.16), this is no longer true, and, unfortunately, the "Wick's theorem" no longer applies in a form convenient for calculations:

$$T[\psi(x_1)\partial_\mu\psi^*(x_2)] \neq \partial_\mu\psi(x_1)\widehat{\psi^*}(x_2). \tag{2.61}$$

This point is worth clarifying. The true interaction Hamiltonian can be obtained from the Lagrangian (2.60) as

$$\mathcal{H}_{int} = \partial_0\psi\frac{\partial\mathcal{L}_i}{\partial_0\psi} + \partial_0\psi^*\frac{\partial\mathcal{L}_i}{\partial_0\psi^*} - \mathcal{L}_i. \tag{2.62}$$

Yet we would not be able to use the "Wick's theorem" to time-order the product of operators because of (2.61). Fortunately, as was demonstrated for the QED [67], one can use an interaction Hamiltonian *different* from (2.62) *and* assume that derivatives

can be pulled outside of Wick's products. The naive Feynman prescription is: take an interaction Lagrangian with the minus sign for the interaction Hamiltonian and treat the derivatives as multiplications by the momentum. This point will be further illustrated in Sec 3.2.2. We thus obtain the interaction Hamiltonian for the relativistic plasma coupled to the electromagnetic fields:

$$\mathcal{H}_i = -\frac{e^2}{\hbar^2} A_\mu A^\mu \psi\psi^* + i\frac{e}{\hbar} A^\mu(\psi^*\partial_\mu\psi - \psi\partial_\mu\psi^*). \tag{2.63}$$

2.3.4 Nonrelativistic Model

From this point on we can apply the formalism of the preceding section to compute perturbatively the evolution of the particle and radiation fields. But, instead of plunging into the development of the relativistic approach to laser-plasma interactions (with which most of this work is concerned), we first derive here a *nonrelativistic* version of laser-plasma interaction. In Section 2.4 we compare the nonrelativistic and relativistic models of third harmonic generation. This both convinces us of the inadequacy of a nonrelativistic description of intense laser-plasma interactions and illustrates the power of the diagrammatic methods.

A nonrelativistic electron plasma can be characterized by a complex function ψ, with the Lagrangian of a noninteracting plasma given by:

$$\mathcal{L}_m = -\frac{i}{\hbar}\psi^*\frac{\partial\psi}{\partial t} - \frac{1}{2}\nabla\psi\cdot\nabla\psi^*. \tag{2.64}$$

Lagrangian (2.64) is, of course, not covariant since it corresponds to the Schrodinger equation. The complex field is still needed to conserve the charge, as mentioned previously in Section 2.3. As in Eq.(2.48), we expand ψ in terms of the free-propagating modes:

$$\begin{aligned} \psi &= \hbar\int\frac{d^3\vec{p}}{(2\pi)^3} q_{\vec{p}}^\dagger e^{-i\vec{p}\cdot\vec{x}+i\varepsilon t} \\ \psi^* &= \hbar\int\frac{d^3\vec{p}}{(2\pi)^3} q_{\vec{p}} e^{i\vec{p}\cdot\vec{x}-i\varepsilon t}. \end{aligned} \tag{2.65}$$

where $q^\dagger$ and q are the creation-annihilation coefficients for the electrons. Note that the positron coefficients do not appear in the nonrelativistic theory— the Schrodinger equation does not admit the anti-particle solutions. We also note the absence of $1/(2\varepsilon_{\vec{p}})$ in the normalization—it will later become clear that it corresponds to the absence of the relativistic correction to the electron mass. The propagator for the electron field is given by

$$\psi^*(\vec{x}_2, t_2)\widehat{\psi}(\vec{x}_1, t_1) = -\int \frac{d^4p}{(2\pi)^4} \frac{e^{ip_0(t_1-t_2)-i\vec{p}\cdot(\vec{x_1}-\vec{x_2})}}{p_0 - \varepsilon_{\vec{p}} - i\epsilon}. \tag{2.66}$$

Following the same reasoning as in deriving Eq.(2.53), we find that a field describing a nonrelativistic cold plasma, with density n_0 and moving with momentum $\vec{p_0}$, is

$$\psi_{nr}(t, \vec{x}) = \hbar\sqrt{n_0} e^{i\varepsilon_{\vec{p_0}} t - i\vec{p_0}\cdot\vec{x}}, \tag{2.67}$$

where $\varepsilon_{\vec{p_0}} = \hbar\vec{p_0}^2/2$. To account for the coupling between the nonrelativistic plasma and electromagnetic fields we modify the unperturbed particle Hamiltonian in the same way as in Eq.(2.59):

$$\begin{aligned} \vec{\nabla} &\rightarrow \vec{\nabla} + ie\vec{A}/\hbar \\ \partial_t &\rightarrow \partial_t - ie\phi/\hbar, \end{aligned} \tag{2.68}$$

where $\vec{A}$ is a vector potential and ϕ is a scalar potential of the electromagnetic field—in non-relativistic electrodynamics the difference between the scalar and vector components of EM field is not nearly as blurred as in the relativistic case. Substituting (2.68) into (2.64) leads to the interaction Hamiltonian $\mathcal{H}_i^{nr}$:

$$\mathcal{H}_i^{nr} = -\frac{e}{\hbar^2}\psi^*\psi\phi + \frac{e^2}{\hbar^2}\frac{\vec{A}^2}{2}\psi\psi^* - \frac{1}{2}\frac{ie}{\hbar}\vec{A}(\psi^*\nabla\psi - \psi\nabla\psi^*). \tag{2.69}$$

2.4 Introductory Example: Third Harmonic Generation

Having set forth field theoretical descriptions of both relativistic and nonrelativistic plasmas, we now examine the third harmonic emission from a plasma with an intense electromagnetic wave, known as a pump, propagating through it. The rigorous solution to this problem is rather complicated and includes the physics that will be included later in this thesis, such as space-charge fields; in the following calculation we analyze a simplified version of this problem in which we (1) reduce the problem to one spacial dimension by assuming that the electromagnetic pump is a plane wave propagating along the $z-$ direction and linearly polarized in the $x-$ direction. The invariance with respect to translation in $x-y$ plane allows us to assume ψ in the form

$$\psi(t,\vec{x}) \equiv \psi(t,z); \tag{2.70}$$

(2) neglect the action of space-charge forces on the plasma (namely, the restoring force of the plasma compressed by ponderomotive force of the pump) and (3) neglect the modification of the phase velocity of the electromagnetic waves propagating in plasma (which is equivalent to assuming that ω_p^2/ω^2 is a small number). From (2) the scalar part of the potential can be neglected and the vector potential can be written in terms of a scalar function $A(z,t)$:

$$\vec{A}(z,t) = \vec{e_x}A(z,t). \tag{2.71}$$

Note that the assumption of linear polarization of the *total* electro-magnetic field *is not* a general choice of gauge, but is justified by the geometry of the problem (one-dimensional) and our neglect of space-charge forces ($\vec{E}_z = 0$). Assumption (3) implies $\omega^2 = \vec{k}^2$, the vacuum dispersion relation for a plane electromagnetic wave (the speed of light is set equal to unity throughout this thesis).

Equation (2.71) reduces the Lagrangian density of the free EM field from Eq.(2.39)

to

$$\mathcal{L}'_{em} = \frac{1}{4\pi}\frac{(\partial_\mu A)^2}{2}. \tag{2.72}$$

We can expand the free-propagating electromagnetic fields analogously to the relativistic expansion in Eq.(2.48) (with the important difference that the field A is real, unlike ψ):

$$A(z,t) = \int \frac{dk_z}{(2\pi)^{1/2}(2\omega_{k_z})^{1/2}}(a^\dagger_{k_z} e^{(-ik_z\cdot z + i\omega_{k_z} t)} + a_{k_z} e^{(ik_z\cdot z - i\omega_{k_z} t)}), \tag{2.73}$$

where

$$\omega_{k_z} = k_z. \tag{2.74}$$

The theory developed here is formally similar to "scalar mesodynamics" for obvious reasons—the charged matter consists of scalar bosons and the electromagnetic fields are described by a single scalar function. But here we do not consider any results which are of nonzero order in $\hbar$.

From Eq.(2.73), using the Poisson bracket relationship between the scalar field A and its canonical momentum $\Pi = \partial_0 A/(4\pi)$ (from Eq.(2.45)), we obtain

$$\{a_{k_1}, a^\dagger_{k_2}\} = 4\pi i\delta(k_1 - k_2). \tag{2.75}$$

For completeness, we calculate the contraction of the scalar EM field:

$$A(z_2,t_2)\widehat{A}(z_1,t_1) = -4\pi \int \frac{d^2k}{(2\pi)^2}\frac{e^{ik_\mu\cdot(x_1^\mu - x_2^\mu)}}{(k_0 + i\epsilon)^2 - \vec{k}^2}, \tag{2.76}$$

where $k^\mu = (k_0, k_z)$ and $x_j^\mu = (t_j, z_j)$ are the covariant vectors. The part of the contraction $4\pi/(k_0 + i\epsilon)^2 - \vec{k}^2$ is conventionally called a propagator in field-theoretical language.

Expansion (2.73) should be understood in the following sense: the total electromagnetic field can be represented as a sum of different modes labeled by their wavenumbers k_z. Recall that in the treatment of a single oscillator in Section 2.2 we only had one oscillation mode at a frequency ω_0. What formally distinguishes the

single-oscillator mechanics from a full-fledged field theory is that for the oscillator there is one oscillatory mode with a corresponding eigenfrequency (ω_0) whereas in a field theory there are infinitely many oscillatory modes, each with its own eigenfrequency (given by Eq.(2.74)). Labeling eigenmodes by their wavenumber is in a way equivalent to setting up a problem in a big rigid box, big enough so that the discreteness of k_z does not affect the physics. To illustrate this point, we consider the process of generation the third harmonic from the standpoint of mode excitation.

Assume that the intense EM wave originally present in the plasma is of the form

$$\vec{a}_0 = \vec{e}_x \frac{a_0}{2} e^{ik_z \cdot z - i\omega_0 t} + c.c., \tag{2.77}$$

where a_0 is a normalized vector-potential given by $a_0 = eA_0/mc^2$. Thus, the mode $\vec{k_0}$ is initially present in plasma and we will calculate the rate at which the mode $3\vec{k_0}$ (initially absent in plasma) is generated. Graphically, we will view the third harmonic generation as a process of absorbing three photons with four-vectors $(\omega_0, \vec{k_0})$ which were originally present in the pump, and emitting one photon with four-vector $(3\omega_0, 3\vec{k_0})$.

One can calculate the rate of the third harmonic generation by computing its amplitude perturbatively to second order in the interaction Hamiltonian. In the analysis of a single oscillator we derived an evolution equation for an arbitrary function of the interaction coordinates. We chose particular combinations of q_i and p_i (a and $a^\dagger$-in Eq.(2.25)) and insured that there is no secular growth of these coordinates with time. As should be clear from expansion (2.73), the Fourier coefficients $a_{\vec{k}_1}$ and $a^\dagger_{\vec{k}_1}$ play the role of interaction coordinates in field theory. The crucial difference between the field theory and single particle mechanics is that in field theory, instead of having one degree of freedom that is coupled to *itself* through the interaction Hamiltonian, we have an infinite number of degrees of freedom coupled to *themselves* and to *each other* through the interaction Hamiltonian. Thus, while we still implement the renormalization program similar to the one in Sec 2.2.4 (adding the counterterms) for the coupling of the different degrees of freedom to themselves, we do not

(and cannot) remove the inter-mode coupling by introducing counter-terms quadratic in the fields.

In fact, harmonic generation in a plasma is a nonlinear excitation of a degree of freedom (which was not initially excited in the plasma) by a strongly excited *different* degree of freedom. When the matching conditions on the wave number and frequency of the harmonic are satisfied, secular growth of the harmonic occurs, until pump depletion becomes important or the resonance condition is no longer satisfied (for instance, due to the appreciable amplitude of the harmonic radiation). It is important to emphasize that, to lowest order in ϵ, one can, in principle, satisfy the matching condition on the wavenumber but not on frequencies. This is related to the fact that the correct linear dispersion relation for the EM radiation in plasma is not Eq.(2.74) but $\omega_{k_z}^2 = k_z^2 + \omega_p^2$. One can show that the resulting phase velocity mismatch leads to the eventual dephasing and saturation of the harmonic [14, 15, 16, 17]. More on the phase velocity mismatch will be presented in Sections 4.1 and 4.4.3.

Since the plane-wave fields are the solutions of the unperturbed Hamiltonian for both the EM fields (as shown in Eq.(2.73)), as well as for the particle fields (as in Eq.(2.65) for non-relativistic plasma and Eq.(2.48) for relativistic plasma), it is natural to label the degrees of freedom by their wave-number. For instance, the fields $q_{\vec{p}}$ and $q_{\vec{p}}^\dagger$ characterize the excitation of the degrees of freedom of a nonrelativistic plasma corresponding to the motion with momentum $\vec{p}$, or the fields a_{k_z}; $a_{k_z}^\dagger$ from Eq.(2.73) characterize the excitation of the k_z mode of the linearly polarized electromagnetic radiation.

2.4.1 Nonrelativistic Third Harmonic Generation (Wick's expansion)

Our assumptions about the polarization (Eq.(2.71)) and the functional dependence of ψ (Eq.(2.70)) lead to a considerable simplification of the interaction Hamiltonian

of nonrelativistic plasma with EM radiation:

$$\mathcal{H}_i^{nr} = \frac{e^2}{2\hbar^2}\vec{A}^2\psi\psi^*. \tag{2.78}$$

To compute the rate of the third harmonic generation we have to obtain an expression for $a^\dagger_{3k_{0z}}$ at time t assuming that, at $t = 0$, there was no radiation at the third harmonic (i.e., $a^\dagger_{3k_{0z}}(0) = 0$) but the pump at the fundamental (ω_0, k_0), with amplitude a_0 (given by (2.77)), was present in a plasma of density n_0, moving with momentum $\vec{p_0}$.

The initial state of plasma is given by (2.67). Then $a^\dagger_{3k_{0z}}$ at time t, to the lowest order, is given by

$$\begin{aligned} a^\dagger_{3k_{0z}}(t) &= \frac{2\cdot 2}{2!}\frac{e^4}{\hbar^4 2^2}\int^x dx_1 \int^x dx_2 A^2(x_2)A(x_1)\psi(x_1)\psi^*(x_2)\psi^*(\widehat{x_1})\psi(x_2)\{A(x_1), a^\dagger_{3k_{0z}}\} \\ &+ \frac{2\cdot 2}{2!}\frac{e^4}{\hbar^4 2^2}\int^x dx_1 \int^x dx_2 A^2(x_2)A(x_1)\psi^*(x_1)\psi(x_2)\psi^*(\widehat{x_2})\psi(x_1)\{A(x_1), a^\dagger_{3k_{0z}}\}, \end{aligned} \tag{2.79}$$

where x is a covariant vector, $x_j = (t_j, z_j)$ and $\int^t dx_j = \int^t dt_j \int_{-\infty}^{+\infty} dz_j$. The numerical factors are easy to understand: 2! in the denominator appears because it is a second-order expansion of the exponential, $2\cdot 2$ in the numerator comes from the two ways of choosing which of the two event points is contracted with $a^\dagger_{3k_{0z}}$ and, once the event point is chosen, which of the two $A(x_1)$'s does the contracting.

Inserting Eqs.(2.73) and (2.75) into Eq.(2.79) gives

$$\begin{aligned} a^\dagger_{3k_{0z}}(t) &= \frac{4\pi e^5}{2(2\pi)^{1/2}\hbar^4}\frac{-i}{(2\omega_{3k_{0z}})^{1/2}}\int^x dx_1 \int^x dx_2 A^2(x_2)A(x_1)\psi(x_1)\psi^*(x_2)\psi^*(\widehat{x_1})\psi(x_2)e^{(i3k_0z_1 - i\omega_{3k_{0z}}t_1)} \\ &+ \frac{4\pi e^5}{2(2\pi)^{1/2}\hbar^4}\frac{-i}{(2\omega_{3k_{0z}})^{1/2}}\int^x dx_1 \int^x dx_2 A^2(x_2)A(x_1)\psi^*(x_1)\psi(x_2)\psi^*(\widehat{x_2})\psi(x_1)e^{(i3k_0z_1 - i\omega_{3k_{0z}}t_1)} \end{aligned} \tag{2.80}$$

Note the similarity between Eq.(2.80) and Eq.(2.35).

Since we have neglected the change of the phase velocity of the wave due to the

plasma, the phase velocities of the pump and the signal match automatically, that is

$$\omega_{3k_0} = 3\omega_{k_0}. \tag{2.81}$$

Inserting the expression for the propagator from Eq.(2.66) and $\psi(x)$ from Eq.(2.67) into Eq.(2.80), we find that the amplitude of third harmonic, a_3, defined by

$$\vec{a} = \vec{e}_x \frac{a_3}{2} e^{i3k_{0z}\cdot z - 3i\omega_0 t} + c.c., \tag{2.82}$$

grows linearly in time. Defining the rate of the harmonic generation

$$\frac{da_3}{dt} \equiv \frac{\Delta a_3}{t}, \tag{2.83}$$

we obtain:

$$i(2\omega_{3k_0})\frac{da_3}{dt} = \frac{4\pi n_0 e^2 a_0^3}{8\hbar^2}\left(\frac{-1}{(\varepsilon_0 + 2\omega_0) - \hbar(p_0 + 2k_0)^2/2} + \frac{-1}{(\varepsilon_0 - 2\omega_0) - \hbar(p_0 - 2k_0)^2/2}\right), \tag{2.84}$$

where $\varepsilon_0 = \hbar p_0^2/2$ is the kinetic energy of a freely moving particle with momentum p_0 (which comprise the unperturbed plasma). The first term in brackets is the propagator that corresponds to first absorbing two photons, then scattering a third photon off the density perturbation created by the first two, and, finally, emitting the third-harmonic photon. Algebraically, this process is described by the first term in Eq.(2.80). The second term in brackets of Eq.(2.84) is the propagator that corresponds to emitting third-harmonic photon first and absorbing the two fundamental photons later (described by the second term in Eq.(2.80)).

2.4.2 Nonrelativistic Diagrams

After calculating the rate of third harmonic generation from nonrelativistic plasma by a "brute-force" method of Wick's expansion, we develop a much more elegant diagrammatic method of perturbative field theory. This section is intended to give the simplest example of diagrammatic field theory, neglecting the important physics

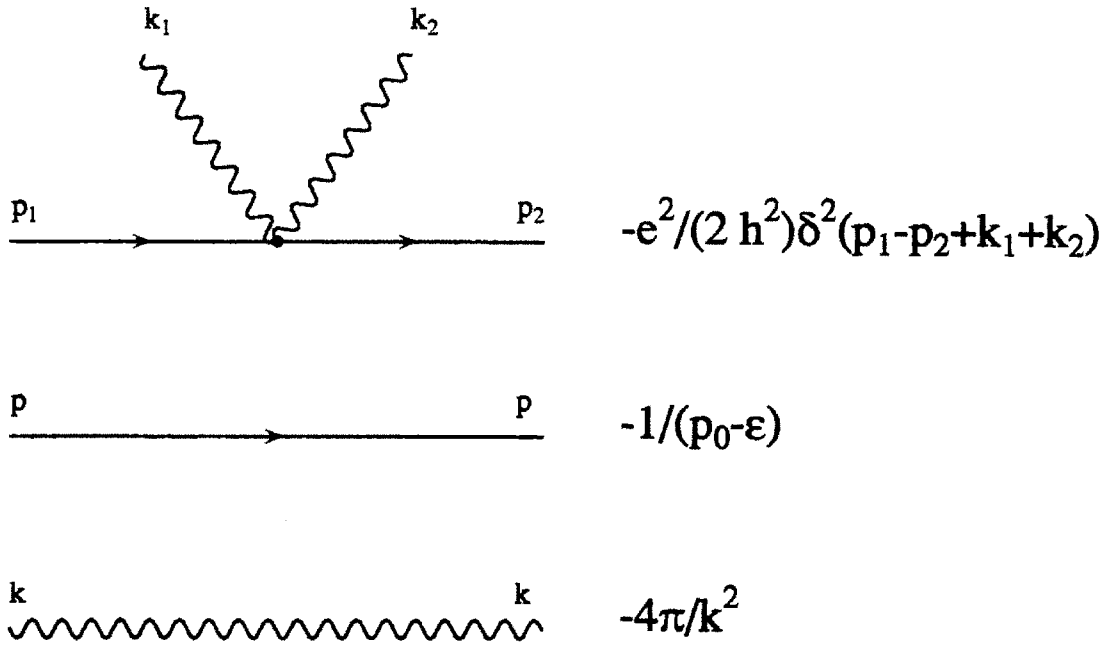

Figure 2-4: Diagrammatic elements of nonrelativistic one-dimensional electrodynamics (slab geometry; no space charge fields).

associated with space-charge forces in plasma, modification of the EM dispersion relation, etc. Clearly, to make the comparison of the results of this and the previous sections meaningful, the calculation is performed under the assumptions (1)-(3) of Section 2.4.

The main result of Section 2.4.1, Eq.(2.84), can be conveniently expressed diagrammatically after we introduce the ingredients of the diagrammatic perturbation theory: the electron propagator,the photon propagator and the interaction vertex. They are shown in Fig. 2-4. Our conventions for drawing the diagrams are similar to the ones we adopted in Section 2.2. The lines that are contracting the modes under study point to the low-right corner of the page and are left "loose", that is, without a cross. The ends of the lines that signify the fields to be evaluated at their unperturbed values are marked with crosses. Particle lines have a directional arrow on them because they are complex. Dirac delta-function at the interaction vertex signifies the momentum conservation at the vertex and is equivalent to integrating over four-space of the Wick's expansion (see below).

In the language of diagrams the process described by (2.80) is shown in Fig. 2-5. A

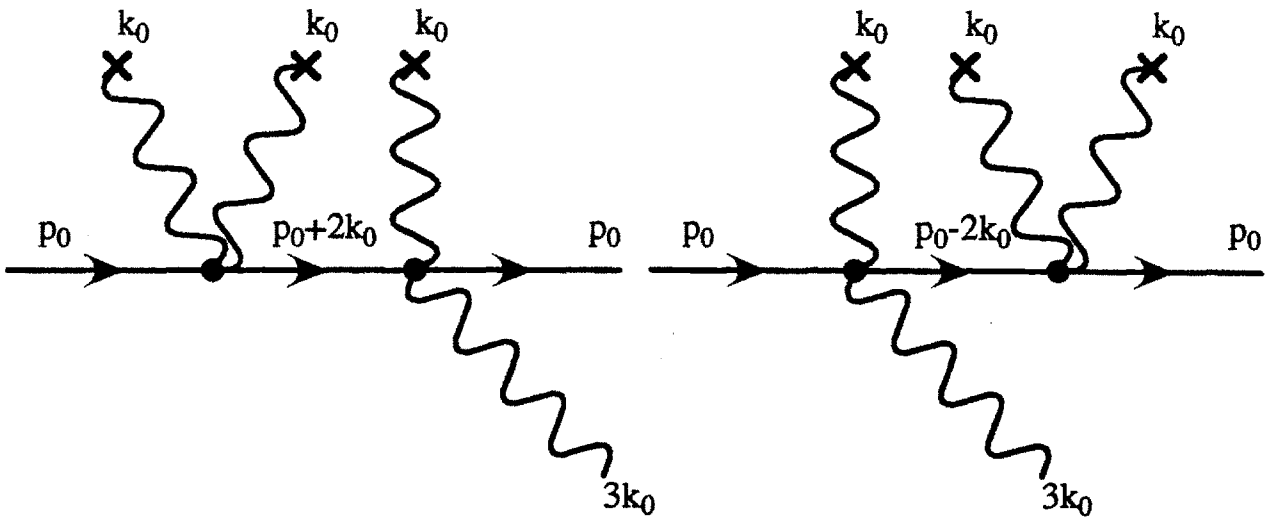

Figure 2-5: Diagrams for the third harmonic generation to lowest order in perturbation theory (slab geometry; no space-charge fields).

detailed comparison of all the diagrammatic elements in Fig. 2-5 with the expansion terms of Eq.(2.79) clarifies the diagrammatic conventions. The first term in Eq.(2.79) corresponds to the first diagram in Fig. 2-5, so we will make a comparison between the two. The Poisson bracket $\{A(x_1), a^{\dagger}_{3k_{0z}}\}$ in Eq.(2.79) corresponds to the "loose" outgoing wiggly line $3k_0$ in Fig. 2-5. The electron field contraction $\psi^*(\widehat{x_1})\widehat{\psi}(x_2)$ corresponds to the electron propagator in Fig. 2-5. The products of the EM fields, $A^2(x_2)A(x_1)$, that have to be evaluated *unperturbed*, are the crossed wiggly lines in the diagram. The product of the electron fields $\psi(x_1)\psi^*(x_2)$ corresponds to the two "loose" electron (straight) lines. To avoid obscuring the drawing, we do not put cross on the particle lines, even though the values of ψ and ψ^* that correspond to "loose" particle lines are to be evaluated at their unperturbed values. The numerical factor $\frac{e^4}{4\hbar^4}$ is identical to the square of the interaction vertex. And, finally, two integrations over four-space in Eq.(2.79) correspond to the product of two delta-functions from the interaction vertices in Fig. 2-5.

It is easy to convince oneself that the final answer (2.84) is obtained from the diagrams by simply reading off the values of the corresponding propagators and multiplying them by the values of vertices and crosses at the external lines. Each cross has to be multiplied by a factor of $a_0/2$, as should be clear from (2.77). For more

detailed description of how the diagrams are quantified see Appendix B.

We also note that we must include *all* possible diagrams that are not topologically equivalent, contain two interaction vertices and lead to third harmonic generation. Missing one of the two diagrams in Fig. 2-5 would result in an unphysical answer inversely proportional to $\hbar$—not a good sign when one is about to assume that $\hbar$ is very small!

Since $p_0^2, \varepsilon_0^2 \gg k_0^2$, or, stated differently, the wavelength associated with electron field ("Compton length") is much smaller than the minimal radiation wavelength, the rate of third harmonic emission becomes (in physical units):

$$i(2\omega_{3k_0})\frac{da_3}{dt} = \frac{a_0^3\omega_{p0}^2}{8}\frac{c^2k_0^2}{(\omega_0 - k_0 \cdot v_0)^2}, \tag{2.85}$$

where v_0 is the initial velocity of the (originally unperturbed) non- thermal plasma. The rate of harmonic generation from Eq.(2.85) is proportional to the first power of ω_{p0}^2. As we know [14, 15], this result is erroneous and is caused by neglecting relativistic corrections.

2.4.3 Relativistic Analysis

We next calculate relativistically the rate of third harmonic generation using identical simplifying assumptions as in Section 2.4.1. Namely, we neglect the space-charge forces, assume that the electromagnetic waves propagate with the speed of light (despite of the presence of the plasma) and limit the analysis to one- dimensional slab geometry. We are led to the same form of the vector-potential as in Eq.(2.71). The interaction Hamiltonian that replaces Eq.(2.78) is then

$$\mathcal{H}_i = \frac{e^2}{\hbar^2}A^2\psi\psi^*. \tag{2.86}$$

This only differs from Eq.(2.71) by factor of two.

Using Eq.(2.86), an expression similar to Eq.(2.80) for the rate of the third har-

monic generation from *relativistic* plasma is

$$a^{\dagger}_{3k_{0z}}(t) = \frac{-2i\cdot 4\pi e^5}{(2\omega_{3k_{0z}})^{1/2}(2\pi)^{1/2}\hbar^4}\int^x dx_1\int^x dx_2 A^2(x_2)A(x_1)\psi(x_1)\psi^*(x_2)\widehat{\psi^*(x_1)\psi}(x_2)e^{(i3k_0z_1-i\omega_{3k_{0z}}t_1)}$$
$$+ \frac{-2i\cdot 4\pi e^5}{(2\omega_{3k_{0z}})^{1/2}(2\pi)^{1/2}\hbar^4}\int^x dx_1\int^x dx_2 A^2(x_2)A(x_1)\psi^*(x_1)\psi(x_2)\widehat{\psi^*(x_2)\psi}(x_1)e^{(i3k_0z_1-i\omega_{3k_{0z}}t_1)}, \quad (2.87)$$

with the same conventions for the integration as in Eq.(2.80). The numerical factor 2 in the numerator arrises because any one of the two photons can be contracted with $a^{\dagger}_{3k_{0z}}$. The difference is that we now have to substitute an expression for the *relativistic* propagator from Eq.(2.51) and an expression for the unperturbed plasma field from Eq.(2.53), obtaining the rate of the third harmonic generation:

$$i(2\omega_{3k_0})\frac{da_{3k_0}}{dt} = 4\pi\frac{n_0}{\hbar^2}e^2a_0^3\left(\frac{-1}{(p_0+2k_0)^2-m^2/\hbar^2}+\frac{-1}{(p_0-2k_0)^2-m^2/\hbar^2}\right), \quad (2.88)$$

where both p_0 and k_0 are four-vectors, with only two nonzero components.

Equation (2.54) and the vacuum dispersion

$$k_0^2 = \omega_0^2 - k_{0z}^2 = 0 \quad (2.89)$$

give

$$\frac{da_3}{dt} = 0. \quad (2.90)$$

This agrees with the findings of Refs.[14, 15, 16, 17] that the rate of the third harmonic generation in plasma vanishes to the lowest order in ω_p^2.

To develop a relativistic diagrammatic theory, we define an electron propagator, a photon propagator and an interaction vertex similarly to the way we did in Fig. 2-4, except that the values of the electron propagator and the interaction vertex change according to (2.51) and (2.86). The "building blocks" for the relativistic calculation are shown in Fig. 2-4.

Applying the same conventions that were used in constructing the diagrams in Fig. 2-5 for a non-relativistic plasma, we obtain their relativistic counter-parts (that

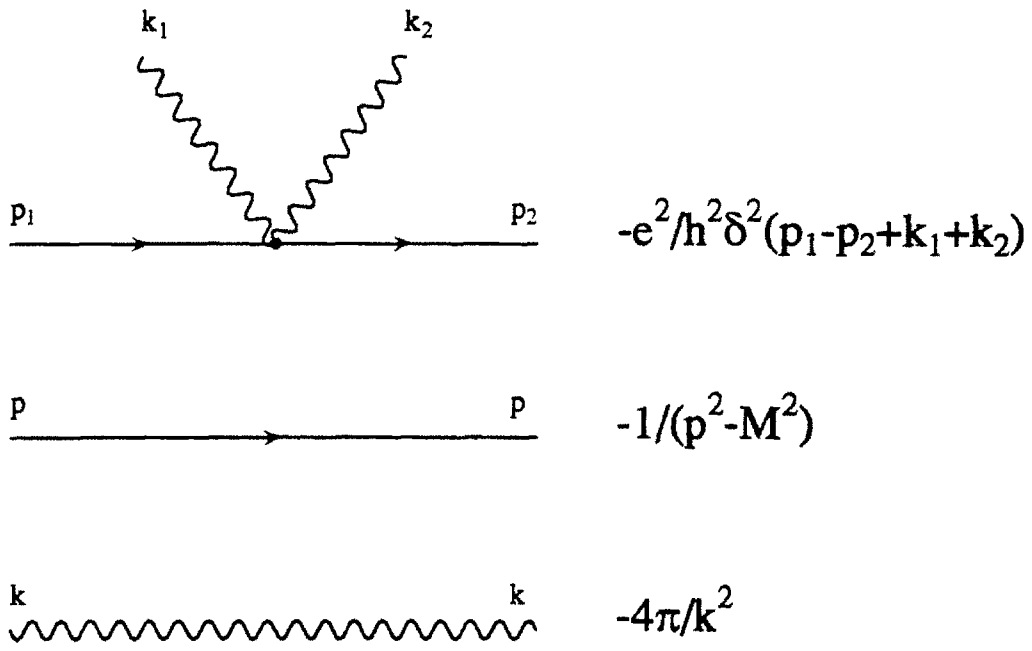

Figure 2-6: Diagrammatic elements of relativistic one- dimensional electrodynamics (slab geometry; no space-charge fields).

look exactly the same, except that the *values* of the propagator and vertices are different). Quantifying the diagrams in Fig. 2-5 with *relativistic* vertices and propagator yields the rate of the third harmonic generation given by Eq.(2.88). For more detail on quantifying the diagrams see Appendix B.

We note that neglecting the restoring space-charge forces in a *single species* plasma is not justifiable on physical grounds (even though the result for the rate of third harmonic generation is correct to lowest order in ω_p^2/ω_0^2 for both relativistic and nonrelativistic plasmas) because the physical mechanism of generating the third harmonic involves creating a longitudinal density modulation and then scattering off it. Creating a longitudinal density perturbation necessarily results in longitudinal electric fields (or space-charge forces). Meanwhile, breaking for the sake of this example, our earlier assumption of no positrons in the system, the following physical scenario can be envisioned, which validates our approximations: in a plasma that contains equal number of electrons and positrons ponderomotive force pushes them in the same direction, thus creating a density perturbation that the light can scatter off but no charge density, and exciting no space-charge fields.

To obtain the harmonic generation rate to the next order, new physics has to be included. Most obvious is the need to include the correct phase velocity of the electromagnetic wave in the plasma. Then Eq.(2.88) would obviously give a nonzero result: instead of Eq.(2.89) we would use

$$k_0^2 = \omega_0^2 - k_{0z}^2 = \omega_p^2. \tag{2.91}$$

The removal of the simplification that the total vector potential of the electromagnetic field in plasma is linearly polarized and can be represented by one scalar function (Eq.(2.71)) will also give a contribution to the rate of harmonic generation. This is done in Chapter 3. Section 3.1 goes beyond the scalar mesodynamics to real three dimensional vector electrodynamics, while Section 3.2.1 accounts for the change of phase velocity of the electromagnetic waves in plasma.

Chapter 3

Gauge and Renormalization

3.1 Choice of Gauge

It is well-known that any consistent field theory that contains electromagnetic interactions has to be formulated in terms of vector-potentials rather than electric and magnetic fields. One of the reasons for this is that $\vec{E}$ and $\vec{B}$ do not form a four-vector and thus are not very convenient for formulating a manifestly covariant theory. A more subtle physical reason is that electromagnetic interaction, in fact, is not local when the wave nature of the electrons is taken into account. The best known illustration of this is the Aharonov-Bohm effect. Forced to use the vector-potential to describe the electromagnetic fields, we have to deal with the fact that there exists an infinite number of vector-potentials that describe the same physical electromagnetic field. This property is known as gauge invariance [66].

A number of different gauges are popular in plasma electrodynamics, some of them relativistically covariant. Among the widely used covariant gauges the most common is the so called Lorentz gauge:

$$\partial_\mu A^\mu = 0. \tag{3.1}$$

It can be shown that the denominator of the propagator of the electromagnetic field, restricted by the Lorentz gauge, is equal to $\omega^2 - \vec{k}^2$. Poles of the propagator (which is just the Fourier transform of a Green function) define a dispersion relation for a

photon. And indeed, for a photon propagating in free space

$$\omega^2 - \vec{k}^2 = 0 \tag{3.2}$$

is the true dispersion relation.

It is difficult to develop a description of plasma wave, perturbatively in plasma density, when using the Lorentz gauge. For instance, the dispersion relation of a plasma wave on a cold nonrelativistic electron beam with density n_0, moving with velocity $\vec{v}_0$, is given by

$$(\omega - \vec{k} \cdot \vec{v}_0)^2 = \omega_{p0}^2. \tag{3.3}$$

The only hope to obtain this dispersion relation perturbatively in ω_{p0}^2/ω^2 is to begin with a dispersion relation $\omega = \vec{k} \cdot \vec{v}_0$ in the absence of plasma (which is quite different from Eq.(3.2)).

It turns out that there is a relativistically covariant gauge that recovers the dispersion relation for a plasma wave perturbatively in ω_p^2. This gauge is the so-called Arnowitt-Fickler gauge [64] given by

$$A_\mu \cdot n^\mu = 0, \tag{3.4}$$

where n^μ is a unit four vector pointing in the direction of motion of the cold plasma, p_0^μ:

$$n^\mu = \frac{p_0^\mu}{\sqrt{p_{0\nu} p_0^\nu}}. \tag{3.5}$$

In Section 2.4 we have developed a simplified description of electromagnetic fields based on a single scalar function A. In the spirit of a field-theoretical calculation, the corresponding canonical momentum was derived and Poisson bracket relationship established. One could naively assume that for a true vector electrodynamics the four components of A_μ are the canonical fields, with corresponding canonical momenta, etc. Yet one immediately finds that a canonical momentum corresponding to A_0, vanishes (see Eqs.(2.39) and (2.44)). This can only mean that not all of the four components of A_μ are independent fields. In fact, only three of them are, which

is precisely the reason why one arbitrary gauge relation is allowed. A brute force approach would be to express one of the components of A_μ in terms of the other three by using Eq.(3.4), substitute this expression into a full Lagrangian, and derive Poisson bracket relations. Defining the field contractions in the usual way (as in Eq.(2.17)), we would find them to be of the form

$$\widehat{A^\mu(x_1)A^\nu}(x_2) = \int \frac{d^4k}{(2\pi)^4} D^{\mu\nu}(k) e^{ik\cdot(x_1-x_2)}, \tag{3.6}$$

where both k and x four-vectors, and $D^{\mu\nu}(k)$ is *defined* by Eq.(3.6). The contraction in (3.6) is a function of $(x_1 - x_2)$ because of the invariance of the Lagrangian with respect to space-time shifts.

Yet a much more elegant method for obtaining $D_{\mu\nu}$ is widely used in field theory under the name of Faddeev-Popov procedure [64]. Without giving a proof of this procedure (which is available in most texts on quantum field theory, for example, Ref. [67]), we present the steps that lead to the vacuum propagator of the fields constrained by gauge condition (3.4).

3.1.1 Faddeev-Popov Ansatz

We rewrite the free field Lagrangian in k space:

$$\mathcal{L}_{em} = \frac{1}{4\pi}\left(-k^2 g^{\mu\nu} + k^\mu k^\nu\right)\frac{A_\mu A_\nu}{2} \equiv \frac{1}{2} O^{\mu\nu} A_\mu A_\nu, \tag{3.7}$$

where $g^{\mu\nu}$ is a symmetric relativistic metric. To obtain a propagator $D_{\mu\sigma}$ of the electromagnetic vector-potential one has to invert the matrix $O^{\mu\nu}$, that is

$$O^{\mu\nu} D_{\mu\sigma} = -\delta^\nu_\sigma, \tag{3.8}$$

where δ^ν_σ is a covariant Kronicle delta equal to unity on the diagonal and to zero elsewhere. Faddeev-Popov procedure is to add a square of the gauge constraint multiplied

by an arbitrary numerical factor to the Lagrangian (3.7). Adding a term

$$-\frac{1}{4\pi}n^\mu n^\nu \frac{A_\mu A_\nu}{2\lambda}, \tag{3.9}$$

where λ is an arbitrary number, to the Lagrangian, modifies the matrix O:

$$O^{\mu\nu} \rightarrow O_1^{\mu\nu} = \frac{1}{4\pi}\left(-k^2 g^{\mu\nu} + k^\mu k^\nu - \frac{n^\mu n^\nu}{\lambda}\right). \tag{3.10}$$

Taking negative of the inverse of the resulting matrix $O_1^{\mu\nu}$ results in the propagator for a gauge field A_μ. Setting $\lambda = 0$ (to insure that the resulting propagator is orthogonal to n^μ) results in an expression for $D_{\mu\nu}$ [64]:

$$D_{\mu\nu} = \frac{4\pi}{k^2(n\cdot k)^2}\left((n\cdot k)^2 g_{\mu\nu} + k^\mu k^\nu - (n\cdot k)(n_\mu k_\nu + n_\nu k_\mu)\right). \tag{3.11}$$

3.1.2 Propagators for Vacuum Electromagnetic Fields

The Faddeev-Popov procedure yields a propagator (3.11), with no apparent structure. Yet the point of the whole exercise was to obtain propagators for an electromagnetic wave as well as for a space-charge wave. It turns out that the propagator (3.11) can be split into two parts, $D^T_{\mu\nu}$ and $D^L_{\mu\nu}$, such that

$$D_{\mu\nu} = D^T_{\mu\nu} + D^L_{\mu\nu} \tag{3.12}$$

and

$$D^L_{\mu\nu}(k) = \frac{-4\pi e^L_\mu e^L_\nu}{(n\cdot k)^2} \tag{3.13}$$

$$D^T_{\mu\nu}(k) = \frac{-4\pi(-g_{\mu\nu} - e^L_\mu e^L_\nu + n_\mu n_\nu)}{k^2}. \tag{3.14}$$

Here

$$e^L_\mu = \frac{-k_\mu + n_\mu(n\cdot k)}{(-k^2 + (n\cdot k)^2)^{1/2}} \tag{3.15}$$

and $e^L_\mu e^{L\mu} = -1$.

The transverse and longitudinal parts of the propagator ($D^T_{\mu\nu}$ and $D^L_{\mu\nu}$ respectively) are chosen to satisfy the following conditions:

$$\begin{aligned} 1 \quad & D^T_{\mu\nu} D^{L\nu\sigma} = 0 && \text{(orthogonal to each other)} \\ 2 \quad & D^T_{\mu\nu} n^\nu = D^L_{\mu\nu} n^\nu = 0 && \text{(each satisfies the gauge)} \\ 3 \quad & D^T_{\mu\nu} k^\nu = 0 && \text{(transverse field).} \end{aligned} \tag{3.16}$$

We note that the quantity $-k^2 + (n \cdot k)^2$ in the denominator of the Eq.(3.15) is always positive which can be seen easily by going to the rest frame of plasma where $n_0 = 1, \vec{n} = 0$.

Thus by the appropriate choice of gauge we have split the total electromagnetic field into two parts—the longitudinal part that will correspond to a plasma wave after we include the EM-plasma interaction, and the transverse part that will correspond to an electromagnetic wave in plasma. As we see in Section 3.2, there is also a technical reason that makes the Arnowitt-Fickler gauge very convenient for perturbative analysis of the interactions of intense lasers with non-thermal plasmas.

To better understand the meaning of the longitudinal and transverse propagators note that both are projection operators. The longitudinal propagator $D^L_{\mu\nu}$ (Eq.(3.13)) projects the component of the total field that is parallel to the polarization vector e^L_μ. And indeed, in a stationary plasma, there exists only one longitudinal (electrostatic) plasma wave corresponding to a given direction of propagation k. On the other hand, the transverse part $D^T_{\mu\nu}$, given by Eq.(3.14), projects the component of the total field which is perpendicular to *both* k and n. Thus the possible polarizations make up a two-dimensional plane in the four-space which is perpendicular to k and n. And indeed, in a stationary plasma an electromagnetic wave can be polarized in any direction in a two-dimensional plane perpendicular to the direction of propagation.

The transverse and longitudinal fields are orthogonal to each other which guarantees that their linear dispersion relations can be renormalized independently, as shown in Section 3.1.3.

3.1.3 Propagators for Dressed Fields (Electromagnetic Fields in Plasma)

Even in the absence of nonlinear effects, the induced polarization currents in plasma lead to renormalization of electromagnetic fields. To the lowest order this renormalization is, of course, just the plasma correction to phase velocity of EM waves. We incorporate this effect by adding a quadratic counter term to the Lagrangian (3.7):

$$\Delta\mathcal{L}_{em} = \frac{\mu^2}{4\pi}\frac{g^{\mu\nu}A_\mu A_\nu}{2}. \tag{3.17}$$

where μ^2 is, for the moment, an arbitrary number. Introduction of this term will be justified in Section 3.2.1, where we will show that this counter term is needed to cancel out the secular growth induced by the interaction term (2.86). It will be also shown that μ^2 is equal to the relativistic plasma density.

As was mentioned earlier, since the longitudinal and transverse waves are orthogonal to each other, the counter term (3.17) can be decomposed into two components: one quadratic in the longitudinal field and one quadratic in the transverse field. It is easy to convince oneself that adding the counter term (3.17) is equivalent to subtracting μ^2 from the denominators of the propagators (3.14). This modifies the propagators of the EM fields to

$$\bar{D}^L_{\mu\nu}(k) = \frac{-4\pi e^L_\mu e^L_\nu}{(n\cdot k)^2 - \mu^2}, \tag{3.18}$$

$$\bar{D}^T_{\mu\nu}(k) = \frac{-4\pi(-g_{\mu\nu} - e^L_\mu e^L_\nu + n_\mu n_\nu)}{k^2 - \mu^2}. \tag{3.19}$$

Even though $\bar{D}^T$ and $\bar{D}^L$ could be found by a straightforward addition of $\Delta\mathcal{L}_{em}$ to the Lagrangian $\mathcal{L}_{em}$ and using the Faddeev-Popov procedure as done in deriving Eqs.(3.13-3.14), we will find them in a slightly different way—employing an approach frequently encountered in quantum field theory.

Fig 3-1 pictorially describes the modification of a propagator that arrises when a $\Delta\mathcal{L}_{em}$ term is added to the Lagrangian. Note that, unlike in the diagrams presented

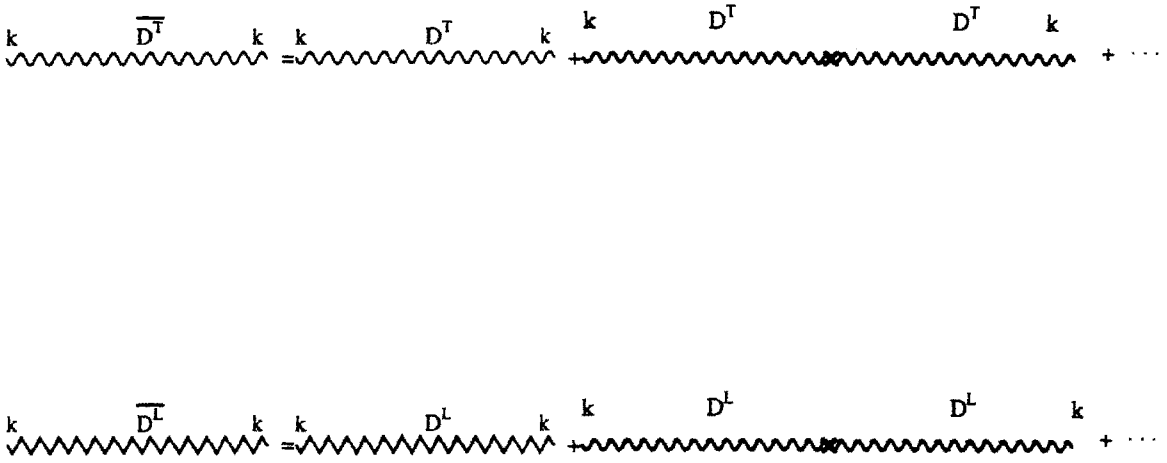

Figure 3-1: Renormalization of the EM propagators by a quadratic term in the Lagrangian.

in Section 2.4, there are no EM-matter interactions involved here, and the counter terms (3.17) appear as crosses, rather than interaction vertices. And, as always, the contributions of each diagram is the product of its propagators and vertices (or counter terms, in this example). By convention we associate wiggly lines with the transverse mode (i.e., a photon) and the zig-zag line is associated with a longitudinal mode (i.e., a plasmon).

We also introduce the purely diadic parts of the longitudinal and transverse propagators, $G^L_{\mu\nu}$ and $G^T_{\mu\nu}$,

$$\begin{aligned} \frac{D^L_{\mu\nu}}{4\pi} &= \frac{G^L_{\mu\nu}}{(n\cdot k)^2} \\ \frac{D^T_{\mu\nu}}{4\pi} &= \frac{G^T_{\mu\nu}}{k^2} \end{aligned} \tag{3.20}$$

Then the diagrammatic series in Fig 3-1 define the new propagators $\tilde{D}^L_{\mu\nu}$ and $\tilde{D}^T_{\mu\nu}$:

$$\begin{aligned} \frac{\tilde{D}^L_{\mu\nu}}{4\pi} &= \frac{G^L_{\mu\nu}}{(n\cdot k)^2} + \frac{\mu^2}{(n\cdot k)^4} G^L_{\mu\alpha} g^{\alpha\sigma} G^L_{\sigma\nu} \\ &+ \frac{\mu^4}{(n\cdot k)^6} G^L_{\mu\alpha} g^{\alpha\sigma} G^L_{\sigma\beta} g^{\beta\gamma} G^L_{\gamma\nu} + \ldots \\ \frac{\tilde{D}^T_{\mu\nu}}{4\pi} &= \frac{G^T_{\mu\nu}}{k^2} + \frac{\mu^2}{k^4} G^T_{\mu\alpha} g^{\alpha\sigma} G^T_{\sigma\nu} \end{aligned} \tag{3.21}$$

$$+ \quad \frac{\mu^4}{k^6} G^T_{\mu\alpha} g^{\alpha\sigma} G^T_{\sigma\beta} g^{\beta\gamma} G^T_{\gamma\nu} + \ldots \tag{3.22}$$

Note that the counter term (3.17) was chosen in such a way that its $1/(4\pi)$ factor cancels out the 4π factor in the propagators. The $1/2$ factor in (3.17) is canceled by the factor of two that arrises since each of the A fields in (3.17) can be contracted independently (as can be seen by examining the Wick's expansion similar to the RHS of Eq.(2.87)).

Because of the properties of the diadic propagators, it is surprisingly easy to carry out the infinite summation. Both $G^L_{\mu\nu}$ and $G^T_{\mu\nu}$ are projection operators and, therefore, satisfy the property that the square of the projection operator is equal to the operator itself. Mathematically,

$$\begin{aligned} G^L_{\mu\alpha} G^{L\alpha}_{\nu} &= G^L_{\mu\nu} \\ G^T_{\mu\alpha} G^{T\alpha}_{\nu} &= G^T_{\mu\nu} \end{aligned} \tag{3.23}$$

Thus the products of the diadic operators that enter the sum in Eqs.(3.21,3.22) are all equal to $G^L_{\mu\nu}$ and $G^T_{\mu\nu}$, respectively. After summing the geometric series

$$\begin{aligned} \frac{1}{(n\cdot k)^2} + \frac{\mu^2}{(n\cdot k)^4} + \frac{\mu^4}{(n\cdot k)^6} + \ldots &= \frac{1}{(n\cdot k)^2 - \mu^2} \\ \frac{1}{k^2} + \frac{\mu^2}{k^4} + \frac{\mu^4}{k^6} + \ldots &= \frac{1}{k^2 - \mu^2} \quad . \end{aligned} \tag{3.24}$$

we recover Eq.(3.19). Notice that the bars over the propagators have been dropped for notational convenience. The technique that we applied to obtain the modified propagator will be used throughout the thesis, in particular, in Section 3.2.2, where we calculate the renormalized electron mass.

3.1.4 Example: Electrostatic and Electromagnetic Fields in a Stationary Plasma

Propagators for the electromagnetic fields given by Eqs.(3.18,3.19) deserve a more careful consideration. Cold unmagnetized plasma at rest provides a familiar ground for classifying electromagnetic waves. As is presented in introductory plasma courses [55], waves in a cold stationary plasma can be classified as electrostatic or electromagnetic. One of the distinctions between these waves is that there is no magnetic field associated with the electrostatic wave while there is no charge density perturbation associated with electromagnetic wave. This distinction is very artificial, especially in the context of a relativistically covariant theory. Indeed, neither magnetic field nor the charge density are relativistically covariant quantities.

Yet there is another distinction between the purely electrostatic and purely electromagnetic waves that should be true in relativistically covariant theory—the former do not have any fields associated with them when the plasma density vanishes while the latter do. Note that if one invokes vector potentials to describe the fields, one can, in principle, have a non-zero value of the vector potential of an electrostatic field even *in the absence* of plasma. Nonetheless, the electric and magnetic fields (which are the only measurable quantities), associated with the vector potential, will be equal to zero in the absence of plasma. From another perspective, electromagnetic waves can escape plasma into the vacuum while electrostatic waves cannot. An example of such a calculation for the rate of the second harmonic generation is presented in Section 4.4, where we find that, despite the presence of the second-harmonic fields *in the plasma*, there is no second-harmonic radiation in the far-field region (to lowest order in ϵ).

The ability of radiation to escape from a finite-size plasma is obviously a relativistically covariant property. To understand how it is related to the transverse and longitudinal operators in Eqs.(3.18),(3.19) we have just derived, consider these covariant propagators in the frame where plasma electrons are, on average, at rest. In

this frame

$$n^\mu = (1, 0, 0, 0). \tag{3.25}$$

For convenience, in the rest of this thesis we will refer to this frame as "the rest frame of plasma". The covariant propagators (3.14) simplify to

$$\begin{aligned} D^L_{00} = D^T_{00} = 0, \\ D^L_{ij} = \frac{-4\pi}{\omega^2 - \mu^2} \frac{k_i k_j}{\vec{k}^2}, \\ D^T_{ij} = \frac{-4\pi}{\omega^2 - \vec{k}^2 - \mu^2} \frac{\vec{k}^2 g_{ij} - k_i k_j}{\vec{k}^2}, \end{aligned} \tag{3.26}$$

where g_{ij} is the identity matrix. The propagators in (3.26) are the well known Green functions for the electrostatic and electromagnetic waves in a cold plasma [55]. Their respective dispersion relations are found by setting the denominators of the propagators to zero, that is:

$$\begin{aligned} \omega^2 &= \mu^2 \quad \text{(electrostatic wave)} \\ \omega^2 - \vec{k}^2 &= \mu^2 \quad \text{(electromagnetic wave)} \end{aligned} \tag{3.27}$$

In Section 3.2.1, using a different method, we show that $\mu^2 = \omega_p^2$. Thus, the modes that we classified in this section as transverse and longitudinal, coincide, in the rest frame of plasma, with electrostatic and electromagnetic waves.

As we return to the reference frame where plasma is moving, these modes are no longer purely electrostatic and electromagnetic. Still, these modes are physically distinct from each other—there are no electric or magnetic fields associated with the longitudinal mode in the absence of plasma while the transverse mode can propagate in vacuum. By analogy with the rest frame of plasma we call the longitudinal wave a plasmon and the transverse mode a photon.

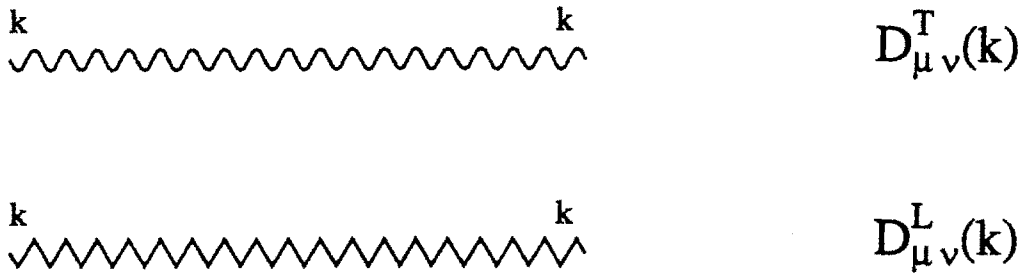

Figure 3-2: Propagators of the EM fields: Photon and Plasmon

3.1.5 Elements of the Perturbation Theory

The main goal of this section—to extend the one-dimensional electrodynamics, introduced in Section 2.4, and to describe longitudinal plasma waves—has been accomplished by introducing two new objects: photons and plasmons. Symbolically, we draw them as wiggly and zig-zag lines, as shown on Fig. 3-2, with their corresponding propagators $D^L_{\mu\nu}$ and $D^T_{\mu\nu}$ given by Eqs.(3.18,3.19).

Now all the diagrammatic elements of a perturbative theory of laser plasma interactions can be put together. The full interaction Hamiltonian, given by (2.63), has two distinct terms:

$$\mathcal{H}_i^{scat} = -\frac{e^2}{\hbar^2} A_\mu A^\mu \psi \psi^* \tag{3.28}$$

$$\mathcal{H}_i^{abs} = i\frac{e}{\hbar} A^\mu (\psi^* \partial_\mu \psi - \psi \partial_\mu \psi^*), \tag{3.29}$$

which correspond to two different kinds of vertices which we will call "scattering" and "absorbing". Photons as well as plasmons enter the interaction vertices in Fig. 3-3. The first two diagrams in Fig. 3-3 are scattering and the last two are absorbing. Recall that when we assumed in Section 2.4 that the total electromagnetic field is polarized perpendicularly to the direction of propagation, the only nonzero term in the Hamiltonian was given by Eq.(3.28), and we only had scattering vertices.

The delta functions in Fig. 3-3 reflect the conservation of the momentum at the vertices. $\mathcal{H}_i^{abs}$ contains derivative terms, which, as noted in Section 2.3, are treated by multiplying by the corresponding momentum whenever one encounters a derivative. This is reflected in the value of the absorbing vertices in the last two diagrams in

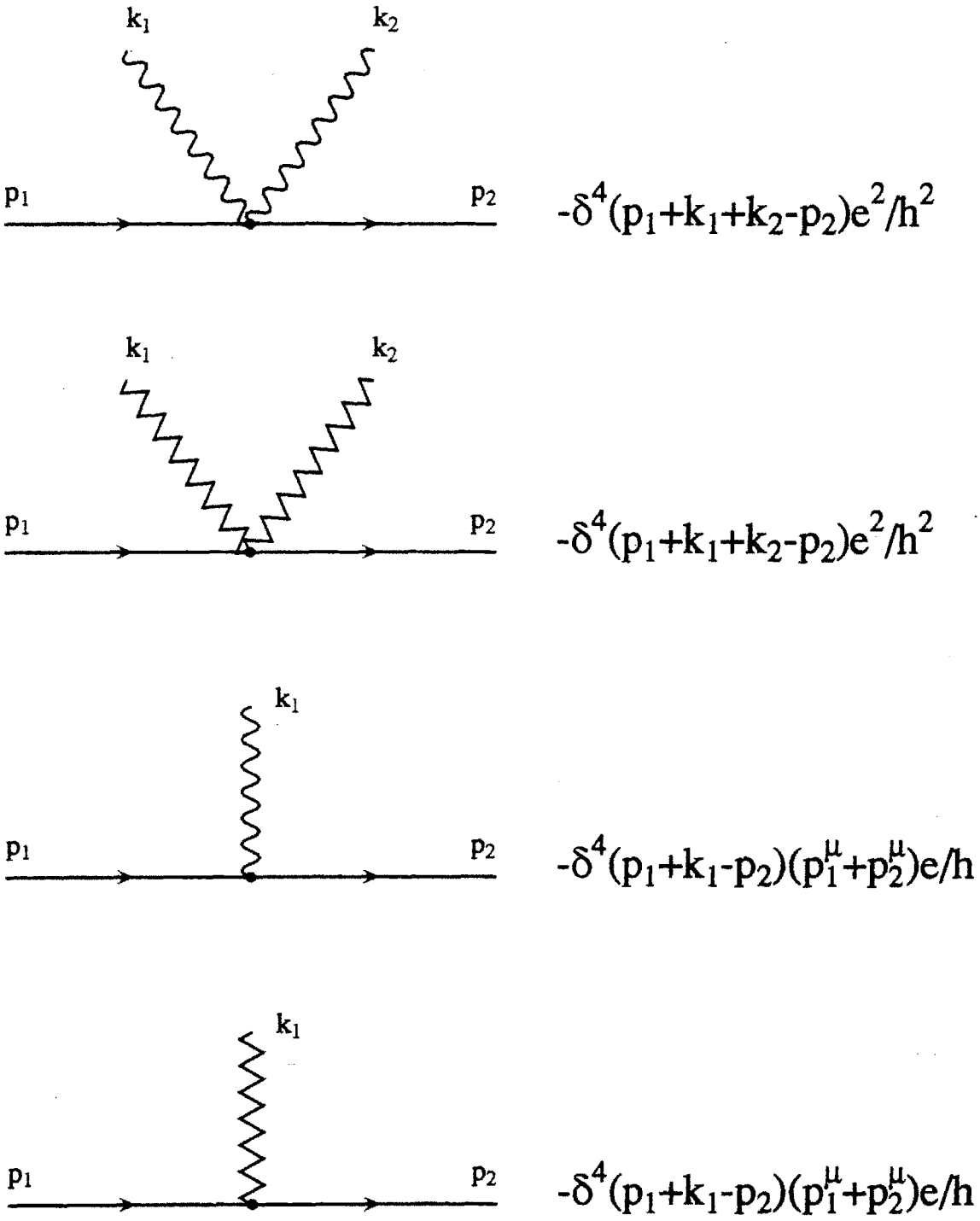

Figure 3-3: Selected diagrammatic elements of three dimensional relativistic electrodynamics

Fig. 3-3.

The list of diagrams in Fig. 3-3 is by no means comprehensive. For instance, one can emit two photons, or absorb one photon and emit another one (as was shown in Fig. 2-5), or even absorb a plasmon and emit a photon (as will be shown in Section 4.4). Perturbative calculations of different physical processes require slightly different diagrammatic components, yet Fig.3-3 gives a fairly good idea of what these building blocks should be.

So far we have not specified the value of μ^2. This is done in the next section by ensuring that the combination of the counter term $\Delta\mathcal{L}_{em}$ from (3.17) and the scattering term $\mathcal{H}_i^{scat}$ from (3.28) do not produce secularly growing terms to the lowest order in ϵ.

3.2 Renormalization of Fields

This section addresses the issues of modification of the index of refraction of the electromagnetic radiation in the presence of plasma as well as the modification of the electron mass in the presence of strong electromagnetic waves and the surrounding electron plasma.

3.2.1 Lowest Order Renormalization of Photons and Plasmons

As we have mentioned in Section 3.1, we have yet to relate μ^2 from Eq.(3.17), which enters the photon and plasmon propagators, to the properties of the surrounding plasma. In physical terms, we have, for example, to calculate how the phase velocity of photons in plasma is different from the speed of light. Attempting to develop a perturbation theory based on an expansion in electromagnetic waves that are moving with the speed of light would lead to secularly growing solutions. Our method is to choose the counter term $\Delta\mathcal{L}_{em}$ to cancel the secular terms arising from the interaction Hamiltonian given by (2.63). This eliminates the secular growth and renormalizes the "photon mass"—in other words, includes the linear polarization current, correcting the dispersion relation to zeroth order.

Another (more concrete) incentive to calculate correctly the speed of EM waves in plasma comes from our attempt in Section 2.4 to calculate the rate of the third harmonic emission. To the lowest order in ϵ the rate was zero, but we have seen that even in the simplified one dimensional case (in slab geometry), with space-charge effects neglected, a nonzero rate of the third harmonic generation could be obtained by allowing $k_\mu k^\mu \neq 0$. We have made the first step in that direction by introducing a counter term $\Delta\mathcal{L}_{em}$ into the zeroth order Lagrangian density of the EM field in the last section. Since the total Lagrangian must not change, we can *subtract* a term from the Lagrangian by *adding* it to the Hamiltonian (recall Feynman prescription from Section 2.3). We add the counter term $\Delta\mathcal{L}_{em}$ to the *interaction* part of the Hamiltonian and evaluate the magnitude of μ^2 by requiring that there is no secular

Figure 3-4: Diagrams for *linear* renormalization of the EM dispersion relation (vanishes by choice of gauge)

growth of a creation operator of the photon and plasmon fields.

We have mentioned in Section 3.1, there is a technical reason for using the $A \cdot n = 0$ gauge. This gauge allows to get rid of the diagrams shown in Fig. 3-4.

With these diagrams removed and the counter term $\Delta\mathcal{L}$ added, the only term in the interaction Hamiltonian that contributes to the propagator of the EM field to the lowest order is

$$\mathcal{H}_i' = -\frac{e^2}{\hbar^2} A_\mu A^\mu \psi\psi^* + \frac{\mu^2}{4\pi}\frac{A_\mu A^\mu}{2}. \tag{3.30}$$

Below, we illustrate how the secularly growing terms originate.

The photonic field polarized in x direction can be expressed as a sum of unperturbed and perturbed terms:

$$A(x) = A_0(x) + A_1(x). \tag{3.31}$$

Then, the Lagrange-Euler equation, with $\mathcal{L}_0 = \mathcal{L}_{em} + \Delta\mathcal{L}_{em}$, takes on the form

$$\frac{1}{4\pi}(\partial_\nu \partial^\nu + \mu^2) A_1 = -\frac{\partial \mathcal{H}_i'}{\partial A}, \tag{3.32}$$

where the RHS of Eq.(3.32) has to be evaluated with the unperturbed ψ and A_0. We have assumed that A_0 is an equilibrium solution to the lowest order, that is, that it

satisfies

$$\frac{1}{4\pi}(\partial_\nu\partial^\nu + \mu^2)A_0 = 0. \tag{3.33}$$

Then, inserting the expression for ψ from Eq.(2.53) into the RHS of Eq.(3.32), we obtain

$$(\partial_\nu\partial^\nu + \mu^2)A_1 = (4\pi e^2 n_0/m - \mu^2)A_0. \tag{3.34}$$

Since A_0 satisfies Eq.(3.33), it follows from (3.34) that A_1 will be growing secularly with time unless the RHS vanishes. This allows us to relate the phenomenological factor μ^2 to the properties of the electron plasma:

$$\mu^2 = \frac{4\pi e^2 n_0}{m\bar{m}}, \tag{3.35}$$

where $\gamma\bar{m}m = \hbar\varepsilon_{\vec{p}_0}$ and $\bar{m} = 1$ for the purpose of this calculation. The factor $\bar{m}$ will be referred to as the dimensionless electron mass. We can see that Eq.(3.35) defines a relativistic plasma frequency:

$$\mu^2 = \frac{\omega_{p0}^2}{\bar{m}}. \tag{3.36}$$

We refer to the process of finding of μ^2 as the photon (or plasmon) renormalization, and to the value of μ^2 itself as the "photon mass" (or "plasmon" mass).

The procedure of renormalizing the photon mass to the lowest order is very simple and essentially consists of making $\mathcal{H}_i'$ vanish, assuming that the electron field ψ is unperturbed and given by Eq.(2.53). As we carry out the renormalization to higher orders, ψ is perturbed by the interactions with EM field, and deriving the corresponding wave equation, similar to Eq.(3.34) becomes increasingly complicated. A systematic diagrammatic expansion becomes the only alternative.

Since to make the Hamiltonian $\mathcal{H}_i'$ we did not assume anything about the field A_μ (whether it is a photon or a plasmon), we realize that μ^2 is the same for both photons and plasmons, which justifies our adding a counter term $\mathcal{L}_{em}$ to the total Lagrangian in Section 3.1. This conclusion will not be true as we renormalize the photon and plasmon masses to higher orders. This, however, will not be true to higher orders in perturbation theory, and photons and plasmons will have to be

renormalized separately, each with its own "mass".

The dimensionless renormalized mass of the electron, $\bar{m}$, is different from unity, its unperturbed value, because, in the presence of a strong electromagnetic wave and the plasma, the effective mass of the electron changes. The renormalization of an electron mass to include oscillations in a strong EM field has been known for many years [46]-[49] and gives rise to a frequency shift of light scattered by a single electron. On the other hand, the effect of the *collective* mass renormalization that occurs through the Coulomb repulsion of plasma electrons when they are bunched by the ponderomotive force of the EM field was recognized only recently [14]. In the next section we first correct $\bar{m}$ for the single-particle oscillation in an intense EM field (which is a zeroth order in ϵ effect) and then develop a power series in ϵ for $\bar{m}$ that will include the first-order result of Rax and Fisch [14].

3.2.2 Renormalization of the Electron Mass and Counting Rules

To calculate the rescaling of the electron mass in the field of the EM pump first assume that a linearly polarized plane-wave pump is present at $t = 0$:

$$\frac{e\vec{A}(x)}{m} = \vec{e}_x \left(\frac{a_0^*}{2} e^{ik_0 \cdot x} + \frac{a_0}{2} e^{-ik_0 \cdot x} \right). \tag{3.37}$$

The change in the electron mass due to the $\mathcal{H}_i'$ is pictorially described in Fig. 3-5. In drawing these diagrams we follow our previous convention: terms that are proportional to $e^{ik_0 \cdot x}$(the absorbed photons) are drawn above and the terms proportional to $e^{-ik_0 \cdot x}$ are drawn below the particle line. Crosses at the ends of the photon lines mean that these fields are unperturbed, or using the language of field theory, that these lines are external sources. Hence, for this particular example, each cross carries a factor $a_0/2$ or $a_0^*/2$, as should be clear from Eq.(3.37). The meaning of the above sequence of diagrams in Fig. 3-5 is that to zeroth order in ϵ only those processes that involve both absorption and emission of the pump photons modify the electron propagator.

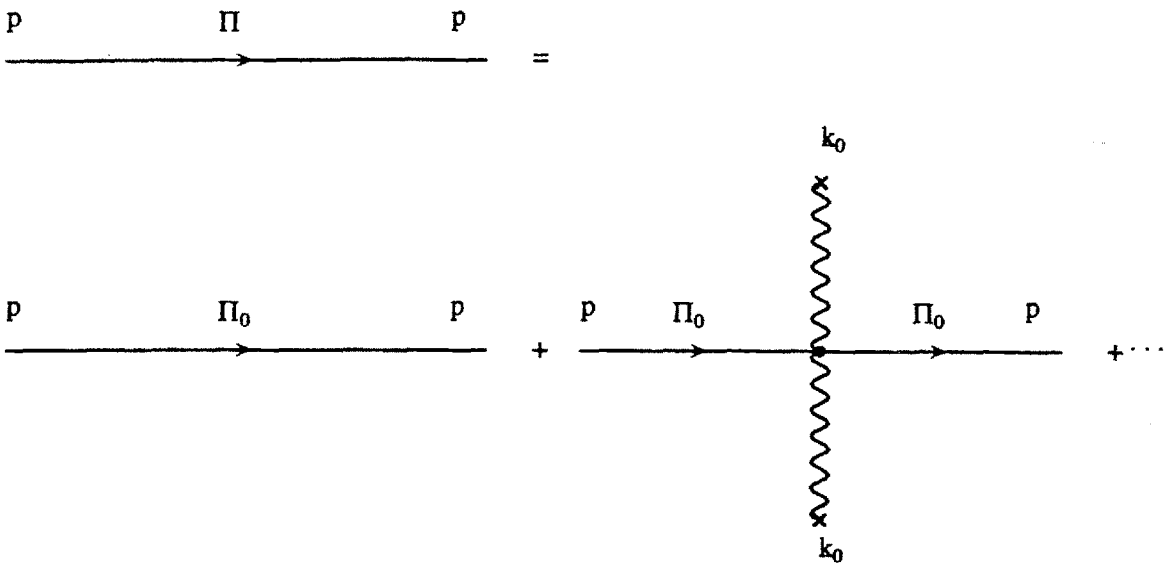

Figure 3-5: Diagrams for renormalizing the electron mass to zeroth order in ϵ (single-particle effect)

We define a space-independent part of the electron propagator, $\Pi(p)$, similarly to the way $D_{\mu\nu}$ was defined for the electromagnetic field in (3.6):

$$\widehat{\psi^*(x_2)\psi}(x_1) = \int \frac{d^4p}{(2\pi)^4}\Pi(p)e^{ip(x_1-x_2)} \tag{3.38}$$

Expanding the diagrammatic sequence and summing the geometric series, analogously to the method used for the modified EM propagator in Section 3.1, we obtain the modified propagator for the electron field:

$$\begin{aligned}\Pi(p) &= \frac{-1}{p^2 - m^2/\hbar^2} + \left(\frac{-1}{p^2 - m^2/\hbar^2}\right)^2 \frac{m^2a_0^2/2}{\hbar^2} + \ldots \\ &= \frac{-1}{p^2 - m^2(1 + a_0^2/2)/\hbar^2}.\end{aligned} \tag{3.39}$$

Note that we have assumed a_0 to be real and that the $a_0^2/2$ factors originate from $(a_0/2)^2$, multiplied by a combinatorial factor 2 (because either one of the A fields in the interaction Hamiltonian $A^2\psi\psi^*$ can be emitted or absorbed).

From the functional form of the modified electron propagator (3.39) we see that the mass of the electron in the presence of an electromagnetic pump is multiplied by

the factor $(1 + a_0^2/2)^{1/2}$. This allows us to calculate the renormalized dimensionless mass of the electron to the zeroth order in ϵ (or μ^2):

$$\bar{m}^2 = (1 + a_0^2/2). \tag{3.40}$$

It is this renormalized mass that has to be used in all calculations, as was done, for instance, in computing the relativistic plasma frequency in Eq.(3.36). The physical meaning of $\bar{m}$ thus becomes clear now—it is equal to time- averaged relativistic factor γ of the electron. We note that this particular result is true only for a linearly polarized pump. The multiplication coefficient for a circularly polarized light would be $(1 + a_0^2)$ instead. The difference between the two cases is that while for a helical pump of amplitude a_0, the rms value of the field is also a_0, for the linear pump the rms is equal to $a_0/\sqrt{2}$.

In Section A we show that the canonical momentum p, which makes the single-particle Hamiltonian space-time independent, corresponds to a "heavier" electron, with the mass given by Eq.(3.39). It is equal to the time-averaged momentum of the electron, as demonstrated by Rax [13].

It is clear that the diagrams in Fig. 3-5 are not the only ones that modify the electron mass. There are higher order diagrams that contribute to renormalization of of the electron propagator, such as the one shown in Fig. 3-6.

The diagrams in Fig. 3-6 are very similar to those in Fig 2-5, which describe the third harmonic generation, which were found to give a zero contribution in Section 2.4.3. And, not surprisingly, the contribution of the diagrams in Fig. 3-6 also vanishes to the lowest order in μ^2. As is true for the third harmonic generation, computing the renormalized electron mass correctly requires both the renormalization of the photons and the inclusion of the restoring space-charge forces that arise in the plasma when it is perturbed by the ponderomotive pressure. The EM wave is again assumed to be of the form given by Eq.(3.37). Diagrammatically, Fig. 3-6 gives the one-level second order (in the interaction Hamiltonian) modification to the electron propagator. As was demonstrated by Eqs.(2.88,2.91), these diagrams give a non van-

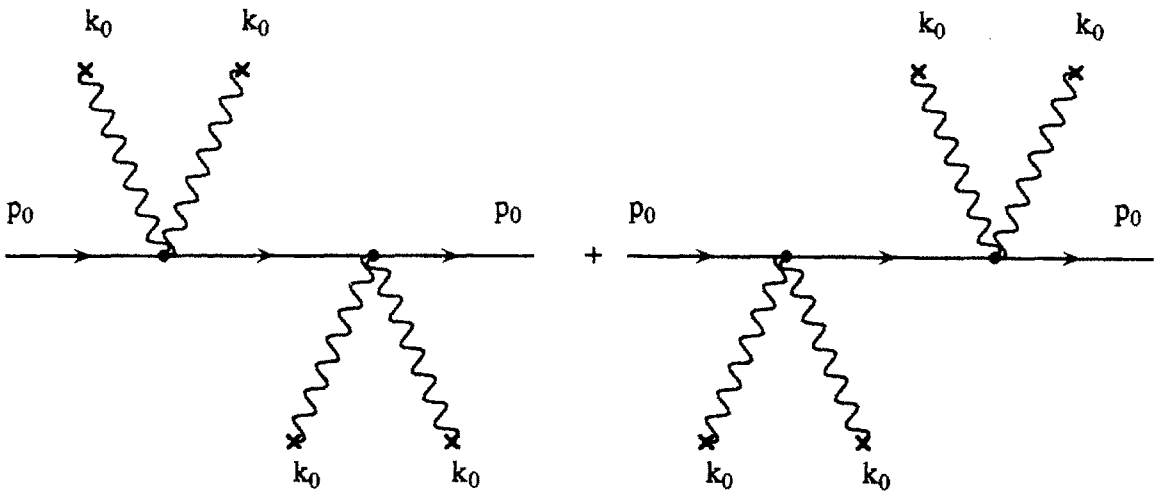

Figure 3-6: Diagrams for renormalizing the electron mass to first order (in ϵ) renormalization; no space charge fields

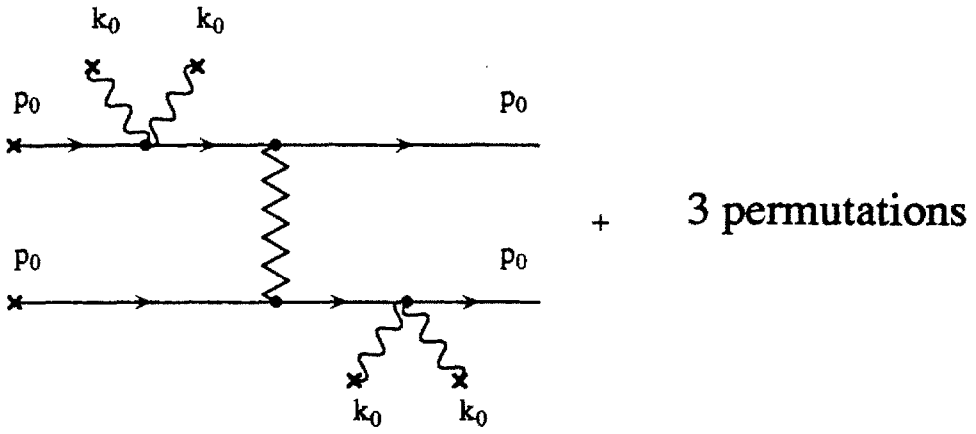

Figure 3-7: First order in ϵ electron mass renormalization, due to space charge fields

ishing contribution if we allow for $k_{0\mu}k_0^\mu \neq 0$. Yet we would obtain an incorrect result if we assume that this is *the only* contribution to the electron mass to this order in ϵ. The diagrams that must be included are shown in Fig. 3-7. The three permutations refer to *all* topologically equivalent diagrams.

The convention for drawing higher order diagrams here and elsewhere is: diagrams consist of multiple levels of electron propagators (straight lines), connected to each other by the photon (wiggly lines) or plasmon (zig-zag lines) propagators, with the photon and plasmon uncontracted lines emitted (below the electron line) and absorbed (above the electron line). As stated earlier, crosses on lines mean that

the field (particle, or photon, or plasmon) has to be evaluated unperturbed. Except for this section, we *will not* put crosses on the electron lines to avoid cluttering the drawing. The contracted EM field lines can be photons as well as plasmons, they can originate from absorbing as well as from the scattering vertices.

For the relatively simple process shown considered here only the contracted *plasmon* propagators give a nonzero contribution to the diagrams. In Section 4.3 we consider some processes that involve contracted *photon* propagators (for instance, parametric instabilities); in Section 4.4 we will see the plasmons originating from the scattering vertices (the rate of the second harmonic emission).

From the example of the electron mass modification we see that the concept of the order of perturbation theory is not necessarily very convenient. For instance, the diagrams in Fig. 3-6 which are of the second order have to be combined with the diagrams in Fig. 3-7 which are of the fourth order to get the correct answer to first order in ϵ. What actually matters is the number of uncontracted EM field lines, which is the same for both figures (four lines). Since an artificially small number $\hbar$ is introduced into the equations of motion of the electrons and EM fields, only those diagrams with overall contributions which are independent of $\hbar$, are physically meaningful.

This motivates the introduction of another convenient concept, the level number of the diagram—the number of uncontracted pairs of electron lines. The origin of the name "level number" is easy to understand by looking at the graphical representation of the diagrams in Fig. 3-6 and in Fig. 3-7. The first set has the level number one while the second one has the level number two.

The power P of $\hbar$ that a given diagrammatic contribution is proportional to is given by the following easily derived rule:

$$P = 2L + EP - A - 2S, \tag{3.41}$$

where L is the level number of the diagram, EP is the number of the electron propagators, A is the number of absorption vertices and S is the number of scattering

vertices. If $P > 0$ the diagram can be discarded as small, if $P < 0$ one expects that some cancellations will result from including the permutations of the diagram. For example, evaluating P for each of the diagrams in Fig. 3-6 gives $P = -1$ but combining them together results in the desired $P = 0$. The mechanics of this cancellation is easy to sketch. The first of the two diagrams in Fig. 3-6 contains a propagator equal to

$$\Pi_1 = \frac{-1}{2p_0 \cdot 2k_0 + 4k_0^2}, \tag{3.42}$$

and would have given a contribution proportional to $\hbar$ (since $p_0 = P_0/\hbar$), as Eq.(3.41) indicates—each electron propagator (EP) adds one power of $\hbar$ to the diagram. Nonetheless, the second diagram contains a propagator equal to

$$\Pi_2 = \frac{-1}{-2p_0 \cdot 2k_0 + 4k_0^2}, \tag{3.43}$$

which cancels Π_1 to first order in $\hbar$. The first non vanishing contribution of the sum of the two diagrams occurs to the second power in $\hbar$, which increases the overall contribution of the process in Fig. 3-6 to $P = 0$.

The level of each of the diagrams in Fig. 3-7 can be immediately evaluated as $P = 0$.

The non-zero correction of order ϵ to the mass from the one level diagrams in Fig. 3-6 arrises because EM waves move faster than speed of light in plasmas whereas the contribution of the two level diagrams in Fig. 3-7 is the result of space- charge forces. Naively, this is not surprising since both terms are proportional to ω_p^2. The presence of the virtual plasmons in Fig. 3-7 reflects the fact that electrons experience space-charge forces when a density perturbation proportional to $\exp 2i(\vec{k}_0 \cdot \vec{x} - \omega_0 t)$ is excited by the ponderomotive force of the laser pump. That these two effects have to considered together was realized in [14, 15, 16, 17].

Mass renormalization is explained in a much greater detail in Appendix B. In this section we do it very briefly. We recall that mass renormalization is the process of adding an extra term of the form $-\Delta\bar{m}_1^2 m^2 \psi\psi^*/\hbar^2$ to the unperturbed particle Lagrangian $\mathcal{L}_m$ (2.41), and subtracting the identical term from the interaction La-

grangian to avoid the secular growth of the electron field ψ, as was explained in Section 3.2.1 for the photons.

Adding the contribution of $\Delta\bar{m}_1^2 m^2\psi\psi^*/\hbar^2$ to the contribution of the diagrams in Fig. 3-6 and requiring no secular growth in ψ results in

$$\Delta\bar{m}_1^2 = -\frac{1}{128}\ \frac{|\ a_0\ |^4\ \omega_p^2}{\omega_0^2\bar{m}^3}. \tag{3.44}$$

Comparing $\Delta\bar{m}_1^2$ with the single-particle mass correction, obtained from Eq.(3.40)

$$\Delta\bar{m}_0^2 = \frac{|\ a_0\ |^2}{2}, \tag{3.45}$$

we find that the ratio $\Delta\bar{m}_1^2/\Delta\bar{m}_0^2$ is indeed of order ϵ.

Assuming that $\Delta\bar{m}_1^2 \ll \Delta\bar{m}_0^2$ we obtain an incremental change in renormalized electron mass:

$$\frac{\Delta\bar{m}_1}{\bar{m}} = -\frac{1}{64}\ \frac{|\ a_0\ |^4\ \omega_p^2}{\omega_0^2\bar{m}^5}. \tag{3.46}$$

Analogously, we compute mass corrections from the diagrams in Fig. 3-7. The result obtained by reading off the values of vertices and propagators of the diagrams given in Fig. 3-7 has to be multiplied by a factor of two since there are two "loose" electron lines in each of the diagrams and, thus, two ways to contract an electron field. For more details on quantifying a diagram see Appendix B. The contribution of the diagrams in Fig. 3-7 is equal to

$$\frac{\Delta\bar{m}_2}{\bar{m}} = \frac{1}{128}\ \frac{|\ a_0\ |^4\ \omega_p^2}{\omega_0^2\bar{m}^5}. \tag{3.47}$$

Combining the results of Eqs.(3.46) and (3.47) yields

$$\frac{\Delta\bar{m}}{\bar{m}} = \frac{-1}{128}\ \frac{|\ a_0\ |^4\ \omega_p^2}{\omega_0^2\bar{m}^5}. \tag{3.48}$$

The result quoted by Fisch and Rax gives a numerical coefficient 1/64.

It is rather straightforward to see how the renormalized electron mass can be calculated to higher orders in ϵ. For example, a typical next order contribution to

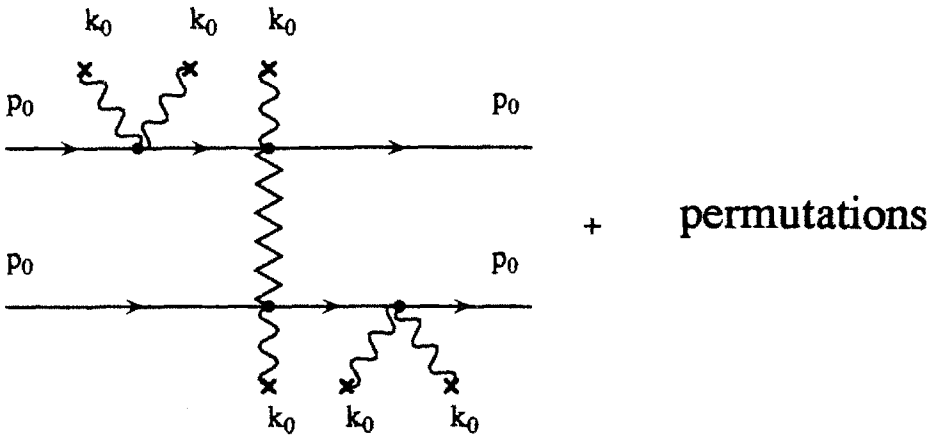

Figure 3-8: An illustration of order ϵ^2 correction to electron mass

the renormalized electron mass is given in Fig. 3-8.

Chapter 4

Application of Diagrammatic Techniques to Laser Plasma Problems

4.1 Third Harmonic Generation with Renormalized Photon Dispersion and Space-Charge Fields

This section revisits the problem of the third harmonic generation by including both the renormalization of the "photon mass" and the space-charge forces ("virtual plasmons" in the language of the diagrams).

The one- and two-level diagrammatic contributions to the third harmonic generation are shown in Fig. 4-1 and Fig. 4-2. This calculation will lead us to an important concept of a "dressed" electron that will be useful in other problems. The non-zero contribution to the third harmonic emission from the one-level diagrams in Fig. 4-1 comes about because EM waves move faster than speed of light in plasmas whereas the contribution of the second-level diagrams in Fig. 4-2 is the result of space-charge forces. The presence of the virtual plasmons in Fig. 4-2 reflects the fact that electrons experience space-charge forces when a density perturbation proportional to $\exp 2i(\vec{k}_0 \cdot \vec{x} - \omega_0 t)$ is excited by the ponderomotive force of the laser pump.

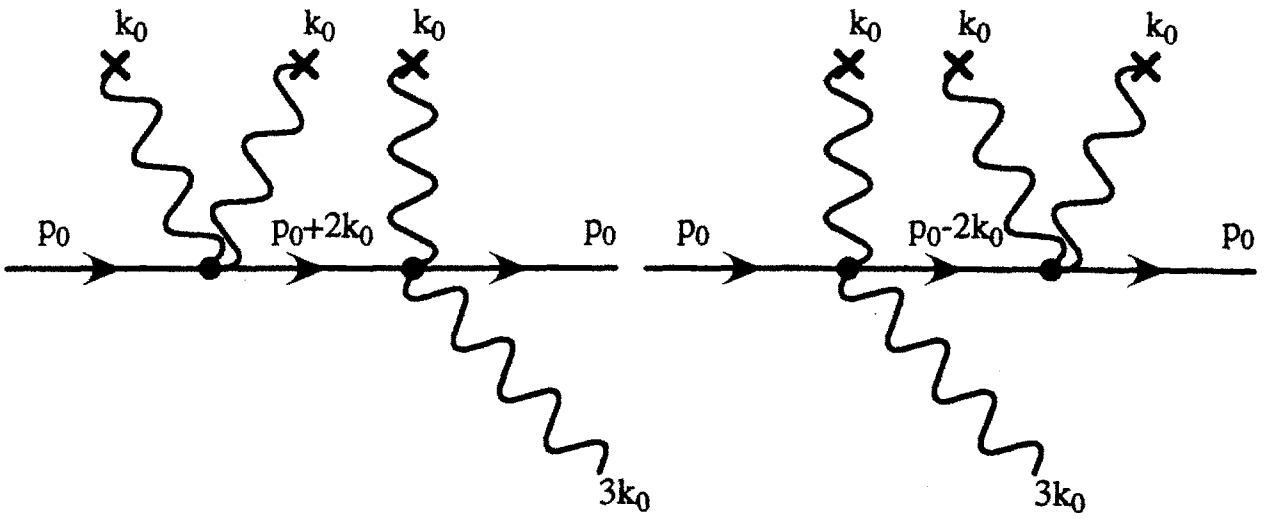

Figure 4-1: Diagrams for the third harmonic generation to first order in ϵ due to modification of phase velocity of the EM waves in the plasma (does not account for space-charge fields).

We notice that all the four diagrams in in Fig. 4-2 are equal to each other to zeroth order in $\hbar$. This allows us to make the following observation: including the virtual plasmons amounts to adding two of the two-level diagrams from Fig. 4-2 to each of the one-level diagrams from Fig. 4-1. Schematically this is shown in Fig. 4-3. In Fig. 4-3 we have temporarily broken our tradition of *not* putting crosses on the uncontracted electron lines in order to emphasize that it is the presence of the surrounding plasma which moves with the four-momentum p_0 that changes the propagation properties of the electron with momentum p.

The diagram in Fig. 4-3 can be quantified as

$$\Pi(p) = \frac{-1}{p^2 - \bar{m}^2/\hbar^2} + \left(\frac{1}{p^2 - \bar{m}^2/\hbar^2}\right)^2 (-\mu^2) \frac{(\delta p \cdot e^L_{\delta p})^2}{(n \cdot \delta p)^2 - \mu^2}, \qquad (4.1)$$

where $\delta p = p - p_0$ and e^L is the unit polarization vector of the plasmon with a four-vector δp, given by Eq.(3.15). The second term in (4.1) is much smaller than the first as long as $\delta p \ll p_0$ (which will always hold for the laser-plasma problems, since $\delta p \propto k_0$), so that we can use the identity $1 + x \approx 1/(1 - x)$ for small x and incorporate the second term in Eq.(4.1) into the denominator of the electron propagator. After some

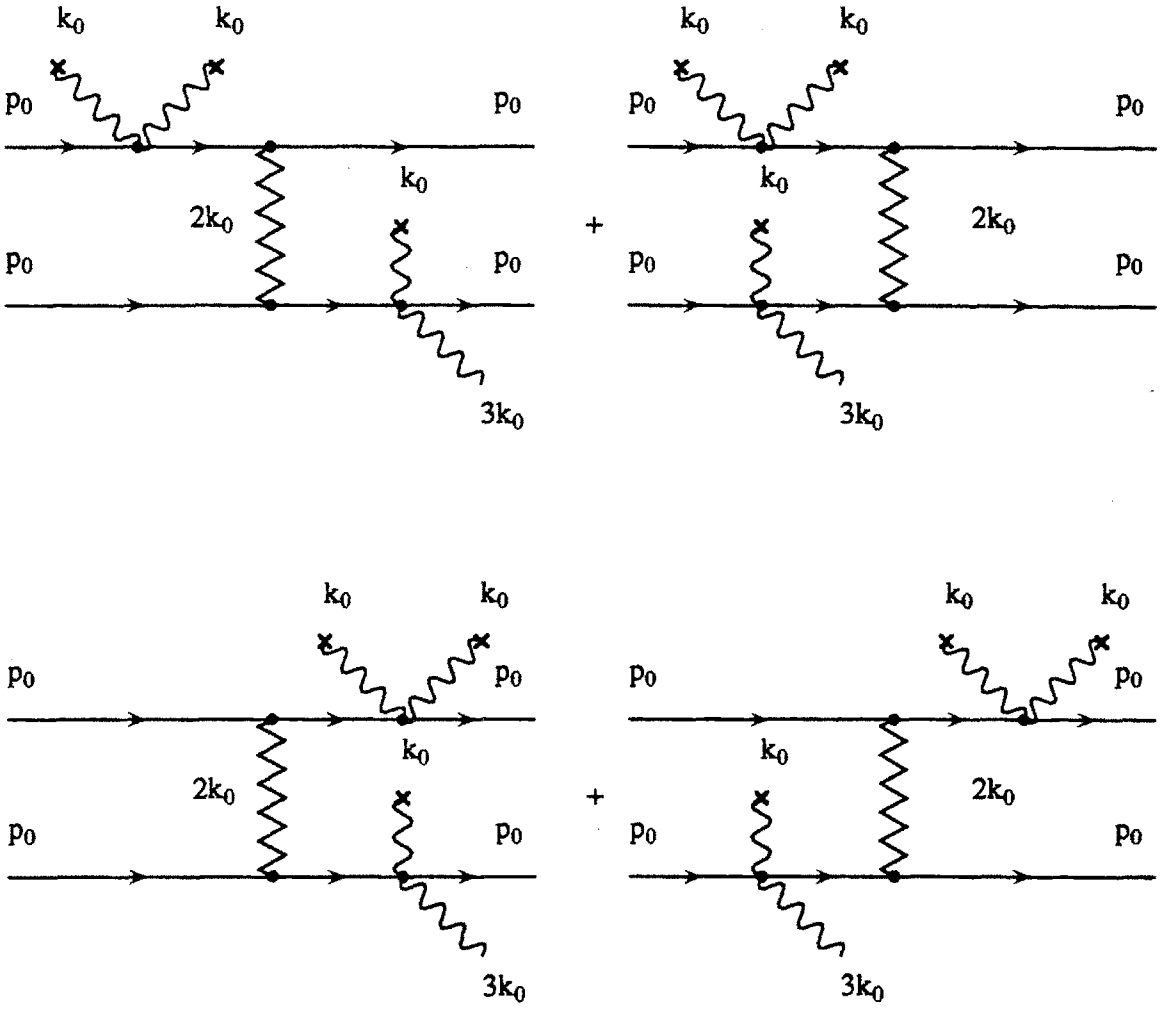

Figure 4-2: Diagrams for the third harmonic generation to first order in ϵ due to space charge fields (does not account for the modification of phase velocity in the plasma).

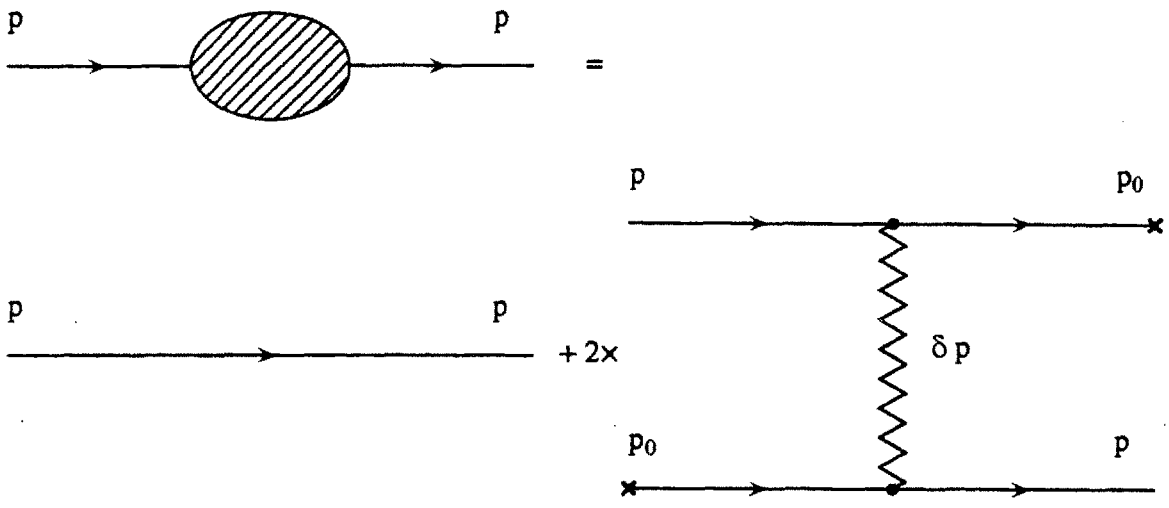

Figure 4-3: Dressed electron propagator

algebra we obtain the following expression for the renormalized electron propagator (which we call the dressed electron propagator):

$$\Pi(p) = \frac{-1}{p^2 - \bar{m}^2/\hbar^2 - \mu^2 \frac{(n\cdot(p-p_0))^2-(p-p_0)^2}{(n\cdot(p-p_0))^2-\mu^2}}. \tag{4.2}$$

This propagator describes the behavior of an electron in the environment of a cold plasma with relativistic plasma density μ^2 moving with a four momentum p_0 pointing in the direction of n in space-time.

We emphasize here that (4.2) is only an approximate propagator, the lowest order of the expansion in powers of $\hbar$. Therefore it can only be used for the processes that need the power P of the diagram to be lowered by one. For some processes (for instance, the second order in ϵ correction to the "photon mass", as shown later in this chapter) more terms in Eq.(4.1) (and, hence, in (4.2)) are needed.

As we have mentioned before, the order P of the diagrams in Fig. 2-5 is to be lowered by one. The concept of a dressed propagator shown in Fig. 4-3 can be used to (schematically) combine the contributions of the diagrams in Figs. 4-1 and 4-2. Combined together, the total contribution (to fist order in ϵ) to the third harmonic generation is now shown in Fig. 4-4.

Assume that the pump wave from Eq.(3.37) is polarized in the direction normal

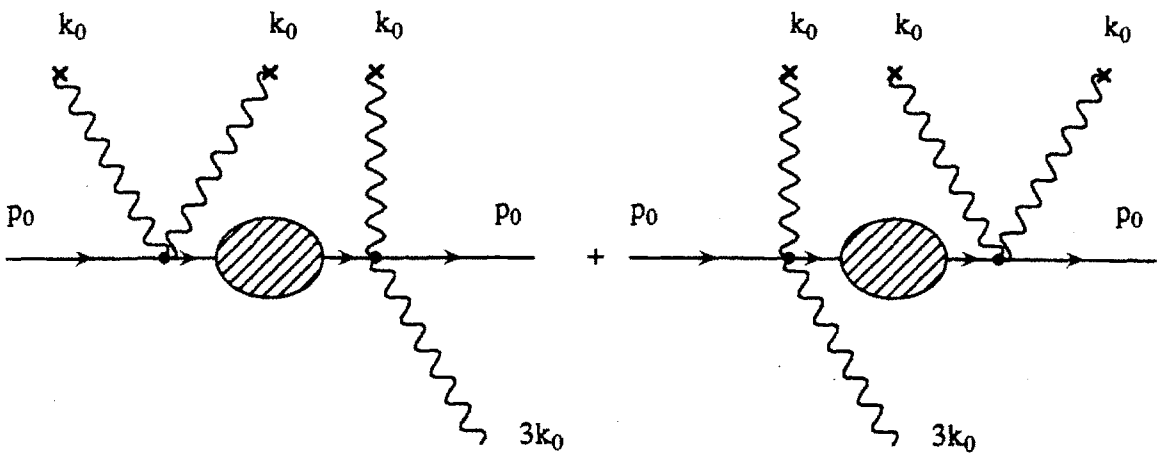

Figure 4-4: Schematic representation of the lowest order third harmonic generation using the dressed electron propagator

to p_0, the direction of the initial plasma motion (which can always be achieved by a Lorentz transformation). This avoids subtleties associated with the rotation of polarization. The polarization of the third harmonic then coincides with the polarization of the pump. Assuming the output radiation in the form of

$$\vec{A}_{3\vec{k}_0} = \frac{\vec{e}_x}{2}\left(A_{3\vec{k}_0}e^{-i3\vec{k}_0 z+i\omega_{3\vec{k}_0}t} + A^*_{3\vec{k}_0}e^{+i3\vec{k}_0 z-i\omega_{3\vec{k}_0}t}\right) \tag{4.3}$$

and quantifying the diagrams in Fig. 4-4 (for details on computing the generation rates with the diagrams, see Appendix B), yields the rate of the 3-d harmonic generation:

$$i2\omega_{3\vec{k}_0}\frac{dA_{3\vec{k}_0}}{dt} = \frac{\mu^2 a_0^3}{16\bar{m}^2}\frac{4k_0^2-\mu^2}{4(n\cdot k_0)^2-\mu^2}. \tag{4.4}$$

In deriving Eq.(4.4) we have neglected the phase velocity mismatch between the pump and the third harmonic. Had we taken the mismatch into account, the amplitude of the third harmonic radiation would not be growing linearly with time. Instead, with the mismatch frequency

$$\Delta\omega = \omega_{3\vec{k}_0} - 3\omega_{\vec{k}_0}, \tag{4.5}$$

we find that the amplitude of the third harmonic oscillates with time and is given by

$$i2\omega_{3\vec{k}_0}A_{3\vec{k}_0} = \frac{e^{\Delta\omega t}-1}{i\Delta\omega}\frac{\mu^2 a_0^3}{16\bar{m}^2}\frac{4k_0^2-\mu^2}{4(n\cdot k_0)^2-\mu^2}. \tag{4.6}$$

The phase velocity mismatch between the pump and the third harmonic limits the amplitude growth, as was found in [14]-[17].

This, in turn, suggests a scheme for generating the third harmonic which consists of a combination of two lasers propagating at a small angle to each other, that does not suffer from the phase velocity mismatch. In Section 4.4, for the first time, we illustrate the basic idea of this scheme by calculating the rate of the *second* harmonic emission. To achieve the phase matching condition the perturbative calculation (of both the third and the second harmonic generation) has to be carried out to second order in ϵ which has not, to our knowledge, been done before.

With a stationary plasma, $n^0 = 1, \vec{n} = 0$ and $\mu^2 \ll \omega_0^2$ we recover the growth rate of the *amplitude* of the third harmonic generation obtained by Rax and Fisch:

$$i2\omega_{3\vec{k}_0}\frac{dA_{3\vec{k}_0}}{dt} = \frac{3\mu^4 a_0^3}{64\bar{m}^2\omega_0^2}. \tag{4.7}$$

Recall that $\mu^2 = \omega_{p0}^2/\bar{m}$, so, for $a_0 \gg 1$ the rate of harmonic generation actually decreases with the strength of the pump.

4.2 Higher Order Nonlinear Correction to Photon Dispersion

The diagrammatic method allows for a straightforward calculation of the higher order corrections to the photon dispersion relation as well. One can calculate a dispersion relation for an electromagnetic wave in the presence of another EM wave. One of the obvious applications of this calculation is the so-called Stimulated Raman Scattering which we analyze later in Section 4.3. As a simpler example we consider the modification to the photon mass μ^2.

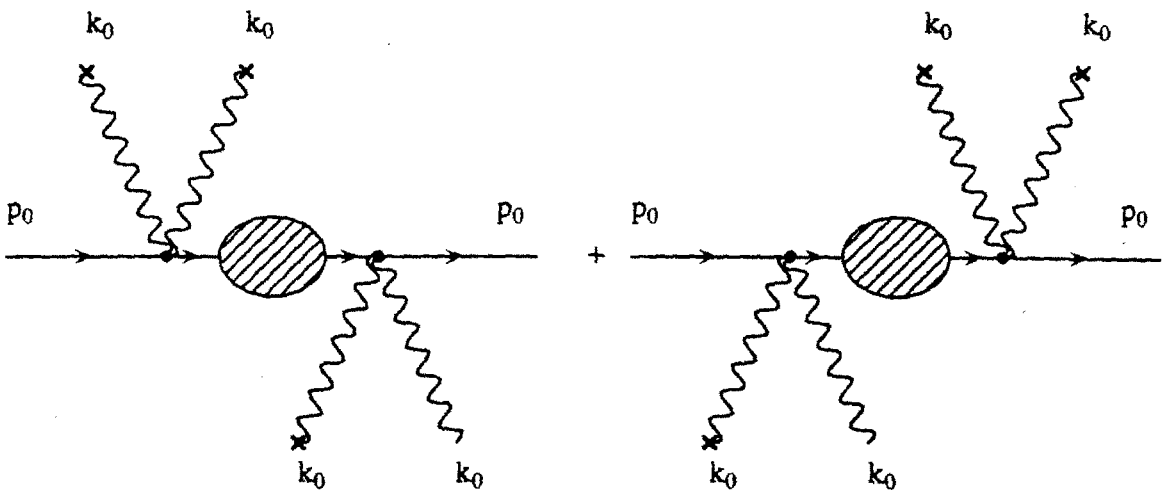

Figure 4-5: Diagrams for the first order in ϵ nonlinear correction to photon dispersion relation in the plasma.

The physics of the first order in ϵ modification is rather straightforward: the high-frequency ponderomotive potential of the electromagnetic wave (which varies as $\exp[i2k_0 \cdot x]$) creates a density perturbation which serves as a scattering grating for the electromagnetic wave. The EM wave is assumed to be of the form given by Eq.(3.37). Diagrammatically, the process is shown in Fig. 4-5.

Again, to account properly for the space-charge forces induced by the laser pulse one has to use the "dressed" propagator for the electron given by Eq.(4.2). Quantifying the diagrams in Fig. 4-5 results in

$$\Delta\mu^2 = -\frac{3\omega_p^4 \mid a_0 \mid^2}{32\tilde{m}^4\omega_0^2}. \tag{4.8}$$

Below we consider the second order in ϵ modification to the photon dispersion relation. It is given here to demonstrate a certain (formal) difficulty that arrises when one tries to cancel out unphysical contributions that are inversely proportional to $\hbar$. The second order correction to μ^2 (neglecting for the moment the space-charge contributions which will be accounted for later) is given schematically in Fig. 4-6. Expanding the contributions of the diagrams in Fig. 4-6 in powers of $\hbar$ results in

$$\frac{\Delta\mu^2}{\mu^2}\frac{16\hbar^4}{a_0^4} = \frac{2}{(2p_0 \cdot \chi)^2} + \frac{6\chi^4}{(2p_0 \cdot \chi)^4}, \tag{4.9}$$

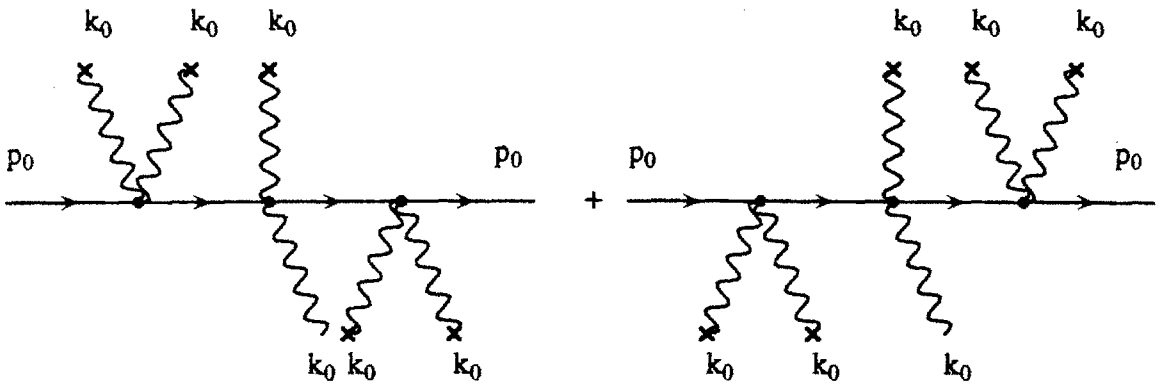

Figure 4-6: Diagrams for the second order in ϵ correction to photon dispersion relation due to the modification of the phase velocity of the EM waves in the plasma (does not account for the space-charge fields).

where $\chi = 2k_0$. Notice that the contribution to $\Delta\mu^2$ from the first term in Eq.(4.9) is inversely proportional to $\hbar^2$. To understand how this anomalous term gets cancelled one has to consider two related sets of diagrams (the top two and the bottom two) given in Fig. 4-7. If $k_1 = k_2 = k_0$ (as it should be since there is only one intense wave in the problem), it is clear that each of the diagrams in Fig. 4-7 involves an infinite propagator (division by zero). This difficulty is formally circumvented by assuming that the absorbed photons have a wavenumber k_1 and the emitted have the wavenumber k_2, as shown in Fig. 4-7. The contributions of the diagrams can be evaluated as

$$\begin{aligned}
\frac{\Delta\mu^2}{\mu^2}\frac{16\hbar^4}{a_0^4} &= \left(\frac{1}{2p_0\cdot\chi_1} - \frac{\chi_1^2}{(2p_0\cdot\chi_1)^2} + \frac{\chi_1^4}{(2p_0\cdot\chi_1)^3}\right)\left(\frac{1}{2p_0\cdot\Delta\chi} - \frac{(\Delta\chi)^2}{(2p_0\cdot\Delta\chi)^2}\right) \\
&+ \left(-\frac{1}{2p_0\cdot\chi_2} - \frac{\chi_2^2}{(2p_0\cdot\chi_2)^2} - \frac{\chi_2^4}{(2p_0\cdot\chi_2)^3}\right)\left(\frac{1}{2p_0\cdot\Delta\chi} - \frac{(\Delta\chi)^2}{(2p_0\cdot\Delta\chi)^2}\right) \\
&+ \left(\frac{1}{2p_0\cdot\chi_2} - \frac{\chi_2^2}{(2p_0\cdot\chi_2)^2} + \frac{\chi_2^4}{(2p_0\cdot\chi_2)^3}\right)\left(-\frac{1}{2p_0\cdot\Delta\chi} - \frac{(\Delta\chi)^2}{(2p_0\cdot\Delta\chi)^2}\right) \\
&+ \left(-\frac{1}{2p_0\cdot\chi_1} - \frac{\chi_1^2}{(2p_0\cdot\chi_1)^2} - \frac{\chi_1^4}{(2p_0\cdot\chi_1)^3}\right)\left(-\frac{1}{2p_0\cdot\Delta\chi} - \frac{(\Delta\chi)^2}{(2p_0\cdot\Delta\chi)^2}\right),
\end{aligned} \tag{4.10}$$

where $\chi_1 = 2k_1$, $\chi_2 = 2k_2$ and $\Delta\chi = 2(k_1 - k_2)$. Rearanging the terms in Eq.(4.10)

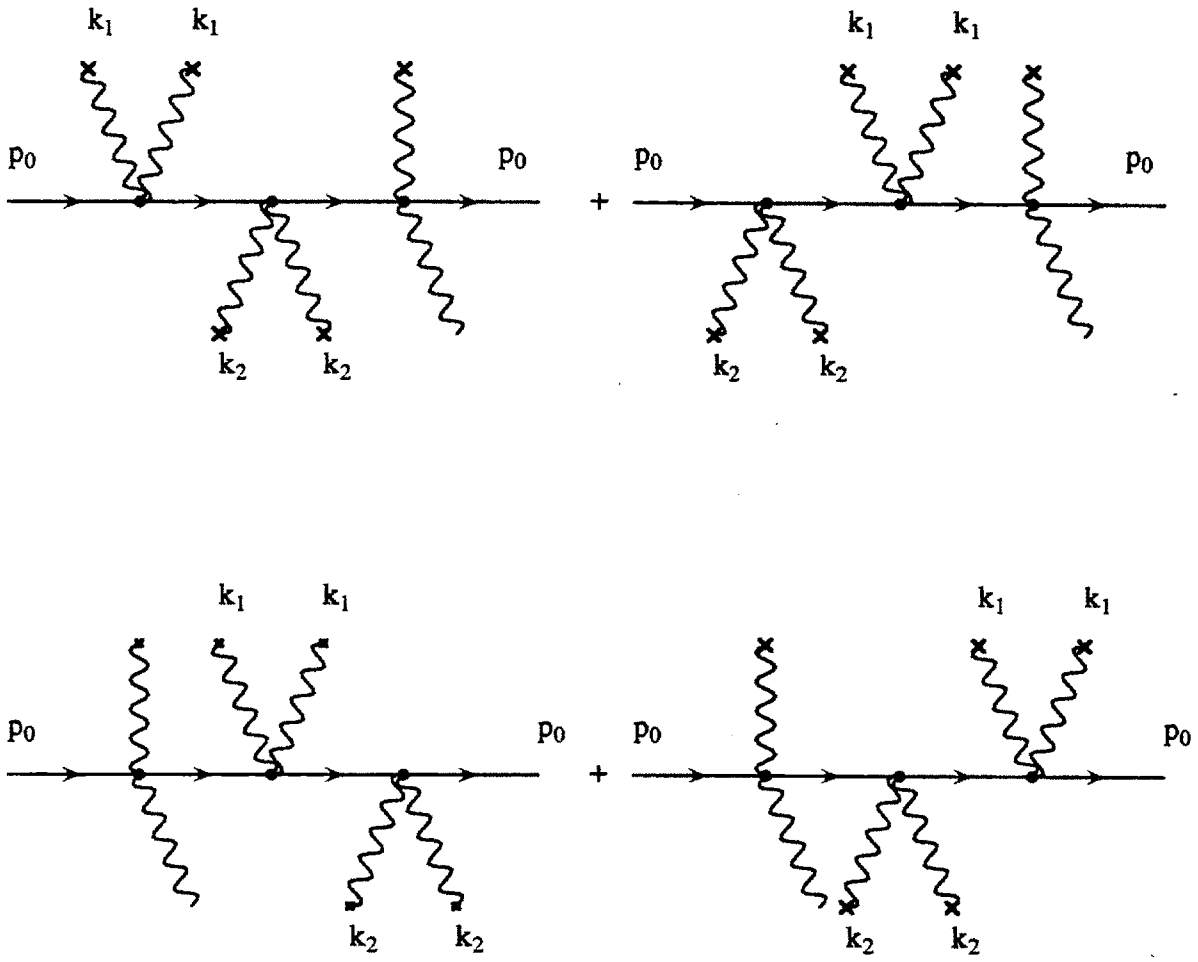

Figure 4-7: Calculation of the "unphysical" contribution to photon dispersion relation; no space charge fields, modified phase velocity

and grouping them by powers of $\hbar$ results in

$$\frac{\Delta\mu^2}{\mu^2}\frac{16\hbar^4}{a_0^4} = -\frac{2}{(2p_0\cdot\chi_1)(2p_0\cdot\chi_2)} + \frac{(\Delta\chi)^2}{(2p_0\cdot\Delta\chi)^2}\left(\frac{2\chi_1^2}{(2p_0\cdot\chi_1)^2}+\frac{2\chi_2^2}{(2p_0\cdot\chi_2)^2}\right) + \frac{2\chi^4}{2p_0\cdot\Delta\chi}\left(\frac{1}{(2p_0\cdot\chi_1)^3}-\frac{1}{(2p_0\cdot\chi_2)^3}\right), \tag{4.11}$$

where $\chi^2 = 4\mu^2$. It is easy to see that the first term in Eq.(4.11) cancels the unphysical contribution of the first term in Eq.(4.9). One can also convince oneself that the second term in Eq.(4.11) is cancelled by the counter term associated with the correction to the electron mass. This counter term is equal and of the opposite sign to $\Delta\bar{m}_1$ given by Eq.(3.46) and shown in Fig. 3-6.

By taking the limit of $k_1 = k_2 = k_0$ in Eq.(4.11) and combining this result with the second term of Eq.(4.9) we obtain for the correction to the "photon mass" from one-level diagrams:

$$\frac{\Delta\mu_1^2}{\mu^2} = 0. \tag{4.12}$$

The representative diagrams contributing to the next level (with the space-charge forces taken into account) are given in Fig. 4-8. Note that the result of the diagrams in Fig. 4-8 has to be multiplied by a factor of four: since the vertex that emits one photon and absorbs one can be drawn either next to the absorbing, or next to the emitting vertex (giving a factor of two) and since the vertex which is drawn on the electron line by itself can be on either side of the plasmon vertex (accounting for another factor of two).

Quantifying the diagrams in Fig. 4-8 yields

$$\frac{\Delta\mu_2^2}{\mu^2} = \frac{12\mu^2\chi^2 D(\chi)a_0^4/16}{(2P_0\cdot\chi)^4}, \tag{4.13}$$

where $D(\chi)$ is a contribution of the "virtual plasmon" in the diagrams in Fig. 4-8, given by

$$D(\chi) = -\frac{(n\cdot\chi)^2-\chi^2}{(n\cdot\chi)^2-\mu^2}. \tag{4.14}$$

Finally, the third level diagrams describing the renormalization of the photon

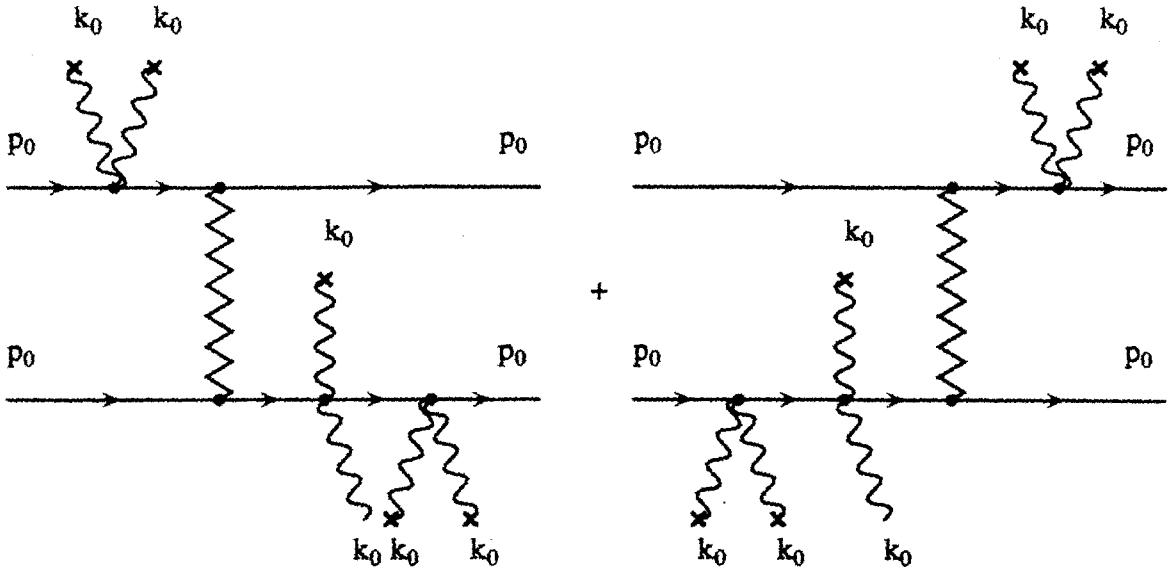

Figure 4-8: Diagrams for the second order in ϵ correction to photon dispersion relation due to *both* space charge fields and modified phase velocity.

mass are given in Fig. 4-9. Here, as in the previous figure, the contributions of the diagrams have to be multiplied by a combinatorial factor four since each of the "sea-gull" vertices can be on either side of the plasmon line. Quantifying the diagrams in Fig. 4-8 yields

$$\frac{\Delta\mu_3^2}{\mu^2} = \frac{2\mu^4 D(\chi)^2 a_0^4/16}{(2P_0\cdot\chi)^4}, \tag{4.15}$$

Adding all three contributions to the renormalized photon mass and keeping the terms up to ϵ^2 results in

$$\frac{\Delta\mu^2}{\mu^2} = \frac{25\omega_{p0}^4 a_0^4}{2048\bar{m}^6\omega_0^4}. \tag{4.16}$$

Using the counting rule Eq.(3.41), it is easy to convince oneself that the diagrams with more than three levels do not contribute to zeroth order in $\hbar$.

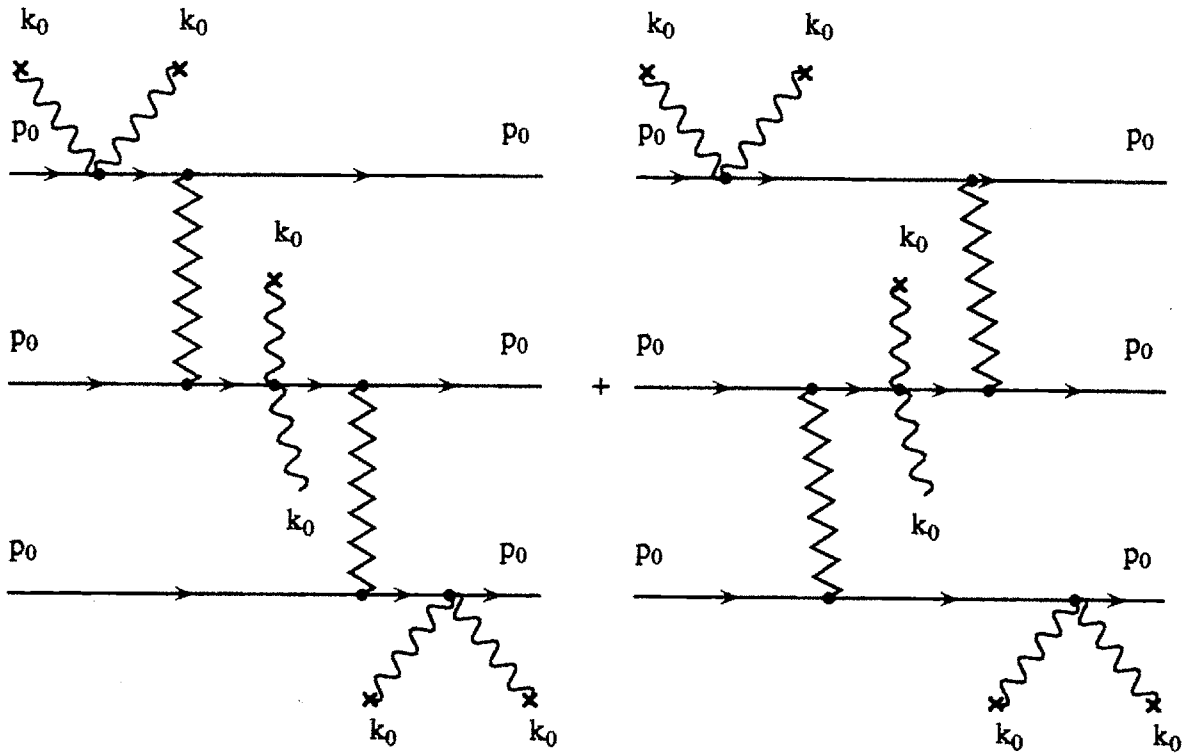

Figure 4-9: Diagrams for the second order in ϵ correction to photon dispersion relation due to space-charge fields (does not account for the modification of the phase velocity of EM waves in the plasma).

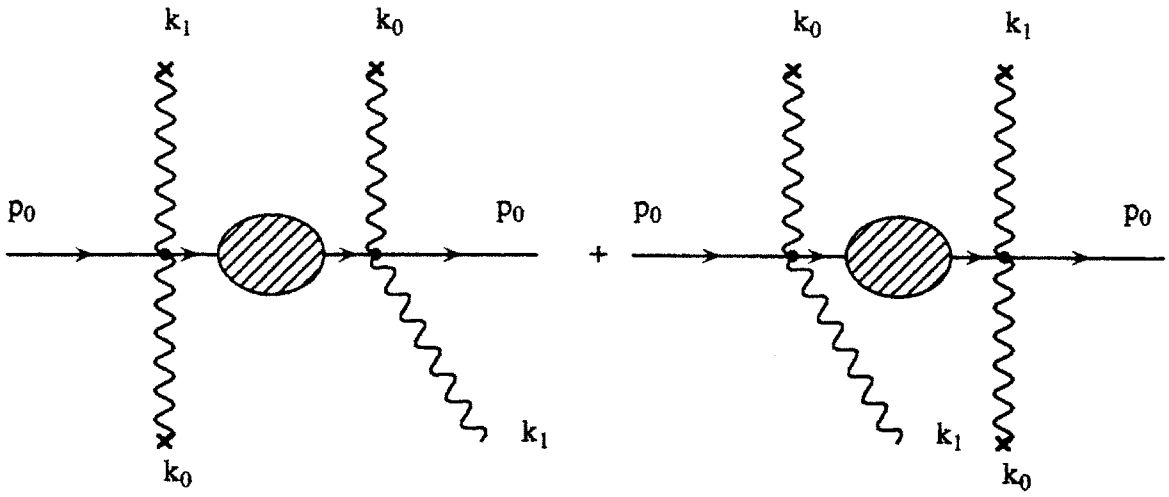

Figure 4-10: Diagrams for the three wave stimulated Raman scattering; both the linear correction to the phase velocity of the EM wave in the plasma *and* the space-charge forces are accounted for by the dressed propagator.

4.3 Parametric Instabilities: Stimulated Raman Scattering

4.3.1 Nonlinear Pump-Probe Interaction

After analyzing various ways the diagrams help to determine the effective masses and cutoff frequencies (an equivalent way of referring to photon masses) in the presence of a single strong electromagnetic wave, it is useful to analyze how the propagation of a weak electromagnetic wave changes in the presence of *another* strong electromagnetic pump. This analysis directly leads us to the description of parametric instabilities in plasma *without* making a weakly-relativistic assumption [34, 35].

Assume that a weak electromagnetic probe a_1, with wavenumber k_1, propagates in a homogeneous plasma in the presence of a strong pump, of amplitude a_0, with wavenumber k_0. Then, to lowest order in μ^2, the correction $\Delta\mu_R^2$ to the refraction index of the probe is described diagrammatically in Fig. 4-10.

Physically, the weak probe a_1 and the pump a_0 ponderomotively drive a density perturbation. The pump then scatters off this density perturbation, reinforcing the probe and resulting in additional polarization current. Since the induced current is

linearly proportional to the amplitude of the probe, a_1, the net result is the change of the probe's index of refraction. Computing the values of the diagrams above results in

$$\frac{\Delta\mu_R^2}{\mu^2} = -\frac{a_0^2}{4\bar{m}^2}\frac{\Delta k^2 - \mu^2}{(n\cdot\Delta k)^2 - \mu^2}, \tag{4.17}$$

where

$$\Delta k = k_1 - k_0. \tag{4.18}$$

For a stationary plasma ($\vec{n} = 0$), Eq.(4.17) takes on the form

$$\frac{\Delta\mu_R^2}{\mu^2} = -\frac{a_0^2}{4\bar{m}^2}\frac{(\Delta k)^2 - \mu^2}{(\Delta\omega)^2 - \mu^2}, \tag{4.19}$$

It is clear from Eq.(4.19) that the correction to μ^2 is not necessarily small for this physical situation. In fact, the correction can become very significant as $\Delta\omega = \omega_1 - \omega_0$ approaches the relativistic plasma density. The new dispersion relation that the electromagnetic wave satisfies is

$$\omega^2 - \vec{k}^2 - \mu^2 = -\frac{\mu^2 a_0^2}{4\bar{m}^2}\frac{(\Delta k)^2 - \mu^2}{(n\cdot\Delta k)^2 - \mu^2}. \tag{4.20}$$

An interesting experiment can be devised to verify the modified dispersion relation (4.20). Assume that the weak continuous probe of frequency $\omega_1 < \omega_p$ is incident on the region of slightly overdense plasma. The detector on the other side of the plasma region does not register any signal because the probe signal is reflected off the plasma. If a sufficiently powerful short laser pulse, with frequency $\omega_0 > \omega_p$ slightly higher than the plasma frequency is sent through the plasma, the RHS of Eq.(4.20) can become large enough to *lower* the cutoff frequency for the probe sufficiently to allow its penetration through the plasma. The physics of this experiment is easy to understand: the pump and the probe beat ponderomotively and excite a density perturbation. The *pump* scatters off this density perturbation and *downshifts* to the frequency of the probe, at which it is detected on the other side of a plasma region. A detector (which can be preceeded by a spectrometer to provide a better frequency resolution) then registers a spike of radiation at frequency ω_1, of duration roughly

equal to the duration of the intense pulse.

Note that the deleterious effects associated with wavebreaking can be easily avoided by ensuring that the magnitude of the excited density perturbation is small. Indeed, assume that the plasma is overdense by an amount Δn with respect to the weak probe. Then the density modulation required to ensure the propagation of the probe is roughly given by $\delta n_{mod} \approx \Delta n a_1/a_0$ (since the *pump*, not the *probe*, scatters of this density ripple). Since the ratio a_0/a_1 can be rather high, the fractional density perturbation in the plasma wave is very insignificant. The pump and the probe pulses can be launched at an angle to each other to avoid the corrections coming from the four-wave nature of the pump-probe parametric interaction (see the next subsection). Technically, it should be easy to accomplish since the low-power probe can be made wide enough to ensure the overlap of the pump and the probe over the whole interaction region.

4.3.2 Four Wave Stimulated Raman Scattering

It is tempting to use Eq.(4.20) as a full dispersion relation and compute the temporal growth rate of the SRS (which occurs when $(\Delta\omega)^2 \approx \mu^2$) but this misses the (generally) four-wave nature of Raman scattering. The physics is rather straightforward—the density perturbation δn that the pump wave is scattering off can be, in general, resonantly driven by both Stokes and anti-Stokes waves (that is, the EM waves with frequencies below and above the pump frequency, respectively). The four waves that participate in SRS are the pump a_0, the scattered wave a_1, the "virtual" photon a_2, with the wavenumber k_2, and the space-charge wave. Here,

$$k_2 = k_1 - 2k_0. \tag{4.21}$$

SRS is one of the fundamental nonlinear laser- plasma instabilities that has been studied for nearly twenty years because of its relevance to pellet preheat in laser fusion [33], for the novel concept of a fast ignitor where the high-energy electrons are used to ignite the compressed fuel [39], in laser- plasma accelerators where it can result

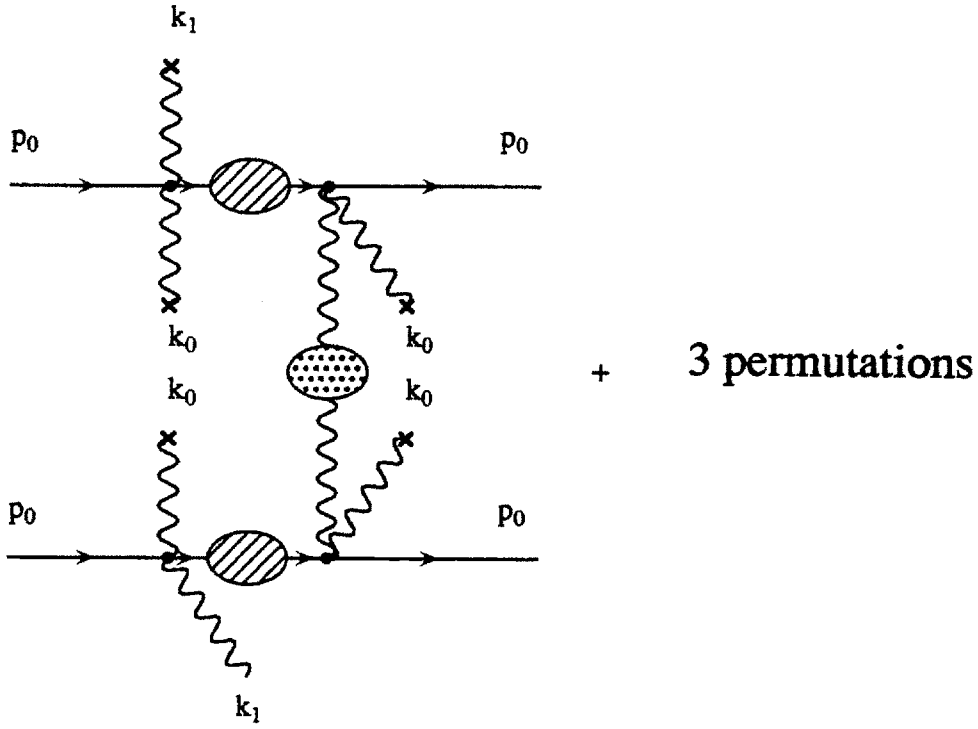

Figure 4-11: Diagrams for the four wave stimulated Raman scattering; both the linear correction to the phase velocity of the EM wave in the plasma *and* the space-charge forces are accounted for by the dressed propagator. The dispersion relation of the virtual photon is modified according to Eq.(4.20), as expressed by the dotted blob.

in a break-up of the laser pulse [15] and distortion of its transverse structure [34, 41]. Note that SRS is not at all restricted to co-linear geometry—the instability can occur when $\vec{k}_1$ *is* or *isn't* parallel to $\vec{k}_0$. In the former case the instability is referred to as forward scattering, while in latter case it is called finite-angle scattering. Another common geometry is the Raman back scattering, when $\vec{k}_1$ points in the direction opposite to $\vec{k}_0$.

In some cases such as Raman back-scattering or large-angle scattering, the instability can be reduced to a three-wave process as only the Stokes component remains resonant [50]. For those processes Eq.(4.20) suffices.

To analyze the small-angle (or forward) Raman scattering one needs to employ two coherent processes: the one shown in Fig. 4-10 and a more complicated processes, diagrammatically shown in Fig. 4-11. The physics behind the diagrams in Fig. 4-10 was explained earlier. For the diagrams in Fig. 4-11, the ponderomotive beating

of the probe a_1 and the pump a_0 results in density perturbation with a wavenumber $\Delta k = k_1 - k_0$, with a space- charge wave associated with it (but by no means necessary for the development of the instability!). The scattering of the pump off this density perturbation results in the emission of a virtual photon a_2 with the wavenumber $k_2 = k_1 - 2k_0$ which, in turn, ponderomotively beats against the pump to result in yet another density perturbation with the wavenumber Δk. Finally, the pump wave scatters off this density perturbation, closing the complicated loop that describes the absorption and emission of a probe wave in the presence of a strong pump. As explained earlier, this process induces polarization currents linear in a_1, which is equivalent to saying that the index of refraction is modified.

The blob on the electron line means that the "dressed" electron propagator has to be used (as given by Eq.(4.2)) to account for the space-charge fields induced by the ponderomotive force. The blob on the "virtual" photon line means that the nonlinear modification to the index of refraction of the "virtual" wave a_2 has to be taken into account, that is, that the relation identical to Eq.(4.20) holds for $(\omega_2, \vec{k}_2)$. Below we calculate the modification of the index of refraction (or change of the photon mass) that results from the SRS process. The resulting dispersion relation can then be used to calculate the temporal rate of the instability, as was done in, for example [35, 50].

Quantifying the above diagram results in

$$\omega_1^2 - \vec{k}_1^2 - \mu^2 = \Gamma(\Delta k) + \frac{\Gamma^2(\Delta k)}{\omega_2^2 - \vec{k}_2^2 - \mu^2 - \Gamma(\Delta k)}, \tag{4.22}$$

where $\Gamma(\Delta k)$ is equal to the RHS of Eq.(4.20):

$$\Gamma(\Delta k) = -\frac{\mu^2 a_0^2}{4\bar{m}^2} \frac{(\Delta k)^2 - \mu^2}{(n \cdot \Delta k)^2 - \mu^2}. \tag{4.23}$$

The first term, Γ, in the RHS of Eq.(4.22) is the renormalization of the first (k_1) photon from the diagrams in Fig. 4-10. The same is the origin of Γ in the denominator of the second term in the RHS, only it reflects the renormalization to the *second* (k_2) photon from the diagrams in Fig. 4-10. Γ^2 in the numerator of the second term in the

RHS is the sum of products of two dressed electron propagators in Fig. 4-11, from all four permutations. Overall, the first term in the RHS of Eq.(4.22) describes the three wave scattering shown in Fig. 4-10 while the second term describes the four wave scattering shown in Fig. 4-11.

Simplifying Eq.(4.22) leads to the dispersion relation:

$$\frac{\mu^2 a_0^2(\mu^2-(\Delta k)^2)}{4\bar{m}^2}\left(\frac{1}{\omega_1^2-\vec{k}_1^2-\mu^2}+\frac{1}{\omega_2^2-\vec{k}_2^2-\mu^2}\right)=(\Delta k\cdot n)^2-\mu^2, \qquad (4.24)$$

where Δk and k_2 are described by Eqs.(4.18, 4.21). Eq.(4.24) describes a linear evolution of a three dimensional stimulated Raman scattering of a strong pump a_0 into a weak wave a_1 by a cold electron beam moving in the direction of a unit four-vector n. The expression is valid for arbitrary pump strength a_0.

A more familiar expression can be obtained by simplifying Eq.(4.25) to the case of the stationary plasma:

$$\frac{\mu^2 a_0^2(\mu^2-(\Delta k)^2)}{4\bar{m}^2}\left(\frac{1}{\omega_1^2-\vec{k}_1^2-\mu^2}+\frac{1}{\omega_2^2-\vec{k}_2^2-\mu^2}\right)=(\Delta\omega)^2-\mu^2, \qquad (4.25)$$

where $\bar{m}^2=(1+a_0^2/2)$ and $\mu^2=\omega_p^2/\bar{m}$. This result is similar to those reported by [34, 35] except that no weakly relativistic assumption is made in deriving Eq.(4.25).

The dispersion relation (4.25) can be used to describe the spatio-temporal evolution of Stimulated Raman Scattering for a finite-angle scattering as well as forward and back-scattering (see, for example, Ref.[52]). We note, though, that the result will be the leading term to order ϵ only for the forward and small-angle scattering (such that $\delta\theta<\mu^2$, where $\delta\theta$ is the angle between the pump and the probe). For the case of, say, back-scattering, the smallness parameter becomes $\tau=\frac{a_0^2/2}{1+a_0^2/2}$, and the higher order corrections in this parameter can be calculated by considering the diagrams given in Fig. 4-12. As was shown by Esarey [16], if one neglects space-charge forces and assumes that EM waves propagate in plasma with exactly the speed of light, all the corrections can be summed, yielding combinations of Bessel functions. We recover these results in the Appendix A. A complete classification of Raman scattering with

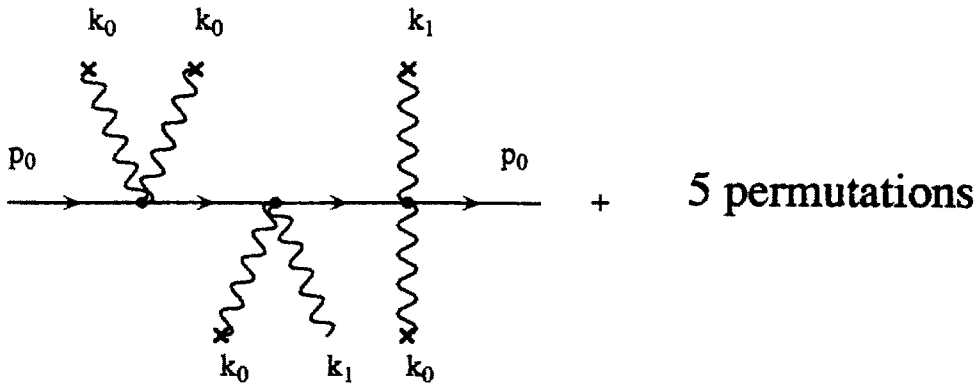

Figure 4-12: Large angle stimulated Raman scattering

the scattering angle $\delta\theta$ for a weakly relativistic case is given by Antonsen [34].

4.4 Second Harmonic Generation from Homogeneous Plasma

4.4.1 Introduction: Second Harmonic Emission From Inhomogeneous plasma

Second harmonic generation from underdense inhomogeneous plasma has been observed in the past [70, 71, 72] and was usually associated with filamentation. The theoretical basis for the second harmonic generation from filamented plasmas is also fairly well developed and understood [16, 70, 71]. Yet the bulk of the experiments [70, 71] was carried out at relatively small laser intensities (typically, $I_0\lambda_0^2 < 10^{15}W\mu^2/cm^2$, or $a \simeq 3 \cdot 10^{-2}$), and thus did not experience significant relativistic (and thus ponderomotive) effects.

We first review the physics of second harmonic generation from a transversely inhomogeneous stratified plasma in slab geometry. This will develop the qualitative foundation for calculating the emission rate from a homogeneous plasma. The mechanism of the harmonic generation is fairly straightforward. The basic model is of a plasma which is non-uniform in one of transverse dimension, so that $n_0 = n_0(x)$, and an intense laser pulse of the form

$$\frac{e\vec{A}}{mc^2} = \vec{e}\left(\frac{a_0^*}{2}e^{ik_0\cdot x} + \frac{a_0}{2}e^{-ik_0\cdot x}\right), \tag{4.26}$$

polarized in $x-y$ plane, and propagating along the z axis. In Eq.(4.26), $\vec{e} = (e_x, e_y)$ is a unit vector in the transverse plane. The laser is uniform in $x-y$ plane (at least on a scale of the amplitude of the electron oscillation, which is only a fraction of the laser wavelength), so that conservation of canonical momentum results in

$$\vec{v}_{0t} = \vec{e}v_{osc}e^{i(k_0z-\omega_0t)} + cc., \tag{4.27}$$

where v_{osc} is the jitter velocity in the field of the laser given by

$$\frac{v_{osc}}{c} = \frac{a_0}{2\gamma}. \tag{4.28}$$

The continuity equation can be used to obtain the density modulation:

$$\delta n = -i\frac{v_{osc}}{\omega_0} e_x \partial_x n_0 \exp i(k_0 z - \omega_0 t) + c.c. \tag{4.29}$$

The laser scatters off this density modulation, δn, driving a nonlinear current $J_{2\omega_0}$

$$J_{2\omega_0} = -i\left(\frac{\lambda_0 e_x \partial_x n_0}{2\pi n_0}\right)\frac{a_0^2 e c n_0}{4\gamma} \exp i(2k_0 z - 2\omega_0 t) + c.c. \tag{4.30}$$

The current $J_{2\omega_0}$ excites the second-harmonic radiation. The rate of second harmonic is found from the eikonal approximation to Maxwell's equations:

$$i2(2\omega_0)\frac{da_2}{dt} = -i\left(\frac{\lambda_0 e_x \partial_x n_0}{2\pi n_0}\right)\frac{\omega_p^2 a_0^2}{2\gamma}, \tag{4.31}$$

where the second harmonic amplitude is a_2.

We see that a plasma density gradient is crucial for producing the second harmonic emission. In low intensity laser-plasma interactions plasma non-uniformities often develop through laser filamentation [70]. Filamentation typically results from self-focusing of laser pulses. Filaments originate either from hot spots of the laser beam, or from the whole-beam self-focusing [70].

One concludes immediately from Eq.(4.31) that, to lowest order in a_0^2, the second harmonic can only be produced if the incident laser is polarized in the direction of density gradient ($x-$ direction in the example above). A laser polarized normal to the density gradient (in $y-$ direction) will not be able to drive the density perturbation (4.29), and thus will be unable to generate the second harmonic.

4.4.2 Lowest Order Second Harmonic Generation from Homogeneous Plasma

The example considered above totally neglected the ponderomotive effects. Thus, its validity is limited to low-power, long-pulse laser- plasma interactions. Ponderomotive forces exerted on plasma electrons by high-intensity lasers lead to a new mechanism for harmonic generation. One might expect that a transversely inhomogeneous laser beam would create a non-uniform current at the second harmonic (through the ponderomotive force) and thus result in second harmonic generation. In fact, it was argued [71] that propagating a Gaussian (in the transverse dimension) laser beam through homogeneous plasma would result in harmonic generation. The authors in [71] have calculated the far-field emission from a finite size (but large compared to the laser wavelength) plasma. Yet in another publication [16] it was proven, using a fluid model for laser-plasma interactions, that no second harmonic is produced from the homogeneous plasma even if the laser pulse itself is inhomogeneous. The calculation in [16] was carried out to the same order in a_0^2 as the one in [71]. Below we resolve this controversy to the lowest order in a_0^2 in favor of [16] by calculating *correctly* the far fields from a finite size plasma. The alternative diagrammatic proof is also given. Note that the conclusion of Ref. [16] is true only to the *lowest* order in a_0^2. In Section 4.4.3 we show, for the first time, that generation of the second harmonic is *possible*, to the next order in a_0^2.

The electron fluid in the field of a strong electromagnetic wave experiences the ponderomotive acceleration [50]:

$$\frac{\partial \vec{v}_2}{\partial t} = -\left(\frac{e}{mc}\right)^2 \nabla(\vec{A}\cdot\vec{A}/2), \tag{4.32}$$

where $\vec{A}(\vec{r},t)$ has an arbitrary spatial profile and is assumed to be given by the incident laser pulse, with frequency ω_0. Consistent with the assumption of a tenuous plasma, we have neglected the re-radiated fields (oscillating with frequency $2\omega_0$).

The accelerated electrons at position $\vec{r}=0$ will emit a second harmonic radiation

with an electric field, at position $\vec{r}$ and time t, given by

$$\vec{E} = \frac{e}{c^2}\frac{\vec{r} \times [\vec{r} \times \dot{\vec{v}}_2(t')]}{r^3}, \tag{4.33}$$

where $t' = t - r/c$ is the delayed time [66].

We now assume that the uniform density plasma occupies a region in space of size $L >> \lambda_0$ and examine the fields outside of plasma at location $\vec{r}$. Assuming $r >> L$ (far field), the electric field of the second harmonic can be expressed as

$$\vec{E} = -\frac{e^3 n_0}{2m^2c^4}\frac{\vec{r}}{r^3} \times \left[\vec{r} \times \int d^3r' \nabla^{(1)}_{r'} \vec{A}^2(r', t')\right], \tag{4.34}$$

where $\nabla^{(1)}_{r'}$ denotes a gradient in the *first* argument of A^2. To the leading (zeroth) order in L/r

$$t' = t - \frac{r}{c} + \frac{\vec{n} \cdot \vec{r}\,'}{c}, \tag{4.35}$$

where $\vec{n} = \vec{r}/r$. Using (4.35), $\nabla^{(1)}_{r'}$ can be expressed as

$$\nabla^{(1)}_{r'} = \nabla_{r'} - \vec{n}\frac{\partial}{c\partial t}. \tag{4.36}$$

Substituting (4.36) into (4.34), integrating the first term by parts and using the obvious identity $\vec{n} \times \vec{r} = 0$, we find that the far-field second harmonic radiation from homogeneous plasma, to the lowest order in $\vec{A}^2$, is equal to zero. Note that one does not even have to assume *any* particular temporal or spatial profile of the incident radiation—the fact that the plasma is homogeneous and the only force acting on the electrons is the ponderomotive force of the laser is sufficient to prove that no second harmonic emission occurs (to first order in a_0^2, of course). Since the spatial and temporal profile of $\vec{A}$ is unspecified, nothing can yet be learned about matching of phase velocities of the fundamental and second harmonics. This issue is addressed in the next subsection.

In the present calculation we have neglected the incoherent component of the radiation which arrises because of the discreteness of the electrons. Also, the result

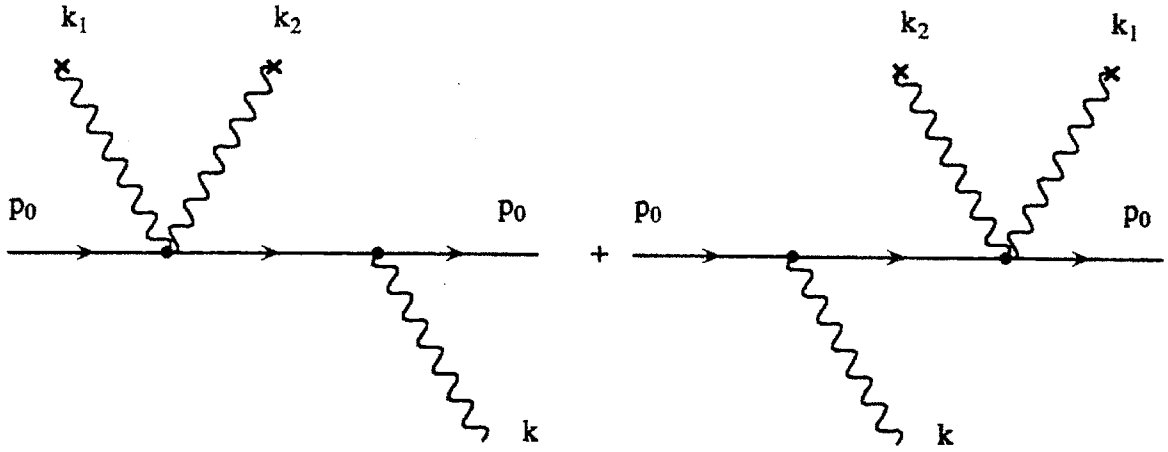

Figure 4-13: Diagrams for the zeroth order in ϵ (vanishing) second harmonic emission.

would not have been zero had the plasma been initially inhomogeneous, since the integration by parts would have resulted in a non-zero term.

We now re-examine the problem of second harmonic generation from a homogeneous plasma, to lowest order in ϵ (and, incidentally, in the amplitude a^2 when it is small) using the diagrammatic technique. Assuming that the laser field at $t = 0$ consists of two non-collinear planar waves with wave numbers k_1 and k_2, the process of emitting a photon with wavenumber $k = k_1 + k_2$ is described diagrammatically in Fig. 4-13. It is easy to see that the emitting vertex is identically equal to zero because the photons, by choice of gauge and orthogonality condition (3.16), are orthogonal both to p_0 and to k. Thus, to the lowest order, the second harmonic generation from a homogeneous plasma is *dynamically* prohibited. We refer to a process as a *dynamically prohibited* if its rate is equal to zero and *kinematically prohibited* if a simultaneous matching of wavenumber and frequencies is not possible. As we show later, the second harmonic is prohibited both kinematically and dynamically, to lowest order. Higher order contributions give a nonzero second harmonic production, as shown below.

4.4.3 Higher Order Second Harmonic Emission

While the vanishing rate obtained in the previous subsection motivates extending the analysis to higher order in a_0, the physics of the second harmonic generation from an inhomogeneous plasma, as explained in Section 4.4.1, lends us an intuition as to *why* going to the next order might give a non-vanishing rate. Indeed, imagine a process where a ponderomotive force of two planar waves creates an inhomogeneous perturbation to the equilibrium plasma density. This inhomogeneous density acts as a seed $n_0(x)$ for the generation process described in Section 4.4.1 by Eq.(4.29). In addition, as we show later, there is a different higher order process that can lead to second harmonic generation. Thus, with a good candidate process for the second harmonic generation established, one has to verify that the secular growth of the second harmonic is kinematically allowed by analyzing the condition for phase matching of a two-wave process involving plane waves with wave numbers k_1 and k_2.

The dispersion relation for the photons is similar to the one for the relativistic particles: $p^2 = m^2/\hbar^2$ for the particles and $k^2 = \mu^2$ for the photons. Examining the interaction in the rest frame of the resulting photon shows that momentum and energy can not both be conserved. Two-into-one decay is *kinematically* prohibited (it is also prohibited *dynamically*, as we have shown in Sec. 4.4.2).

Another approach is to assume that

$$\omega_1 = \omega_2 = \omega_0$$

and try to add k_1 and k_2 to get a second harmonic. A simple calculation shows that

$$| \vec{k_1} | + | \vec{k_2} | < | \vec{k}(2\omega_0) | . \tag{4.37}$$

That is, if the frequencies are matched, the geometric sum of the wavenumbers of the incident waves is too short to insure wavenumber matching.

The obvious solution is shown in Fig. 4-14. One can view this process as three-into-two decay: three photons with wave numbers k_1 decay into two photons with

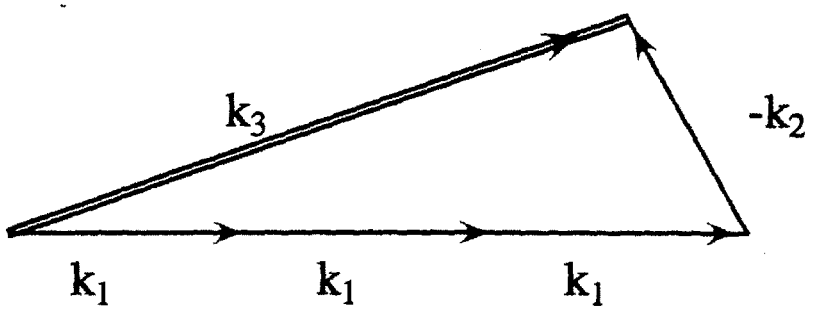

Figure 4-14: Nonlinear phase velocity matching for the second harmonic generation.

wave numbers k_2 and $k_3 = 3k_1 - k_2$. We will later calculate the angle between $\vec{k_1}$ and $\vec{k_2}$ which insures the matched phase velocities of the harmonic and the pump.

Second harmonic generation is, clearly, not the only laser-plasma process which is affected by the phase velocity mismatch. As was calculated in Section 4.1, the growth of the third harmonic is arrested by phase velocity mismatch. The physical reason is the same—in three-into-one process momentum and energy cannot be conserved simultaneously. The solution to this problem is the same as for the second harmonic generation—one has to go to the next order in a^2 and use four-into-two process for generating the third harmonic.

Having established the necessity for calculating the rate of the second harmonic to the fourth order in amplitude we note that the fourth order current that drives the harmonic radiation can be represented as the sum of two distinct terms:

$$j^{(4)} = n^{(3)}v^{(1)} + n^{(2)}v^{(2)}. \tag{4.38}$$

Each quantity is computed to order of its superscript in a. The origin of the first term was already discussed in the context of harmonic emission by non-uniform plasma: two pumps crossed at an angle ponderomotively drive a second order density perturbation, which serves as an initial density inhomogeneity in Eq.(4.29) for the third order density perturbation. The second term represents the coupling of density and velocity perturbations which are both ponderomotively driven. These two contributions are physically different and are given by topologically distinct diagrams. We distinguish between these separate contributions by calling them "absorptive" and

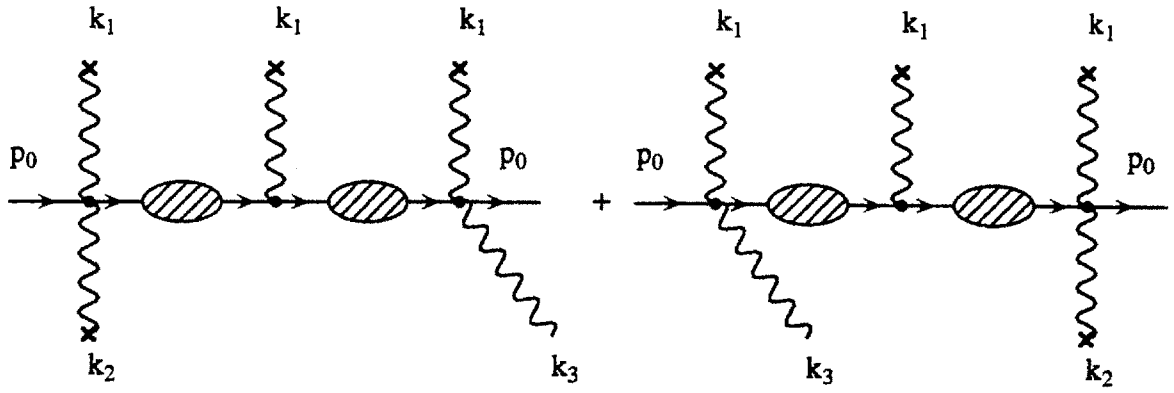

Figure 4-15: Diagrams for the first contribution to the second harmonic generation ("absorption channel").

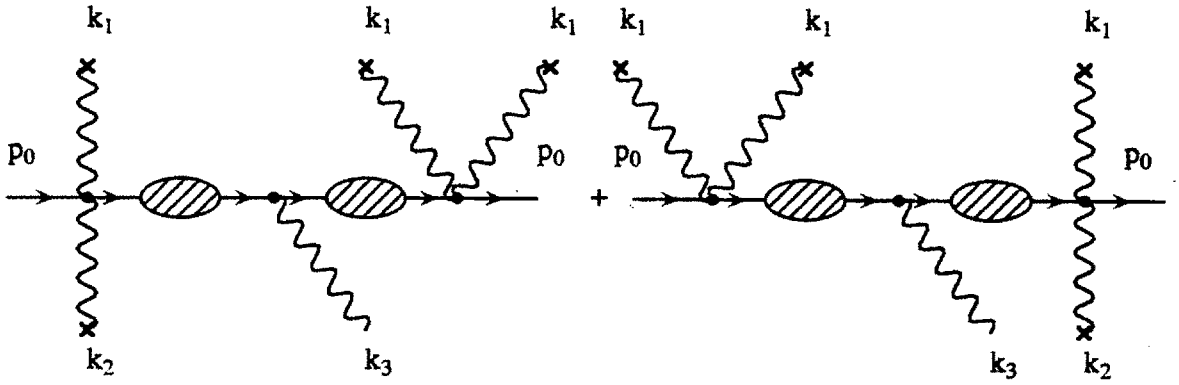

Figure 4-16: Diagrams for the first contribution to the second harmonic generation ("ponderomotive channel").

"ponderomotive" channels. The absorptive channel is diagrammatically expressed in Fig. 4-15, and the ponderomotive channel is shown in Fig. 4-16. The distinction between these different channels can be further appreciated by analyzing the dependence of each of them on the polarization of the incident radiation. For instance, if the two incident electromagnetic waves are polarized *perpendicularly* to the plane of their incidence, it is easy to see that the absorptive channel *will not* contribute: the second order density perturbation, which plays the role of inhomogeneous seed in Eq.(4.29), will have a density gradient in the plane of incidence while the lasers are polarized *perpendicularly* to the plane of incidence. On the other hand, the ponderomotive channel *will* contribute to harmonic generation. In fact, the outgoing second harmonic will be polarized *in* the plane of incidence. This presents a novel method

for nonlinear polarization rotation using laser-plasma interactions. The identification and complete analysis of these two distinct processes of the second harmonic generation are carried out in this thesis for the first time, to our knowledge.

We carry out the calculation for the absorptive channel in great detail since the calculation for the ponderomotive channel is technically almost identical.

As it is clear from the diagram in Fig. 4-15, second harmonic generation involves two "virtual" space-charge waves, with wave numbers

$$\chi_1 = k_1 - k_2 \tag{4.39}$$

and

$$\chi_2 = 2k_1 - k_2. \tag{4.40}$$

The incident waves are assume polarized in the directions $\vec{e}_1$ and $\vec{e}_2$ respectively, and the outgoing wave is polarized in $\vec{e}_3$ direction, with $e_1 = (e_{10}, \vec{e}_1)$,$e_2 = (e_{20}, \vec{e}_2)$ and $e_3 = (e_{30}, \vec{e}_3)$ satisfying the gauge and orthogonality conditions for the photons.

With this notation, the contribution of the diagrams above is calculated, by reading off the propagators and vertices of the diagrams in Fig. 4-15, to be equal to

$$\left(i2\omega_{\vec{k_3}}\frac{da_{\vec{k_3}}}{dt}\right)_{(1)} = \frac{\mu^2(e_1\cdot e_2)(e_1\cdot e_3)(e_1\cdot\chi_1)a_1^3a_2^*}{16\bar{m}^3}\left(\frac{1}{n\cdot\chi_1}\frac{\chi_2^2-\mu^2}{(n\cdot\chi_2)^2-\mu^2}+\frac{1}{n\cdot\chi_2}\frac{\chi_1^2-\mu^2}{(n\cdot\chi_1)^2-\mu^2}\right). \tag{4.41}$$

As before, $\bar{m}$ stands for the renormalized mass of the electron, and is given (to the lowest order in a^2) as

$$\bar{m} = (1+\mid a_1\mid^2/2+\mid a_2\mid^2/2)^{1/2}. \tag{4.42}$$

Examining Eq.(4.41) in the limit that the unperturbed plasma is stationary and that the two waves are monochromatic shows that the term that contains $(n\cdot\chi_1)$ in the denominator becomes infinite. As one expects, there is another contribution to the absorptive channel shown in Fig. 4-17. Using the expression (4.1) for the "dressed"

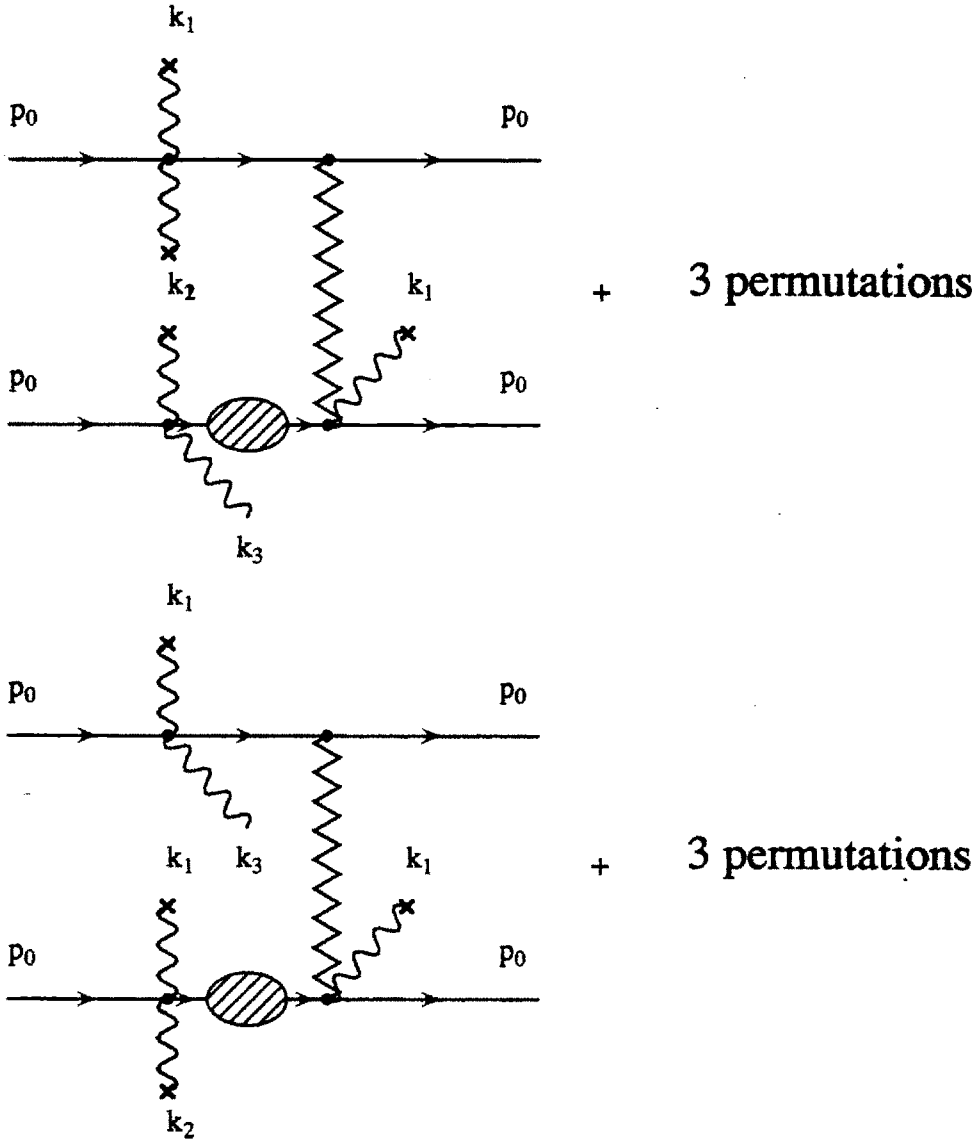

Figure 4-17: Diagrams for the second contribution to the second harmonic generation ("absorption channel").

electron propagator from Section 4.1, one obtains:

$$\left(i2\omega_{\vec{k}_3}\frac{da_{\vec{k}_3}}{dt}\right)_{(2)} = \frac{\mu^2(e_1\cdot e_2)(e_1\cdot e_3)(e_1\cdot\chi_1)a_1^3a_2^*}{16\bar{m}^3} \times \left[\frac{(\chi_2^2-\mu^2)\mu^2}{((n\cdot\chi_2)^2-\mu^2)((n\cdot\chi_1)^2-\mu^2)(n\cdot\chi_1)} + \frac{(\chi_1^2-\mu^2)\mu^2}{((n\cdot\chi_1)^2-\mu^2)((n\cdot\chi_2)^2-\mu^2)(n\cdot\chi_2)}\right]. \quad (4.43)$$

Adding Eq.(4.41) to Eq.(4.43) yields the total contribution of the absorption channel to the rate of the second harmonic generation:

$$\left(i2\omega_{\vec{k}_3}\frac{da_{\vec{k}_3}}{dt}\right)_{abs} = \frac{\mu^2(e_1\cdot e_2)(e_1\cdot e_3)(e_1\cdot\chi_1)a_1^3a_2^*}{16\bar{m}^3}\ \frac{(n\cdot\chi_1)(\chi_2^2-\mu^2)+(n\cdot\chi_2)(\chi_1^2-\mu^2)}{((n\cdot\chi_2)^2-\mu^2)((n\cdot\chi_1)^2-\mu^2)}. \quad (4.44)$$

The contribution from the ponderomotive process can be computed in a similar fashion. Since the intermediate density and velocity perturbations for this channel differ from the ones in the absorptive channel, we introduce the corresponding wave numbers: $\kappa_1 = k_1 - k_2$ and $\kappa_2 = 2k_1$. Calculating the correct rate requires the single-level diagrams in Fig. 4-16 and the two-level diagrams shown in Fig. 4-18. We find:

$$\left(i2\omega_{\vec{k}_3}\frac{da_{\vec{k}_3}}{dt}\right)_{pond} = \frac{\mu^2(e_1\cdot e_2)(e_3\cdot\kappa_1)a_1^3a_2^*}{16\bar{m}^3}\ \frac{(n\cdot\kappa_1)(\kappa_2^2-\mu^2)+(n\cdot\kappa_2)(\kappa_1^2-\mu^2)}{((n\cdot\kappa_2)^2-\mu^2)((n\cdot\kappa_1)^2-\mu^2)}. \quad (4.45)$$

For a stationary plasma, $n^0 = 1, \vec{n} = 0$, and

$$e^0_{(i)} = 0, \quad \vec{e}_{(i)}\cdot\vec{k}_{(i)} = 0. \quad (4.46)$$

Further assuming that both incident waves have the same frequency and are polarized in the plane of incidence results in

$$\left(i2\omega_{\vec{k}_3}\frac{da_{\vec{k}_3}}{dt}\right) = \frac{3\mu^2\delta\theta a_1^3a_2^*}{32\bar{m}^3}\left(\frac{k_\perp^2}{\mu^2}+1\right), \quad (4.47)$$

where $\delta\theta$ is the small angle between $\vec{k}_1$ and $\vec{k}_2$ and $k_\perp = \mid \vec{\chi}_1 \mid \approx \omega_0/c\delta\theta$. The angle $\delta\theta$ can be computed by requiring that both wave number and frequency are conserved

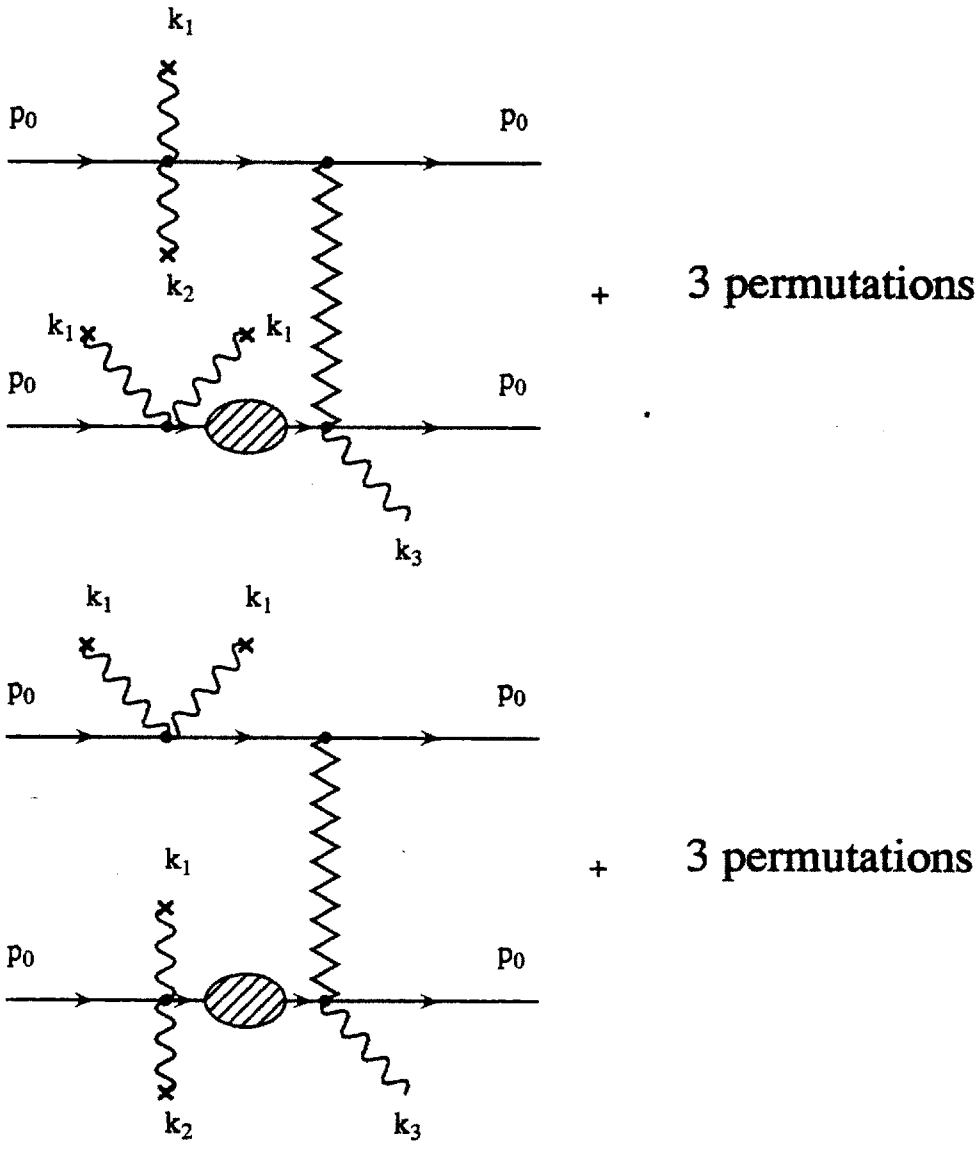

Figure 4-18: Diagrams for the second contribution to the second harmonic generation ("ponderomotive channel").

in the process of harmonic generation, that is

$$\mid 3\vec{k}_1 - \vec{k}_2 \mid = \mid \vec{k}(2\omega_0) \mid . \tag{4.48}$$

Eq.(4.48) results in

$$\delta\theta \approx \mu/\omega_0, \tag{4.49}$$

yielding

$$\left(i2\omega_{\vec{k}_3}\frac{da_{\vec{k}_3}}{dt}\right) = \frac{3\omega_p^3 a_1^3 a_2^*}{16\omega_0 \bar{m}^{4.5}}. \tag{4.50}$$

If the incident waves were polarized perpendicularly to the plane of incidence, the result would be reduced by a factor of three because the absorptive channel wouldn't have contributed.

Here we present a plausibility argument for an interesting experiment that involves nonlinear polarization rotation. Assume that two intense pumps polarized perpendicularly to the plane of incidence, with normalized vector potentials $a_1 = a_2 = 1$ and wavelength $\lambda_0 = 1\mu$, are propagating through underdense plasma of density $n_0 = 10^{20}\text{cm}^{-3}$. For this example $\lambda_p/\lambda_0 = 3.0$. Using Eq.(4.50) (reduced by a factor three, as explained above) and assuming that the polarizer at the end of interaction can discriminate between perpendicular polarizations with accuracy 10:1, we obtain the length of plasma after which the second harmonic component $a_{\vec{k}_3} = 0.1$:

$$L_{harm} \approx \frac{5\lambda_p^3}{\lambda_0^2}. \tag{4.51}$$

The two beams are incident at an angle $\delta\theta$ (see Eq.(4.49)). The minimum spot size of each of the beams that insures an overlap over distance L_{harm} is roughly equal to $d \propto \lambda_p^2/\lambda_0$. Calculating the Rayleigh length that corresponds to the spot size d results in $Z_R \approx \pi\lambda_p^4/\lambda_0^3$. We thus see that for underdense plasma diffraction should not present a considerable problem since $Z_R > L_{harm}$. It is easy to calculate that with a spot size d and normalized vector potentials of order unity, the power requirement on the pump is about 2.5 Terawatt, putting the nonlinear polarization rotation experiment within reach for most tabletop CPA laser systems.

Chapter 5

Laser Propagation in Plasma Channels

5.1 Laser/Plasma Based Accelerator Schemes

High-energy particle accelerators have been advancing the frontier of our knowledge about the building blocks of matter since Lawrence built the first synchrotron in the 30's [73]. Since then the particle energy has increased exponentially. Whenever an old technology reached its limit, the new approach was developed. It is clear at this point in history of accelerators that the conventional radio-frequency technology limits the accelerating gradients to about $100MV/m$. Extending the existing technology to higher frequencies is unlikely to yield gradients greater than $200MV/m$. Even though the next grand accelerator project, such as the Next Linear Collider (NLC) [23], will almost certainly rely on RF technology, physicists are looking beyond the NLC to identify new accelerating media that would sustain much higher accelerating gradients, thus allowing to reach TeV energies without making the machine prohibitively large in size and costly.

Plasma has been considered as a possible accelerating medium. There are several recent reviews of its potential role in accelerators [23, 25]. Plasma-based accelerators have been investigated theoretically [28] and experimentally [11] for over a decade. The basic idea behind any plasma accelerator is to excite an intense plasma wave

moving with the speed close to the speed of light. The longitudinal electric field of this wave can then accelerate charged particles. Accelerating gradients generated by plasma waves can be enormous: from the Poisson equation one can derive an approximate expression that relates accelerating gradient to the density of ambient plasma n_0 and the fractional density perturbation, $\delta n/n_0$:

$$E_z = 100GeV/m\sqrt{\frac{n_0(cm^{-3})}{10^{18}}}\frac{\delta n}{n_0}. \tag{5.1}$$

Thus accelerating gradients in the 10-100 GeV/m range are achievable. Fractional density perturbations as high as 23% have been experimentally demonstrated by Joshi and coworkers at UCLA [11], allthough with a relatively low ambient plasma density ($9\times10^{15}cm^{-3}$). A collaboration at the Institute of Laser Engineering at Osaka University reported generating plasma waves with accelerating gradient 30GeV/m.

Several schemes have been proposed for generating intense plasma waves. At present, plasma beat-wave accelerator [28] and laser wakefield accelerator [28, 15, 23] appear to have achieved the most theoretical and experimental maturity. In the plasma beat-wave scheme two co-propagating lasers are focused into plasma. The lasers beat against each other, and, if the beat frequency is close to plasma frequency ω_p, the density modulation is driven resonantly. The phase velocity of the plasma wave is then approximately equal to the group velocity of the incident lasers [24]:

$$\frac{\omega_p}{k_p} = \frac{\omega_1 - \omega_2}{k_1 - k_2} \approx v_g \approx c\left(1 - \frac{\omega_p^2}{2\omega^2}\right). \tag{5.2}$$

Here the electromagnetic waves in plasma satisfy $\omega = \sqrt{k^2c^2 + \omega_p^2}$. An important advantage of the beat-wave scheme over the laser-wakefield accelerator, which is discussed below, is that it does not require very high power lasers—the resonantly driven plasma wave grows linearly with time. One of the important disadvantages is the requirement of uniformity imposed on plasma density in order to satisfy the resonance condition.

The scheme that we are mostly concerned in this thesis is the laser wakefield accel-

erator. Unlike a beat-wave scheme, which requires two precisely tuned lasers to excite the plasma wave, laser wakefield accelerator uses a single, extremely intense, short (on the order of plasma period) laser pulse, which travels through the underdense plasma and leaves behind a strong longitudinal wave. This scheme does not excite the plasma wave resonantly and, thus, does not require the same degree of plasma uniformity as the beat-wave approach. The trade-off is the necessity to produce very short, high-power pulses. This will become less of a limitation as more powerful lasers become widely available. Even with a Terawatt laser at $1\mu m$, focused to a spotsize of $6\mu m$, one can excite a fractional density perturbation $\delta n/n_0$ of over 60%. The physics of ponderomotive excitation of plasma wakes and the stability of the short laser pulses will be the focus of the remaining part of this thesis.

There are a number of limitations on the final energy that can be achieved using laser-plasma acceleration schemes. Since the phase velocity of the plasma wave is somewhat smaller than the speed of light, accelerated particles will eventually get out of phase with the accelerating field. Assuming that the particle is moving with the speed c and the phase velocity of the wave is equal to group velocity of the driving laser (as given by Eq.(5.2)), the velocity mismatch can be evaluated as

$$\frac{c - v_{ph}}{c} \approx \frac{\omega_p^2}{2\omega_0^2} \tag{5.3}$$

where ω_0 is the frequency of the laser radiation and we have assumed that

$$\frac{\omega_p^2}{\omega_0^2} \ll 1. \tag{5.4}$$

Assuming that the particle has to slip by about $\lambda_p/2$ ahead of the plasma wave to start losing energy, we find the distance over which acceleration remains in effect

$$L_{deph} = 2\lambda_p \frac{\omega_0^2}{\omega_p^2}, \tag{5.5}$$

where $\lambda_p = 2\pi c/\omega_p$ is the wavelength of the plasma wave. For a typical example of $1\mu m$ laser pulse traveling through plasma of density $n_0 = 10^{18} cm^{-3}$ we obtain

$L_{deph} \approx 6cm$.

Dephasing is not, however, the most severe limitation on the interaction length. Diffraction imposes a much more severe limit. Laser light of wavelength λ, focused to a spot size σ, diffracts over a distance $Z_R = \pi\sigma^2/\lambda$, where Z_R is known as a Rayleigh range. For the previous example of $\lambda = 1\mu m$ and $\sigma = 6\mu m$, $Z_R \approx 0.1mm$. Increasing the spot size at fixed intensity is clearly impractical because it requires higher laser power.

Another limit on the acceleration distance comes from pump depletion. As the pump laser pulse propagates through plasma, it leaves behind a plasma wave. The energy of the plasma wave is provided by the pump, which is depleted. Pump depletion becomes more severe as the intensity of the laser increases. The reason for this is that the *amplitude* E_z of the generated longitudinal field is proportional to P, the power of the pump. Thus, the energy in the wake is proportional to P^2 and, since the total energy in the pump is proportional to P, the depletion distance L_{depl} is inversely proportional to P. A back-of-the-envelope calculation gives, for a weakly relativistic pulse of size λ_p, a depletion length L_{depl} that scales as

$$L_{depl} \propto L_{deph}/a_0^2, \tag{5.6}$$

where a_0 is the normalized vector-potential of the pump. As the scaling in Eq.(5.6) indicates, keeping $a_0 < 0.3$ should keep pump depletion secondary to dephasing. This is indeed seen in numerical simulations [74].

5.2 Desirability of Channels

As was demonstrated in Section 5.1, diffraction is by far the most severe limit for laser-plasma acceleration. Thus, a successful design of a plasma based accelerator must include some form of optical guiding. Two schemes have been proposed: relativistic optical guiding and plasma channel guiding.

Relativistic guiding [29, 30, 31, 32] relies on the energy dependence of the plasma

frequency, ω_{p0}^2/γ, where $\gamma = \sqrt{1 + \vec{p} \cdot \vec{p}/m^2c^2}$. The electron momentum $\mid \vec{p} \mid$ will be largest where the laser pulse is most intense, and therefore the plasma frequency will be lower there, and the pulse will generate a nonlinear index of refraction which is larger at the center of the pulse than at the pulse edges. Analysis has shown [30] that, in steady-state, relativistic guiding can focus the pulse whenever the total power is greater than $P_c = 16.2(\omega/\omega_{p0})^2$ GW.

For the short pulses (of order a plasma wavelength) envisioned in many wakefield accelerators, however, relativistic guiding is substantially reduced [15]. This is due to the tendency of the ponderomotive force from the front of the pulse to push plasma electrons forward and generate a density increase which balances the relativistic mass increase. The plasma frequency then has no transverse variation and cannot optically guide the laser pulse. Relativistically guided long laser pulses suffer from Raman forward and sidescatter instabilities [34, 35]. The instability leads to the break-up of the pulse into small pulselets of order one plasma wavelength. The utility of using these pulselets themselves for acceleration is at present unclear [36].

An alternative scheme which has been investigated [37] envisions guiding the laser pulse with a plasma density channel. The channel should have a higher density on the outside than on the inside, giving it an index of refraction which decreases from the channel axis. A fixed plasma channel is analogous to an optical fiber, and its guiding properties can be similarly analyzed. The plasma channel can be used to guide short pulses, and has been studied using axisymmetric models for parabolic density variation [37] and for hollow channels [40].

It was demonstrated analytically [41] that a small perturbation to the guided (transverse) equilibrium of the laser pulse, which occurs abruptly on a scale of a plasma wavelength, can lead to wakefield instability. A perturbation to the laser profile excites, through the ponderomotive force, a plasma density perturbation (or wake) which, in turn, couples back to the perturbed field. A detailed calculation of the wakefield instability of a short laser pulse, guided by a parabolic channel, is given in Chapter 6.

Calculations show that a hollow channel, apart from optically guiding the laser

pulse, supports a plasma wake with very attractive properties for acceleration [40]. The laser excites a surface mode on the inside of the channel. The fringe fields of the surface mode extend into the channel, providing the accelerating field E_z which is almost uniform, along with the transverse electric and magnetic fields which linearly focus the beam. In Chapter 7 we derive a general formalism for studying the ponderomotively generated wakefields in inhomogeneous plasmas and apply it to hollow channels.

5.3 Basic Equations of Wake Excitation in Uniform Plasmas

Excitation of plasma wakes in non-uniform plasmas is a formidable theoretical problem. A complete solution to this problem is complicated by several effects: 1) the excited wake is no longer purely electrostatic, as in the case of uniform plasma 2) there are regions in plasma where the local plasma frequency matches the frequencies of the plasma eigenmodes, which leads to singularities in the electric field. We thus see that the complete problem is not just *formally* difficult, but, rather, contains the physics (such as resonant absorption at the singularities of the electric field) that is not easily amenable to calculations. We return to inhomogeneous plasmas and address some of these issues in Chapter 7.

For the purpose of exciting the wakefields, plasmas can be considered uniform if the ponderomotive force is confined to regions much smaller than the scale over which plasma is uniform. For example, if a parabolic plasma channel in a slab is studied, with density profile given by

$$n(x) = n_0 \left(1 + \frac{x^2}{L^2}\right), \tag{5.7}$$

and the ponderomotive force is given by

$$f = f_0 e^{-x^2/w^2} \tag{5.8}$$

with $w \ll L$, then plasma can be considered uniform in the region where ponderomotive force is appreciable.

An important point to note is that, for the purpose of designing the best wakefield accelerator, going to high a_0's *is not* desirable. For the best acceleration one should avoid over-bunching the plasma to prevent wave-breaking, profile steepening and related nonlinear effects, undesirable for particle acceleration. In addition, as was mentioned in Section 5.1, increasing a_0 leads to substantial pump depletion. We thus assume that

$$a_0 \leq 0.3. \tag{5.9}$$

Thus, here and in the rest of this thesis, we use a weakly relativistic approximation [34], which is justified by assumption Eq.(5.9). In contrast to the previous chapters, where we developed a systematic perturbation theory to all orders in $\frac{\omega_p^2 a_2}{\omega^2(1+a^2)^{3/2}}$, here all the calculations of density perturbation and relativistic index of refraction will be performed to second order in laser fields, neglecting the terms proportional to a_0^4.

Since the duration of the laser pulse is assumed to be short compared to $2\pi/\omega_{pi}$, where $\omega_{pi}^2 = 4\pi e^2 n_0/m_i$, the ions can be considered immobile. Plasma electrons will be described by a fluid model, which is applicable in a cold plasma before wave breaking [58] has occurred. The short pulse durations and relatively low value of a_0 insures that the wave breaking is not a concern for a laser wakefield accelerator. For the plasma to be considered cold the thermal velocity of an electron must be less than the oscillatory velocity imparted to it by the laser field.

We further assume that the plasma is very underdense, so that (5.4) is satisfied. This allows to separate time scales into the fast scale of order laser period, $1/\omega_0$, and slow scale of order plasma period, $1/\omega_p$. Plasma electrons move in the combined electric and magnetic fields of the laser, $\vec{E}_L$ and $\vec{B}_L$, and the (slow-scale) space-charge field $\vec{E}_s$, induced by the laser, in plasma. The nonlinear equation of motion of the

electron fluid is given by

$$\frac{\partial \vec{v}}{\partial t} + (\vec{v} \cdot \nabla)\vec{v} = \frac{e}{m}\left(\vec{E}_L + \frac{\vec{v}}{c} \times \vec{B}_L + \vec{E}_s\right). \tag{5.10}$$

We further assume that the laser field is purely electromagnetic (which is a valid assumption in a homogeneous plasma), described by a vector potential $\vec{A}$, with a varying on a slow scale:

$$\vec{A} = \frac{mc^2}{2e}\vec{a}(\vec{x}_\perp, z, t)e^{i(k_0 z - \omega_0 t)} + c.c., \tag{5.11}$$

where

$$\vec{a} \cdot \vec{e}_z = 0. \tag{5.12}$$

The spot size of the laser is assumed to be much larger than the wavelength λ_0, validating the assumption of transverse polarization in Eq.(5.12). Under the weakly relativistic assumption (5.9), the peak particle displacement in the transverse plane is negligible compared with the spot size of the laser. Thus the transverse component of the second term in the LHS of Eq.(5.10) can be neglected in comparison with the corresponding component of the first term. This is equivalent to conserving the transverse canonical momentum.

Separating electron velocity into fast and slow parts,

$$\vec{v} = \vec{v}_f + \vec{v}_s, \tag{5.13}$$

using the conservation of transverse canonical momentum,

$$\vec{v}_f = -\frac{e\vec{A}}{mc}, \tag{5.14}$$

and averaging over the fast time-scale yields

$$\frac{\partial \vec{v}_s}{\partial t} = \frac{e}{m}(\vec{E}_s + \nabla f), \tag{5.15}$$

where f is the ponderomotive potential given by

$$f = -\frac{mc^2}{4e} \mid \vec{a} \mid^2 . \tag{5.16}$$

Assuming the plasma density $n = n_0 + \delta n$, we obtain from the continuity equation:

$$\frac{\partial}{\partial t}\frac{\delta n}{n_0} = -\nabla \cdot \vec{v}_s. \tag{5.17}$$

Combining Eqs.(5.15,5.17) with the Poisson equation

$$\nabla \cdot \vec{E}_s = 4\pi e \delta n \tag{5.18}$$

results in

$$\left(\frac{\partial^2}{\partial t^2} + \omega_{p0}^2\right)\frac{\delta n}{n_0} = -\frac{e}{m}\nabla^2 f, \tag{5.19}$$

where $\omega_{p0}^2 = 4\pi e^2 n_0/m$ is the unperturbed plasma frequency.

We note that in the case of homogeneous plasma the induced field $\vec{E}_s$ is purely electrostatic, and there is no magnetic field associated with it. This can be most easily seen by considering wave equation for the magnetic field $\vec{B}_s$:

$$\left(\frac{\partial^2}{\partial t^2} - \nabla^2\right)\vec{B}_s = \frac{4\pi}{c}\nabla \times \vec{J}_s, \tag{5.20}$$

where $\vec{J}_s$ is the slow component of the plasma current given by

$$\vec{J}_s = e n_0 \vec{v}_s. \tag{5.21}$$

Taking the time derivative of Eq.(5.20) and using Eqs.(5.21,5.15) together with the second Maxwell equation, we obtain

$$\left(\frac{\partial^2}{\partial t^2} - \nabla^2 + \omega_{p0}^2\right)\frac{\partial \vec{B}_s}{\partial t} = 0. \tag{5.22}$$

Hence, the ponderomotive force *does not* excite a magnetic field in the homogeneous

plasma. As we show in Chapter 7, this statement is false for inhomogeneous plasmas.

Equation (5.19) contains the essential physics of wakefield generation in homogeneous plasma. It describes the laser-wakefield accelerator as well as the beat-wave accelerator. In the latter scheme the ponderomotive potential f is formed by the beating of two lasers. It is clear from Eq.(5.19) that if $f \propto \exp(i\omega_{p0}t)$, then the density perturbation grows secularly with time, as would a displacement of any resonantly driven oscillator. On the other hand, if one assumes a transversely uniform laser pulse, the only way to appreciably excite plasma is to make a pulse short compared to plasma wavelength.

The ponderomotive potential f bears some resemblance to the driving electron bunch in electron-beam wakefield accelerator [75, 76]. In this scheme a low-energy intense bunch generates a strong plasma wake that accelerates a trailing bunch to high energy. The corresponding equation [75], for the plasma that is overdense (compared with the driving bunch), is

$$\left(\frac{\partial^2}{\partial t^2} + \omega_p^2\right)\frac{\delta n}{n_p} = \omega_p^2 \frac{n_b}{n_p}, \tag{5.23}$$

where n_b and n_p are the densities of the bunch and plasma, respectively. The optimally designed longitudinal profile of the driving beam is a bunch with a slow (over several plasma wavelengths) rise in density and a very abrupt termination [76]. If the laser pulse is designed in the same way, no appreciable wakefield is generated, as is evident from Eq.(5.19). This emphasizes the difference between the laser-driven and beam-driven wakes—in the former case the second derivative of the pulse shape excites the wake, while the *shape itself* excites the wake in the latter case.

Chapter 6

Stability of Pulse Propagation in Parabolic Channels

6.1 Physical Problem and Previous Work

This chapter considers the dynamic stability of channel-guided pulses in the presence of plasma wakes. A perturbation to the guided equilibrium leads, through the ponderomotive force, to a plasma density perturbation which, in turn, couples back to the perturbed field. Thus, the plasma couples different longitudinal slices of the laser pulse.

The main finding of this chapter is that (initially small) perturbation of the transverse profile of the laser grows exponentially as the pulse propagates through the plasma channel [cite gsprl]. A general equation is derived, which describes the spatio-temporal evolution of arbitrary distortions of the transverse laser shape, such as hosing, breathing, quadrupole deformation, etc.

For example, a transverse instability of channel-guided pulses occurs when the laser pulse is initially not centered on the channel axis. The underlying physics is straightforward: the off-centered laser produces a ponderomotive force with a dipole component; this causes the surrounding plasma electrons to try to follow the laser pulse. Thus the shape of the channel is distorted and its guiding properties are perturbed. The result is that the perturbation has exponential spatio-temporal growth.

The laser pulse starts exhibiting hosing. The degree of hosing will be increasing as a function of distance traveled by the pulse, as well as of the distance along the pulse from its head. In general, there will be a coupling between higher-order multipoles, so that the back of the laser pulse will be hosing and widening at the same time.

The wakefield instabilities that are discussed here are closely related to small-angle Raman scattering that affects unfocused intense laser pulses. Raman scattering of laser pulses in plasma has been investigated by numerous authors. Antonsen and Mora examined [34] the stability of relativistically guided pulses using a mildly relativistic fluid model, and Bingham and Mckinstrie made an analysis [35] including relativistic effects. They found a dispersion relation assuming that the perpendicular wave number is large compared to the inverse of the transverse spot size. In this calculation the plasma channel externally guides the laser pulse. Scattering, for the quadratic density channel, is restricted to a discrete set of transverse modes. Our analysis explicitly includes the finite transverse size of the pump, which leads to coupling between different modes and is not restricted to perturbed wavenumbers which are large compared to the inverse of the equilibrium mode size. Valeo investigated [77] the dynamic stability of an equilibrium consisting of a long laser pulse guided by a self-induced (by the pulse) channel. His analysis is of the temporal single mode growth on a hydrodynamic time scale and without relativistic effects. The analysis here is of the short pulse (plasma oscillation timescale) dynamics, including mildly relativistic electron motion. Other papers [78, 79] have examined the consequences of self-induced channels and filamentation on Raman instabilities. Their theoretical model is based on pressure balance equilibrium, nonrelativistic electron motion, and they derive only purely temporal growth rates. A nonrelativistic analysis of the temporal evolution of Raman scattering in a sinusoidally modulated plasma density has been made by Barr, et al. [80]. These investigations do not yield results for the short time scales and cold plasmas appropriate for high intensity laser accelerators.

6.2 Basic Equations

With a quadratic density variation, the stability analysis of the laser pulse propagation can be solved exactly. The physical model consists of a preformed neutral plasma channel with an unperturbed density given by

$$n_0(\vec{x}_\perp) = \bar{n}_0(1 + \frac{r^2}{W^2}), \tag{6.1}$$

where $r^2 = x^2 + y^2$. The channel density is taken to vary over a distance much larger than collisionless plasma skin-depth, so that

$$K = c/\bar{\omega}_p W \ll 1, \tag{6.2}$$

where $\bar{\omega}_p = 4\pi\bar{n}_0/m$ is the plasma frequency at the channel center. Then, as shown below, the unperturbed laser pulse has a spotsize w $= \sqrt{Wc/\bar{\omega}_p} \ll W$, so that the density does not vary appreciably in the region where the ponderomotive force is nonzero. Therefore, in deriving the equations for the wake generation, we will be able to use the results obtained under quasi-uniform plasma assumption in Section 5.3. We also assume that, in the region where the laser amplitude is non-negligible, $\omega_p^2 << \omega^2$, where $\omega_p^2 = 4\pi e^2 n(\vec{x_\perp}, z, t)/m$.

We consider the circularly polarized laser radiation, with the normalized vector-potential $\vec{a}$, defined by Eq.(5.11):

$$\vec{a} = a(x_\perp, z, t))(\vec{e}_x + i\vec{e}_y) \tag{6.3}$$

We note that a circularly polarized field *is not* a valid solution in inhomogeneous plasma. In fact, the solutions to Maxwell equations separate into TM and TE modes which have nonzero E_z and B_z, respectively. These two kinds of modes can be linearly combined to approximate the circularly polarized field represented by Eq.(6.3). The accuracy of this representation is insured by the fact that the spot size of the laser is

much greater than the optical wavelength:

$$\mathrm{w} \gg \frac{c}{\omega_p} \gg \frac{c}{\omega_0}. \tag{6.4}$$

The approximation breaks down for very high multipoles of the transverse laser profile which correspond to scattering at almost 90°. Large-angle scattering with $k_\perp \gg 1/\sigma$ is beyond the interest of this calculation and is better approached by the method of Ref. [34].

The field equation is, in the weakly relativistic limit ($\mid \vec{a} \mid^2 < 1$),

$$\left(-\frac{1}{c^2}\frac{\partial^2}{\partial t^2} + \frac{\partial^2}{\partial z^2} + \nabla_\perp^2 - \frac{\omega_p^2(x_\perp, z, t)}{c^2}\left(1 - \frac{\mid a \mid^2}{2}\right)\right)(a \exp\left(i(k_0 z - \omega_0 t)\right)) = 0. \tag{6.5}$$

We use z and $s = t - z/v_{g0}$ (the retarded time) instead of z and t. Group velocity of the laser, $v_{g0}/c = k_0 c/\omega_0$, will be assumed to be constant in the rest of the calculation. In the paraxial approximation (see, for example, Ref. [52]) s can be thought of as an index that labels a given slice of the laser. The choice of coordinates is typical for analyzing cumulative instabilities [81].

Using the eikonal approximation to Eq.(6.5) results in

$$\left(\frac{\omega_0^2}{c^2} - k_0^2 + \nabla_\perp^2 - \frac{\omega_p^2}{c^2}\left(1 - \frac{\mid a \mid^2}{2}\right) + 2ik_0\frac{\partial}{\partial z}\right) a(z, s, \vec{x}_\perp) = 0, \tag{6.6}$$

Formally, eikonal approximation amounts to neglecting the second derivatives in s and z. Using the eikonal (or paraxial, as it is often called) approximation neglects some of the important physics, for instance, Raman Forward Scattering. To recover RFS the second derivative in s has to be kept. An important physical consequence of the paraxial approximation is that the total laser power of a given longitudinal slice s is conserved, that is

$$\frac{\partial}{\partial z}\int d^2\vec{x}_\perp \mid \vec{a} \mid^2 (\vec{x}_\perp, s, z) = 0. \tag{6.7}$$

Nonetheless, the laser power at a given position s can spread out transversely, as the laser travels through plasma, without violating Eq.(6.7). An extensive discussion of

the validity of the paraxial approximation for unfocused laser propagation is given in Ref. [52].

The amplitude of the laser is expanded as a sum of the unperturbed guided laser pulse and a perturbation driven by the generation of plasma density modulations: $a(\vec{x}_\perp, s, z) = a_0(\vec{x}_\perp, s) + a_1(\vec{x}_\perp, s, z)$. Note that the equilibrium is chosen to be independent of distance z, so that it travels through the plasma undistorted with velocity v_{g0}. This neglects the spreading of the pulse due to dispersion, as well as pulse depletion. Retaining leading order terms in Eq.(A.8), and using the dimensionless transverse coordinates $\bar{x} = x/\mathrm{w}, \bar{y} = y/\mathrm{w}$, $\bar{\nabla}_\perp = \mathrm{w}\nabla_\perp$, results in

$$(-\bar{\nabla}_\perp^2 + \bar{r}^2)a_0(s, \vec{\bar{x}}_\perp) = \mathrm{w}^2\left(\frac{\omega_0^2}{c^2} - k_0^2 - \frac{\bar{\omega}_p^2}{c^2}\left(1 - \frac{|\,a_0\,|^2}{2}\right)\right)a_0(s, \vec{\bar{x}}_\perp). \tag{6.8}$$

In deriving Eq.(6.8) we have also neglected the wakes in the unperturbed field a_0, created by the nonadiabaticity in the unperturbed $a_0(s)$ dependence. Thus, it is more accurate to say that $a_0(\vec{\bar{x}}_\perp)$ describes the steady state of a guided laser pulse which was adiabaticlly turned on from zero to its final value.

Since the primary concern in this paper is guiding by a channel and not relativistic self-focusing, we will assume that the laser power is below the self-focusing threshold P_c [30]. In our notation, this is equivalent to requiring

$$|\,a_0^2\,|/8K = |\,a_0^2\,|\,\mathrm{w}^2\bar{\omega}_p^2/8c^2 \ll 1. \tag{6.9}$$

This allowed us to neglect the nonlinear terms in Eq.(6.8).

The calculation proceeds by linearizing Eq.(A.8) and expanding the perturbation a_1 in a complete set eigenfunctions of the transverse operator $\mathcal{L}_T$ defined by

$$\mathcal{L}_T\psi \equiv (-\bar{\nabla}_\perp^2 + \bar{r}^2)\psi. \tag{6.10}$$

Thus the laser field eigenfunctions in a parabolic channel are identical to the eigenfunctions of a two-dimensional harmonic oscillator. The operator $\mathcal{L}_T$ is separable in $(\bar{r}, \theta)$ cylindrical coordinates. The eigenfunctions ψ_n^m, where m is the azimuthal and

n is the radial numbers, form a complete set and can be expressed, as

$$\psi_n^m(\bar{r},\theta) = \exp(-\bar{r}^2/2)\bar{r}^m L_n^m(\bar{r}^2)\exp(im\theta), \tag{6.11}$$

where L_n^m are the modified Laguerre polynomials [88]. The eigenfunctions $\psi_n^m(\bar{r},\theta)$ are orthogonal to each other and satisfy the following spectral equation:

$$(-\bar{\nabla}_\perp^2 + \bar{r}^2)\psi_n^m(\bar{r},\theta) = \lambda_n^m \psi_n^m(\bar{r},\theta), \tag{6.12}$$

where $\lambda_n^m = 2 + 2m + 4n$. The orthogonality condition for $\psi_n^m(\bar{r},\theta)$ is [88]

$$\frac{1}{2\pi}\int d^2x_\perp \psi_{n_1}^{m_1}(\bar{r},\theta)\psi_{n_2}^{m_2}(\bar{r},\theta) = \delta_{n_1 n_2}\delta_{m_1 m_2}\frac{(n_1+m_1)!}{n_1!}, \tag{6.13}$$

where δ_{kl} is a Kronicker symbol.

The unperturbed equilibrium profile a_0, consistent with the assumption that the field is small enough so that self-guiding is unimportant, can be taken as

$$a_0(s,z,\vec{\bar{x}}_\perp) = \bar{a}_0(s)\exp(-\bar{r}^2/2), \tag{6.14}$$

which corresponds to the lowest $(m = 0, n = 0)$ eigenfunction. The corresponding dispersion relation for the fundamental mode is thus

$$\left(\frac{{\omega_0}^2}{c^2} - k_0^2 - \frac{\bar{\omega}_p^2}{c^2}\right) = \frac{2}{\mathrm{w}^2}. \tag{6.15}$$

Using Eqs.(A.8) and (6.15), the equation for the perturbed field is

$$\left[(2 + \bar{\nabla}_\perp^2 - \bar{r}^2) + 2ik\mathrm{w}^2\frac{\partial}{\partial z}\right] a_1 = \frac{\bar{\omega}_p^2}{c^2}\mathrm{w}^2\left(\frac{\delta n}{n_0} - \frac{a_0^* a_1}{2} - \frac{a_0 a_1^*}{2}\right) a_0. \tag{6.16}$$

We have neglected the relativistic guiding term, proportional to $(\bar{\omega}_p^2/c^2)\mathrm{w}^2 a_0^2$, within the bracket on the LHS of Eq.(6.16). This is consistent with our assumption that the relativistic guiding corrections to the unperturbed profile can be neglected.

Since we have assumed that $\mathrm{w} \ll W$, the results of Section 5.3 are valid, and we

can linearize Eq.(5.19) to obtain the equation for the density modulation δn:

$$\left(\frac{\partial^2}{\partial s^2}+\omega_{p0}^2\right)\frac{\delta n}{n_0}=\frac{c^2\nabla^2}{2}\left(a_0^* a_1+a_0 a_1^*\right). \tag{6.17}$$

Note that the terms on the RHS of Eq.(6.16), while of the same order as the relativistic guiding term, are the ponderomotive driving terms for the density perturbation on the LHS of Eq.(6.17). Equation (6.17) for $\delta n/n_0$ can be broken into a longitudinal and a transverse piece by use of the quasistatic approximation,

$$\nabla_{\parallel}^2 \approx \frac{1}{c^2}\frac{\partial^2}{\partial s^2}. \tag{6.18}$$

Changing Eq. (6.17) into an integral equation, integrating twice by parts, and inserting the resulting expression for $(\delta n/n_0)$ into Eq.(6.16), yields

$$\left(2+\bar{\nabla}_{\perp}^2-\bar{r}^2+2ik\mathrm{w}^2\frac{\partial}{\partial z}\right)a_1(s,z)=$$
$$\frac{a_0(s)}{2}\int_{-\infty}^{s}\bar{\omega}_p ds'\sin\bar{\omega}_p(s-s')\left(\bar{\nabla}_{\perp}^2-\frac{1}{K}\right)\left(a_0^*(s')a_1(s',z)+a_0(s')a_1^*(s',z)\right). \tag{6.19}$$

Here both a_0 and a_1 are implicitly assumed to depend on $\vec{\bar{x}}_{\perp}$.

The fundamental has $m=0$, so that perturbed modes with differing azimuthal numbers are decoupled. Thus, we can concentrate on the evolution of a particular azimuthal mode, a_1^m, with an arbitrary radial profile. This profile can be decomposed as a weighted sum of radial eigenmodes with the same azimuthal mode number:

$$a_1^m(\vec{\bar{x}}_{\perp},z,s)\equiv\sum_{n=0}^{\infty}\bar{a}_n^m(z,s)\psi_n^m(\bar{r},\theta). \tag{6.20}$$

It is convenient to introduce dimensionless time and space coordinates, normalizing them to a plasma period and Rayleigh length, respectively:

$$\bar{s}=\bar{\omega}_p s,\ \bar{z}=z/k\mathrm{w}^2. \tag{6.21}$$

Multiplying Eq.(6.19) and its complex conjugate by $\psi_{n_1}^m(r,\theta)$, integrating over the

transverse dimensions and making use of the orthogonality condition for Laguerre polynomials (6.13), we obtain

$$\left(2-\lambda_{n_1}^m+2i\frac{\partial}{\partial\bar{z}}\right)\bar{a}_{n_1}^m(\bar{s},\bar{z})\frac{(n_1+m)!}{n_1!}$$
$$=\frac{\bar{a}_0(s)}{2}\sum_{n_2}G_{n_1n_2}^m\int_{-\infty}^{\bar{s}}d\bar{s}'\sin(\bar{s}-\bar{s}')(\bar{a}_0^*(\bar{s}')\bar{a}_{n_2}^m(\bar{s}',\bar{z})+\bar{a}_{n_2}^{m*}(\bar{s}',\bar{z})\bar{a}_0(\bar{s}')) \qquad (6.22)$$

and its complex conjugate. The coupling coefficients are, using relations between Laguerre polynomials [88]:

$$G_{n_1n_2}^m=-\frac{N!}{n_1!n_2!2^{N+1}}\left(\frac{1}{K}+\frac{N+1}{2}\right). \qquad (6.23)$$

where $N=n_1+n_2+m$. Equation (6.22) can be used to find the evolution of the instability for a finite duration pulse. If $\bar{a}_0(s)$ has an arbitrary longitudinal profile, these equations need to be solved numerically. Yet since we have neglected the zeroth order wakes created by the temporal dependence of $\bar{a}_0(s)$ in Eq.(6.8), it is natural to assume that the pump is constant in amplitude, $\bar{a}_0(s)\equiv\bar{a}_0$. Then Eq.(6.22) can be solved by Fourier transforming in $\bar{s}$.

By introducing a new (real) variable

$$b_n^m=\bar{a}_0\bar{a}_n^{m*}+\bar{a}_0^*\bar{a}_n^m \qquad (6.24)$$

and Fourier transforming Eq.(6.22) in $\bar{s}$, a set of coupled differential equations is derived:

$$\left(\frac{\partial^2}{\partial\bar{z}^2}+(m+2n_1)^2\right)b_{n_1}^m=\mid\bar{a}_0^2\mid/2(m+2n_1)2^{-m-1}\frac{1}{1-\bar{\omega}^2}\sum_{n_2}A_{n_1n_2}^m b_{n_2}^m, \qquad (6.25)$$

where

$$A_{n_1n_2}^m=\frac{(m+n_1+n_2)!}{(m+n_1)!n_2!}2^{-n_1-n_2}\left(\frac{1}{K}+\frac{m+n_1+n_2+1}{2}\right). \qquad (6.26)$$

The dimensionless frequency $\bar{\omega}$ is the Fourier transform variable of $\bar{s}$.

Eq.(6.25) constitutes one of the main results of this chapter. It describes the

evolution of any initial perturbation to a flat-top laser pulse propagating in plasma channel. As it is obvious from Eq.(6.25), all the radial modes are coupled to each other. This is a consequence of both the nonlinear nature of the laser-plasma interaction and the finite transverse size of the unperturbed equilibrium. This formalism can describe various perturbations to a laser pulse, such as hosing, breathing, and other modulational instabilities such as quadrupole distortion. While the dynamics of short transversely uniform laser pulses in the homogeneous plasma has been explored in a number of recent publications [34, 35], this is the first analysis of the stability of externally focused laser pulses.

The coupling between different modes through the non-diagonal matrix $A^m_{n_1 n_2}$ also has to be considered for predicting the spatio-temporal character of the instability. Note that each radial mode has its own (using the analogy with electron beam instabilities) "betatron frequency", equal to, in normalized units,

$$\bar{k}_{\beta n} = m + 2n. \tag{6.27}$$

Different radial modes can be intuitively viewed as trapped modes, bouncing inside the channel with different (but very small!) angles of incidence. Their longitudinal phase velocities are, therefore, different from each other, and from that of the unperturbed pump. If the phase difference of 2π is accumulated between the pump and the n-th mode over a distance $\bar{L}_{\beta n}$, then the mode is said to have a betatron frequency $\bar{k}_{\beta n} = 2\pi/\bar{L}_{\beta n}$.

Thus the betatron frequency is an increasing function of the radial number of a mode, introducing a spread in betatron frequency and resulting in phase mixing. For *continuous* mode spectrum, as has been shown in the studies of the resistive hose instability [82, 83, 84], the ion-hose instability [85] and the electron-hose instability [86], this spread makes the instability convective instead of absolute. Important difference between these cases and laser wakefield instability is that the latter has a *discrete* set of eigenmodes. As we show in Section 6.3, the spatial growth rate of the instability is smaller than unity (in normalized units), because of the assumption (6.9), and fur-

ther decreases with propagation distance z. Hence, the growth rate is smaller than the spacing between different modes, as given by Eq.(6.27), and coupling between different modes should not affect the instability. The inclusion of the mode coupling is the subject of future investigations.

6.3 Example: Dipole Instability (Laser-Hose)

It is instructive to examine the evolution of a laser pulse which is initially displaced from the center of the channel as a "rigid body," which corresponds to the $(m, n) = (1, 0)$ mode. The physics of the resulting (simplified) instability bears a strong resemblance to the electron-hose instability [81]. In the electron-hose instability, an electron beam propagates through the underdense plasma, expels plasma electrons and is, thereby, linearly focused by the remaining ions. At the same time, electron beam interacts with plasma electrons outside of the ion channel. If, for example, the head of the electron beam is rigidly displaced off axis of the channel, it leaves behind a dipole plasma wake which then interacts with the following slices of the beam, resulting in the electron-hose instability. The electron-hose instability is absolute in propagation distance, that is, the perturbation of a given slice of the electron beam (fixed s) grows as a function of propagation distance z.

In the case of a laser pulse propagating through plasma, the laser itself plays the role of a particle beam. The focusing is accomplished by a parabolic plasma density profile, which is the counterpart of the ion channel. The single-mode instability (only approximate due to mode coupling, as we have alluded earlier) resulting from the displacement of the laser pulse off the channel axis then proceeds very much like the electron-hose instability. For this reason we will be referring to this dipole type of the wakefield instability as the laser-hose instability (LHI). Note that Eq.(6.25) is not restricted to studying the hosing instability and is valid for arbitrary azimuthal number m, thus allowing us to study breathing modes $m = 0$, quadrupole modes $m = 2$, and other higher multipole distortions of the laser pulse.

Neglecting the coupling of the lowest $n = 0$ mode to other radial modes with

$n = n_2$ can be somewhat justified by considering the coupling coefficient $A^1_{0n_2}$:

$$A^1_{0n_2} = \frac{1+n_2}{2^{n_2}}\left(\frac{1}{K} + \frac{n_2+2}{2}\right). \tag{6.28}$$

We see that the strength of coupling of the lowest radial mode to other modes falls of exponentially with the mode number. Thus, to elucidate the physics, we choose A^1_{00} to be the only nonvanishing element of the matrix A. The dispersion relation for the dipole mode, obtained by keeping only the diagonal element, is:

$$\bar{k}^2 = \left(1 - \frac{\mu}{1-\bar{\omega}^2}\right), \tag{6.29}$$

where

$$\mu = \frac{|\,\bar{a}_0^2\,|}{8}\left(1 + \frac{1}{K}\right) \approx \frac{|\,\bar{a}_0^2\,|}{(8K)} \tag{6.30}$$

and $\bar{k}$ is the Laplace transform variable of $\bar{z}$. A more accurate treatment would involve keeping a finite number of modes and solving the resulting matrix equation on the computer. Note that the dispersion relation (6.29) corresponds to the following linear differential equation in space-time variables:

$$\left(\frac{\partial^2}{\partial \bar{s}^2} + 1\right)\left(\frac{\partial^2}{\partial \bar{z}^2} + 1\right) b_1 = \mu b_1. \tag{6.31}$$

Asymptotic behavior of the solutions of Eq.(6.31) for $\bar{z} \geq 1, \bar{s} \geq 1$ can be obtained by the steepest descent integration (see, for example, [81]) in regimes that are delineated by relations between the length of the pulse s, the interaction length z and the coupling parameter μ. For the analysis presented above to be valid, $\mu \ll 1$. With $z_R = k_0 \mathrm{w}^2$ and returning to dimensional variables, the asymptotic amplitudes are:
(i) Long pulses:

$$\bar{\omega}_p s \gg 1/\mu(z/z_R)$$

$$\bar{a}_1 \sim \bar{a}_{10} \exp\left[\frac{\sqrt{3}}{4}\,|\,a_0^2/(8K)\,|^{1/3}\,(z/z_R)^{\frac{2}{3}}(\bar{\omega}_p s)^{\frac{1}{3}}\right] \tag{6.32}$$

(ii) Intermediate pulses:

$$\mu(z/z_r) \ll \bar{\omega}_p s \ll 1/\mu(z/z_R)$$

$$\bar{a}_1 \sim \bar{a}_{10} \exp\left[\mid a_0^2/(8K) \mid^{1/2} (z/z_R)^{\frac{1}{2}} (\bar{\omega}_p s)^{\frac{1}{2}} \right] \tag{6.33}$$

(iii) Short pulses:

$$\bar{\omega}_p s \ll \mu(z/z_R)$$

$$\bar{a}_1 \sim \bar{a}_{10} \exp\left[\frac{3\sqrt{3}}{4} \mid a_0^2/(8K) \mid^{1/3} (z/z_R)^{\frac{1}{3}} (\bar{\omega}_p s)^{\frac{2}{3}} \right] \tag{6.34}$$

The following numerical example which satisfies the basic assumptions of our theory gives the scale of the instability. For 10μ radiation propagating through a plasma of $n_0 = 4 \cdot 10^{16} cm^{-3}$, focused to a $0.1mm$ spotsize, $z_R \approx 0.6cm$. For the above parameters $K = 0.0625$ (see Eq.(6.2)), so choosing $a_0 = 0.4$ satisfies our assumption that self-focusing can be ignored compared to channel focusing. Equation(6.29) for these parameters was inversely Fourier-Laplace transformed and solved numerically for the real part of the perturbed field which is plotted as a function of propagation distance in Figure 6-1. The perturbation was evaluated at a distance $s = \lambda_p/2$ behind the onset of the instability (at $s = 0$). We can see that after 20 Rayleigh ranges the initial perturbation, set equal to $a_1 = 0.01$, has grown tenfold. An ultrashort laser pulse, initially displaced by 1% of axis, will acquire a 10% displacement after propagating in plasma for a distance less than $6cm$. The obvious consequence for the acceleration is that the accelerating mode will now be displaced off axis, and the electron bunch, initially injected *on axis*, will experience a transverse deflecting force which is very hard to control precisely. Thus a successful design of the laser-wakefield accelerator, with its stringent requirements of the phase and amplitude stability of the accelerating field (plasma wake), critically depends on our ability to control the wakefield instabilities. In Section 6.4.2 we briefly review the concept of BNS damping and apply it to the laser-hose instability.

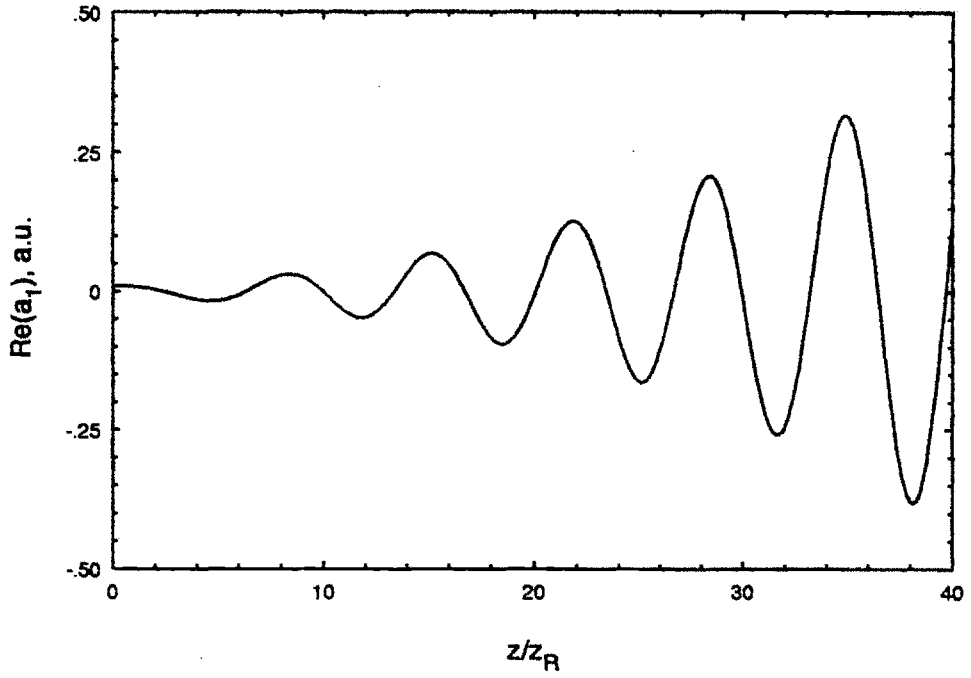

øfiFigure 6-1: Evolution of the normalized off-axis displacement of the laser pulse a_1 with propagation distance z/z_R. Initial displacement at $z = 0$ is $a_1 = 0.01$ and the pulse length $\omega_p s = \pi$.

6.4 Envelope Equation and BNS Damping

6.4.1 Relativistic Guiding and Laser Wakefield Instability

As we have seen in Section 6.3, the initial perturbation on the laser pulse exponentiates as $(z/z_R)^q(s\bar{\omega}_p)^r$ where $q+r=1$. This exponentiation is typical of beam break-up instabilities [89] in conventional accelerators where a charged particle bunch interacts with its electromagnetic environment. Here the laser pulse is somewhat analogous to the particle beam and the electron plasma to the metallic structures through which the beam propagates. The electron beam excites a higher order mode in the metallic structure which acts on the following beam slices as a wake. In the case of the laser wakefield accelerator, the wake is excited in the plasma.

While the analogy fails in detail, it is useful in suggesting cures for the instability. In linear electron accelerators, a technique known as BNS [90] damping has been employed to mitigate the effect of beam break-up instabilities. The BNS damping works by introducing a head-to-tail variation in the transverse oscillation frequencies of the accelerated particles. A similar approach to damping the instability can be employed in case of laser wakefield instability. Betatron frequency of a particular transverse mode (m,n) is given by

$$k_\beta = \frac{(m+2n)\lambda_0}{2\pi \mathrm{w}^2}. \tag{6.35}$$

From Eq.(6.35) it is clear that a variation of k_β can be imposed through a frequency chirp (which changes the wavelength λ_0), or may occur naturally, for sufficiently intense pulses, when relativistic guiding corrections from $a_0(s)$ are included in the analysis (since $a_0(s)$ affects the spot size $w(s)$ at a particular slice s through partial relativistic focusing). While the former method of inducing the head-to-tail spread in betatron frequency is very easy to understand, the later one is more complicated and is better approached by the method of envelope equation.

The envelope equation is widely used for analysing self-focusing of lasers in plasma [19, 20], laser pulse self-modulation [22], and other phenomena. For the purpose of il-

lustrating how relativistic guiding affects the evolution of laser wakefield instabilities, we consider a dipole LHI in slab geometry. A very similar treatment can be carried out without an assumption of stratified plasma.

Similarly to Eq.(6.1), we assume a quadratic dependence of plasma density on the transverse coordinate x:

$$n_0(x) = \bar{n}_0 \left(1 + \frac{x^2}{W^2}\right). \tag{6.36}$$

Then, in the eikonal approximation, in planar geometry, assuming weakly relativistic laser field, we obtain

$$\begin{aligned} \left(2i\frac{\partial}{\partial \bar{z}} + \frac{\partial^2}{\partial \bar{x}^2}\right) a &= \frac{\omega_{p0}^2 \mathrm{w}^2}{c^2}\left(\frac{\delta n}{n_0} - \frac{|\, a\,|^2}{2}\right) a \\ &+ \bar{x}^2 a, \end{aligned} \tag{6.37}$$

where the transverse coordinate x is scaled to w, and longitudinal coordinates are made dimensionless according to Eq.(6.21). Note that in Eq.(6.37) we have neglected the constant quantities such as ω_{p0}^2 since they can be incorporated as phase factors in a. As was shown in Section 5.3, the density equation is

$$\left(\frac{\partial^2}{\partial \bar{s}^2} + 1\right)\frac{\delta n}{n_0} = \frac{c^2\nabla^2}{\omega_{p0}^2}\frac{|\, a\,|^2}{2}. \tag{6.38}$$

It is convenient to introduce a nonlinear index of refraction

$$\chi = \frac{\delta n}{n_0} - \frac{|\, a\,|^2}{2}, \tag{6.39}$$

which satisfies

$$\left(\frac{\partial^2}{\partial \bar{s}^2} + 1\right)\chi = (K\bar{\nabla}_\perp^2 - 1)\frac{|\, a\,|^2}{2}, \tag{6.40}$$

where we have assumed that the quasistatic approximation (6.18) holds. We assume, as previously, that the channel is many collisionless skin depths wide, or that Eq.(6.2) is satisfied. Hence, the first term on the RHS of Eq.(6.40) can be neglected.

One can proceed solving Eqs.(6.37) and (6.40) analogously to the way it was

done in Section 6.2 by linearizing about an approximate equilibrium. Neglecting the relativistic focusing is essential for obtaining the equilibrium field a_0. Expanding the linearized solution of Eq.(6.37) in eigenmodes provides a very detailed information about the mode structure and coupling. Yet the goal of this section is to study the effects of relativistic focusing on the evolution of wakefield instabilities. We therefore use an alternative approach, the envelope equation.

The envelope equation derives relationships between the global characteristics (or moments) of the laser pulse, such as the total energy of the pulse, average spot size, average off-axis displacement, and so on. The obvious drawback of this approach is that, in general, infinite number of global quantities is needed to characterize the laser pulse. Therefore, a truncation (or closure) has to be made, based on our intuition and judgement about the importance of various moments. Another, more subtle shortcoming of the envelope approach, is that, by neglecting the mode structure of the laser field, effects related to mode coupling and phase mixing could be missed out. Conceptually, this is somewhat similar to the fact that certain kinetic effects, such as Landau damping, cannot be derived from the fluid treatment of plasma. Yet, as was mentioned at the end of Section 6.2, we speculate that the mode coupling does not play a significant role in the evolution of the instability.

To analyze the laser hose instability, we introduce a power-weighted transverse displacement of the laser:

$$\zeta = \frac{\int_{-\infty}^{+\infty} d\bar{x}\bar{x} \mid a \mid^2}{N}, \tag{6.41}$$

where N is the conserved quantity equal to the power flux:

$$N = \int_{-\infty}^{+\infty} d\bar{x} \mid a \mid^2 . \tag{6.42}$$

From Eq.(6.37) we derive

$$\frac{\partial \mid a \mid^2}{\partial \bar{z}} = -\frac{i}{2}\frac{\partial}{\partial \bar{x}}\left(a\frac{\partial a^*}{\partial \bar{x}} - a^*\frac{\partial a}{\partial \bar{x}}\right). \tag{6.43}$$

Integrating Eq.(6.43) by parts results in

$$\frac{\partial N}{\partial \bar{z}} = 0. \tag{6.44}$$

As mentioned in Section 6.2, this is a consequence of the paraxial approximation: adjacent slices of radiation do not exchange energy with each other because all the radiation moves forward at a constant group velocity v_{g0}.

Using Eq.(6.43) and the definition of ζ we find that

$$\frac{\partial \zeta}{\partial \bar{z}} = \frac{i}{2N} \int d\bar{x} \left(a \frac{\partial a^*}{\partial \bar{x}} - a^* \frac{\partial a}{\partial \bar{x}} \right). \tag{6.45}$$

Taking another derivative of Eq.(6.45) and using Eq.(6.37), we derive an "equation of motion" for the average laser displacement:

$$\frac{\partial^2 \zeta}{\partial \bar{z}^2} + \zeta = -\frac{1}{2NK} \int d\bar{x} \mid a \mid^2 \frac{\partial \chi}{\partial \bar{x}}. \tag{6.46}$$

Equation (6.46) has to be solved together with the wake equation

$$\left(\frac{\partial^2}{\partial \bar{s}^2} + 1 \right) \chi = -\frac{\mid a \mid^2}{2}, \tag{6.47}$$

which is obtained from Eq.(6.40) by assuming that $K \ll 1$.

Equations (6.46) and (6.47) are linearized and an appropriate closure has to be selected. Let assume that

$$\begin{aligned} \mid a \mid^2 (\bar{s}, \bar{z}, \bar{x}) &= \mid a \mid^{2(0)} (\bar{s}, \bar{x}) + \mid a \mid^{2(1)} (\bar{s}, \bar{z}, \bar{x}), \\ \chi(\bar{s}, \bar{z}, \bar{x}) &= \chi^{(0)}(\bar{s}, \bar{x}) + \chi^{(1)}(\bar{s}, \bar{z}, \bar{x}), \end{aligned} \tag{6.48}$$

where it is assumed that the zeroth order quantities are even functions of $\bar{x}$ and the first order quantities are odd in $\bar{x}$, and $\mid a \mid^{2(0)} (\bar{s}, \bar{x})$ changes adiabatically on a scale of a plasma oscillation. An approximate expression for $\chi^{(0)}(\bar{s}, \bar{x})$ can then be obtained

by

$$\chi^{(0)}(\bar{s},\bar{x}) = -\frac{\mid a \mid^{2(0)}(\bar{s},\bar{x})}{2}. \tag{6.49}$$

Not that, in reality, laser pulse *will not* be adiabatic on a scale of plasma oscillation, for two reasons—because long pulses do not excite appreciable wakes and because, as we show later, BNS damping becomes inefficient for long pulses. Hence, $\chi^{(0)}$ will be smaller than in Eq.(6.49)—relativistic guiding is not effective for short pulses [15]. Nevertheless, analytical progress can be made when the zeroth order wakes are neglected. The obtained physical insights justify using the adiabatic assumption (6.49).

At this stage we introduce a semi-empirical relation between the dipole perturbation of the laser field, $\mid a \mid^{2(1)}$, and the centroid displacement ζ—we assume that the laser pulse is displaced as a rigid body, that is

$$a(\bar{s},\bar{z},\bar{x}) = a^{(0)}[\bar{s},\bar{x}-\zeta(\bar{s},\bar{z})]. \tag{6.50}$$

Note that definition of ζ (6.41) is consistent with (6.50), and Eq.(6.44) remains valid as well.

From Eq.(6.50), assuming $\zeta \ll 1$, we obtain

$$\mid a \mid^{2(1)}(\bar{s},\bar{z},\bar{x}) = -\zeta\frac{\partial \mid a \mid^{2(0)}}{\partial\bar{x}}. \tag{6.51}$$

Linearizing Eq.(6.47) and substituting (6.51) results in

$$\left(\frac{\partial^2}{\partial\bar{s}^2}+1\right)\chi^{(1)} = \frac{\zeta}{2}\frac{\partial \mid a \mid^{2(0)}}{\partial\bar{x}}. \tag{6.52}$$

Linearizing Eq.(6.46) and combining it with Eq.(6.52) yields

$$\left(\frac{\partial^2}{\partial\bar{s}^2}+1\right)\left(\frac{\partial^2}{\partial\bar{z}^2}+1+T^2(\bar{s})\right)\zeta = T^2(\bar{s})\zeta, \tag{6.53}$$

where

$$T^2(\bar{s}) = \frac{1}{4NK}\int d\bar{x}\left(\frac{\partial \mid a \mid^{2(0)}(\bar{s},\bar{x})}{\partial\bar{x}}\right)^2. \tag{6.54}$$

$T^2(\bar{s})$ is the BNS term we were looking for. Its physical meaning is transparent: when relativistic focusing is included, those radiation slices with higher values of $\mid a \mid^2$ are focused stronger than the low-power slices. Therefore, the longitudinal shape of the equilibrium laser pulse creates a natural head-tail spread in betatron frequency, and can be very important in determining the evolution of a wakefield instability. As was mentioned earlier, this result is valid for laser pulses longer than plasma oscillation period. For shorter pulses *the RHS* of Eq.(6.53) is still given by Eq.(6.54), while *the BNS* term is smaller than predicted by Eq.(6.54), as explained earlier.

In principle, we have obtained the evolution equation for the pulse centroid in terms of the integral over the transverse equilibrium profile, whatever it happens to be. To make a realistic estimate of the magnitude of T^2 we assumed that the channel focusing is much stronger than relativistic guiding. The approximate profile of the equilibrium laser radiation is then given by

$$a_0(\bar{s},\bar{x}) = a_0(\bar{s}) \exp\left(-\bar{x}^2/2\right). \tag{6.55}$$

Then the expression for $T^2(\bar{s})$ can be simplified to give

$$T^2(\bar{s}) = \frac{k_p^2 \mathrm{w}^2 a_0^2(\bar{s})}{4\sqrt{2}}. \tag{6.56}$$

Equation (6.53), which describes the analog of BNS damping in laser wakefield instabilities, thus simplifies to

$$\left(\frac{\partial^2}{\partial \bar{z}^2} + 1 + \frac{k_p^2 \mathrm{w}^2 a_0^2(\bar{s})}{4\sqrt{2}}\right)\left(\frac{\partial^2}{\partial \bar{s}^2} + 1\right)\zeta = \frac{k_p^2 \mathrm{w}^2 a_0^2(\bar{s})}{4\sqrt{2}}\zeta, \tag{6.57}$$

Equation (6.57) was solved numerically for the following parameters:

$$a_0(\bar{s}) = a_0 \sin\left(\pi \bar{s}/s_{max}\right) \quad \text{for} \quad 0 < \bar{s} < s_{max}, \tag{6.58}$$

with $s_{max} = 3.0$, $a_0 = 0.4$, $n_0 = 4 \cdot 10^{16} cm^{-3}$ and $\mathrm{w} = 0.16$. In Fig. 6-2 the relativistic

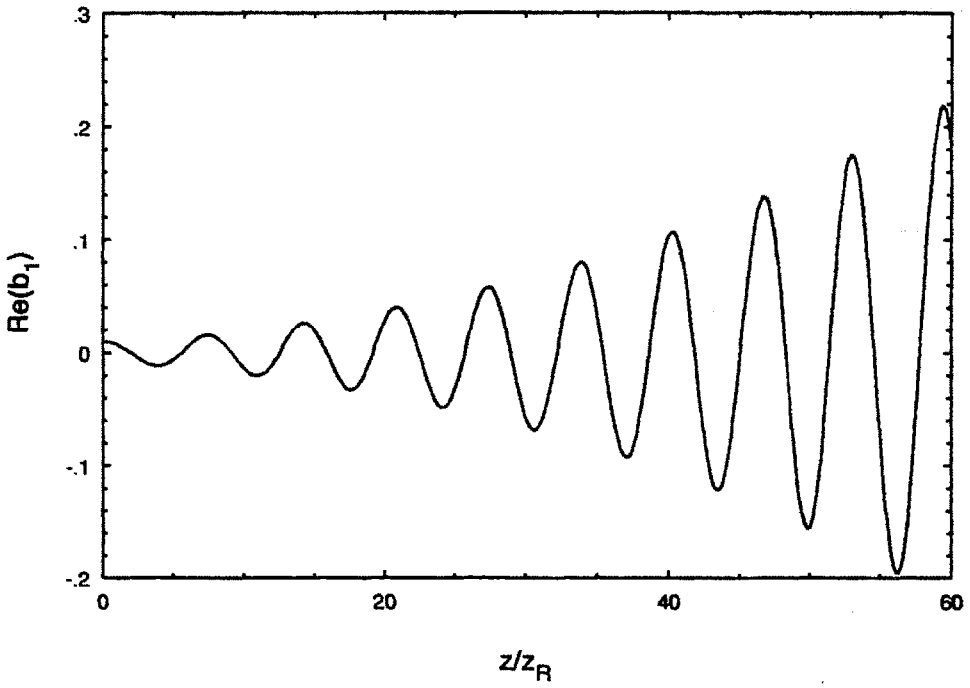

ÆfiFigure 6-2: Evolution of the normalized off-axis displacement of the laser pulse a_1 with propagation distance z/z_R. The pump profile is given by Eq.(6.58), with $s_{max} = 3.0$ and $a_0 = 0.4$. Initial displacement at $z = 0$ is $a_1 = 0.01$. Relativistic guiding is neglected.

modification to the betatron frequency was neglected. An initially seeded 1% modulation ($\zeta = 0.01$) has grown by a factor of 20. When the relativistic correction was included, as shown in Fig. 6-3, the instability saturates at $\zeta = 0.04$. In both cases the average centroid displacement was measured half-way into the pulse at $\bar{s} = 0.5 s_{max}$.

In the next numerical example, shown in Fig. 6-4, Eq.(6.57) is integrated for the same set of parameters, except that $s_{max} = 6.0$. We see that BNS damping is significantly decreased for longer pulses.

This is intuitively correct since longer pulses phase mix slower, and, thus, can undergo more exponentiations. Thus, a simplified prescription for avoiding laser

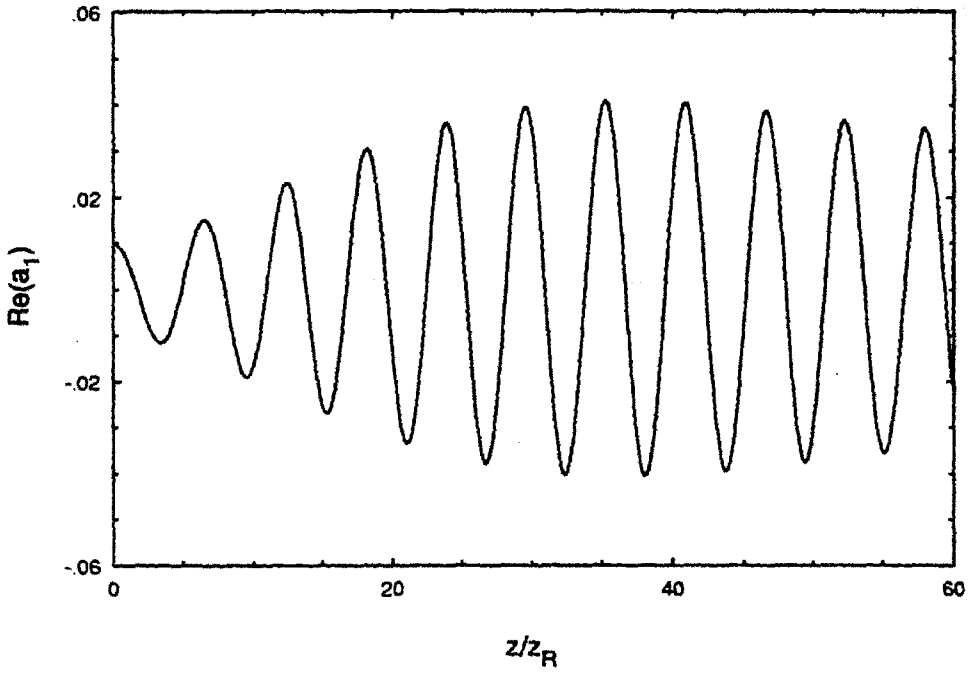

ŒfiFigure 6-3: Evolution of the normalized off-axis displacement of the laser pulse a_1 with propagation distance z/z_R. The pump profile is given by Eq.(6.58), with $s_{max} = 3.0$ and $a_0 = 0.4$. Initial displacement at $z = 0$ is $a_1 = 0.01$. Relativistic guiding is included.

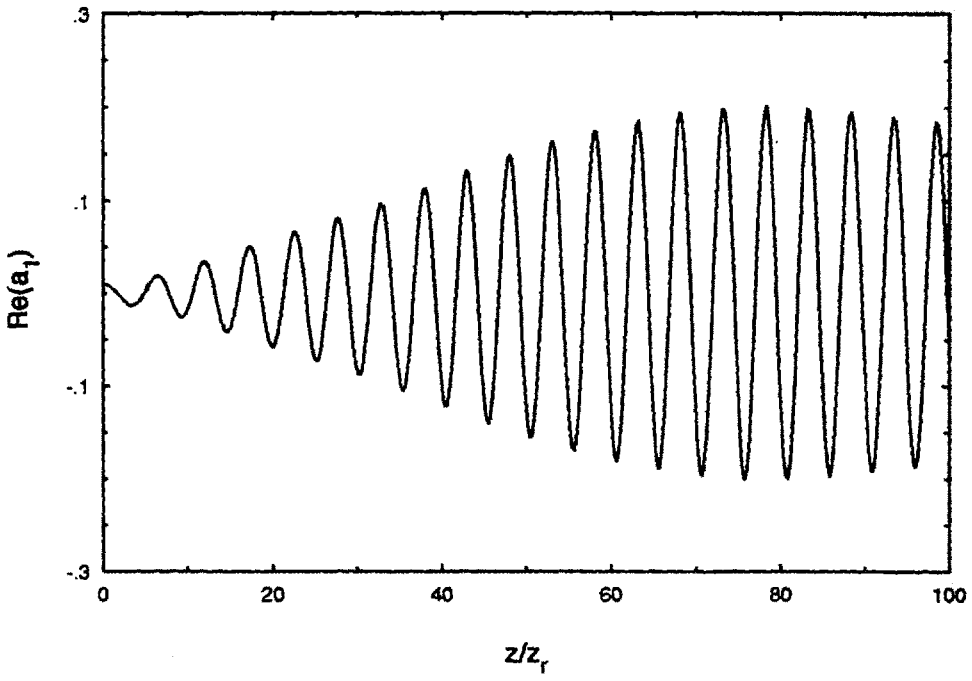

ØfiFigure 6-4: Evolution of the normalized off-axis displacement of the laser pulse a_1 with propagation distance z/z_R. The pump profile is given by Eq.(6.58), with $s_{max} = 6.0$ and $a_0 = 0.4$. Initial displacement at $z = 0$ is $a_1 = 0.01$. Relativistic guiding is included.

wakefield instabilities is to operate with short pulses. To understand why this is the case, one has to develop a better understanding of the BNS damping. In the next subsection we analytically develop a model for BNS damping for the case of linear variation in the betatron frequency and quantitatively justify the results of numerical calculations presented here.

6.4.2 Brief Theoretical Treatment of BNS Damping

In this section we sketch the theoretical underpinnings of the BNS damping technique and make quantitative estimates of the degree of BNS damping necessary to suppress a wakefield instability.

We modify the simplified equation for the LHI (6.31) by including a phenomenological variation in betatron frequency as a function of $\bar{s}$:

$$\left(\frac{\partial^2}{\partial \bar{s}^2}+1\right)\left(\frac{\partial^2}{\partial \bar{z}^2}+1+\Delta\bar{k}_\beta^2(\bar{s})\right)b_1=\mu b_1, \tag{6.59}$$

where μ is defined by Eq.(6.30). Since this variation can be imposed by chirping the laser frequency as well as through the relativistic guiding, we do not, for the purpose of this calculation, restrict $\Delta\bar{k}_\beta(\bar{s})$ to the functional form obtained in Eq.(6.57).

The logic behind the BNS suppression is rather straightforward: since the instability we are trying to suppress is cumulative, that is, a given slice of radiation is affected by all the preceeding slices, to suppress the instability one should somehow decouple the slices from each other, or make their contributions decohere. This can be accomplished by making the betatron frequencies of different slices vary along the pulse. If $\Delta\bar{k}_\beta(\bar{s})$ variation is imposed, then, for two slices separated by distance $\Delta\bar{s}$ to get out of phase, they have to propagate a distance of order

$$\bar{z}\approx\frac{\pi}{\bar{k}'_\beta\Delta\bar{s}}, \tag{6.60}$$

where $\bar{k}'_\beta=\partial\bar{k}_\beta/\partial\bar{s}$ is a typical rate of chirping. Alternatively, Eq.(6.60) can interpreted as giving an effective "coherence length" along the pulse, $\Delta\bar{s}$, as a function

of propagation distance $\bar{z}$. Therefore, as $\bar{z}$ increases, any pulse becomes effectively "short", which puts us into the assymptotic regime given by Eq.(6.34). Substituting $\Delta\bar{s}$ for $\bar{s}$ in Eq.(6.34) shows that the growth of the instability with $\bar{z}$ stops for large propagation distances. We see that the physics behind BNS damping is phase mixing.

An important issue to address is by how much the instability grows before the BNS damping becomes effective. To do that, we choose a simple functional form of $\Delta\bar{k}_\beta(\bar{s})$, easily amenable to analytic calculations:

$$\Delta\bar{k}_\beta(\bar{s}) = \alpha\frac{\bar{s}}{s_{max}}, \tag{6.61}$$

and assume that the pulse is at least a few plasma periods long ($s_{max} \gg 1$), and the propagation distance is such that the pulse is in either the intermediate, or long regime (see Eqs.(6.32) and (6.33)). Then, Laplace transforming Eq.(6.59) in $\bar{z}$ and assuming that $b_1 = e^{-i\bar{s}}\bar{b}_1(\bar{s})$, with the envelope variable $\bar{b}_1$ slowly varying with $\bar{s}$, results in

$$\frac{d\bar{b}_1(\bar{s},\bar{k})}{d\bar{s}} - i\frac{\mu/2}{1+\Delta\bar{k}_\beta(\bar{s})-\bar{k}^2}\bar{b}_1(\bar{s},\bar{k}) = 0. \tag{6.62}$$

Eq.(6.62) is integrated between $\bar{s} = 0$ and $\bar{s} = s_{max}$, with the betatron frequency given by Eq.(6.61), and then inversely Laplace transformed in $\bar{k}$ to yield an integral expression for $b_1(\bar{s},\bar{z})$:

$$b_1(\bar{s},\bar{z}) \propto e^{-i\bar{s}}\int_{-\infty}^{+\infty}\frac{d\bar{k}}{2\pi}e^{i\Phi(\bar{s},\bar{z},\bar{k})}\bar{b}_1(\bar{s}=0,\bar{k}), \tag{6.63}$$

where

$$\Phi = \frac{\mu\bar{s}}{2\alpha}\ln\left(1+\frac{\alpha}{1-\bar{k}^2}\right) + \bar{k}\bar{z}. \tag{6.64}$$

To find the assymptotic behavior of b_1 integral (6.64) has to be integrated by the steepest descent. It is easy to check that in the limit of $\alpha \to 0$ the assymptotic expressions (6.32) and (6.33) are recovered. Note that, for notational convenience, we are using $\bar{s}$ instead of s_{max}.

Integrating (6.64) by steepest descent requires finding a saddle point in the com-

plex $\bar{k}-$ plane which satisfies $d\Phi/d\bar{k} = 0$. The result is

$$\frac{\mu\bar{s}\bar{k}}{(1-\bar{k}^2+\alpha/2)^2-\alpha^2/4} = -\bar{z}. \tag{6.65}$$

From Eq.(6.65) it is obvious that for long pulses ($\bar{z}/(\mu\bar{s}) \ll 1$) BNS damping is not effective since $\bar{k}^2 \gg 1, \alpha$.

The significance of phase mixing becomes obvious in the opposite regime, where $\bar{z}/(\mu\bar{s}) \gg 1$. Choosing $\bar{k} = \sqrt{1+\alpha/2}+\kappa$ and inserting it in Eq.(6.65) results in

$$\kappa^2 = -\mu\sqrt{1+\alpha/2}\bar{s}/\bar{z} + \alpha^2/4. \tag{6.66}$$

We see from Eq.(6.66) that, at a given distance $\bar{s}$ the growth of the instability stops for $\bar{z} > \bar{z}_{cr}$, where

$$\bar{z}_{cr} = \frac{4\mu\sqrt{1+\alpha/2}\bar{s}}{\alpha^2}. \tag{6.67}$$

We estimate the number of exponentiations, N_{exp}, the instability undergoes before it phase-mixes, by inserting $\bar{z} = \bar{z}_{cr}$ into the asymptotic solution given by Eq.(6.33):

$$N_{exp} = 2\mu\bar{s}/\alpha. \tag{6.68}$$

Therefore, to have of order one exponentiation, the fractional variation of betatron frequency, per unit pulse length, should be of order

$$\frac{\alpha}{\bar{s}} > 2\mu, \tag{6.69}$$

which is not a very stringent requirement, considering that $\mu \ll 1$. In physical units, requirement (6.69) means providing a fractional chirp per plasma period of order P/P_c.

The results we have obtained in this section are limited to long and intermediate pulses, as expressed by Eqs.(6.32- 6.33). Since a typical laser pulse of duration of order $\bar{s} \approx 1$ first goes through the intermediate regime, and then saturates according

to Eq.(6.66), less than one exponentiation is guaranteed if

$$\bar{z}_{cr} < \frac{\bar{s}}{\mu}. \tag{6.70}$$

The RHS of (6.70) is equal to the normalized propagation distance past which the pulse is in the "short pulse" regime, according to Eq.(6.34). For $\bar{s} \approx 1$ and $\mu < 1$, condition (6.70) is a less stringent requirement than (6.69). Expressed in terms of the chirp parameter α, condition (6.70) becomes:

$$\alpha > 2\mu. \tag{6.71}$$

Thus, the prescription for effective BNS damping becomes: for a short pulse of order $1/\omega_p$, the betatron frequency has to be chirped, with $\Delta k_\beta^2/k_\beta^2 \approx 2\mu$.

The result we have derived is limited to linear variation of betatron frequency. Nonetheless, the qualitative conclusions are most likely to hold for other temporal profiles of betatron frequency, including the one given by Eqs.(6.57,6.58). As the number of exponetiations before the phase mixing increases with the length of the pulse (μ and α kept constant), as given by Eq.(6.68), BNS damping will be less efficient for longer pulses. This explains why the instability saturated at a much higher amplitude for a twice long pulse in Fig 6-4 than in Fig 6-4.

Some of the conclusions drawn in this paper rely on the quadratic radial variation of the plasma density. Another simple model [40], which also has better accelerating properties, is an inverted step-function radial density dependence, which, due to finite variation in the plasma density, will have only a finite number of discrete eigenmodes. By a careful choice of parameters, the unstable dipole mode can be pushed into the continuum, which may reduce the instability.

6.4.3 Conclusions

In summary, a new instability of the propagation of a laser pulse in a plasma channel has been analyzed for the case of a quadratic density variation. The instability is

significant when pulses need to be propagated many Rayleigh lengths, as is envisioned in laser wakefield accelerators. Explicit growth rates have been obtained for the dipole instability over a wide range of parameters. The growth rate is seen to be nonzero even for short pulses, of order a plasma wavelength. Future investigations need to examine in more detail the influence of the nonlinearities in the unperturbed equation, especially wakes generated by the equilibrium mode, relativistic electron velocities, coupling between modes, and different density profiles and pulse shapes.

Chapter 7

Laser Wakefields in Inhomogeneous Plasmas

7.1 General Formalism

In Chapter 6 we made a detailed analysis of the excitation of wakefields in quasi-uniform plasmas. The plasma was treated as being uniform when the induced density perturbations were calculated. Plasma inhomogeneity was taken into account only when calculating the transverse modes of the laser field. The approximation of quasi-uniformity (Eq.(6.2)) and a parabolic unperturbed density profile allowed us to derive a matrix dispersion relation for the transverse modal structure of the laser-plasma system.

The focus of this section, however, will be to develop a general formalism for analyzing wakefield generation in plasma *without* making an approximation of uniformity. The motivation for developing such a general formalism comes from the idea of a hollow channel laser wakefield accelerator [40]. In this scheme an evacuated channel in the plasma serves as an optical fiber which guides the laser pulse over many Rayleigh lengths. At the same time, the ponderomotive force of the laser excites wakefields at the surface of the channel, which extend to the center where they can be used for particle acceleration. In order for this acceleration scheme to be efficient, the size of the laser pulse should be comparable with the size of the channel. Since the interface

between the evacuated channel and the surrounding plasma is relatively sharp (on a scale of laser spot size), the approximation of uniform plasma clearly breaks down.

Other assumptions that were used in Chapters 5 and 6 will remain valid in this chapter. We assume that plasma is uniform in the direction of the laser propagation and is very underdense, so that Eq.(5.4) holds everywhere in the plasma. We also assume that the motion of plasma electrons in the field of the laser is weakly relativistic. While Chapter 6 was mainly concerned with the evolution of the laser in response to the induced plasma wakes, the main focus of this section is the excitation of the *wakes themselves.* Laser pulse will be assumed unaffected by its interaction with the plasma. Treating *both* the laser and nonuniform plasma at the same time is very complicated, which motivated this (artificial) breaking of the problem into two. While the laser eigenmodes for a parabolic unperturbed density profile can be calculated analytically, the equations for the plasma wake are not amenable to analytical calculations. On the other hand, the wake excitation in a hollow channel (which will serve as a starting point for the exploration of nonuniform plasmas in this Chapter) is very straightforward, while the laser eigenmodes cannot be obtained in a closed form.

The plasma is assumed to have an arbitrary transverse profile, with a local plasma density defined as

$$\omega_{p0}^2(x) = \frac{4\pi n_0(x) e^2}{m}, \tag{7.1}$$

where $n_0(x)$ is the unperturbed plasma density. As discussed in Section 5.3, assumption (5.4) allows the separation of time time scales into fast (laser period) and slow (order of plasma period). All the relations derived in this chapter are for the *slow* time scale variables. We therefore drop the superscript s that was used in Section 5.3 in relation to the induced electric fields.

As is known from the earlier work on interaction of obliquely incident p-polarized lasers with inhomogeneous plasmas [51, 91], calculations are more easily performed in terms of the magnetic field $\vec{B}$. Fourier transforming the Faraday's law in time and

introducing a new quantity

$$\vec{P} = \frac{ic}{\omega}\vec{B}$$

results in

$$\vec{E} + \frac{4\pi i}{\omega}\vec{j} = \vec{P}. \tag{7.2}$$

Combining Eq.(7.2) with Eq.(5.15) and recalling that the current in the electron plasma is given by $\vec{j} = en_0\vec{v}$ yields:

$$\vec{E} = \frac{\omega_{p0}^2(x)/\omega^2}{1-\omega_{p0}^2(x)/\omega^2}\vec{\nabla}f + \frac{\vec{\nabla}\times\vec{P}}{1-\omega_{p0}^2(x)/\omega^2}. \tag{7.3}$$

Later in the section we show that for the case of a homogeneous plasma vector $\vec{P}$ goes to zero and the wake becomes electrostatic, confirming the results of Section 5.3 (see Eq.(5.22)).

From Maxwell's Equations,

$$\nabla\times\nabla\times\vec{E} + \frac{1}{c^2}\frac{\partial^2\vec{E}}{\partial t^2} = -\frac{4\pi}{c^2}\frac{\partial\vec{j}}{\partial t}. \tag{7.4}$$

Combining Eq.(7.4) with Eq.(7.3) we obtain:

$$\nabla\times\nabla\times\left(\frac{\nabla\times\vec{P}}{1-\omega_{p0}^2(x)/\omega^2} + \vec{\nabla}f\frac{\omega_{p0}^2(x)}{\omega^2}\frac{1}{1-\omega_{p0}^2(x)/\omega^2}\right) = \\ = \frac{\omega^2}{c^2}\nabla\times\vec{P}. \tag{7.5}$$

Equation (7.5) can be simplified to a scalar differential equation in instances where the plasma has planar or azimuthal symmetry. In these limits, the outer curl in Eq.(7.5) can be removed and the Eq.(7.5) is substantially simplified:

Case 1. Slab geometry, $n = n(x), f = f(x,z)$ and the TM space-charge mode is exited, with $\vec{P} = \vec{e}_y P(x,z)$.

Case 2. Cylindrical geometry, $n = n(r), f = f(r,z)$. Also, the TM wave is generated with $\vec{P} = \vec{e}_\phi P(r,z)$.

The physical reason for this simplification is that, from the symmetry of the

cylindrical and slab geometries, magnetic field is unidirectional. In this chapter we concentrate on case 1. The extension to azimuthally symmetrical case is straightforward.

By introducing $\vec{P} = \vec{e}_y P(x,z)$, Eq.(7.5) is reduced to

$$-\nabla^2 P + \frac{\partial P}{\partial x}\frac{\partial}{\partial x}\ln\left(1-\frac{\omega_{p0}^2(x)}{\omega^2}\right) - \frac{\omega^2-\omega_{p0}^2(x)}{c^2}P = \\ = -\frac{\partial f}{\partial z}\frac{\partial}{\partial x}\ln\left(1-\frac{\omega_{p0}^2(x)}{\omega^2}\right). \tag{7.6}$$

Equation (7.6), in a slightly modified form, was used for analyzing the resonant absorption of obliquely incident p polarized radiation by inhomogeneous plasma [50, 51, 91]. It is for the first time, to our knowledge, that it is used for studying ponderomotively induced plasma wakes for particle acceleration.

We will concentrate on the wakes left by laser pulses moving with speeds close to the speed of light. This is equivalent to considering all the quantities of interest as functions of x and a single longitudinal variable $\zeta = ct - z$, and assumes that the laser pulse is nonevolving. Then, since

$$\frac{\partial}{\partial z} = -\frac{\partial}{c\partial t}, \tag{7.7}$$

Eq.(7.6) simplifies to

$$-\frac{\partial^2 P}{\partial x^2} + \frac{\partial P}{\partial x}\frac{\partial}{\partial x}\ln\left(1-\frac{\omega_{p0}^2(x)}{\omega^2}\right) + \frac{\omega_{p0}^2(x)}{c^2}P = \\ = -i\frac{\omega}{c}\tilde{f}\frac{\partial}{\partial x}\ln\left(1-\frac{\omega_{p0}^2(x)}{\omega^2}\right), \tag{7.8}$$

where

$$\tilde{f}(x,\omega) = \int_{-\infty}^{+\infty} dt e^{i\omega t} f(x,t). \tag{7.9}$$

Eq.(7.8) holds for any transverse density profile $\omega_{p0}^2(x)$, including those with density discontinuities. Equation (7.3) and a knowledge of the $\vec{P}(x,\zeta)$ is sufficient for computing the electric field.

For continuous density profiles Eq.(7.8) can be solved for P using the following boundary condition:

$$\lim_{x\to\pm\infty} P(x) = 0. \tag{7.10}$$

In a homogeneous plasma ($\frac{\partial}{\partial x}\omega_{p0}^2(x) = 0$) it is evident that $P = 0$ is the only solution satisfying Eqs.(7.8-7.10). This implies that the plasma wake is electrostatic in a homogeneous plasma.

For discontinuous density profiles (e.g. hollow channel) one has to match the solutions in each region of continuous density, at the discontinuities. The usual way of matching the solutions at discontinuities is to find invariants that remain continuous across the density jump. Close inspection of Eq.(7.8) gives the following continuity conditions:

$$P(x) \to \text{continuous} \tag{7.11}$$

$$\frac{\frac{\partial P}{\partial x} + i\frac{\omega}{c}\tilde{f}}{1 - \frac{\omega_{p0}^2(x)}{\omega^2}} \to \text{continuous}, \tag{7.12}$$

where one can show that Eq.(7.12) is equivalent to demanding the continuity of E_z and Eq.(7.11) is equivalent to balancing the jump in E_x with the surface charge. In deriving the continuity conditions (7.11-7.12) we have assumed that ponderomotive potential f is continuous across the boundary. Since f is proportional to the amplitude of laser radiation (which is guided by the channel itself), it is clear that some discontinuity of f at the boundary in unavoidable if, for example, the laser is polarized in x direction. Yet, since $\omega_p^2 \ll \omega_0^2$, this discontinuity can be neglected compared to the discontinuity of $\frac{\partial P}{\partial x}$. In the next Section we apply the general formalism developed here to a hollow channel.

7.2 Example: Hollow Channel Laser Wakefield Accelerator

The eigenmodes of a hollow channel can be found by solving Eq.(7.8) with $f = 0$. Equation (7.8) then becomes an eigenvalue equation for wakes, moving with the speed of light, supported by inhomogeneous plasma:

$$-\frac{\partial^2 P}{\partial x^2} + \frac{\partial P}{\partial x}\frac{\partial}{\partial x}\ln\left(1 - \frac{\omega_{p0}^2(x)}{\omega^2}\right) + \frac{\omega_{p0}^2(x)}{c^2}P = 0. \tag{7.13}$$

The wake is assumed to be proportional to $e^{-i\frac{\omega}{c}(ct-z)}$, and ω is an eigenvalue of Eq.(7.13). For an arbitrary density profile $n_0(x)$ Eq.(7.13) is very hard to study analytically (as well as numerically), as will be explained in Section 7.3. Analytical progress can be made for a simple hollow channel geometry in which

$$\begin{aligned} \omega_{p0}^2(x) &= 0 \quad \text{for} \quad |\, x \,| < a \\ \omega_{p0}^2(x) &= \omega_p^2 \quad \text{for} \quad |\, x \,| > a \end{aligned} \tag{7.14}$$

We now look for the eigenfunctions $P(x)$, satisfying Eq.(7.13) and continuity conditions (7.11- 7.12), with $f = 0$, at $x = \pm a$. The symmetry of the problem with respect to an $x \rightarrow -x$ transformation makes clear that the eigensolutions will be either even or odd in x. In fact, in the rest of this chapter we will be only considering the *odd* modes since they correspond to *even* accelerating gradients and are excited by laser pulses which are symmetric in x. The *even* modes that are excited by an initially offset laser pulse or one that has degraded through instabilities (such as hosing), can be analyzed by techniques similar to those given here. Also, note that the only modes that are considered here are the accelerating modes which have a phase velocity equal to speed of light.

The eigensolution of Eq.(7.13) with $\omega_{p0}^2(x)$ given by Eq.(7.14) is given by

$$P = A\frac{x}{a} \quad for \quad |\, x \,| < a$$

$$P = Ae^{-k_p(x-a)} \quad for \quad x > a$$
$$P = -Ae^{k_p(x+a)} \quad for \quad x < -a, \tag{7.15}$$

where $k_p = \omega_p/c$ and A is an arbitrary constant. The eigenfrequency of this mode is found by applying the continuity condition (7.12), with $f = 0$:

$$\frac{1}{a} = \frac{-k_p}{1 - \omega_p^2/\omega^2}, \tag{7.16}$$

resulting in $\omega = \omega_{ch}$, where

$$\omega_{ch} = \frac{\omega_p}{\sqrt{1 + k_p a}}. \tag{7.17}$$

Using Eq.(7.3) we find the accelerating gradient inside the channel to be transversely uniform:

$$E_z = \frac{A}{a}. \tag{7.18}$$

This attractive property of the hollow channel laser wakefield accelerator was first realized in [40]. Transverse inhomogeneities in the accelerating field introduce unwanted energy spread in the bunch and impose stringent limitations on the transverse emittance.

It is easy to show that the density perturbation associated with the eigenmode (7.15) is equal to zero inside the plasma and creates a surface charge layer at the edge of the plasma. The fields inside the channel are the fringing fields from this surface charge. Plasma particle trajectories are ellipses in $x - z$ plane, with an aspect ratio equal to $k_p a$. Note a similarity between particle motion in the surface mode (7.15) and gravitational surface waves in water.

To relate the amplitude of the wake A to the strength of the laser driver f, continuity condition (7.12) is applied to the eigensolution (7.15), resulting in

$$\frac{A}{a} = \omega_p^2 \frac{i\omega \bar{f}}{c(1 + k_p a)(\omega^2 - \omega_{ch}^2)}, \tag{7.19}$$

where

$$\bar{f} = \tilde{f}(x = a). \tag{7.20}$$

Assuming that $f = f(\zeta, x)$, the accelerating field inside the channel can be expressed as

$$E_z(\zeta) = \frac{k_p^2}{(1 + k_p a)} \int_{-\infty}^{\zeta} d\zeta' \frac{\sin k_{ch}(\zeta - \zeta')}{k_{ch}} \frac{df(\zeta', x = a)}{d\zeta'}. \tag{7.21}$$

Note that this result is just the homogeneous plasma result with the small difference that k_p is replaced by k_{ch} in the sine and the coupling constant is reduced by a factor $(1 + k_p a)$. Another, somewhat unexpected consequence of Eq.(7.21), is that the amplitude of the wake is driven by the *longitudinal* rather than transverse shape of the ponderomotive potential f. Hence, despite the significant ponderomotive pressure a narrow laser pulse exerts on the plasma *transversely*, it still has to be short to create substantial wakes inside the channel.

7.3 Resonant Layers

7.3.1 Physical Picture and Basic Scalings

In Section 7.2 we were able to calculate exactly the evolution of the plasma wake, driven by the ponderomotive force. Yet a hollow channel with a step function density profile is clearly an idealization. In a realistic hollow channel plasma density will rise smoothly from zero (inside the channel) to a constant value far away from the channel. To quantitatively anticipate the new physics exhibited by a smooth channel, imagine that the thickness of the "channel wall" (the distance over which plasma density changes from 0 to n_0) is much smaller than the size of the channel. Then, it is logical to expect that the eigenfrequency of the channel mode, ω_{ch} does not change much from (7.17). Since

$$0 < \omega_{ch} < \omega_p, \tag{7.22}$$

there exists a location x_r inside the channel wall where the channel frequency matches the local plasma frequency:

$$\omega_p(x_r) = \omega_{ch}. \tag{7.23}$$

At this location a resonant enhancement of the electric field is expected. The coefficient of the first derivative of P in the eigenmode equation (7.13) becomes singular.

Expanding the coefficients of Eq.(7.13) in the vicinity of $x = x_r$ to the lowest order in $(x - x_r)$ and assuming that

$$\frac{d\left(\frac{\omega_p^2}{\omega_{ch}^2}\right)}{dx}(x = x_r) = \frac{1}{L}, \tag{7.24}$$

we obtain

$$-P'' + \frac{P'}{x - x_r} + \frac{\omega_{ch}^2}{c^2} P \left(1 + \frac{x - x_r}{L}\right), \tag{7.25}$$

where a prime denotes $\frac{d}{dx}$.

A general solution of Eq.(7.25) in the vicinity of $x = x_r$ can be expressed as a series in $\xi = (x - x_r)$:

$$\begin{aligned} P &= A\left(\frac{k_{ch}^2 \xi^2}{2} \ln(k_{ch}\xi) + 1 + \cdots\right) \\ &+ B(k_{ch}^2 \xi^2 + \cdots), \end{aligned} \tag{7.26}$$

where only the first terms in the power series are given, and A and B are numerical constants. The solution (7.26) inside the ramp region should match at the ramp boundaries with the corresponding solutions inside the channel and inside the homogeneous plasma (given by Eq.(7.15)).

A simple illustration of how the matching occurs is helpful: we assume, for simplicity, that $k_p a = 1$. Then, using Eq.(7.17), we find that $k_{ch} = k_p/\sqrt{2}$, and the boundaries of the ramp are located at $x_b = \pm L$. We further assume that $L \ll a$. Then, to provide the *amplitude* matching with solutions (7.15), constant A in Eq.(7.26) should be equal to the A in Eq.(7.15). On the other hand, the constant B has to be chosen so as to match the *derivatives* of the solutions of (7.26) with those of (7.15). It is

a matter of simple algebra to see that $B = a/L$. Notice that $B \to \infty$ as the wall thickness L approaches zero, yet B *does not* contribute to the amplitude of P in this limit! The increase of B in the limit of an infinitely thin wall is related to the fact that there is a jump in transverse field E_x due to the surface charge at the edge of the plasma. As a result, for a step function density profile P has a discontinuous derivative at the channel edge (as seen from Eq.(7.15)), while for a channel with a finite-thickness wall P has a smooth maximum at $x = x_r$.

Using Eq.(7.3) we find that the axial and transverse electric field diverge as $x \to x_r$:

$$E_z \propto k_{ch} A \ln(k_{ch}\xi)(k_{ch}L) \tag{7.27}$$

$$E_x \propto k_{ch} A (k_{ch}\xi)^{-1}(k_{ch}L). \tag{7.28}$$

The merit of using P (or B_y) to characterize the eigenmodes of an inhomogeneous plasma, instead of the electric field, is now very clear. Both components of $\vec{E}$ are divergent at the resonant location, which would make an equation for E, equivalent of Eq.(7.13), hard to analyze even numerically. On the other hand, P stays finite and differentiable at $x = x_r$, as seen from the assymptotic expansion (7.26). The robustness of P to small changes in the wall thickness suggests that the eigenfrequency of the channel ω_{ch} does not change much from (7.17) if the wall thickness is small.

We see that, as the channel wall becomes thinner ($L \to 0$), for a fixed A (which corresponds to the accelerating gradient inside the channel, see Eq.(7.18)), the amplitude of the singularity decreases, vanishing for a step function density profile. Obviously, the electric field at $x = x_r$ neither builds up to high values instantaneously, nor does it ever become infinite because of the various nonlinear effects. To understand the dynamics of the build up of the electric field, Section 7.3.3 examines the time-dependent process of exiting the wake.

But before developing the time-dependent theory, Section 7.3.2 perturbatively examines the eigenmode of a hollow channel with thin walls. The analysis of the next Section is needed to: (a) develop an operator approach to the problem of wake excitation in an inhomogeneous plasma; (b) to perturbatively calculate the structure of the

eigenmode inside the channel wall, proving rigorously that neither the eigenfrequency, nor the mode itself are greatly affected.

7.3.2 Thin-Wall Hollow Channel

In this section we present numerical and analytical solutions to the eigenvalue equation (7.13), with the plasma density linearly tapered from 0 to n_0 over a distance short compared with the size of the channel, a.

By introducing a linear operator

$$\mathcal{L} = -\epsilon(x,\omega)\frac{\partial}{\partial x}\left(\frac{1}{\epsilon(x,\omega)}\frac{\partial}{\partial x}\right) + \frac{\omega_p^2(x)}{c^2}, \tag{7.29}$$

where

$$\epsilon(x,\omega) = 1 - \frac{\omega_p^2(x)}{\omega^2}, \tag{7.30}$$

Note that the frequency dependence of $\mathcal{L}$ is suppressed for notational convenience. Eq.(7.13) can be symbolically rewritten as

$$\mathcal{L}P(x) = 0. \tag{7.31}$$

It is straightforward to prove a useful identity which holds for arbitrary functions $\psi_1(x)$ and $\psi_2(x)$:

$$\int_0^{+\infty} dx \frac{\psi_1(x)}{\epsilon(x,\omega)}\mathcal{L}\psi_2(x) = \int_{-\infty}^{+\infty} dx \frac{\psi_2(x)}{\epsilon(x,\omega)}\mathcal{L}\psi_1(x). \tag{7.32}$$

Thus, with the weighting factor $\frac{1}{\epsilon(x,\omega)}$, $\mathcal{L}$ is a Hermitian operator (assuming that ω is real). Therefore, it has a set of real eigenvalues λ_n and corresponding eigenfunctions ψ_n (that can be also chosen to be real):

$$\mathcal{L}\psi_n(x) = \lambda_n\psi_n(x), \tag{7.33}$$

where $\lambda_n = \lambda_n(\omega)$ since the operator $\mathcal{L}$ is frequency dependent. Note that the lower

limit of integration is chosen to 0 (instead of $-\infty$) since, as was mentioned earlier, only odd modes are considered in this chapter.

The orthogonality condition for the eigenfunctions is derived from Eqs.(7.32) and (7.33):

$$\begin{aligned} \int_0^{+\infty} \frac{dx}{\epsilon(x,\omega)} \psi_{n_1}\psi_{n_2}(x) &= 0 \quad \text{for } n_1 \neq n_2 \\ &= U_{n_1} \quad \text{for } n_1 = n_2, \end{aligned} \tag{7.34}$$

where U_n is the weighting coefficient. Note that all the integrals are defined in a principle value sense since $\epsilon(x,\omega)$ can contain poles and that the index n *does not* imply a purely discrete spectrum. In fact, the spectrum contains both discrete ($\lambda < k_p^2$) and continuous ($\lambda > k_p^2$) eigenvalues. For continuous part of the spectrum the eigenfunctions, obviously, are not normalizable.

The mode we are presently concerned with is the self-supported wake, corresponding to $\lambda = 0$. The unperturbed solution for a step-function profile ψ_0 is given by Eq.(7.15), and its eigenfrequency $\omega_u = \omega_{ch}$. We now assume that the thin-wall dielectric function is given by

$$\begin{aligned} \epsilon &= 1 \quad \text{for} \quad |x| < a(1-\delta/2) \\ \epsilon &= 1 - \frac{\omega_p^2(x-a+a\delta)}{\omega^2 a\delta} \quad \text{for} \quad a(1-\delta/2) < |x| < a(1+\delta/2) \\ \epsilon &= 1 - \frac{\omega_p^2}{\omega_2} \quad \text{for} \quad |x| > a(1+\delta/2), \end{aligned} \tag{7.35}$$

where $\delta \ll 1$ is the ratio of a channel thickness to the half-width of the channel. Note that the *average* position of the channel wall remains unchanged at $x = a$ to exclude the obvious effect of the channel width on the eigenfrequency. The goal of the following calculation, as was mentioned at the end of Section 7.3.1, is to estimate, to linear order in δ, the influence of density ramp on the eigenfrequency of the wake mode.

Equation (7.31) for the wake eigenfunction ψ can be rewritten as

$$\frac{\partial}{\partial x}\left(\frac{1}{\epsilon(x,\omega)}\frac{\partial\psi}{\partial x}\right)=\frac{\omega_p^2(x)}{c^2\epsilon(x,\omega)}\psi. \tag{7.36}$$

The solutions ψ in the regions $0<x<a(1-\delta/2)$ and $x>a(1+\delta/2)$ are known and given by Eq.(7.15). Therefore, Eq.(7.36) can be integrated across the density ramp to yield a jump in $\psi'/\epsilon \propto E_z$. Note that in the case of a step function density profile the size of the density ramp is equal to zero, and, thus, the jump also vanishes, as expressed by Eq.(7.16).

We can write

$$\begin{aligned}
\psi &= \frac{A_1 x}{a(1-\delta/2)} \quad \text{for} \quad x<a(1-\delta/2)\\
\psi &= 1-B(x-x_r)^2 \quad \text{for} \quad a(1-\delta/2)<x<a(1+\delta/2)\\
\psi &= A_2 e^{-k_p(x-a-a\delta/2)} \quad \text{for} \quad x>a(1+\delta/2),
\end{aligned} \tag{7.37}$$

where A_1, A_2 and B are constants that are determined by matching ψ and its derivatives at the boundaries. The functional dependence of ψ inside the ramp is chosen in accordance with Eq.(7.26); one can easily show that other terms in the expansion (7.26) can be neglected to linear order in δ. The plasma frequency at the resonant location

$$x_r = a\left(1-\frac{\delta(k_p a-1)}{2(k_p a+1)}\right). \tag{7.38}$$

is equal to the *unperturbed* channel frequency, given by Eq.(7.17).

Using $\xi = x-x_r$ instead of x, we find the coordinates of the inner and outer edges of the ramp:

$$\begin{aligned}
\xi_{in} &= -\frac{a\delta}{1+k_p a}\\
\xi_{out} &= \frac{k_p a^2\delta}{1+k_p a}.
\end{aligned} \tag{7.39}$$

By matching the derivatives at ξ_{in} and ξ_{out} we find

$$B = -\frac{1 + k_p a}{2a^2\delta}, \tag{7.40}$$

and, using Eq.(7.40) and continuity of ψ, recover

$$\begin{aligned} A_1 &= 1 - \frac{\delta}{2(1 + k_p a)} \\ A_2 &= 1 - \frac{\delta k_p^2 a^2}{2(1 + k_p a)}. \end{aligned} \tag{7.41}$$

Expressing the plasma quantities inside the density ramp (using $\omega = \omega_{ch}$) in the new coordinates yields

$$\begin{aligned} \epsilon(\xi) &= -\frac{(1 + k_p a)\xi}{a\delta} \\ k_p^2(\xi) &= k_p^2 \frac{\xi - \xi_{in}}{a\delta}. \end{aligned} \tag{7.42}$$

Substituting Eq.(7.42) in Eq.(7.36) and integrating it across the ramp gives

$$\frac{-k_p A_2}{1 - \omega_p^2/\omega_2} - \frac{A_1}{a(1 - \delta/2)} = -\frac{k_p^2}{1 + k_p a} \int_{\xi_{in}}^{\xi_{out}} \frac{d\xi}{\xi}(1 - B\xi^2)(\xi - \xi_{in}). \tag{7.43}$$

The integral on the RHS of Eq.(7.43) has a singularity at $\xi = 0$ and must be taken in the principal value sense.

After some algebra, assuming $\omega = \omega_{ch} + \Delta\omega$, we find, to linear order in δ

$$\frac{\Delta\omega}{\omega_p} = \delta \frac{k_p^2 a^2 (k_p a - 1 - 2\ln k_p a)}{4(1 + k_p a)^{5/2}}. \tag{7.44}$$

The perturbed channel frequency is thus a function of both the width of the channel wall and the average width of the channel. The dependence of the frequency shift on the channel width a and channel wall thickness δ is seen in Fig 7-1. where $\Delta\omega/\omega_p$ is plotted as function of δ for wall boundaries given by: (i) for $x_{in} = a$, $x_{out} = a(1 + \delta)$; (ii) for $x_{in} = a(1 - 0.5\delta)$, $x_{out} = a(1 + 0.5\delta)$; (iii) for $x_{in} = a(1 - \delta)$, $x_{out} = a$. In all three cases $k_p a = 1$. Note that the frequency shift is almost equal to zero in case

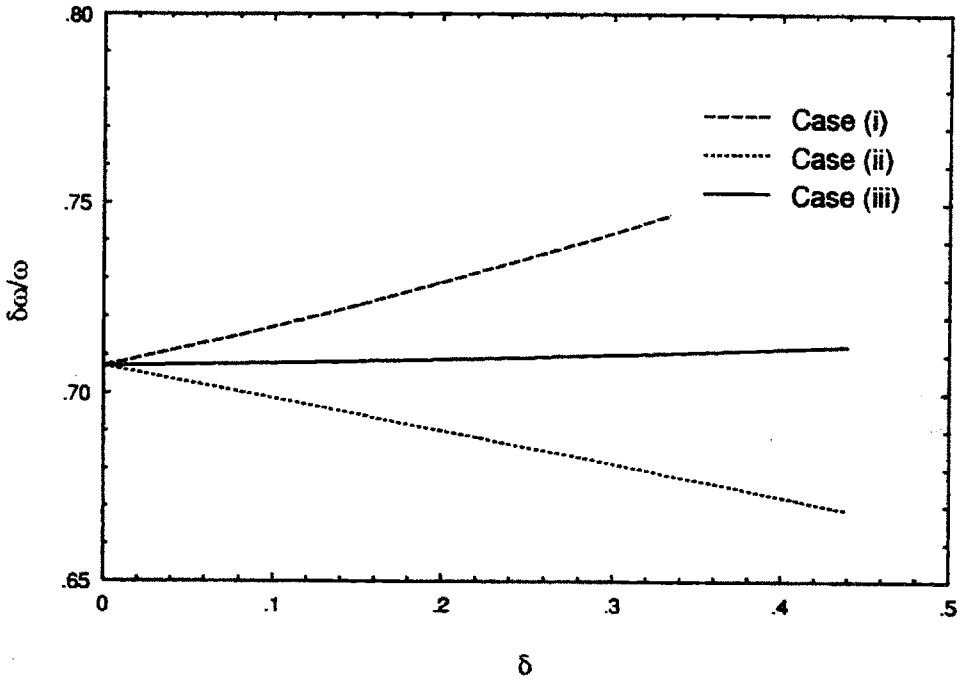

fiFigure 7-1: Normalized frequency shift as a function of a fractional wall thickness, for three different positions of the channel walls. In all cases $k_p a = 1$

(ii), since $\Delta\omega$, given by Eq.(7.44) vanishes for $k_p a = 1$. Case (i) gives a frequency shift almost identical to the shift that corresponds to making a step-function channel *wider* by a factor $(1 + \delta/2)$, while case (iii) corresponds to making a step-function channel *narrower* by a factor $(1 - \delta/2)$.

As Eq.(7.44) indicates, for some typical parameters $k_p a \approx 2$ the relative frequency shift of the wake mode due to 10% wall thickness, is about 0.7%. Hence, our intuition is correct and the frequency of the wake excited inside a smooth wall channel is very robust to variations in thickness of the channel wall (as is the structure of the accelerating field inside the channel). Yet the diverging fields at the resonance location x_r are worrisome, and, as we show in the next section, they result in the eventual

disintegration of the channel wake excited by an intense laser pulse.

A careful analysis of how the wake is excited by an external driver is crucial since, obviously, the fields at the resonant location do not become infinite instantaneously. In the next section we examine time evolution of the electric field inside the channel wall and show that wave breaking eventually destroys the wake, thereby introducing an effective quality factor Q of the plasma channel.

7.3.3 Excitation of the Wake Field

After studying in a great detail the properties of the channel eigenmodes in Section 7.3, we now examine the excitation of these wakes are excited by the ponderomotive driver (laser pulse). To do that we rewrite Eq.(7.8) in the operator form:

$$\mathcal{L}P = -i\frac{\omega}{c}\tilde{f}\frac{\partial \ln \epsilon(x)}{\partial x}. \tag{7.45}$$

P can be expanded in a complete set of eigenmodes ψ_n of the operator $\mathcal{L}$ given by Eq.(7.33):

$$P(x,\omega) = \sum p_n(\omega)\psi_n(x,\omega) \tag{7.46}$$

One of the important conclusions of Section 7.3 is that the eigenfunctions ψ and the eigenvalues are only slightly perturbed by the finite thickness of the channel wall. Hence, to a high degree of accuracy, the ψ_n's can be chosen to be the eigenfunctions (and λ_n the eigenvalues) of Eq.(7.31) with a step-function density profile, with $\omega_p^2(x)$ given by Eq.(7.14). Using the orthogonality conditions Eq.(7.34), the expansion coefficients can be expressed as

$$p_n = \frac{i\omega/c}{\lambda_n U_n}\int_0^{+\infty} dx' f(x',\omega)\psi_n(x',\omega)\frac{\partial}{\partial x'}\left(\frac{1}{\epsilon(x',\omega)}\right). \tag{7.47}$$

By examining the spectrum of Eq.(7.33) with a step function density profile one can demonstrate that the only eigenvalue function $\lambda_n(\omega)$ that has a pole for *any* complex ω is one of the discrete spectrum eigenvalues $\lambda_0(\omega)$, which vanishes at $\omega = \pm\omega_{ch}$. Alternatively, from the results of Section 7.3.2, there exists *only one* self-supported

eigenmode (these self-supported modes correspond to poles of eigenvalue functions).

From Eqs.(7.3),(7.46) and (7.47) we can find the induced accelerating field inside the channel. Since $\lambda_0(\omega)$ has a pole at at $\omega = \pm\omega_{ch}$, we need to find its behavior in the vicinity of the pole. Since $\lambda_0(\omega)$ is regular in the vicinity of the pole, we consider $\omega > \omega_{ch}$, which, as we prove later, is equivalent to $\lambda > 0$. Solutions to Eq.(7.33) are then given by

$$\begin{aligned} \psi &= \frac{\sin \lambda^{1/2} x}{\sin \lambda^{1/2} a} \quad \text{for} \quad x < a \\ \psi &= e^{-(k_p^2+\lambda)^{1/2}(x-a)} \quad \text{for} \quad x > a, \end{aligned} \tag{7.48}$$

where we have dropped the subscript from λ. Applying the continuity condition (7.12), with $f = 0$, yields an implicit $\lambda(\omega)$:

$$\frac{\tan(\lambda^{1/2} a)}{\lambda^{1/2} a} = \frac{\frac{\omega_p^2}{\omega^2} - 1}{k_p a (k_p^2 - \lambda)^{1/2}}. \tag{7.49}$$

Linearizing Eq.(7.49) in the vicinity of $\omega = \pm\omega_{ch}$ and $\lambda = 0$ yields:

$$\lambda = \frac{(1 + k_p a)^2}{k_p a(-1/2 + k_p^2 a^2/3)} \frac{\omega^2 - \omega_{ch}^2}{c^2}. \tag{7.50}$$

We also compute the normalization constant

$$U_n = \int_0^\infty \frac{dx}{\epsilon} \psi_n^2, \tag{7.51}$$

which, for $\omega = \pm\omega_{ch}$, is equal to

$$U_0 = \frac{-1/2 + k_p^2 a^2/3}{k_p^2 a}. \tag{7.52}$$

The accelerating gradient inside the channel is computed by observing that inside the channel $\omega_p^2(x) = 0$, so that the first term of Eq.(7.3) can be combined with

Eq.(7.47) to obtain:

$$E_z(x,\zeta) = \int \frac{d\omega}{2\pi c} e^{-i\frac{\omega}{c}(\zeta-\zeta')} \sum_n \frac{\psi_n'(x,\omega)}{U_n \lambda_n(\omega)} \times \int_{-\infty}^{+\infty} dx' \psi_n(x',\omega) \frac{\partial}{\partial x'} \left(\frac{1}{\epsilon(x',\omega)} \right) \frac{\partial f(x',\zeta')}{\partial \zeta'}, \tag{7.53}$$

where the first integration is carried out along a contour in complex ω plane, above the real axis, to ensure causality. Even though this calculation appears to be much more cumbersome than the one used in Section 7.2, it is worthwhile to prove that Eq.(7.53) yields the same result as Eq.(7.21). The method of modal expansion, while almost being "too powerful" for finding E_z inside the channel, is the only method for finding the temporal evolution of the laser-driven fields inside the channel wall.

As mentioned earlier, only the lowest eigenmode of the discrete spectrum has an eigenvalue function $\lambda(\omega)$ with a pole. Thus, after closing the integration contour in the lower half of complex ω plane, summation in Eq.(7.53) contains only one non-vanishing term—the lowest discrete mode. Since the residues at the pole of $\lambda(\omega)$ at $\omega = \pm\omega_{ch}$ were computed earlier, we substitute Eqs.(7.50) and (7.52) into Eq.(7.53), and, adding the two residues, recover Eq.(7.21).

The goal of this Section is to establish how the fields grow in time at the resonant location $x = x_r$. Formally, one expects the field to grow indefinitely since the field of the wake eigenmode diverges near resonant location (see Eq.(7.26)). An unusual physical situation occurs: as the laser pulse passes through plasma, it generates a wakefield, which, near the resonant point, continues to grow *indefinitely* (in the linear theory, of course) *after* the laser pulse is gone!

As Eq.(7.3) indicates, the total electric field inside plasma is given by a sum of two contributions. The first term in the RHS of Eq.(7.3), at a given location x, has a simple pole in $\omega-$ plane, and, thus, cannot lead to infinite growth of the field. Physically, the laser pulse excites an oscillation which continues at the *local* plasma frequency $\omega_p(x)$. Thus we can neglect this term in this calculation and compute the contribution of the second term on the RHS of Eq.(7.3). Similarly to Eq.(7.53), we

can derive a modal expansion for E_x at an arbitrary location in plasma:

$$E_x(x,\zeta) = -\int \frac{d\omega}{2\pi c} e^{-i\frac{\omega}{c}(\zeta-\zeta')} \sum_n \frac{\psi_n(x,\omega)}{U_n \lambda_n(\omega)\epsilon(x,\omega)} \times \int_{-\infty}^{+\infty} dx' \psi_n(x',\omega) \frac{\partial}{\partial x'} \left(\frac{1}{\epsilon(x',\omega)} \right) \frac{\partial^2 f(x',\zeta')}{\partial \zeta'^2}, \tag{7.54}$$

As in the previous example of calculating E_z, only $n = 0$ can contribute to indefinite growth of the electric field. Other modes, while giving a nonzero contributions (unlike the case of E_z inside the channel), have an effect similar to that of the first term on the RHS of Eq.(7.3), with a simple pole at the local plasma frequency. By retaining only the $n = 0$ mode, and setting $x = x_r$, observe that the integrand in Eq.(7.54) has a double pole at $\omega = \pm\omega_{ch}$. We thus obtain:

$$E_x(\zeta, x_r) = \frac{k_p^2 a}{1 + k_p a} \int_{-\infty} d\zeta' G_x(\zeta - \zeta') \frac{d^2 f(\zeta', x = a)}{d\zeta'^2}, \tag{7.55}$$

where $\bar{f}$ is given by Eq.(7.20), and $G_x(\zeta - \zeta')$ is a Green function of the transverse electric field at resonant point given by

$$G_x(\zeta) = \frac{\zeta}{2} \cos(k_{ch}\zeta) + \frac{\sin(k_{ch}\zeta)}{k_{ch}}. \tag{7.56}$$

The wake has the temporal behavior we expected—it grows indefinitely with time. Similarly, one can estimate that the axial field at x_r will be growing logarithmically with time. If E_{x0} is the transverse field at the edge of the channel, the amplitude of the field at $x = x_r$ roughly grows as

$$E_x(x_r) \propto \frac{k_{ch}\zeta}{2} E_0. \tag{7.57}$$

Thus, after the laser passes through the channel, electric field inside the ramp region continues to grow *in the absence* of an external driver.

The situation here (at least formally) is very similar to excitation of a linear plasma profile by an external capacitor. Refs. [26, 93, 94] analyze the following model problem: inhomogeneous plasma with a linear density ramp is subject to a sinusoidally

varying with time electric field produced by a plane capacitor. Electric field is co-linear with the density gradient and its frequency matches the local plasma frequency at resonant location $x = x_r$. An obliquely incident $p-$ polarized electromagnetic wave can also play the role of a capacitor. Secular growth of the electric field at resonant point which saturates through collisions, relativistic corrections, wavebreaking, particle ejection, etc., was predicted [93, 94]. The important difference between the hollow channel and the model problem described above is that *no external capacitor* is needed in our case. Instead, a hollow channel mode is excited, which serves *as a capacitor* to drive the internal modes of inhomogeneous plasma.

Initially the fields *inside* the channel and in the inhomogeneous plasma region are not influenced by the dramatic growth of the field at resonant point. But later, as E_x builds up, wavebreaking [58] occurs, energetic electrons are ejected into the channel, thereby dissipating the wake. The process of wavebreaking and electron acceleration (in the direction of decreasing plasma density, that is, into the channel) has been extensively discussed in the literature [26, 93, 94].

The basic physics behind wavebreaking is the crossing of particle trajectories. When the boundary is sharp, particles execute elliptic motion, of typical size $r_0 = \frac{2eE_0(1+k_pa)}{m\omega_p^2}$ (this motion becomes circular for $k_pa = 1$). No trajectory crossing occurs since all the particles are moving in tandem, with frequency ω_{ch}. When a finite-size wall is introduced, particles inside the homogeneous plasma start coherently dephasing. At the point in time when trajectories cross wavebreaking occurs, with subsequent production of energetic electrons and the dissipation of the surface charge. This crossing occurs because, due to finite size of their orbits, surface electrons actually spend some time in the ramp region of the plasma. The accelerating channel mode is driven by the surface charge. Thus, trajectory crossing of the surface electrons results in the damping of the mode.

As the first illustration of the mechanism for wavebreaking we assume that $r_0 \gg a\delta$, that is, that the boundary is very sharp. Qualitatively, as the electron passes through the resonance region, it gets a kick from the electric field in $x-$ direction, of magnitude Δv_x, which leads to the displacement of its guiding center, by roughly

$\Delta z \propto \Delta v_x/\omega_{ch}$, in the $z-$ direction, with the corresponding change of phase angle $\Delta\phi \propto \Delta v_x/(\omega_{ch} r_0)$. Another important observation [93] is that, due to dephasing, the size of the resonant region shrinks inversely proportional to time. Since the amplitude of the resonant field grows linearly with time (see Eq.(7.57)), the magnitude of the kick, Δv_x, remains roughly the same. By considering two electrons, with guiding centers infinitely close to each other, one can verify that it takes about

$$Q = \omega_{ch} t \propto r_0/(a\delta) \tag{7.58}$$

channel oscillations for the wave to break. And indeed, as numerical simulations indicate [27], no deterioration of the wake is observed for many channel oscillations when the step function plasma density profile is used.

The mechanism for wave breaking in the limit of $r_0 \ll a\delta$ was discussed in literature [93, 26]. Briefly, the spatio-temporal structure of the field near resonance point is such that it has the form of a wave packet, moving with a characteristic phase velocity $v_{ph} \approx \omega\Delta L$, where ΔL is the size of a resonance region. Wave breaking occurs when electron velocity (which grows linearly with time) matches v_{ph} (which decreases linearly with time). The number of oscillations before the wave breaks is roughly given by

$$Q = \omega_{ch} t \simeq (a\delta/r_0)^{1/2} \tag{7.59}$$

(see [95]). In the case of $r_0 \simeq a\delta$ wavebreaking was numerically observed [27] to occur after the first oscillation.

Wave breaking of the accelerating mode imposes serious limitations on the operation of future laser wakefield accelerators. It introduces an effective Q of the plasma channel, which can be quite low [27] and prevents accelerating multiple bunches by the wake created in a single laser shot. It appears that to increase Q one either has to use channels with very sharp (Eq.(7.58)), or very smooth boundaries (Eq.(7.58)).

Chapter 8

Conclusions

In the first part of this thesis we developed a novel diagrammatic approach to intense laser plasma interactions. By restricting our model to non-thermal homogeneous electron plasma and sufficiently short laser pulses, so that ion motion can be neglected, we described laser- plasma interactions as a fully covariant field theory. No restriction on the intensity of laser radiation was made.

To illustrate the use of a diagrammatic perturbation theory in solving nonlinear classical problems, we first applied it to a simplified problem of an anharmonic oscillator. The formal similarity between the methods of quantum electrodynamics (QED) and nonlinear perturbation theory was revealed in Section 2.2.2 by proving the classical analog of Wick's theorem in QED.

A field-theoretical description of the electron plasma was developed which treats electrons as waves, with a very short artificial wavelength λ_c associated with them. In all calculations λ_c was assumed shorter than any relevant spatial scale. Despite the analogy with QED, the theory remains *classical.*

An unusual gauge (Arnowitt-Fickler) was used to develop an elegant relativistically covariant description of electromagnetic waves in a moving nonthermal plasma. Using the Faddeev-Popov procedure, electromagnetic waves were classified into photons and plasmons, which are relativistic extensions of electromagnetic and electrostatic waves in a stationary plasma. The distinction between photons and plasmons, which remains valid in any moving frame (covariance) is that photons can escape

plasma while plasmons cannot.

The concept of renormalization was introduced and applied to electromagnetic fields and electrons. The effective mass of electron in a strong electromagnetic wave in plasma was calculated to higher orders in ϵ (see Eq.(1.1)) without assuming that the normalized laser amplitude $a < 1$. For the first time the nonlinear corrections to phase velocity of an electromagnetic wave was computed, using the diagrammatic perturbation theory, up to order ϵ^2. The nonlinear modification of the index of refraction of a weak laser probe in the presence of the strong electromagnetic wave was studied. An experiment aimed at studying the nonlinear interaction between two laser pulses was proposed. In this experiment a weak laser probe, unable to propagate through the overdense plasma in the *absence* of a stronger laser pulse, penetrates through the plasma in the *presence* of another laser pulse of sufficient strength.

The diagrammatic formalism was applied to the interaction between a plasma and two laser pulses. The dispersion relation for four-wave stimulated Raman scattering (SRS) was derived without recoursing to the weakly relativistic approximation.

The diagrammatic formalism was further used to calculate the rate of a second harmonic emission from the homogeneous plasma. For the first time we were able to carry out the calculation to order a^4 in the amplitude of incident radiation *and* account for a finite angle between the incident laser pulses. This calculation resulted in a non-vanishing rate of the second harmonic generation, disproving the previously held opinion that an *external plasma inhomogeneity is necessary to produce the second harmonic*. In addition, an interesting effect of nonlinear polarization rotation was predicted: two intense electromagnetic waves polarized *perpendicularly* to the plane of their incidence, produce the second harmonic polarized *in the plane* of incidence.

We have developed a novel method for overcoming the ubiquitous phase velocity mismatch in harmonic generation. The proposed technique uses *two* intense lasers propagating at a small angle to each other. A detailed discussion of how this method applies to the second harmonic generation is given (See Sec. 4.4.3).

In the second part of this thesis we studied various physics issues related to laser

wakefield acceleration. We identified and analyzed a new instability in channel guided laser propagation. The instability is of a cumulative nature, similar to beam breakup instability (BBU), and amplifies distortions in the transverse profile of a channel guided laser as it propagates through the plasma. By considering a parabolic density profile, we derived a matrix dispersion relation for a complete set of transverse modes, given by Laguerre polynomials. This dispersion relation was simplified and studied analytically and numerically for a particular case of a dipole distortion. It was found that the instability becomes important after a number of Rayleigh lengths for laser pulses of order plasma period.

A method for suppressing the instability, similar to BNS damping (which is routinely used in linear accelerators), was proposed. Two sources of BNS damping were identified: external chirping of the laser wavelength and naturally occurring relativistic self-focusing. An alternative derivation of the hosing instability—the envelope equation—was presented, and relativistic corrections were incorporated, thus allowing us to derive a simplified linear equation which contains the effects of the BNS damping. For an idealized case of a linear chirp in the effective "betatron frequency" of the hosing instability an analytical description of BNS damping was developed and the criterion for saturating the instability at a controllable level was derived.

For realistic laser pulses (where the chirp in the betatron frequency is not linear) the BNS equation was solved numerically. It was found that for short (less than plasma period) intense ($P \propto P_c$) laser pulses the naturally occurring BNS can saturate the instability.

In this thesis we have also analyzed the problem of wake excitation in an inhomogeneous plasma. The general formalism for excitation of the accelerating mode in nonuniform plasma was developed and the results were applied to a particular case of a hollow channel accelerator, with a step-function density profile. The eigenfrequency of the accelerating mode was derived and the excellent properties of the mode for particle acceleration (uniformity in the transverse dimension) were demonstrated. The time-dependent excitation of the mode by the ponderomotive force of a laser pulse was derived and the accelerating gradient inside the channel was expressed as

a causal time convolution of the ponderomotive force at the edge of the channel and the wake Green function.

For the first time a more realistic case of a channel with a smooth interface between vacuum and plasma was considered. We have rigorously proven that the structure of the accelerating mode is only slightly perturbed by the finite thickness of the channel walls. The corrections to the eigenfrequency of the accelerating mode due to finite thickness of the channel was obtained analytically and numerically. The interaction between the channel mode and the inhomogenious plasma inside the channel was considered. It was shown analytically that the transverse electric field at the resonant location inside the channel wall, where the local plasma frequency matches the channel eigenfrequency, is driven resonantly. A Green function for the transverse electric field at the resonant location was derived, predicting a linear growth of the amplitude of the field with time.

A somewhat exotic scenario was predicted, in which the transverse electric field at resonant location grows indefinitely (in linear theory) *after* the short laser pulse (which excited the wake) has already propagated downstream. Nonlinear effects, most notably wavebreaking, which arrest the growth of the electric field, were briefly discussed. The important implication of these effects is that the accelerating wake is dissipated, thereby introducing an effective quality factor Q for the channel accelerator and limiting the number of electron bunches that can be accelerated in the wake of a single laser pulse. The effect of wake dissipation due to resonant absorption inside the channel wall have already been observed in PIC simulations and will, undoubtedly, have to be taken into consideration when designing a laser wakefield accelerator.

8.1 Topics for Future Research

We briefly describe some extensions and further applications of this work.

1. Thus far the diagrammatic formalism is limited to the homogeneous nonthermal plasmas and plane electromagnetic waves of infinite duration. Extending the

formalism to inhomogenious plasmas and pulsed propagation would allow investigation of interesting phenomena such as the generation of intense magnetic fields at the plasma boundary.

2. Extending the diagrammatic formalism to cold *magnetized* plasma will allow for the systematic description of phenomena such as electron-cyclotron resonance [92].

3. One can develop a classical theory which does not have the artificial scale $\hbar$ and, instead of describing the electron plasma by a field ψ, describe it by a classical action. The action function can be obtained as a series in ϵ of canonical transformations. The benefits of the Arnowitt-Fickler gauge and the relativistically covariant classification of the electromagnetic waves can still be realized by gauge at each order in ϵ (since the canonical momentum will be changing with each canonical transformation).

4. The relativistic particle Lagrangian can describe both electrons and positrons. Studying electron-positron plasmas in astrophysical environments appears to be an interesting application.

5. Parametric decay of a neutrino wave into another neutrino wave and a plasma wave has been recently proposed as a possible process to explain the energy transfer from neutrinos to the electrons in the supernovae [96]. Diagrammatic approach developed here for the EM-electron interaction can be extended to include the neutrino fields.

6. The modal formalism for laser propagation in the parabolic channel is quite general. Analytical and numerical study of will predict the evolution of an arbitrary initial pulse distortion, including laser mode coupling. Even for dipole distortions, the inclusion of different radial modes will predict the extent of transverse spreading that occurs along with the centroid displacement.

7. The calculations for the laser stability in parabolic channels neglected the zeroth order wakes caused by non-adiabaticity of the laser pump. These wakes are

important in order to evaluate the initial distortions that serve as seeds for the instability. They also help to quantify such effects as BNS damping and relativistic self-focusing.

8. Calculations for the parabolic channel were carried out under the assumption that the plasma is uniform in the region where the ponderomotive force of the laser is appreciable. Removal of this assumption would allow one to address such effects as phase mixing of the electrons with different local plasma frequencies, wavebreaking, and generation of energetic electrons, just as was studied for the hollow channel.

9. Dissipation of the hollow channel wake through wavebreaking inside the channel wall has must be studied numerically. It is important to carry out PIC simulations for different thicknesses of the channel wall (much larger or much smaller than the excursion of a surface electron, etc.) to identify the most promising regime of operating the hollow channel laser wakefield accelerator.

Appendix A

Plasma Physics Through Klein-Gordon Equation

In Chapters 2-5 we have described laser-plasma interactions as a field theory in which the electron fluid is represented by a complex field $\psi(t, \vec{x})$ and is coupled to an electromagnetic vector-potential $A^{\mu}(t, \vec{x})$. A rather involved perturbation theory was developed that can be roughly described as first evaluating the perturbation to the electron trajectories by the EM fields, generating new ("virtual") EM fields from these perturbations, which in turn act back on the electrons, and so on. A fully self-consistent model, such as the diagrammatic approach, can be systematically used to evaluate a wide variety of nonlinear plasma problems, as seen in Chapter 4.

One of the difficulties in developing a self-consistent theory of laser-plasma interactions is the fact that the electrons are *not* moving in the prescribed EM fields. The plasma response is collective by nature, which is, for example, manifested in the induced space-charge forces (plasma waves). Yet some important insights into laser-plasma interactions can be gained from studying the motion of the electrons in *prescribed* fields and analyzing the currents and fields generated by this motion. In diagrammatic language, this is equivalent to analyzing only one-level diagrams. No virtual photons or plasmons are thus included. The goal of this Appendix is, therefore, to calculate the contributions of one-level diagrams in a different way and compare the results with diagrammatic calculations of Chapters 2- 4.

A free-electron laser (FEL) operated in Compton regime presents a typical example of a calculation which neglects virtual plasmons. In a Compton FEL induced space-charge forces are not important for the instability and can be neglected. Hence, the only fields that act on the electrons of the beam are the fields of a wiggler and the amplified EM wave. The currents that are generated as result of this interaction are then substituted into the Maxwell's equation for the EM wave.

The appropriate equation for ψ, the field describing the electron with unperturbed Lagrangian (2.41), coupled to the EM field, is the perturbed Klein-Gordon equation.

To simplify the calculation we consider a one-dimensional problem with the direction of propagation chosen along z axis and the *total* EM field polarized along x axis. This would be violated if we included the collective space-charge forces. We address three different problems from laser- plasma interactions: (1) that no harmonics are generated by EM waves propagating through plasma at the speed of light; (2) large-angle Raman scattering of a high-intensity EM wave (this recovers the results of Ref. [12] for Raman back- scattering); (3) the third harmonic generation, the electron mass corrections and the "photon mass" corrections. These results will be compared with the results of the diagrammatic calculations presented in the Chapters 2-4.

A strong electromagnetic wave with a vector potential

$$\vec{a}_0 = \vec{e}_x a_0 cos(k_0^\mu x_\mu), \tag{A.1}$$

where $x^\mu = (t, z)$, is assumed to be present in the plasma. If the EM wave propagates with the speed of light (neglecting the induced polarization currents in plasma)

$$k_{0\mu} k_0^\mu = 0. \tag{A.2}$$

In general, condition (A.2) need not be satisfied, and the "photon mass" has to be consistently renormalized (as will be shown later). With space-charge fields neglected (that is, no plasmons), the "absorbing" part (3.29) of the interaction Hamiltonian

vanishes. The evolution equation for the electron field ψ is then given by

$$\partial_\mu \partial^\mu \psi + \frac{m^2}{\hbar^2}[\bar{m}^2 + a_0^2/2\cos(2k_0 \cdot x)]\psi = 0, \tag{A.3}$$

where $\bar{m}^2 = (1 + a_0^2/2)$. Since quantum mechanical effects are outside of the scope of this calculation, we assume, as before, that

$$\frac{k_0 \hbar}{m} \ll 1 \tag{A.4}$$

It turns out that Eq.(A.3) can be solved exactly when (A.2) is satisfied. Following the classical treatment of relativistic Hamilton-Jacobi equation from Ref. [60] results in

$$\psi_0(x) = \frac{\hbar^{1/2}\sqrt{n_0}}{(2\epsilon_{\vec{p}_0})^{1/2}} e^{i\left(p_0 \cdot x + \frac{m^2 a_0^2 \sin(2\phi)}{\hbar^2 (8 k_0 \cdot p_0)}\right)}, \tag{A.5}$$

where

$$\phi = k_0 \cdot x \tag{A.6}$$

and p_0 is a constant four vector. As before, the pre-exponential factor was chosen to insure that the time-averaged density is equal to n_0. We note that the pre- exponential factor is numerically equal to $\hbar\mu/\sqrt{2}.$, where μ is the relativistic plasma density defined by Eq.(3.35).

Once the equation (and the solution) for the electron field is obtained, the induced plasma currents can be calculated and substituted into the wave equation for the EM fields. Assuming that the EM field is polarized in $x-$ direction,

$$\vec{a}(t, \vec{x}) = \vec{e}_x a(t, \vec{x}), \tag{A.7}$$

we arrive at the wave equation:

$$\partial_\mu \partial^\mu a = -\frac{2\psi\psi^* m^2}{\hbar^2} a. \tag{A.8}$$

The RHS of Eq.(A.8) represents the induced currents in the plasma. Since only the

physical processes represented by one-level diagrams are considered in this Appendix, a in the RHS has to be taken be equal to a_0. We thus proceed to compute ψ, calculate the perturbed square of its absolute value and insert it into the wave equation (A.8), and then examine Problems (1-3).

(1) **Absence of harmonics generation by freely propagating EM waves.**

This is true since Eq.(A.5) implies that $\mid \psi_0 \mid^2=$ const and thus the RHS of Eq.(A.8) does not contain any harmonics of the field a_0. This result will not be valid if one drops the assumption (A.2), as we show in part (3).

(2) **Simplified analysis of Stimulated Large-Angle Raman Scattering.**

Here we give a simplified linear analysis of Raman Scattering which neglects the space-charge waves generated in plasma as well as the four-wave nature of Raman Scattering, as discussed in Section 4.3. This analysis is justified for large- angle scattering [50]. As before, we assume that the pump a_0 propagates through plasma with the speed of light, i.e. that Eq.(A.2) holds. The linear nature of the calculation implies that a weak probe a_1 propagates in plasma along with the large amplitude pump a_0.

The evolution equation for the electron field ψ, to linear order in a_1, is

$$\partial_\mu \partial^\mu \psi + \frac{m^2}{\hbar^2}[\bar{m}^2 + a_0^2/2 \cos(2k_0 \cdot x)]\psi = -\frac{2a_0 a_1 m^2}{\hbar^2}\psi. \qquad \text{(A.9)}$$

Equation (A.9) can be solved by the Green function method. Green function $G(x, x')$ satisfies

$$\left(\partial_\mu \partial^\mu + \frac{m^2}{\hbar^2}[\bar{m}^2 + a_0^2/2] \cos(2k_0 \cdot x)\right) G(x, x') = -\delta^4(x - x'). \qquad \text{(A.10)}$$

In solving for $G(x, x')$ we follow closely the analysis of Reiss and Eberly [46] and borrow some of their formal results.

We would like to point out that the problems addressed in [46]-[49] are very different from the one we are considering. Refs. [46]-[49] are concerned with the behavior of a *single* electron in intense EM wave. This is precisely the reason why Refs. [46]-[49] did not need to introduce a classification of EM waves into plasmons

and photons—a single electron *does not* perturb the wave. On the other hand, in this thesis we are concerned with the waves propagating in the *continuous plasma.* Even though our assumption of no plasmons does not imply that the plasma *vector* momentum is perpendicular to the wave vector potential (as we have assumed by choosing $\psi \equiv \psi(z,t)$ and $\vec{a} \parallel \vec{e}_x$), this condition can be achieved through canonical transformation. Hence, in the continuous plasma, under assumption of no plasmons, the "absorbing part (3.29) of the interaction Hamiltonian identically vanishes. On the other hand, the classification into plasmons and photons is meaningless for a plasma consisting of a single electron. This is why the "absorbing" part of the Hamiltonian does not vanish in Ref. [46].

And indeed, the main formal difference between the two treatments is that in this calculation we consider the "scattering" part (3.28) of the interaction Hamiltonian, while the "absorbing part (3.29) vanishes. On the contrary, Ref. [46] assumes circular polarization for a_0, which makes the "scattering" vanish, and includes the "absorbing" part (3.29).

We look for the solutions of Eq.(A.10) in the form

$$G(x,x') = \int \frac{d^4p}{(2\pi)^4} e^{-ip\cdot(x-x')} f(\phi,\phi'). \tag{A.11}$$

Inserting Eq.(A.11) into Eq.(A.10) yields

$$f' + \Phi(\phi) f = D, \tag{A.12}$$

where $f' = \partial f/\partial\phi$ and

$$\Phi(\phi) = \frac{i}{2k_0\cdot p}\left(-p^2 + \frac{m^2\bar{m}^2}{\hbar^2} + \frac{m^2 a_0^2\cos(2\phi)}{2\hbar^2}\right), \tag{A.13}$$

$$D = \frac{-i}{2k_0\cdot p}. \tag{A.14}$$

The solution of Eq.(A.12) is

$$f = uv, \tag{A.15}$$

with

$$u = \exp\left(-\int_{\phi''}^{\phi}\Phi(\alpha)d\alpha\right),$$
$$v = D\int_{\phi'}^{\phi}\exp\left(\int_{\phi''}^{\beta}\Phi(\alpha)d\alpha\right)d\beta. \tag{A.16}$$

The value of the lower limit of integration, ϕ'', in u and v is immaterial. Integration over α then yields

$$\int^{\beta} d\alpha\Phi(\alpha) = i\zeta\sin(2\beta) - 2i\sigma\beta, \tag{A.17}$$

where

$$\zeta = \frac{m^2a_0^2}{8k_0\cdot p\hbar^2}, \tag{A.18}$$

and

$$\sigma = \frac{p^2-\hbar^2}{4k_0\cdot p}. \tag{A.19}$$

The calculation of $f(\phi,\phi')$ parallels the one of Reiss and Eberly [46], except that ζ is defined differently. The difference can be again traced to the fact that in our calculation the scattering part of the Hamiltonian remains nonvanishing, while in Ref. [46] the absorbing part is nonzero. One can show that the order of magnitude of ζ is

$$\zeta \sim a_0^2\frac{\lambda_0}{\lambda_c}. \tag{A.20}$$

In the context of this work ζ is infinite since the artificial "Compton wavelength" was chosen to be smaller than any scale of interest. It is interesting to calculate ζ for the actual value of Planck's constant to assess the importance of quantum mechanical effects. For visible light with $\lambda_0 \sim 400nm$ and $\lambda_c \approx 2\cdot 10^{-12}m$ we find

$$\frac{\lambda_0}{\lambda_c} \approx 2\cdot 10^5. \tag{A.21}$$

Since today's lasers at $0.3\mu m$ reach the intensities high enough to have $a_0 > 0.1$, our neglect of quantum effects is well justified, and the assumption $\zeta \to \infty$ is the correct one even for a consistent quantum calculation.

It is rather amusing that at the time when Ref. [46] was published, the maximum available a_0^2 from a pulsed-ruby laser was of order 10^{-8}, thus validating the assumption of $\zeta \to 0$, which was used in [46]! A leap from zero to infinity in the past 30 years is wonderful evidence of the progress in laser technology. Yet one should refrain from characterizing this leap as "quantum" since, to the contrary, the increased power of modern lasers brings us securely into classical domain.

Solving for f in a similar fashion as in [46] we arrive at

$$f = (4k_0 \cdot p \sin \pi\sigma)^{-1} J_{-\sigma}(\zeta) e^{-i\zeta \sin 2\phi} e^{2i\sigma\phi}, \tag{A.22}$$

where σ is required to be an integer and J_n is the Bessel function of order n. One observes from Eq.(A.22) that the Green function of the electron in intense EM field has poles corresponding to integer σ's. Calculating the poles at each σ allows one to rewrite the Green function as

$$G(x,x') = \sum_{\sigma=-\infty}^{+\infty} (2\pi)^{-4} \int d^4p \frac{e^{-ip\cdot(x-x')} J_\sigma(\zeta) e^{-i\zeta \sin 2\phi} e^{2i\sigma\phi}}{(p - 2\sigma k_0)^2 - \bar{m}^2/\hbar^2}. \tag{A.23}$$

From (A.9), Eq.(A.8) becomes

$$\partial_\mu \partial^\mu a_1 = R a_1, \tag{A.24}$$

with

$$\begin{aligned} R &= \frac{4m^2 a_0(x)\psi_0(x)}{\hbar^4} \int d^4x' G(x,x') a_0(x') a_1(x') \psi_0^*(x') \\ &+ \frac{4m^2 a_0(x)\psi_0^*(x)}{\hbar^2} \int d^4x' G(x,x') a_0(x') a_1(x') \psi_0(x'). \end{aligned} \tag{A.25}$$

Inserting the Green function $G(x,x')$ from Eq.(A.23) into Eq.(A.25) and using a well-known identity for Bessel functions,

$$\sum_{k=-\infty}^{\infty} J_{l+k}(t) J_k(z) = J_l(t-z) \tag{A.26}$$

results in

$$R = \frac{a_0^2 \mu^4 m^2}{4\bar{m}^2} \sum_{m=-\infty}^{\infty} \frac{(J_m(\zeta_0 - \zeta_1) + J_{m-1}(\zeta_0 - \zeta_1))^2 [k_1 - (2m-1)k_0]^2}{\bar{m}^2 [(k_1 - (2m-1)k_0) \cdot n]^2}, \tag{A.27}$$

where

$$\zeta_1 = \frac{m^2 a_0^2}{8\hbar^2 (p_0 \cdot k_0 - k_1 \cdot k_0)}$$
$$\zeta_0 = \frac{m^2 a_0^2}{8\hbar^2 (p_0 \cdot k_0)}. \tag{A.28}$$

Both ζ_0 and ζ_1 become infinite in the limit of $\hbar \to 0$ but the difference between them is finite, provided $p_0 \gg k_0, k_1$. Calculating the argument of the Bessel functions to the lowest (zeroth) order in $\hbar$, Eq.(A.27) can be simplified to

$$R = \frac{\mu^2 a_0^2}{4(1 + a_0^2/2)} \sum_{m=-\infty}^{\infty} \frac{(J_m(b) - J_{m-1}(b))^2 [k_1 - (2m-1)k_0]^2}{(1 + a_0^2/2)[(k_1 - (2m-1)k_0) \cdot n]^2}, \tag{A.29}$$

where

$$b = \frac{a_0^2 (k_1 \cdot k_0)}{8(1 + a_0^2/2)[n \cdot k_0]^2}. \tag{A.30}$$

The dispersion relation for the probe (which can be used to calculate its spatio-temporal evolution, in the linear regime) is then given by

$$\omega_1^2 - \vec{k}_1^2 = R. \tag{A.31}$$

It is easy to convince oneself that Eqs.(A.31) and (A.29) recover the dispersion relation derived in [12] for a particular example of back scattering. This is not surprising since both calculations have been carried out under the same set of assumptions, namely (i) the space-charge effects were neglected and (ii) the pump was assumed to be moving with the speed of light despite the presence of plasma.

It is also worth pointing out that the solutions of Eq.(A.3)

$$\psi_{p0}(x) = e^{i\left(p_0 \cdot x + \frac{m^2 a_0^2 \sin(2\phi)}{\hbar^2 (8 k_0 \cdot p_0)}\right)}, \tag{A.32}$$

form a complete set satisfying the orthogonality relation

$$(2\pi)^{-4}\int d^4p\psi_p^*(x)\psi_p(x') = \delta^4(x-x'). \tag{A.33}$$

The four-vector index p_0 in Eq.(A.32), satisfying the "mass shell" dispersion relation

$$p_\mu p^\mu = \frac{\bar{m}^2 m^2}{\hbar^2} \tag{A.34}$$

labels the time-averaged momenta and energy and, as it is clear from Eq.(A.33), represents a canonical variable which makes the single-particle Hamiltonian space-time independent. This property of the time-averaged momentum was used by Rax [13] to study single-particle dynamics in the combined fields of the pump a_0 and the perturbing (smaller) probe a_1.

Unfortunately, one cannot generalize the Green function (A.23) to the regimes for which either of assumptions (i) or (ii) is invalid. For those cases the order-by- order diagrammatic calculation seems to be the appropriate systematic approach.

(3) **Third harmonic generation; electron and photon renormalization** We now develop a perturbative solution to Eq.(A.3) when (A.2) is not valid. Namely, we assume that

$$k_{0\nu}k_0^\nu = \mu^2 \tag{A.35}$$

and solve Eq.(A.3) for ψ using μ^2 as a perturbation parameter. Space-charge effects are still neglected in this calculation. Note that μ^2 is the consistently renormalized photon mass that has to be obtained to all orders in ϵ by calculating the resonant currents into the RHS of wave equation (A.8). The exact procedure will be illustrated below in the calculation of the renormalized photon mass.

We rewrite Eq.(A.3) in the form

$$\partial_\mu\partial^\mu\psi + \frac{m^2}{\hbar^2}\bar{m}^2 + a^2(\phi)\psi = 0, \tag{A.36}$$

where the functional dependence of $a^2(\phi)$ is unspecified. Later we will assume

$$a^2(\phi) = \frac{a_0^2}{2}\cos 2\phi \tag{A.37}$$

and compare these results for the rate of harmonic generation, electron mass renormalization and "photon mass" correction with the predictions of the diagrammatic calculations in Sections 4.1,3.2.1,3.2.2, 4.2.

Solutions of Eq.(A.36), parametrized by the average four momentum p, are sought in the form

$$\psi_p(x) = \frac{\hbar^{1/2}\sqrt{n_0}}{(2\epsilon_{\vec{p}})^{1/2}} q(\phi) e^{i\left(p\cdot x + \frac{m^2\int^\phi d\phi' a^2(\phi')}{\hbar^2(2k_0\cdot p)}\right)}, \tag{A.38}$$

where $q(\phi)$ is a function which is equal to unity for $\mu^2 = 0$, and must be determined perturbatively, order by order, in μ^2. Canonical momentum p makes the single particle Hamiltonian time- independent *to zeroth order* in μ^2. We will be seeking the appropriate canonical transformation which makes the Hamiltonian time-independent order by order in μ^2.

The zeroth order (in μ^2) phase Φ_0 is given by

$$\Phi_0 = p\cdot x + \frac{\int^\phi d\phi' a^2(\phi')}{\hbar^2(2k_0\cdot p)}. \tag{A.39}$$

Noting that

$$\partial_\mu q(\phi) = k_{0\mu} q'(\phi) \tag{A.40}$$

and substituting (A.38) into (A.36) results in the equation for $q(\phi)$:

$$\mu^2 q'' + 2i\left[(k_0\cdot p) + \frac{\mu^2 m^2 a^2(\phi)}{2\hbar^2(k_0\cdot p)}\right] q' + \mu^2 q\left[\frac{ia^{2\prime}(\phi)m^2}{2\hbar^2(k_0\cdot p)} - \frac{a^4(\phi)m^4}{4\hbar^4(k_0\cdot p)^2}\right] = 0. \tag{A.41}$$

Since Eq.(A.41) is homogeneous in q, we look for the solutions in the form

$$q(\phi) = \exp\left(\mu^2\Phi_1(\phi) + \mu^4\Phi_2(\phi) + \ldots\right). \tag{A.42}$$

Substituting (A.42) into (A.41) yields

$$\Phi_1(\phi) = -\frac{a^2(\phi)m^2}{4\hbar^2(k_0\cdot p)^2} - \frac{im^4\int^\phi d\phi' a^4(\phi')}{8\hbar^4(k_0\cdot p)^3} \tag{A.43}$$

$$\Phi_2(\phi) = \frac{a^4(\phi)m^4}{8\hbar^4(k_0\cdot p)^4} + \frac{im^6\int^\phi d\phi' a^6(\phi')}{16\hbar^6(k_0\cdot p)^5}. \tag{A.44}$$

The real and imaginary parts of the phases Φ_1 and Phi_2 have different physical meanings. The real parts change the absolute value of ψ and thus affect the RHS of the wave equation (A.8), resulting in harmonics generation, modification of the "photon mass", etc. The imaginary parts of renormalize the electron mass but do not affect the wave equation.

We now assume the particular form of $a^2(\phi)$ given by (A.37). As a simple check of the diagrammatic formalism in the context of the KG model, we calculate the lowest order of the electron mass renormalization and compare it with the corresponding diagrams. Averaging over the oscillating quantities, we obtain (to the first order in μ^2):

$$\langle\Phi_0 + \Phi_1\rangle = \left(p - k_0\frac{\mu^2m^4(a_0^2/2)^2}{16\hbar^4(k_0\cdot p)^3}\right)\cdot x. \tag{A.45}$$

The ordering of Φ's assumed that each successive term is smaller that the previous one. This is insured by choosing the canonical momentum in such a way that phases do not grow secularly as a function of x. As the second term in the brackets in the RHS of Eq.(A.45) indicates, Φ_1 would grow secularly, unless the new canonical momentum is chosen to be

$$p_1 = p - k_0\frac{\mu^2m^4(a_0^2/2)^2}{16\hbar^4(k_0\cdot p)^3}. \tag{A.46}$$

From another perspective, canonical transformation (A.46) is equivalent to transforming to oscillation center coordinates. Recalling that the square of the mass is equal to square of a four- momentum (see Eq.(A.34)), we calculate from Eq.(A.46)

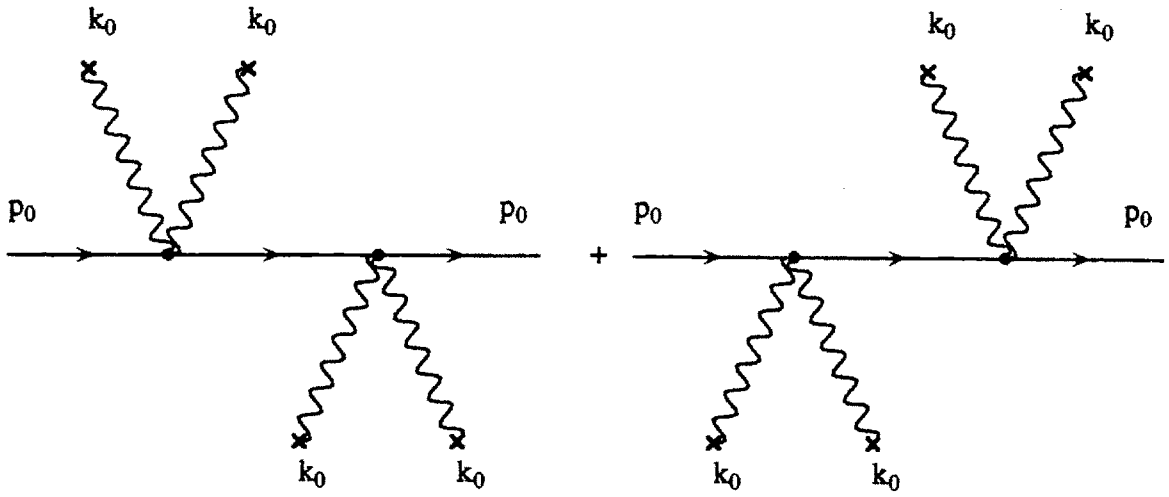

Figure A-1: First order in ϵ correction to the electron mass; phase velocity correction, no space-charge fields

the fractional correction to the electron mass

$$\frac{\Delta m^2}{m^2} = -\frac{\mu^2 a_0^4}{32\bar{m}^2(n\cdot k_0)^2}. \tag{A.47}$$

This value of Δm^2 has to be compared with that obtained from diagrammatic contribution of Fig. A-1. These diagrams takes into account the lowest order "photon mass", but neglect the space-charge effects. Reading off the values of the propagators in the same way it was done in Section 3.2.2 results in

$$-\Delta m^2 = \frac{m^4}{\hbar^2}\left(\frac{a_0}{2}\right)^2\left(\frac{-1}{(p_0+2k_0)^2-\bar{m}^2/\hbar^2}+\frac{-1}{(p_0-2k_0)^2-\bar{m}^2/\hbar^2}\right), \tag{A.48}$$

which, after simplification, can be easily seen to yield exactly (A.47). Another check of the diagrammatic approach is to calculate, to the lowest order in μ^2, the rate of the third harmonic emission. Neglecting the Φ_2 phase, because it is of higher order, we write the RHS of the wave equation (A.8) as

$$R = \mu^2 e^{2\mu^2 Re(\Phi_1)} a_0 \cos k_0\cdot x. \tag{A.49}$$

Expanding the exponential to the first order and extracting the third harmonic com-

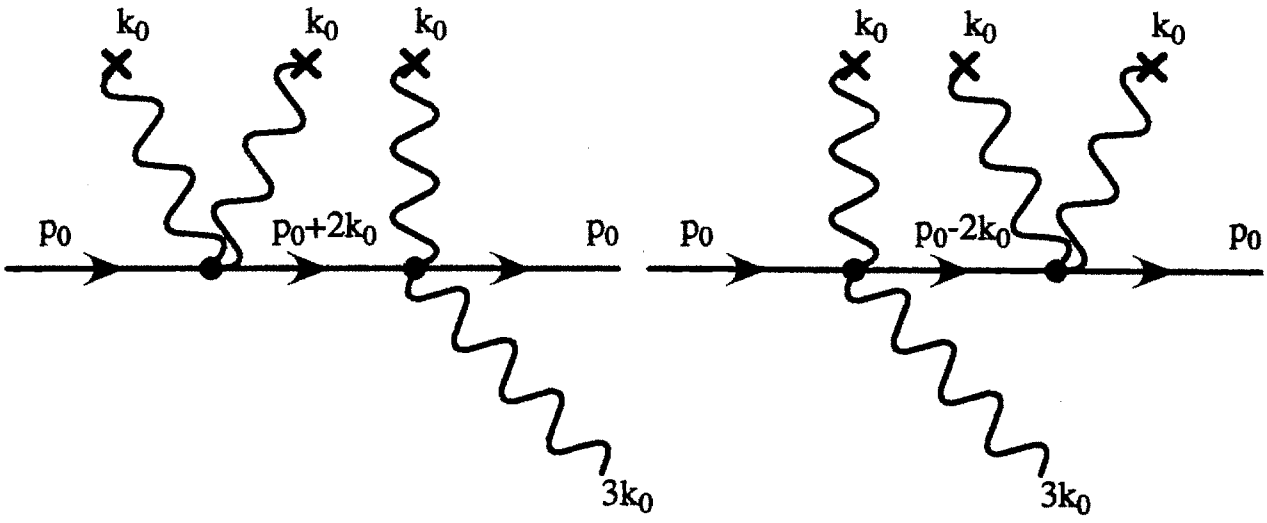

Figure A-2: Third harmonic generation to lowest order in ϵ; phase velocity correction, no space-charge fields

ponent results in

$$R = \frac{\mu^4 a_0^3 \cos 3k_0 \cdot x}{8\bar{m}^2 (n \cdot k_0)^2}. \tag{A.50}$$

This result agrees with evaluating the diagrammatic contributions of Fig. A-2 (for more details, see Section 2.4.3)

Check to the next order in μ^2 which involves Φ_2, is to calculate the modification of the "photon mass" to order μ^6 and compare it with the corresponding diagrammatic contribution that was computed in Section 4. To make a valid comparison it is important that the results of both calculations use the same (renormalized) quantities. For instance, the diagrammatic calculation in Section 4.2 uses the renormalized to the first order in ϵ electron momentum given by Eq.(A.46). It is important to realize that momentum transformation (A.46) cannot be achieved by incorporating a constant into the Hamiltonian, as it was done to the lowest order with p. Indeed, p satisfies

$$p \cdot p = \frac{\bar{m}^2}{\hbar^2} = \frac{m^2(1 + a_0^2/2)}{\hbar^2}, \tag{A.51}$$

and is a true canonical momentum of the single-particle Hamiltonian with the time-averaged part of $a_0^2(x)$ included in the electron mass. On the contrary, the mass correction given by (A.47) is momentum-dependent and thus cannot be generated by

adding a constant term to the Hamiltonian. We still need to develop a perturbation theory in terms of p_1 and not p (renormalization to every order in ϵ, in compliance with our diagrammatic logic!), and this can be accomplished through a canonical transformation given by (A.46). This is a contact transformation since it transforms momenta independently of the coordinates. We have noted, but have not rigorously proven, that to ensure that the wave function ψ_p obtained from Eq.(A.38) with the expansion (A.43- A.44), describes the same object as an eigenstate of the new momentum p_1, with unperturbed (time- averaged) density n_0, ψ_p has to be rescaled the by a factor $1/\sqrt{\rho}$, where

$$\rho^{1/2} = \det\left(\frac{\partial p_1^\mu}{\partial p^\nu}\right)^{1/2}. \tag{A.52}$$

The physical reason for this "squeezing" of the coordinate space is that the contact transformation (A.46) *expands* the momentum space, and, since the total phase volume is preserved by the canonical transformation, the coordinate space has to shrink. From Eqs.(A.46) and (A.52) we obtain

$$\rho = \det\left(\delta_{\alpha\beta} + \frac{3\mu^2 a_0^4 k_{0\alpha} k_{0\beta}}{64\hbar^2 (k_0 \cdot p)^4}\right). \tag{A.53}$$

Using an easily proven identity,

$$\det\left(\delta_{\alpha\beta} + \sigma e_\alpha e_\beta\right) = 1 + \sigma, \tag{A.54}$$

where e_α is an arbitrary unit four vector, we obtain

$$\rho = 1 + \frac{3\mu^4 a_0^4}{64(k_0 \cdot p)^4}. \tag{A.55}$$

Overall, the properly rescaled solutions of the Klein-Gordon equation to order ϵ^2 are given by

$$\psi_{p1}(x) = \frac{\hbar^{1/2}\sqrt{n_0}}{(2\epsilon_{\vec{p_1}})^{1/2}\rho^{1/2}} \exp\left(\bar{\Phi}_0 + \mu^2\bar{\Phi}_1 + \mu^4\bar{\Phi}_2\right), \tag{A.56}$$

where

$$\begin{aligned}
\bar{\Phi}_0 &= i\left(p_1\cdot x+\frac{a_0^2\sin 2\phi}{8\hbar^2(k_0\cdot p_1)}\right)\\
\bar{\Phi}_1 &= -\frac{a_0^2\cos 2\phi}{8(k_0\cdot p_1)^2}-\frac{ia_0^4\sin 4\phi}{256\hbar^2(k_0\cdot p_1)^3}\\
\bar{\Phi}_2 &= \frac{a_0^4\cos^2 2\phi}{32(k_0\cdot p_1)^4}-\frac{ia_0^6(\sin 6\phi/6+\sin 2\phi/2)}{64\hbar^2(k_0\cdot p_1)^5}.
\end{aligned}\tag{A.57}$$

Simple calculation confirms that there is no *additional*, to order μ^6, first harmonic in the RHS of the wave equation, as was proven in Section 4.2 for the one-level diagrams (see Eq.(4.12)).

It is worthwhile to note that, in principle, one needn't start with the modified momentum p satisfying Eq.(A.51), nor was it required to absorb the $a_0^2/2$ time-averaged term of the Klein-Gordon equation into the zeroth order electron mass. Instead of assuming $a^2(\phi)$ in the form of (A.37), alternatively, one could use

$$a^2(\phi)=a_0^2\cos^2\phi \tag{A.58}$$

and "real" (kinematic) particle momentum p_0. The calculation would then proceed by performing the zeroth order canonical transformation

$$p_1=p_0+k_0\frac{a_0^2}{4k_0\cdot p_0}, \tag{A.59}$$

rescaling the fields to the *first* order in ϵ (unlike the rescaling in (A.55) which was done to the second order in ϵ), and so on. The result would look formally slightly different from that of (A.56 -A.57) but would be identical to it order by order. The path we have taken is easier and utilizes the known fact that p is the canonical momentum of the Hamiltonian which is time- independent to zeroth order in μ^2.

Another important lesson that can be learned from the solutions of Klein-Gordon equation is that laser-plasma interactions in the fluid (for plasma electrons) limit can be studied by methods of successive canonical transformations, with μ^2 being the smallness parameter. Both photons and plasmons can be incorporated into this

treatment, thus removing assumption (i). The idea of using Arnowitt- Fickler gauge $A \cdot p_0 = 0$ can still be used, where p_0 is a canonical momentum, redefined order by order in μ^2. Development of purely classical (no artificial scale $\hbar$) theory of laser-plasma interactions based on successive canonical transformations is the subject of future work.

Appendix B

Tutorial on Diagrammatic Calculations

The goal of this Appendix is to formulate the rules for using the diagrams rather than giving rigorous proofs and presenting all the algebra. The rules are illuminated by solving three problems: (i) electron mass renormalization due to lowest order modification of phase velocity of EM waves in plasmas, (ii) renormalization of photon mass due to lowest order modification of phase velocity of EM waves in plasmas, and (iii) third harmonic generation due to space-charge field. Emphasis is placed on how an arbitrary diagram is quantified.

As in Chapter 3, we assume that the unperturbed state of EM fields and the electron plasma is given by

$$\psi = \hbar^{1/2} \frac{e^{ip_0^\mu \cdot x_\mu}}{(2p_0^0)^{1/2}} \sqrt{n_0} \tag{B.1}$$

and

$$\frac{e\vec{A}_0(x)}{m} = \vec{e}_x \left(\frac{a_0^*}{2} e^{ik_0 \cdot x} + \frac{a_0}{2} e^{-ik_0 \cdot x} \right), \tag{B.2}$$

and we use a four-vector notation for the polarization:

$$e_x^\mu = (e_0, \vec{e}_x). \tag{B.3}$$

We further assume that (1) the initial field is a photon, satisfying the Arnowitt-

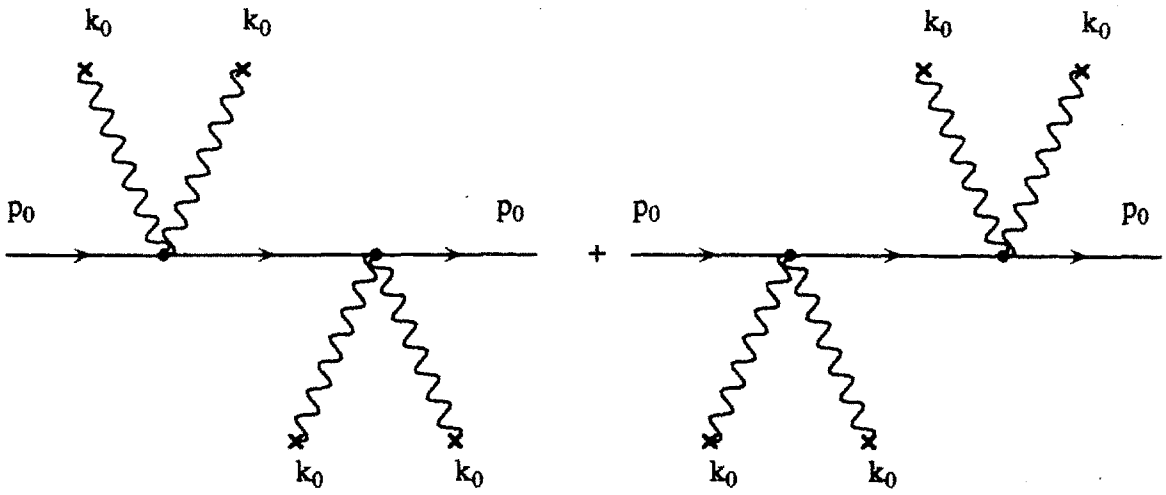

Figure B-1: Diagrams for renormalizing the electron mass to first order in ϵ due to modification of phase velocity in the plasma (no space charge fields).

Fickler gauge and propagating in $z-$ direction, so that $e_x^\mu \cdot k_{0\mu} = e_x^\mu \cdot p_{0\mu} = 0$ and $e_x^\mu = (0,1,0,0)$; and (2) the plasma is moving in $z-$ direction with four momentum $p_0 = (p_0^0, 0, 0, p_{0z})$ (which can be always achieved by a Lorentz transformation).

Problem (i). The diagrams corresponding to the electron mass renormalization due to the lowest order modification of the phase velocity of EM waves are given in Fig. B-1. Crosses on the photon lines in Fig. B-1 indicate that the EM field has to be evaluated unperturbed, as given by Eq.(B.2). Each cross corresponds to multiplication by $ma_0/2e$ for the lines coming from the top (or $ma_0^*/2e$ for the lines coming from the bottom), as should be clear from Eq.(B.2). By convention, we do not put crosses on the electron lines despite the fact that they *also* have to be evaluated unperturbed. Every electron line that *enters* a vertex should be multiplied by ψ from Eq.(B.1) and every electron line that *exits* the vertex has to be multiplied by ψ^*.

The term "renormalization" refers to adding a quadratic piece $-\Delta m^2 \psi\psi^*/\hbar^2$ to the free partcle Lagrangian given by Eq.(2.41). To preserve the total Lagrangian, the counter term

$$\mathcal{H}^{(1)}_{count} = -\Delta m^2 \psi\psi^*/\hbar^2 \tag{B.4}$$

has to be added to the interaction *Hamiltonian* (2.63)

$$\mathcal{H}_i = -\frac{e^2}{\hbar^2} A_\mu A^\mu \psi\psi^* + i\frac{e}{\hbar} A^\mu(\psi^*\partial_\mu\psi - \psi\partial_\mu\psi^*)$$

(see discussion in the beginning of Section 3.2.1). The magnitude of Δm^2 is computed order by order so as to cancel the contributions of the higher-order wave-particle interactions from $\mathcal{H}_i$.

An example of such an interaction, calculated to second order in the Hamiltonian from Eq.(3.28) is given in Fig. B-1. Note that when the space-charge forces are neglected, the absorbing part of the interaction Hamiltonian from Eq.(3.29) does not contribute. Schematically, we can write that

$$\Delta m^2\psi\psi^*/\hbar^2 + (\text{contribution} \quad \text{of} \quad \text{Fig. B} - 1) = 0, \tag{B.5}$$

or

$$-\Delta m^2 \frac{n_0\hbar}{2\bar{m}m}/\hbar^2 = (\text{contribution} \quad \text{of} \quad \text{Fig. B} - 1), \tag{B.6}$$

where $\bar{m} = p_0^0$.

Starting from left to right, the contribution of each of the two diagrams in Fig. B-1 consists of a product of (1) an unperturbed electron field ψ, (2) a first interaction vertex $e^2/\hbar^2$, (3) two unperturbed photon lines $-(ma_0/2e)^2$, (4) electron propagator

$$\frac{-1}{(p_0 \pm 2k_0)^2 - m^2\bar{m}^2/\hbar^2},$$

where $+$ is used in evaluating the first diagram and $-$ in evaluating the second diagram, (5) a second interaction vertex $e^2/\hbar^2$, (6) two unperturbed photon lines $-(ma_0^*/2e)^2$, and (7) an unperturbed electron field ψ^*. Note that for this particular example the $\psi\psi^*$ term in the counter term exactly cancels the product of (1) and (7) in Fig. B-1. If a diagram has more than one pair of electron lines (as in example in Fig. 3-7), its contribution has to be multiplied by a combinatorial factor $M!$, where M is the number of pairs of electron lines. In covariant notation $e_x \cdot e_x = -1$, which

explains the minus sign in front of the $-(ma_0/2e)^2$ and $-(ma_0^*/2e)^2$ terms.

From Eq.(B.6), we obtain:

$$-\Delta m^2/\hbar^2 = \left(\frac{e^2}{\hbar^2}\right)^2 \left(\frac{m^2 \mid a_0 \mid^2}{4e^2}\right)^2 \left(\frac{-1}{(p_0+2k_0)^2 - m^2\bar{m}^2/\hbar^2} + \frac{-1}{(p_0-2k_0)^2 - m^2\bar{m}^2/\hbar^2}\right). \tag{B.7}$$

Recalling that $p_0^2 = m^2\bar{m}^2/\hbar^2$ and $k_0^2 = \mu^2 = \omega_p^2/\bar{m}$, we obtain, to zeroth order in $\hbar k_0/(mc)$

$$\frac{\Delta m^2}{\bar{m}^2} = -\frac{a_0^4\omega_p^2}{32\bar{m}^5(n\cdot k_0)^2}. \tag{B.8}$$

In the reference frame where the plasma is stationary, assuming that $\Delta m^2 \ll \bar{m}^2$, Eq.(B.8) can be simplified to yield Eq.(3.46).

(ii) Some diagrammatic terms contribute to several laser plasma processes. For example, the diagrammatic expansion to second order in the scattering Hamiltonian from Eq.(3.28) contributes to both the renormalization of the electron mass (as explained in the previous example) and to the renormalization of the photon mass (subject of the present example). The diagrams corresponding to the first order in ϵ correction to photon mass is shown in Fig. B-2. We schematically distinguish between the two examples by not putting a cross on one of the emitted photon lines in Fig. B-2. This can be interpreted as scattering of the external (crossed) photon into the "loose" photon. Similarly to example (i), renormalizing the photon mass is equivalent to adding the counter term

$$\mathcal{H}^{(2)}_{count} = \frac{\Delta\mu^2}{4\pi} g^{\mu\nu}\frac{A_\mu A_\nu}{2} \tag{B.9}$$

to the interaction Hamiltonian. Following the same logic as in the previous example, we obtain

$$\frac{\Delta\mu^2}{2\cdot 4\pi} \times (ma_0^*/2e)\epsilon_x^\mu + (\text{contribution of Fig. B}-2) = 0, \tag{B.10}$$

The contribution of the diagrams in Fig. B-2 is calculated identically to the previous example. Starting from left to right, the contribution of each of the two diagrams

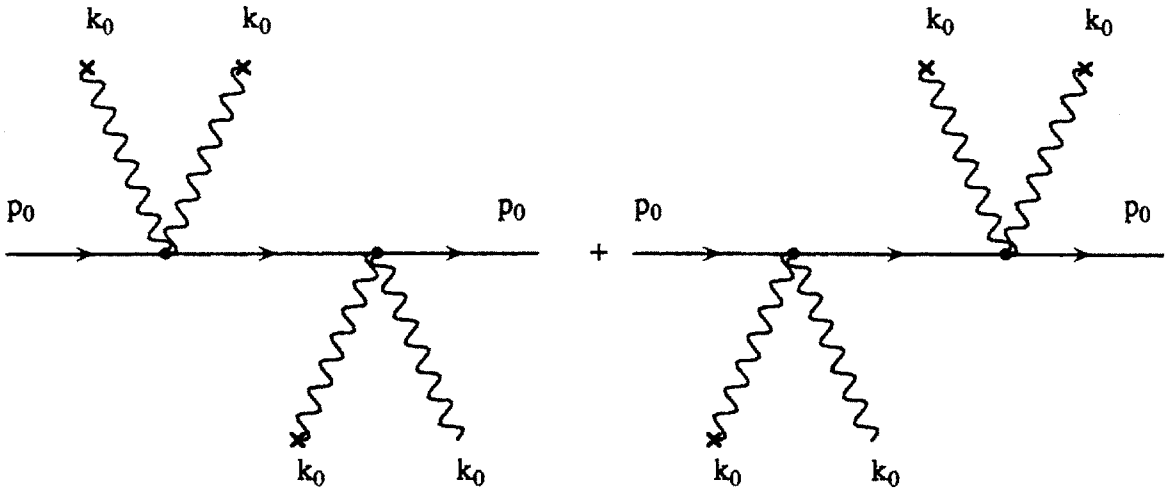

Figure B-2: Diagrams for renormalizing the photon mass to first order in ϵ due to modification of phase velocity in the plasma (no space charge fields).

in Fig. B-2 consists of a product of (1) the unperturbed electron field ψ, (2) the first interaction vertex $e^2/\hbar^2$, (3) two unperturbed photon lines $-(ma_0/2e)^2$, (4) the electron propagator

$$\frac{-1}{(p_0 \pm 2k_0)^2 - m^2\bar{m}^2/\hbar^2},$$

where $+$ is used in the first and $-$ in the second diagrams, (5) the second interaction vertex $e^2/\hbar^2$, (6) one unperturbed photon lines $(ma_0^*/2e)e_x^\mu$, and (7) the unperturbed electron field ψ^*.

Altogether, from Eq.(B.10) we find

$$\begin{aligned}\frac{\Delta\mu^2}{4\pi} &= 2 \times \frac{\hbar^2 n_0}{2\bar{m}} \times \frac{e^2}{\hbar^2} \times \frac{-m^2 a_0^2}{4e^2} \\ &\times \left(\frac{-1}{(p_0 + 2k_0)^2 - \bar{m}^2 m^2/\hbar^2} + \frac{-1}{(p_0 - 2k_0)^2 - \bar{m}^2 m^2/\hbar^2} \right), \end{aligned} \tag{B.11}$$

which simplifies to

$$\frac{\Delta\mu^2}{\mu^2} = -\frac{\omega_p^2 a_0^2}{8\bar{m}^3\omega_0^2}. \tag{B.12}$$

The physical interpretation of Eq.(B.12) is a nonlinear lowering of the cutoff frequency for the photons in the plasma. For the full derivation of $\Delta\mu^2$ including the space charge forces, see Section 4.2.

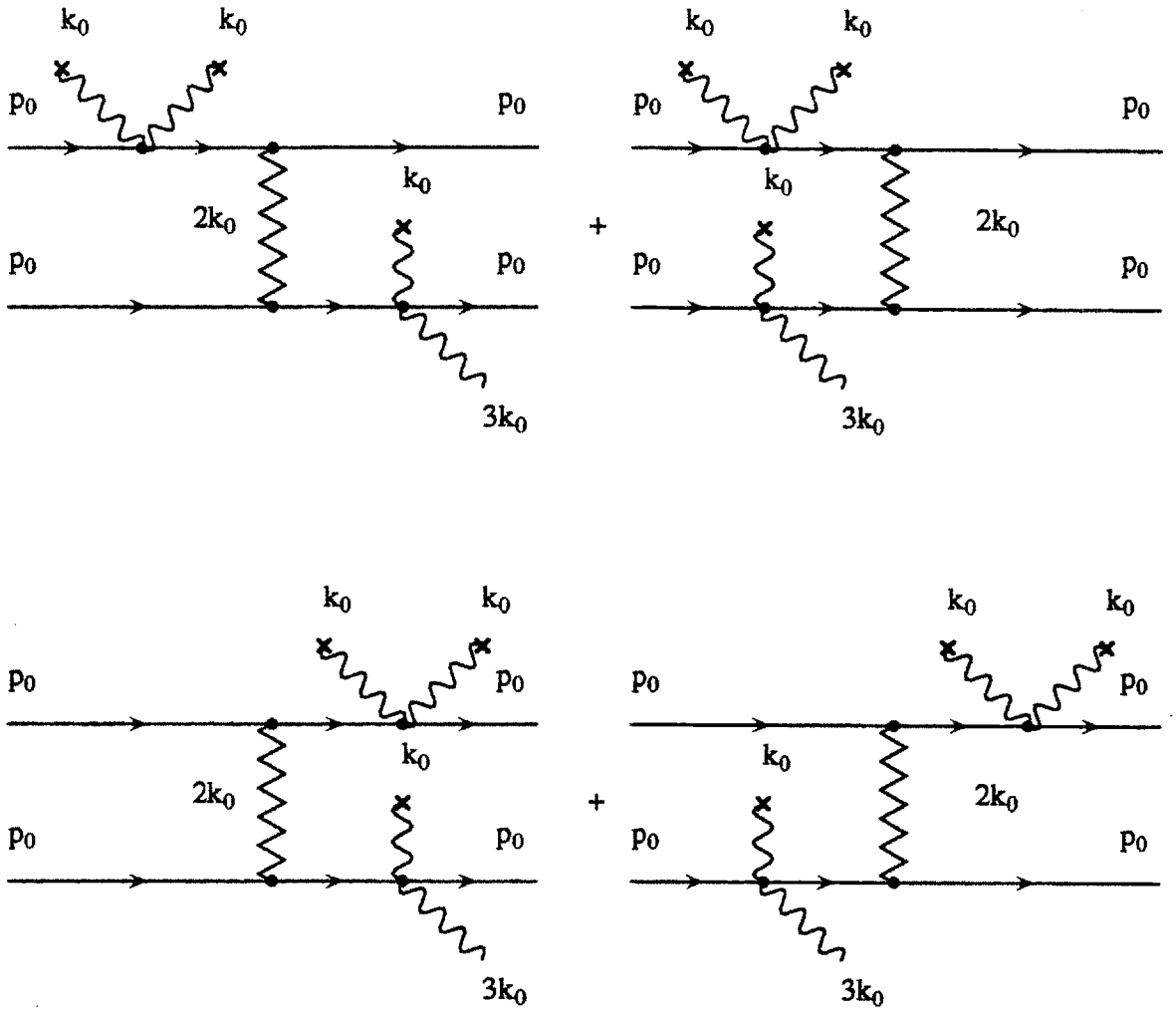

Figure B-3: Diagrams for the third harmonic generation to first order in ϵ due to space charge fields (does not account for the modification of phase velocity in the plasma).

(iii) As discussed in Section 4.1, two mechanisms allow for the generation of the third harmonic to order ω_p^4 in plasma frequency. These are due to the modification of the phase velocity of the EM waves in the plasma ($v_{ph} \neq c$) and the space-charge forces induced in the ponderomotively driven electron plasma. This example describes the third harmonic generation due to space-charge forces. The diagrammatic representation of this process is given in Fig. B-3. The calculation of the rate of the third harmonic is somewhat complicated by the fact that there are two different types of EM waves in the plasma: photons and plasmons. In addition, photons can be polarized in any direction in a two-dimensional plane, as mentioned in Section 3.1.2. For

the example presented here, it is obvious that the third harmonic is polarized in $x-$direction. However, for the sake of pedagogy, we calculate the generation rate for a third harmonic *photon* field polarized in the direction e_3^μ (the subscript 3 labels the third harmonic!). The combination of the emitted field being photonic and satisfying the Arnowitt-Fickler gauge condition implies that $e_3 \cdot p_0 = 0$ and $\vec{e}_3 \cdot \vec{k}_0 = 0$. Thus, we will be looking for the growth rate of a field given by

$$\frac{eA^\mu_{3\vec{k}_0}(x)}{m} = e_3^\mu \left(\frac{a_3^*}{2} e^{i3k_0 \cdot x} + \frac{a_3}{2} e^{-i3k_0 \cdot x} \right), \tag{B.13}$$

where we have assumed that phase velocities of the fundamental and the harmonic match.

The loose ($3k_0$) lines of the diagrams in Fig. B-3 denote taking a contraction of the fields at the interaction vertex with the third harmonic field. If the field of interest $A^\mu_{3\vec{k}_0}(x)$ is photonic (as in the present example), the corresponding contraction is given by Eq.(3.6), where the transverse part of the propagator $D_{\mu\nu}$ has to be taken from Eq.(3.19). It can be easily shown that, under the assumption of phase velocity matching, the integration over the event (vertex) coordinates in Wick's integral (analogous to integration over x_1 and x_2 in Eq.(2.87)) ensures that $D_{\mu\nu}(k)$ is evaluated at $k = 3k_0$. In general, the diadic part of the propagator $D_{\mu\nu}(k)$ has to be evaluated *at the wavenumber of the emission.* For instance, in Section 4.4.3, where we evaluated the rate of second harmonic generation, $D_{\mu\nu}(k)$ was evaluated at $k = 3k_1 - k_2$. To calculate the rate of third harmonic emission polarized in e_3^μ direction, one simply projects $D_{\mu\nu}(k)$ on e_3^μ.

Another element of the diagrams in Fig. B-3 is the "virtual plasmon" propagator $D^L_{\mu\nu}(2k_0)$ given by Eq.(3.18). By the "naive" Feynman rule (as outlined at the end of Section 2.3.2) this propagator has to be multiplied by the sum of the electron momenta at the interaction vertices. For the first diagram in Fig. B-3 this is $(p_0 + 2k_0) + p_0$ for the top absorption vertex and $p_0 + (p_0 + 2k_0)$ for the bottom absorption vertex. The last thing that has to be accounted for is the $-4\pi/(k^2 - \mu^2)$ term in the propagator (3.19). It can be shown that when the rate of generation of a_3 (the component of

vector potential that goes as $e^{-ik\cdot x}$) is calculated, this term becomes equal to

$$\frac{-4\pi}{i2\omega_{3\vec{k}_0}}, \tag{B.14}$$

where, in general, the frequency in the denominator of Eq.(B.14) is equal to the *frequency of the emitted radiation.*

We can now write down the contribution of the first diagram in Fig. B-3 (in fact, all of them are equal to lowest order in $\hbar$) as a product of the following terms (from left to right, from top to bottom): (1) the unperturbed electron field ψ, (2) the first scattering vertex $e^2/\hbar^2$, (3) two unperturbed photon lines $-(ma_0/2e)^2$, (3) the electron propagator

$$\frac{-1}{(p_0+2k_0)^2-\bar{m}^2m^2/\hbar^2},$$

(4) the first absorptive vertex $e(p_0^\mu+2k_0^\mu)/\hbar$, (5) an unperturbed electron field ψ^*, (6) plasmon propagator

$$D^L_{\mu\nu}(2k_0)=-\frac{4\pi e^L_\mu(2k_0)e^L_\nu(2k_0)}{(n\cdot 2k_0)^2-\mu^2},$$

(7) the unperturbed electron field ψ, (8) the second absorptive vertex $e(p_0^\nu+2k_0^\nu)/\hbar$, (9) electron propagator

$$\frac{-1}{(p_0+2k_0)^2-\bar{m}^2m^2/\hbar^2},$$

(10) the second scattering vertex $e^2/\hbar^2$, (11) the unperturbed photon field $e_x^\alpha ma_0/2e$, (12) outgoing photon operator, multiplied by the projection vector e_3^β:

$$-\frac{4\pi(-g_{\alpha\beta}-e^L_\alpha(3k_0)e^L_\beta(3k_0)+n_\alpha n_\beta}{2i(3\omega_0)},$$

(13) the unperturbed electron field ψ^*.

A few observations simplify the calculation. Recall that $D^L_{\mu\nu}\cdot p_0^\mu=0$ by choice of gauge, so that $D^L_{\mu\nu}$ only has to be multiplied by $2k_0$. Also, by choice of gauge and restricting the calculation to photonic fields, $e_3\cdot p_0=e_3\cdot e^L(3k_0)=0$. Another useful

relation for an arbitrary vector χ is

$$\chi \cdot D^L(\chi) \cdot \chi = -4\pi \frac{(n\cdot\chi)^2 - \chi^2}{(n\cdot\chi)^2 - \mu^2}. \tag{B.15}$$

With all this in mind, the rate of the third harmonic generation is found to be

$$\begin{aligned} i2(3\omega_0)\frac{da_3}{dt} &= \frac{e}{m} \times 4 \times \left(\frac{\hbar^2 n_0}{2\bar{m}m}\right)^2 \times \left(\frac{e^2}{\hbar^2}\right)^2 \\ &\times \left(\frac{e}{\hbar}\right)^2 \times [2k_0 \cdot D^L(2k_0) \cdot 2k_0] \left(-\frac{m^2 a_0^2}{4e^2}\right) \\ &\times (-4\pi(-g_{\alpha\beta} - e^L_\alpha(3k_0)e^L_\beta(3k_0) + n_\alpha n_\beta)\cdot e_3) \times \left(\frac{-1}{(p_0+2k_0)^2 - \bar{m}^2m^2/\hbar^2}\right)^2, \end{aligned} \tag{B.16}$$

where the factor four stands for four different diagrams in Fig. B-3 and the factor e/m is used for conversion to normalized vector potential.

Using Eq.(B.15), Eq.(B.16) simplifies, to zeroth order in $\hbar$, to yield

$$i2(3\omega_0)\frac{da_3}{dt} = \frac{\omega_p^4 a_0^3 \vec{e}_x \cdot \vec{e}_3}{32\bar{m}^4} \frac{(n\cdot k_0)^2 - \mu^2}{4(n\cdot k_0)^2 - \mu^2}. \tag{B.17}$$

Equation (B.17) definitely indicates that the third harmonic is polarized in $x-$ direction, as is the fundamental.

We note that the calculation of renormalized corrections to a photon mass can be reduced to calculating the emission rate of the *fundamental*, stemming from the interaction terms and from the counter terms, and requiring that the total rate vanishes. In complicated geometries, when several waves are present, the rate calculation is the most reliable approach to renormalizing the EM dispersion relation.

The three examples considered in this Appendix cover some common problems in laser-plasma interactions and should provide a good guide for most practical calculations.

Appendix C

List of Notation

n_0	Unperturbed plasma density
ω_{p0}, ω_p	Plasma frequency
μ	Relativistic plasma frequency (in Chapters 1-5)
μ	Coupling parameter for laser- hose instability (in Chapters 5-6)
ϵ	Smallness parameter
$\vec{A}$	Vector potential
ϕ	Scalar potential
A_μ	Four- vector potential
a	Normalized vector potential
(q, p)	Canonical coordinate and momentum
$\{f, g\}$	Poisson bracket of functions f and g
(q_i, p_i)	Interaction canonical coordinate and momentum
$a^\dagger, a$	Creation and annihilation functions
β	Nonlinearity coefficient in Chapter 2
$C_2^{(n)}$	Counter terms of order n in nonlinearity β
$\hbar$	Scaling constant, has dimension of Planck const.
λ_c	Spatial scale associated with electron wavelength
ψ	Electron field
$\epsilon_{\vec{p}}$	Energy of electron with momentum $\vec{p}$
$(p_0^0, \vec{p}_0)$	Initial four momentum of plasma electrons (in units 1/Length)
$(P_0^0, \vec{P}_0)$	Initial four momentum of plasma electrons (regular units)

γ	Relativistic factor
n_μ	Unit vector in the direction of electron motion
$\widehat{A(x_1), B(x_2)}$	
$b^\dagger_{\vec{p}}, b_{\vec{p}}$	Creation and annihilation functions of the *relativistic* electron with momentum
$q^\dagger_{\vec{p}}, q_{\vec{p}}$	Creation and annihilation functions of the *nonrelativistic* electron with momen
$e^L_\mu(k)$	Unit polarization vector of longitudinal wave with wavenumber k
$D^L_{\mu\nu}$	Longitudinal (plasmon) propagator
$D^T_{\mu\nu}$	Transverse (photon) propagator
$\Pi(p)$	Electron propagator
$\bar{m}$	Renormalized dimensionless electron mass
v_{g0}	Group velocity of laser radiation
W	Width of the parabolic channel
$\mathrm{w} = \sqrt{Wc/\omega_p}$	Laser spot size
$K = \frac{c}{\omega_p W}$	Channel smoothness parameter
χ	Nonlinear index of refraction

Bibliography

[1] M. D. Perry and G. Mourou, Science **264**, 917 (1994).

[2] D. Strickland and G. Mourou, Opt. Commun. **56**, 219 (1985).

[3] P. Maine, D. Strickland, P. Bado, M. Pessot, G. Mourou, IEEE J. Quantum Electron. **24**, 398 (1988).

[4] M. M. Murnane, H. C. Kapteyn, M. D. Rosen, and R. W. Falcone, Science **251**, 531 (1991).

[5] H. Hamster, A. Sullivan, S. Gordon, and R. W. Falcone, Phys. Rev. E **49**, 671 (1994).

[6] C. B. Darrow et al., Phys. Rev. Lett. **69**, 442 (1992).

[7] X. Liu and D. Umstadter, Phys. Rev. Lett. **69**, 1935 (1992).

[8] J. Kmetec et al., Phys. Rev. Lett. **68**, 1527 (1992).

[9] W. Priedhorsky, D. Lier, R. Day, D. Gerke, Phys. Rev. Lett. **47**, 1661 (1981).

[10] C. Y. Chien et. al., Opt. Lett. **18**, 1535 (1993).

[11] C.E. Clayton, et al., Phys. Rev. Lett. 30, 37 (1993).

[12] P. Sprangle and E. Esarey, Phys. Rev. Lett. **67**, 2021 (1991).

[13] J. M. Rax, Phys. Fluids B **4**, 3962 (1992).

[14] J. M. Rax and N. J. Fisch, Phys. Rev. Lett. **69**, 772 (1992); J. M. Rax and N. J. Fisch, IEEE Trans. Plasma Phys. **21**, 105 (1993).

[15] P. Sprangle, E. Esarey, and A. Ting, *Phys. Rev. Lett.* **64**, 2011 (1990); Phys. Rev. A **41**, 4463 (1990); A. Ting, E. Esarey, and P. Sprangle, Phys. Fluids B **2**, 1390 (1990).

[16] E. Esarey, A. Ting, P. Sprangle, D. Umstadter, and X. Liu, IEEE Trans. Plasma Phys. **21**, 95 (1993).

[17] W. B. Mori, C. D. Decker, and W. P. Leemans, IEEE Trans. Plasma Phys. **21**, 110 (1993).

[18] K.-J. Kim, S. Chattopadhyay, C. V. Shank, Nucl. Instrum. Methods Phys. Res. A, **341**, 351 (1994).

[19] A. B. Borisov *et. al.,* Phys. Rev. A **45**, 5830 (1992).

[20] X. L. Chen and R. N. Sudan, Phys. Rev. Lett. **70**, 2082 (1993).

[21] T. Katsouleas and J. M. Dawson, Phys. Rev. Lett. **51**, 392 (1983).

[22] E. Esarey, J. Krall, and P. Sprangle, Phys. Rev. Lett. **72**, 2887 (1994).

[23] J. S. Wurtele, Phys. Fluids B **5**, 2363 (1993), and references therein.

[24] J. S. Wurtele, Physics Today **47** (no. 7), 33 (1994).

[25] P. Sprangle, E. Esarey, Phys. Fluids B **4**, 2241 (1992).

[26] S. V. Bulanov, L. M. Kovrizhnykh, and A. S. Sakharov, Physics Reports, **186**, 1 (1990).

[27] T. Katsouleas, Private Communication.

[28] T. Tajima and J. M. Dawson, *Phys. Rev. Lett.* **43**, 267 (1979); L. M. Gorbunov and V. I. Kirsanov, Zh. Exp. Teor. Fiz. **93**, 509 (1987) [Sov. Phys. JETP **66**, 290 (1987)]; C. Joshi, W. B. Mori, T. Katsouleas, *et al.*, Nature, **311**, 525 (1984).

[29] C. E. Max, J. Arons, and A. B. Langdon, *Phys. Rev. Lett.* **33**, 209 (1974).

[30] G. Schmidt and W. Horton, *Comments Plasma Phys. Controlled Fusion* **9**, 85 (1985).

[31] G. Z. Sun, E. Ott, Y. C. Lee, and P. Guzdar, Phys. Fluids **30**, 526 (1987).

[32] W. B. Mori, C. Joshi, J. M. Dawson, D. W. Forslund and J. M. Kindel *Phys. Rev. Lett.* **60**, 1298 (1988).

[33] D. W. Forslund, J. M. Kindel, and E. L. Lindman, Phys. Fluids **18**, 1002 (1975); K. Estabrook and W. L. Kruer, Phys. Fluids **26**, 1892 (1983).

[34] T. M. Antonsen, Jr.,and P. Mora, *Phys. Rev. Lett.* **69**, 2204 (1992); T. M. Antonsen, Jr., and P. Mora, Phys. Fluids B **5**, 1440 (1993).

[35] C. J. McKinstrie and R. Bingham, Phys. Fluids B **4**, 2626 (1992).

[36] C. Decker, W. B. Mori, and T. Katsouleas, *Phys. Rev. Rap. Comm.*, in press 1994.

[37] P. Sprangle, E. Esarey, J. Krall, and G. Joyce, *Phys. Rev. Lett.* **69**, 2200 (1992).

[38] S. C. Wilks, W. Kruer, M. Tabak, and A. B. Langdon, Phys. Rev. Lett. **69**, 1383 (1992).

[39] M. Tabak et al., Phys. Plasmas **1**, 1626 (1994).

[40] T. Katsouleas, T. C. Chiou, C. Decker, W. B. Mori, J. S. Wurtele, G. Shvets, and J. J. Su, in *Advanced Accelerator Concepts*, edited by J. S. Wurtele, (AIP, New York, 1993), p. 480; T. C. Chiou, T. Katsouleas, C. Decker, W. B. Mori, J. S. Wurtele, G. Shvets, J.J. Su, Phys. Plasmas **2**, 310 (1995).

[41] G. Shvets and J. S. Wurtele, Phys. Rev. Lett., **73**, 3540 (1994).

[42] J. F. Ward, Rev. Mod. Phys. **37**, 1 (1965); T. K. Yee and T. K. Gustafson, Phys. Rev. A **18**, 1597 (1978); J. G. Fujimoto and T. K. Yee, IEEE Journ. Quant. Elect. **QE-22**, 1215 (1986).

[43] V. N. Tsytovich, Nonlinear effects in plasma (Plenum Press, New York, 1970).

[44] V. N. Tsytovich, An introduction to the theory of plasma turbulence (Pergamon Press, Oxford, 1972).

[45] B. Coppi, private communication.

[46] H. R. Reiss and J. H. Eberly, Phys. Rev. **151**, 1058 (1966).

[47] J. H. Eberly and H. R. Reiss, Phys. Rev. **145**, 1035 (1966).

[48] T. W. B. Kibble, Phys. Rev. **138**, 740 (1966).

[49] T. W. B. Kibble, Phys. Rev. **150**, 1060 (1966).

[50] W. L. Kruer, The physics of laser plasma interactions (Addison-Wesley, 1988), and references therein.

[51] J. P. Freidberg, R. W. Mitchell, R. L. Morse, and L. I. Rudsinski, Phys. Rev. Lett. **28**, 795 (1972).

[52] W. B. Mori, C. D. Decker, D. E. Hinkel, *Phys. Rev. Lett*, **72**, 1482 (1994).

[53] Yu. L. Klimontovich, 1957, Zh. Eksp. Teor. Fiz. **33**, 982 [Sov. Phys. JETP **6**, 753 (1958)].

[54] S. Ichimaru, Basic Principles of Plasma Physics (Benjamin, Reading, Mass., 1973).

[55] N. A. Krall and A. W. Trivelpiece, Principles of plasma physics (McGraw-Hill, New York, 1973).

[56] S. I. Braginskii, Reviews Of Plasma Physics, **1**, 205, (1965).

[57] F. F. Chen, Introduction to plasma physics and controlled fusion (Plenum Press, New York, 1984).

[58] J. M. Dawson, *Phys. Rev.*, vol. 113, p.383, 1959.

[59] . W. Littlejohn, The semiclassical evolution of wave packets (University of California Santa Barbara, Internal Report NSF-ITP-85-53, 1985), and references therein.

[60] L. D. Landau, Mechanics (Pergamon Press, Oxford, 1976).

[61] A. Deprit, Cel. Mech. **1**, 12 (1969).

[62] R. L. Dewar, J. Phys. A **11**, 9)1978).

[63] J. R. Cary, Lie transforms and their use in Hamiltonian perturbation theory (U.S. Department of Energy, Internal Report DOE/ET-0074, 1979).

[64] P. Ramond, Field theory: a modern primer (Addison-Wesley, Reading, MA, 1990).

[65] N. Minorsky, Non Linear Oscillations (Van Nostrand, Princeton, 1962).

[66] J. D. Jackson, Classical electrodynamics (Wiley, New York, 1975).

[67] S. Coleman, Aspects of symmetry (Cambridge University Press, Cambridge, 1983).

[68] U. A. Mitropolskii, Assymptotic methods in the theory of non-linear oscillations (Gordon and Breach, New York, 1961).

[69] L. D. Landau, The classical theory of fields (Pergamon Press, Oxford, 1989).

[70] J. A. Stamper *et. al.,* Phys. Fluids **28**, 2563 (1985).

[71] J. Meyer and Y. Zhu, Phys. Fluids **30**, 890 (1987).

[72] M. J. Herbst, J. A. Stamper, R. R. Whitlock, R. H. Lehmberg, and B. H. Ripin, Phys. Rev. Lett. **46**, 328 (1981).

[73] S. Humphries, Principles of charged particle acceleration (J. Wiley, New York, 1986), and references therein.

[74] C. Decker, private communication.

[75] P. Chen, J. M. Dawson, R. W. Huff, and T. Katsouleas, Phys. Rev. Lett. **54**, 693 (1985).

[76] T. Katsouleas, Phys. Rev. A **33**, 2056 (1985).

[77] E. Valeo, *Phys. Fluids* **17**, 1391 (1974).

[78] C. S. Liu and V. K. Tripathi, *Phys. Fluids* **29**, 4188 (1986).

[79] R. W. Short, W. Seka, and R. Bahr, *Phys. Fluids 30*, 3245 (1987).

[80] H. C. Barr, T. J. M. Boyd, and G. A. Coutts, *Phys. Rev. Lett.*, **56**, 2256 (1986).

[81] D.Whittum, W. M. Sharp, S. S. Yu, M. Lampe, and G. Joyce, *Phys. Rev. Lett.* **67**, 991 (1991).

[82] E. P. Lee, Phys. Fluids **21**, 1327 (1978).

[83] M. Lampe, W. M. Sharp, R. F. Hubbard, E. P. Lee, and R. J. Briggs, Phys. Fluids **27**, 2921 (1984).

[84] M. Lampe, W. M. Sharp, and H. S. Uhm, Phys. Fluids **25**, 1456 (1982).

[85] J. Krall, K. Nguyen, and G. Joyce, Phys. Fluids B **1**, 2099 (1989).

[86] M. Lampe, G. Joyce, S. P. Slinker, and D. H. Whittum, Phys. Fluids **5**, 1888 (1993).

[87] J. F. Drake, P. K. Kaw, Y. C. Lee, G. Schmidt, C. S. Liu, and M. N. Rosenbluth, Phys. Fluids **17**, 778 (1974).

[88] I. S. Gradshtein, and I. M. Ryzhik, *Table of Integrals, Series, and Products* (Academic Press, New York, 1980).

[89] Y. Y. Lau, *Phys. Rev. Lett.* **63**, 1141 (1989).

[90] V. E. Balakin, A. V. Novokhatsky, and V. P. Smirnov, in *Proceedings of the 12th International Conference on High-Energy Accelerators*, edited by F. T. Cole and R. Donaldson (Fermi National Accelerator Laboratory, Batavia, IL, 1984), pp.119 and 120.

[91] V. L. Ginsburg, Propagation of Electromagnetic Waves in Plasma, Addison-Wesley, Reading, Mass. (1964).

[92] B. Coppi, private communication.

[93] J. Allbritton and P. Koch, Phys. Fluids **18**, 1136 (1975).

[94] L. M. Kovrizhnykh and A. S. Sakharov, Sov. L. Plasma Phys. **5**, 470 (1979).

[95] P. Koch, Phys. Fluids **16**, 651 (1973).

[96] R. Bingham, J. M. Dawson, J. J. Su, H. A. Bethe, Physics Letters A, **193**, 279 (1994); J. J. Su, R. Bingham, J. M. Dawson, H. A. Bethe, Phys. Scr. **T52**, 132 (1994).